DEPARTMENT OF MECHANICAL ENGINEERING

MALAVIYA NATIONAL INSTITUTE OF TECHNOLOGY

(Deemed University)

JAIPUR (RAJASTHAN) – 302017.

CERTIFICATE

This is to certify that the thesis entitled "Effect of Pressure, Concentration and Heat Flux on Flow Boiling Heat Transfer Characteristics of Nanofluids" being submitted by Mr. Om Shankar Prajapati to the Malaviya National Institute of Technology, Jaipur for the award of the degree of DOCTOR OF PHILOSOPHY is a record of bona fide research work carried out by him.

Mr. Om Shankar Prajapati worked under my guidance and supervision and has fulfilled the requirement for the submission of this thesis, which to our knowledge has reached the requisite standard.

To the best of my knowledge, the results contained herein have not been submitted in part or full, to any other University or Institute for the award of any degree.

Date: 21/05/2016

(Dr. Nirupam Rohatgi)
Associate Professor and Supervisor
Department of Mechanical Engineering
Malaviya National Institute of Technology
Jaipur-302017, India.

ACKNOWLEDGEMENT

It gives me great pleasure in expressing my sincere thanks to my dissertation supervisor, Dr. Nirupam Rohatgi, Associate Professor, Mechanical Engineering Department, Malaviya National Institute of Technology, Jaipur, for their valued guidance, their commitment in providing me with the guidance, advice and support at each and every step in the completion of this work. Their scientific and analytic approaches to new problems, wide knowledge and discerning remarks really have helped me at every stage of my work. It was due to their immense keenness and continuous attention that this present work could take a final picture.

A quote of special thanks to Late Professor A.K. Rajvanshi, Mechanical Engineering Department, Malaviya National Institute of Technology, Jaipur, for engaging me as Junior Research Fellow and Senior Research Fellow on Board of Research in Nuclear science, Mumbai, India sponsored research project (2009/36/95-BRNS/3234; 23 Feb. 2010) entitled "Investigation of Heat Transfer Characteristics of Nano-fluids in Subcooled Flow Boiling" collaborated with Dr. R.K. Duchaniya, Principal co-investigator and Assistant Professor, Metallurgical and Materials Engineering Department, Malaviya National Institute of Technology, Jaipur and Dr. A.K. Nayak, Scientist-F, Bhabha Atomic Research Centre, Mumbai, India lavishing special care and all time support to me. The financial help given by Board of Research in Nuclear science, Mumbai, India is gratefully acknowledged.

I immensely thankful to Dr. Puli Ugandhar for their experimental set-up and guidance. I am indebted for their help and suggestions on different matters and for the constant motivation.

I am very much indebted to Mr. Ramswaroop Meena for their help in making the experimental facility and help in conducting the experiments.

I also express my profound sense of gratitude and deep respect to Dr. G.S. Dangayach, Professor, Head of Mechanical Engineering Department and DRC Chairman for allowing me to work on the topic of my choice and providing me with all possible support.

I am also thankful to Dr. S. Mishra, Head of Mechanical Engineering Department and my senior colleagues at Rajasthan Technical University, Kota, Rajasthan for all their cooperation.

I am grateful to my beloved parent and family members for their invariable throughout encouragement and good wishes for my successful completion of my work.

Lastly, but not the least I thank one and all who have helped me directly or indirectly in completion of the report.

Date: 21/05/2016

(Om Shankar Prajapati)
Department of Mechanical Engineering
Malaviya National Institute of Technology
Jaipur-302017, India.

ABSTRACT

Nanofluids are liquid suspensions containing nanoparticles that are smaller than 100 nm. Nanofluid is emerging coolant for heat exchange due to high thermal conductivity and many benefits over other coolants. Nanofluids in pool boiling conditions is being studied broadly but data for nanofluid flow boiling, which is the situation of interest for the nuclear reactors and other engineering applications, are very scarce. Understanding of flow boiling is still elusive due to complexity and irreproducibility of process involved. This makes them very attractive as heat transfer fluids in many applications.

Flow boiling is characterized by the presence of small bubbles, which grow and collapse rapidly near the heated surface. Flow boiling is influenced by operational parameters like system pressure, mass flux, heat flux and channel geometry as well as microscopic parameters like void fractions and surface conditions.

In this study, selected nanofluids like Al_2O_3-water nanofluid, TiO_2-water nanofluid, ZnO-water nanofluid and Multi Walled Carbon Nano-Tubes-water nanofluid with concentration varying from 0.0001 to 0.1% are prepared using ultrasonic vibration mixer. The thermal conductivity of the selected nanofluids has been measured for different sonication time using thermal property analyzer (KD2-Pro). The nanofluids having maximum thermal conductivity have been used further for heat transfer study. The bubble parameters in an annular test section and heat transfer coefficient for variable pressure from 1 to 2.5 bar and heat flux from 0 to 400 kW/m^2 at a sub cooling of 20ºC and constant mass flux of 400 kg/m^2s have been investigated.

All the selected nanofluids are studied for samples of nanofluids having maximum thermal conductivity. Bubble images were captured with high-speed video camera using XCAP SV-642 software. High speed photography at the rate of 20,000 fps is used to capture bubble images. These images are processed by using National Instrument's Labview IMAQ Vision Builder 6.1 image processing software. The bubble size, bubble density and void fraction with respect to

variation in pressure, concentration of nanoparticles and heat flux have been evaluated for different selected nanoparticles by automated image processing and analysis algorithms. The surface roughness of the heating rod also has been measured before and after the experiments. The study shows that, the thermal conductivity of selected nanofluids increases with increase in sonication time in the beginning until it reaches a maximum value and then decreases. Heat transfer coefficient of nanofluids increases with increases in pressure, concentration of nanoparticles and heat flux. The empirical relations also have been developed for heat transfer coefficient of the nanofluids. The empirical relations predict the experimental results reasonably. Compared with water, significant increase in pressure drop is found for all pressurized nanofluids. Pressure drop increases with increase in Concentration of the nanoparticles and with increase in heat flux in flow boiling.

The bubble diameter, bubble density and void fraction for distilled water and for all nanofluids decreases and boiling is delayed with increase in external pressure on bubbles. Results also show that bubble diameter, bubble density and void fraction for distilled water and for all nanofluid increases with increase in heat flux. The bubble diameter of Al_2O_3-water nanofluid and TiO_2-water nanofluid is larger than bubble diameter of water while the bubble diameter of ZnO-water nanofluid and MWCNT-water nanofluid is smaller than bubble diameter of water. The void fraction increases with increase in concentration of the nanofluids for Al_2O_3-water nanofluid and TiO_2-water nanofluid. While the initial void fraction for ZnO-water nanofluid and MWCNT-water nanofluid observed less than water. The surface roughness, Ra (μm), of heater rod for selected nanofluids increases gradually with increase in concentration of nanoparticles in the nanofluid.

Key words: Nanoparticle, Nanofluid, Flow boiling, Two-phase heat transfer, High speed visualization, Bubble behavior, Void fraction.

CONTENTS

LIST OF TABLES

LIST OF FIGURES

NOMENCLATURE

a	cross-sectional area, m^2
A	cross-sectional area, m^2
AC	Alternative current, A
A_b	bubble area, mm^2
C	constant defined appropriately
CHF	Critical Heat Flux, W/m^2
c_p	specific heat at constant pressure, J/kg K
D	outer diameter, m
DAQ	Data Acquisition System
DC	Direct Current, A
d	inner diameter, m
f	friction factor (dimensionless)
FDB	Fully developed boiling
g	acceleration due to gravity, 9.8 m/s^2
G	mass flux, kg/m^2 s
h	heat transfer coefficient, W/m^2 K
i	specific enthalpy, J/kg K
I	current, A
k	thermal conductivity, W/m K
l	length, m
m	mass, kg
$\dot{m}$	mass flow rate, kg/s
N	total number
n_B	bubble density, $1/m^2$
NB	nucleate boiling.
NVG	Net vapour generation
ONB	Onset of nucleate boiling
OSV	Onset of significant void
p	pressure, bar
P_h	Heated perimeter, m
Δp	pressure drop, bar
q	heat flux, W/m^2
r	radius, m
r_i	radius of inner wall, m
r_o	radius of outer heated wall, m
Ra	surface roughness, µm
SS	Stainless Steel
t	time, s
T	temperature, K
TK	thickness, m

ΔT	temperature difference, K
u	velocity, m/s
UVM	Ultrasonic Vibration Machine
v	specific volume, m^3/kg
V	Volume, m^3
ΔV	control volume, m^3
$\dot{V}$	Volumetric flow rate, m^3/s
VF	Void fraction (dimensionless)

Greek Letters

η	thermal diffusivity, m^2/s
ν	kinematic viscosity, m^2/s
μ	viscosity, N-s/m
ρ	density, kg/m^3
ε	error
σ	surface tension, N/m
τ	Shear stress, N/m^2

Subscripts

b	bulk
c	convective
eff	effective
eq	equilibrium
f	liquid
g	gas/ vapor
h	hydraulic
i	inner
in	inlet
l	liquid
o	outlet
s	solid surface heater
sat	saturation
scb	subcooled boiling
sp	single-phase
spl	single-phase liquid
sub	sub cooling
sat	saturated
tp	two-phase
v	vapour
w	wall

1.

INTRODUCTION

Heat transfer plays an important role in all thermal applications such as nuclear reactors, power generation, refrigeration and air-conditioning, cryogenics and high power electronic components. In all such applications, heat transfer is realized through heat exchangers i.e. intercooler, evaporators, condensers and heat sinks. Conventional heat transfer technologies are becoming inadequate to transfer heat from one medium to another or to diffuse the accumulated heat. The researchers are looking for newer technologies to enhance heat transfer. Several methods are used to improve the heat transfer efficiency such as utilization of extended surfaces, imparting vibration to the heat transfer surfaces, use of micro-channels and increasing the thermal conductivity of the working fluid.

1.1 Background and Motivation

Heat transfer occurs through three modes i.e. conduction, convection, and radiation or through their combinations. Though each mode of heat transfer has specific application, convection is gaining momentum in areas of high rate of heat dissipation like space vehicles, turbine blades, electronic components, nuclear reactors, etc. Hence a lot of research is being focused on this mode of heat transfer.

Convective heat transfer may occur with or without phase change process. Of these, phase change cooling is an extremely effective way to cool the components. A typical example of phase change process is boiling of water. Boiling occurs when surface temperature of the heater surface exceeds saturation temperature of the fluid and it is always accompanied by phase change. The nucleation, transition and film boiling are mechanisms of boiling heat transfer. Boiling can be natural or forced. Natural boiling in stationary liquid is called pool boiling whereas forced boiling in the presence of liquid motion is called flow boiling. Examples of flow boiling are cooling of nuclear fuel core, cooling of microprocessors, etc. Currently, established cooling medium for nuclear fuel rod cooling is distilled water. However, world-over, efforts are being made to improve the heat transfer rate further. Putra et al. (2003), Yang et al. (2005), Heris et al. (2006) have opined that enhancement of convective flow boiling heat transfer is

vital and it is going to make inroads into all major and critical industrial applications in future.

Boiling heat transfer has been found to be an effective method to dissipate high heat loads. Extensive research has been done to further improve boiling heat transfer. Efforts are mainly aimed at finding techniques to initiate earlier onset of boiling, enhance nucleate boiling heat transfer rates and increase the critical heat flux (CHF), etc. Several boiling enhancement methods including surface roughening (Suriyawong and Wongwises (2009) and Shahmoradi (2013)) and use of various combinations of fluids (Henderson et al. (2010) and Tang et al. (2014)) have shown good potential.

Convective heat transfer rate can also be increased by increase in thermal conductivity of the working fluid. Commonly used heat transfer fluids such as water, ethylene glycol and engine oil have relatively low thermal conductivities. Solid materials such as oxides, metals and carbon nano-tubes (CNT) have 10 to 1000 times higher thermal conductivity than the liquids. High thermal conductivity of solids can be used to increase thermal conductivity of a fluid by adding small particles of the solid to the fluid. In the last century, solid particles with sizes of the order of millimeter to micrometers were mixed with liquid to increase their thermal conductivity.

Feasibility of the usage of these particles was investigated by several researchers and significant drawbacks were observed. These drawbacks are sedimentation, clogging of channels, increased pressure drop and erosion of channel walls. These drawbacks dissuaded from the use of suspensions of nanoparticles in base fluids as advanced working fluids in heat transfer applications (Bang and Chang (2005) and Qu et al. (2003)). Fresh efforts were made to use particles of smaller sizes. The sizes of particles were reduced from micrometer (10-6 m) to nanometer (10^{-9} m) and researchers shifted their focus to nanoparticles.

A Nanofluid is a fluid containing particles having their size in 1–100 nm range. The term Nanofluid was coined by Choi in 1995. The first nanofluid was produced by Choi (1995) at Argonne National Laboratory, USA.

Limited research work on pool boiling heat transfer characteristics of nanofluids is available in published literature. Heat transfer characteristics such as thermal conductivity, viscosity, critical heat flux, surface roughness, wettability, pressure drop in micro channels, stability of fluids, etc. has been discussed by Qu et al. (2003), Lee and Mudawar (2007), Liu et al. (2007), Park et al. (2007), Park and Jung (2007), Peng et al. (2009), Ahn et al. (2010). One area of importance which still remains unexplored is flow boiling, where its ability to enhance heat transfer would improve the overall efficiency of the system and reduce operational cost. The reported work on the heat transfer characteristics of nanofluids is conflicting and the effect of nanofluids on convective and flow boiling heat transfer is currently difficult to predict. Further investigation is required in this field.

There are many factors like thermal conductivity, viscosity, stability, wettability, size of particles, type of nanoparticles, base fluids, etc. that influence convective and flow boiling heat transfer. Parameters like sonication time, pressure, heat flux and type of nanoparticles also appear to be of paramount importance.

Sonication is one of the preparation methods of nanofluids using ultrasonic vibrations. Sonication time plays a significant role in preparation of nanofluids. Very few papers are available in the literature on the effect of sonication time on thermal conductivity of the nanofluids. Literature on sonication time reveals large discrepancy and disagreement in results as reported by Murshed et al. (2005) and Ismaya et al. (2013). Therefore the effect of sonication time on thermal conductivity of the selected nanofluids has been studied in this work.

Pressure plays a significant role in heat transfer. Little work is found in literature on the effects of pressure on boiling heat transfer for water. However, the effect of pressure on flow boiling heat transfer with nanofluids has not been studied so far. Therefore, the effect of pressure on convective and flow boiling heat transfer coefficient has been studied in this work.

Types of nanoparticles play a significant role on heat transfer. Considerable work on oxidized (Al_2O_3, TiO_2, ZnO, SiO_2, etc.) micro-particle is

available in the literature. Literature on nanoparticles is relatively less and at times self-contradictory as reported by Putra et al. (2003) and Mostafizur (2014). Therefore convective and flow boiling heat transfer performance of a few nanoparticles has been studied in this work.

Concentration of nanoparticles plays a significant role on heat transfer. Several researchers worked on the heat transfer characteristics of nanofluids in pool boiling heat transfer. The results of pool boiling heat transfer with nanofluids are contradictory. Witharana (2003) reported increased heat transfer whereas Das et al. (2003) reported decreased heat transfer. Relatively little work has been done so far on convective heat transfer characteristics of nanofluids. Similar to pool boiling heat transfer, contradictory results of convective heat transfer are reported. Kim et al. (2010) reported unchanged heat transfer at low heat fluxes and very less increase in heat transfer at high heat fluxes, whereas Bang et al. (2011) reported increased heat transfer at low and high heat fluxes. Therefore, effect of concentration of nanoparticles on convective and flow boiling heat transfer performance has been studied in this work.

Surface roughness is an important factor in increasing the heat transfer. Concentration of nanoparticles plays a significant role on the surface roughness. Contradictory results have been reported on effect of concentration on surface roughness by different researchers. Shahmoradi (2013) reported that surface roughness increases with increase in concentration of nanoparticles while White (2010) reported the opposite. Considerable work is available in literature on pool boiling for effects of concentration of nanoparticles on the surface roughness but very less work is available on the effects of concentration of nanoparticles on the surface roughness for convective heat transfer. Therefore, the effect of concentration of nanofluids on surface roughness has also been studied in this work.

In fluid medium, heat transfer coefficient depends on heat flux. This area has witnessed considerable publications. A few findings were also reported on nanofluids. Some researchers like Liu et al. (2007) and Kim et al. (2010) observed that for nanofluids, heat transfer coefficient increases with increase in heat flux. There is a recent interest in enhancing heat transfer by employing nanofluids. In

this work, effect of heat flux on the heat transfer coefficient for nanofluids has been studied.

High speed visualization technique is used to study bubble behavior as they are non-intrusive and suitable for study of flow boiling. The study of bubble behavior for water and refrigerants is available for pool and flow boiling but very little work on bubble behavior is available for pool boiling in nanofluids. The bubble behavior in flow boiling in nanofluids has not been studied so far. Therefore bubble behavior in flow boiling of nanofluids has been studied in this work.

In this study, selected nanofluids like Al_2O_3-water nanofluid, TiO_2-water nanofluid, ZnO-water nanofluid and Multi Walled Carbon Nano-Tubes–water nanofluid with concentration varying from 0.0001 to 0.1% are prepared using ultrasonic vibration mixer. The thermal conductivity of the selected nanofluids has been measured for different sonication time using thermal property analyzer (KD2-Pro). The nanofluids having maximum thermal conductivity have been used further for heat transfer study. The bubble parameters in an annular test section and heat transfer coefficient for variable pressure from 1 to 2.5 bar and heat flux from 0 to 400 kW/m^2 at a sub cooling of 20ºC and constant mass flux of 400 kg/m^2s have been investigated.

Bubble images are also captured with high-speed video camera using XCAP SV -642 software. High speed photography at the rate of 20,000 fps is used to capture bubble images. Bubble images are processed by using National Instrument's Labview IMAQ Vision Builder 6.1 Image Processing software. The bubble size, bubble density and void fraction with respect to variation in pressure, concentration of nanoparticles and heat flux have been evaluated by automated image processing and analysis algorithms.

1.2 Research Objectives

The present study enables effect of operational parameters such as concentration of nanoparticles, pressure in the test section and heat flux on heat

transfer coefficient of nanofluids, pressure drop and bubble parameters. The research objectives of this work can be summed up as following:

1. To study the effect of concentration, pressure and heat flux on:-
   - Heat transfer coefficient,
   - Pressure drop in the test section, and
   - Bubble parameters such as bubble diameter, bubble density and void fraction in flow boiling in few selected nanofluids.

   Heat transfer coefficient depends on thermal conductivity of the fluid and roughness of heat transfer surface. Therefore, along with the above, following effects were also investigated.
2. Effect of sonication time on thermal conductivity and
3. Effect of nanofluids on surface roughness of the heating rod.

Therefore in the present work the effect of Pressure, Concentration and Heat-Flux on Heat Transfer characteristics of Nanofluids has been investigated.

1.3 Organization of Thesis

There are seven chapters in thesis. A brief description of each chapter is given below.

Chapter-1. Introduction

Chapter-1 gives brief background of the problem to increase the heat transfer by using different nanofluids. The objectives of the research are enumerated and a brief description of the organization of the thesis is given.

Chapter-2. Literature Review

Chapter-2 gives a summary of the research work done hitherto in the related areas. The literature review has been divided into three broad topics - a) Thermal Conductivity of Nanofluids, b) Heat Transfer in Nanofluids c) Visualization of bubble parameters. Review of the salient papers reveals the gaps observed in the reported work. The chapter concludes with identification of specific objectives and scope of the present work.

Chapter-3. Experimentation

Chapter-3 describes experimental setup, details of the instruments used and the experimental procedure adopted. Fabrication and commissioning of the test section and commissioning of various instruments used in setup are discussed in this chapter. Specifications of the various instruments and equipment are also presented in this chapter. Detailed methodology of various measurements is also presented in this chapter.

Chapter- 4. Bubble Visualization

Chapter- 4 describes visual study of flow boiling process using 'National Instrument's Labview IMAQ vision builder' software.

Chapter- 5. Results and Discussion

This chapter gives results and their analysis. Parametric study based on available literature is also included in this chapter.

Chapter- 6. Empirical Relations for Heat Transfer Coefficient

In this chapter Response Surface Regression Analysis method has been used to develop empirical relations for heat transfer coefficient (HTC) of the nanofluids.

Chapter- 7. Conclusions

Chapter - 7 summarizes the conclusions drawn from the present investigation. Suggestion for the future work has also been included in this chapter.

Appendices contain information that has not been included under main chapters, which nevertheless is important and forms the integral part of the study.

2.

LITERATURE REVIEW

Nanofluids have higher thermal conductivity than base fluids, and hence may improve the efficiency of heat transfer, which is a main requirement of the industries. Therefore, efforts have been going on from last two decades to improve the heat transfer efficiency of fluids using nanofluids. The heat transfer system depends not only on pressure, temperature and surface morphology but also on properties of the nanofluids.

The thermo-physical properties of nanofluids vary with size of nanoparticle, concentration of nanoparticles, sonication time, sonication power, temperature and pressure of the fluid, pH level of the base fluid and presence of surfactants.

Researchers over the last two decades have been exploring high thermal conductive fluids to improve the efficiency of heat transfer fluid systems. The bubbles play a crucial role in heat transfer and bubble phenomenon has been extensively documented for water. Review of work done on bubble visualization has also been included in this chapter. An extensive study on the effect of concentration on heat transfer, pressure drop and surface roughness has also been included.

Literature review has been broadly divided into three sections:

1. Thermal conductivity of nanofluids.
2. Heat transfer in nanofluids. This has further been divided into three sections, i.e. -
    - Convective heat transfer
    - Pool boiling heat transfer
    - Flow boiling heat transfer
3. Visualization of bubble parameters

2.1 Thermal Conductivity of nanofluids

In this section, available literature on the effect of sonication time, type of nanoparticles and concentration of nanoparticles on thermal conductivity have been reviewed.

Eastman et al. (1997) studied thermal conductivity of nanofluids containing Al_2O_3, CuO, or Cu nanoparticles with two different base fluids i.e. water and HE-200 oil. They found that thermal conductivity increases with addition of nanoparticles. Maximum 60% increase in thermal conductivity was achieved compared to the corresponding base fluids for 5% (v/v) of Cu nanoparticles.

Lee et al. (1999) measured thermal conductivity for CuO and Al_2O_3 nanoparticles suspended in two different base fluids i.e. water and ethylene glycol (EG). They observed that nanofluids have substantially higher thermal conductivities than the base liquids. The increment for CuO/EG nanofluids thermal conductivity was more than 20% at 4% (v/v) concentration of nanoparticles. They also observed that, in the low volume fraction range (<0.05%), the thermal conductivity ratio increases almost linearly with concentration of nanoparticles.

Wang et al. (1999) measured thermal conductivity of nanofluids by steady-state parallel-plate technique. They used Al_2O_3 and CuO nanoparticles which had average diameters of 28 nm and 23 nm respectively, suspended in different base fluids i.e. water, ethylene glycol (EG), vacuum pump oil and engine oil. They concluded that thermal conductivities of all nanofluids were higher than the respective base fluids. They observed that CuO nanoparticles performed better, as observed by Lee et al. (1999).

Xuan and Li (2000) measured thermal conductivity for Cu and CuO nanoparticles of 100 nm and 36 nm respectively, in water. They observed that increase in thermal conductivity for Cu nanoparticles of larger size was higher than CuO nanoparticles of the smaller size. They also worked for an appropriate selection of dispersants to improve the stability of the suspension. They used oleic acid for transformer oil-Cu suspension and laurate salt for water-Cu suspension in their study. They found that Cu nanoparticles in transformer oil had superior characteristics as compared to the suspension of Cu particles in water.

Similarly, Eastman et al. (2001) used pure Cu nanoparticles of less than 10 nm size and achieved 40% increase in thermal conductivity for 0.3% (v/v) fraction

of Cu nanoparticles dispersed in ethylene glycol. They indicated that the increased surface to volume ratio with decrease in size is an important factor for increase in thermal conductivity. They also observed that the additive acid may stabilize the suspension and thus increase the effective thermal conductivity.

The largest increase in thermal conductivity has been observed with suspensions of carbon nanotubes, which have a very high aspect ratio and very high thermal conductivity. The first report on the synthesis of nanotubes was conducted by Iijima (1991). Later, nanotubes (multi-walled carbon nanotubes or MWCNTs)-oil (α-olefin) mixtures were investigated by Choi et al. (2001). They concluded that the measured thermal conductivity was anomalously greater than the theoretical predictions and was nonlinear with nanotubes concentration. As compared to other nanostructured materials discussed previously, carbon-nanotubes achieved the highest conductivity increment and offered opportunities for effective management of heat transfer.

Xie et al. (2002a) prepared nanofluid with 26 nm and 0.6 μm SiC suspensions in de-ionized water and EG respectively and measured the thermal conductivity using a transient hot-wire method. They found that the nanofluids with the same solid particles in different base fluids had similar improvement in their respective thermal conductivity. Later, Xie et al. (2002b) extended their research to study the effect of pH value of the suspension, specific surface area (SSA) of the dispersed Al_2O_3 nanoparticles and the crystalline phase of the solid particle on thermal conductivity of the nanofluid. They found that increase in the difference between the pH value and iso-electric point (the pH at which a molecule carry no net electrical charge) of Al_2O_3 resulted in enhancement of the effective thermal conductivity. They also observed that the thermal conductivity enhancements were highly dependent on the specific surface area (SSA) of the nanoparticles however the crystalline phase of the nanoparticles does not affect the thermal conductivity of the suspensions.

Biercuk et al. (2002) measured the thermal conductivity of suspensions of single wall carbon nanotubes (SWCNTs) and vapor grown carbon fibers (VGCF) in epoxy using a comparative method developed by Llaguno et al. (2001). Their experiments showed 125% and 45% improvements in thermal conductivity for

SWCNTs and VGCF respectively, at 1% w/w suspensions compared to effective thermal conductivity of water. Similarly, Choi et al. (2003) found that thermal properties of SWCNTs-epoxy composites give similar improvement in thermal conductivity.

Assael et al. (2003) experimentally studied the enhancement of thermal conductivity of carbon-multiwall nanotubes (C-MWNTs)-water suspensions with 0.1% w/w of sodium dodecyl sulfate (SDS) as dispersant. They found that the maximum thermal conductivity enhancement was 38% for a 0.6% (v/v) suspension. Results also showed that the SDS interacts with C-MWNT and the surface roughness of the container was increased when SDS is added

Das et al. (2003) examined the effect of temperature on thermal conductivity enhancement for nanofluids containing Al_2O_3 (38.4 nm) and CuO (28.6 nm) through an experimental investigation using the temperature oscillation method. They observed that a 2 to 4-fold increase in thermal conductivity can take place over the temperature range of 21ºC to 52ºC. They suggested application of nanofluids as cooling fluids for devices with high energy density, where cooling fluid is likely to work at a temperature higher than the room temperature. They also mentioned that the inherent stochastic motion of nanoparticles could be a plausible explanation for the thermal conductivity enhancement as smaller particles show greater enhancement of thermal conductivity with temperature.

Patel et al. (2003) used gold and silver nanoparticles for the first time to prepare nanofluids. They used a transient hot wire method for measuring thermal conductivity. The most important observation in their study was a perceptible enhancement in thermal conductivity for vanishingly small concentrations. It was reported that at room temperature, the conductivity of toluene-gold nanofluid was enhanced by 3–7% for a 0.005–0.011% (v/v) nanofluid, whereas the enhancement for water–gold nanofluid was 3.2–5% for a vanishingly small concentration of 0.0013–0.0026% (v/v). The main reason for such an enhancement was the small size (~10–20 nm) of the particles. The enhancement was greater with water-based nanofluids because bare particles were used, and was lower for toluene-based nanofluids where the nanoparticles were protected by a layer of thiolate coating, which was used to prevent agglomeration. Also, the increments in thermal

conductivity of the nanofluids were found to be nonlinear with temperature and almost linear with particle volume fraction.

Xie et al. (2003) also proposed a method to produce stable and homogeneous suspensions of multi-walled carbon nanotubes (MWCNTs) in de-ionized water (DW), ethylene glycol (EG), and decene (DE). They introduced oxygen-containing functional groups on MWCNT surfaces to form more hydrophilic surfaces. They observed that the thermal conductivity increases with increase in concentration of nanotubes in the base fluid.

Wen and Ding (2004) studied thermal conductivity of carbon nanotubes in water. They found that the thermal conductivity increases with addition of CNT nanotubes. Later, Wen and Ding (2004a) examined the effect of temperature on the thermal conductivity of MWCNT (20-60 nm in diameter and a few tens of micrometers in length)/water nanofluids. They found that increase in thermal conductivity with temperatures for temperatures lower than 30ºC was approximately linear. However, the dependence on temperature decreased at temperatures higher than 30ºC and thermal conductivity became more or less constant. Later, Assael et al. (2005) repeated similar measurements using multiwall carbon nanotubes (MW CNTs) and double-walled carbon nanotubes (DW CNTs). Thermal conductivity of the MWCNT-water nanofluid for MWCNTs of 130 nm average diameter and 40 μm average length was found to increase by 34% for the concentration of 0.6% v/v in water, whereas that of double walled CNTs of approximately same size was found to increase by 8% for the concentration 1% v/v in water.

Ding et al. (2005) measured thermal conductivity with addition of carbon nanotubes (CNT) at different temperatures. They found that the effective thermal conductivity increases with addition of CNT and increase in the fluid temperature. They found that the improvement of the thermal conductivity is slightly higher than that reported by Assael et al. (2003), Xie et al. (2003), and Wen and Ding (2004a), but much lower than that found by Choi et al. (2001). They attributed discrepancy to difference in properties in CNT used, the aspect ratio, the inclusion of dispersants and experimental errors.

Hwang et al. (2005) compared the thermal conductivity of four kinds of nanofluids, i.e. MWCNTs in water, CuO in water, SiO_2 in water and CuO in ethylene glycol. They concluded that thermal conductivity increases with addition of nanoparticles in the respective base fluids. They found that the thermal conductivity of MWCNT-water nanofluid increases by up to 11.3% at 1% (v/v) suspension, which was higher than the other nanofluids.

Murshed et al. (2005) used ultrasonication method to prepare TiO_2 nanofluids in two hours. They observed that thermal conductivity increases with increase in sonication time. They also observed that for the same concentration of nanoparticles thermal conductivity increases nearly by 33% and 30% for TiO_2-water nanofluids over the base fluid for particle size of 10 nm and 15 nm, respectively.

Hong and Yang (2005) prepared Fe-nanofluid and Cu-nanofluids using ethylene glycol as base fluid. The average size of nanoparticles was 10 nm. They found that Fe nanofluids exhibited higher enhancement of thermal conductivity than Cu-nanofluids. They also observed that the material with high thermal conductivity is not always the best option for the suspension to improve the thermal characteristics of the base fluids. They also concluded that the thermal conductivity of nanofluids increased non-linearly with increasing concentration of nanoparticles in the base fluids.

Hong et al. (2006) investigated the effect of clustering of Fe nanoparticles on the thermal conductivity of the nanofluids. They found that the thermal conductivity of nanofluids was directly related to the agglomeration of Fe nanoparticles which resulted in the nonlinear relation between the Fe volume fraction and thermal conductivity of nanofluids.

Hays et al. (2006) used ultrasonication method to prepare Al_2O_3 nanofluids. They dispersed nanoparticles of 47 nm average size in de-ionized water and found that nanofluids can be prepared in 3-4 hours by using the UVM at a fixed energy level of 4W. They found that thermal conductivity of nanofluids increases with increase in sonication time and concentration of nanoparticles. They also studied the effect of addition of HCl to the base fluid. They found that

addition of HCl prior to the addition of nanoparticles helps in reducing the no. of larger colloids as compared to the case in which HCl is added after the addition of nanoparticles to the base fluid.

Li and Peterson (2006) conducted an experiment to examine the effects of variations in temperature and the volume fraction on the thermal conductivity of CuO (29 nm) and Al_2O_3 (36 nm) water suspensions. Results demonstrated that nanoparticle material, volume fraction and bulk temperature have significant effect on the thermal conductivity of the nanofluids. They found that thermal conductivity increases with increase in temperature and volume fraction. They reported that Al_2O_3/water suspensions have higher thermal conductivity than CuO/water suspensions and increase in the mean temperature from 27ºC to 34.7ºC results in the enhancement of thermal conductivity by three times.

Putnam et al. (2006) did not observe significant increase in the thermal conductivity of nanofluids by addition of small volume fractions of nanoparticles such as C_{60}–C_{70} and Au (with aspect ratio, $\varphi << 1$). The largest increase in thermal conductivity for 4 nm Au particles was observed as 1.3%±0.8%, which conflicted with the results of Patel et al. (2003).

Zhang et al. (2007) measured the thermal conductivity and diffusivity of Au/toluene, Al_2O_3/water, TiO_2/water, CuO/water nanofluids using the transient short-hot-wire (SHW) technique, which was developed from the conventional transient hot wire technique and is based on the numerical solution of two-dimensional transient heat conduction for a short wire with the same length-to-diameter ratio and boundary conditions as those used in the actual measurements. The diameters of Au, Al_2O_3, TiO_2 and CuO spherical particles were 1.65, 20, 40 and 33 nm respectively. They did not find increase in thermal conductivity of the nanofluids and the same was predicted accurately by the equations of the Hamilton and Crosser model. Later, Zhang et al. (2007a) investigated the thermal conductivity and thermal diffusivity of CNT/water nanofluids using the transient SHW technique. The average length and diameter of CNTs were 10 μm and 150 nm respectively. However, the measured results demonstrated that there was no increase in thermal conductivity of the nanofluids as predicted by the unit-cell model equation of Yamada and Ota (1980) for carbon nano-fibers.

Xuan and Li (2008) measured the thermal conductivity of Cu nanoparticle suspensions in water. They found that the thermal conductivity of nanofluids increases remarkably with increase in the volume fraction of nanoparticles. They also suggested that experimental research is urgently required to investigate the heat transfer process of nanofluids.

Yurong et al. (2008) measured the thermal conductivity of TiO_2 nanofluid prepared in distilled water with particle size of 95 nm and compared it with the Hamilton-Crosser model. They found that thermal conductivity of nanofluid increased non-linearly with increase in particle concentration while the Hamilton-Crosser model predicted lower values of thermal conductivity, increasing linear with concentration. The exact reason for this disparity was not clear but they suggested that size of nanoparticle and concentration of nanoparticles used in the model might be responsible for this behavior.

Murshed et al. (2009) developed a model by taking both static and dynamic mechanisms on which thermal conductivity of nanofluid depends. The model formulation was done by considering factors such as Brownian motion of nanoparticles, particle size, fluid temperature and interfacial nano-layer. They measured the thermal conductivity of TiO_2, Al_2O_3 and Fe_3O_4 nanoparticles in distilled water by hot wire transient method. They found that thermal conductivity increases with increase in Brownian motion, temperature and interfacial nano-layers, while it decreases with increase in particle size. The results of experiment and that of model developed were also compared with Maxwell and Parasher model. They found a good agreement between the experimental values and the values calculated by the suggested model. However, Maxwell and Parasher models under-predicted the experimental values since these models did not include the effect of particle movement, surface chemistry and interfacial layer, all of which have a significant role in the thermal conductivity of nanofluids.

Murshed et al. (2010) measured thermal conductivity for Al_2O_3-water nanofluids and CuO-water nanofluids. The size of nanoparticles was also considered. They reported that nanofluids containing different nanoparticles have different thermal conductivities. The result indicated that the Al_2O_3 (33 nm)/water nanofluid has an enhancement of 29% for 5% volume fraction while for Al_2O_3 (20

nm)/water nanofluid has an enhancement of 16% for 1% volume fraction. Similarly CuO nanoparticles of 36 nm and 50 nm diameter mixed with water have an enhancement of 60% and 17% in thermal conductivity of nanofluids for 5% (v/v) and 0.4% (v/v) fraction respectively.

Gowda et al. (2010) studied the effect of surface charge, base fluid and dispersion methods on thermal conductivity of alumina and copper oxide nanofluids. The surface charge was varied by changing the pH value of the fluids. They observed that higher surface charge (low pH value) of nanofluids improves dispersion of nanoparticles in base fluids. They suggested that the viscosity of base fluid reduces the Brownian motion of nanoparticles and thus the agglomeration of particles reduces in nanofluids. They also observed that high power sonication significantly improved the thermal conductivity and the stability of the nanofluids. They concluded that, the thermal conductivity of nanofluids could be effectively improved by changing the pH of the fluids, using more viscous fluids and high power sonication.

Das et al. (2012) compared the enhancement of thermal conductivity for various nanofluids having nanoparticles such as metallic, oxides, graphene and carbon nanotubes at different concentrations maintaining the same temperature. They found that the increase in thermal conductivity for graphene nanofluid and CNT nanofluid was more as compared to the increase in thermal conductivity for metallic nanofluid and oxides nanofluid having same concentration and temperature. It was assumed that the long chains of inter-connected networks between the particles acted as conducting paths, which enhanced thermal conductivity of CNT-nanofluids and grapheme-nanofluids. However, increment in thermal conductivity in case of CNT was 2.5 times more than graphene.

Murugesan et al. (2012) gave the upper and lower limit for thermal conductivity of nanofluids. The upper limit was based on heat transport mechanisms considering nano-layer thickness in the interface of particle and fluid, Brownian motion and particle shape. They considered maximum heat transfer for setting up the upper limit. It was found that at 5% volume concentration, a minimum of 30% and a maximum of 50% enhancement was observed when the nanofluid was prepared in distilled water. Thus, they identified that the increase in

thermal conductivity of the nanofluids having concentration of nanoparticles up to 5% varies between 50% and 30%.

Ismay et al. (2013) studied thermal conductivity of water-based TiO_2 (rutile) nanofluid over a range of volume fraction, temperature, pH, particle size and sonication time. The rutile is a mineral composed primarily of titanium dioxide and it is the most common natural form of it. The thermal conductivity was measured using a KD2-Pro apparatus. They found that thermal conductivity increases with increase in volume fraction, sonication time, nanoparticle size reduction and temperature. It was found that thermal conductivity improved by 2% due to change in pH, with large spikes in enhancement as fluid pH approached isoelectric point of TiO_2. Furthermore, the results of the experiments indicated that the placement of the KD2-Pro sensor needle was critical in the study of nanofluids having aggregated nanoparticles. They further reported that the sonication time required to completely break up the aggregated particles was considerably greater than those reported in the literature.

Xia et al. (2014) measured thermal conductivity for Al_2O_3/de-ionized water nanofluids of different volume fractions with different mass fractions of sodium dodecyl sulphate (SDS) and polyvinylpyrrolidone (PVP) surfactants. The thermal conductivity ratio of surfactant solutions mainly depends on the length of alkyl chain; they also studied the effect of alkyl chain length for the same kind of surfactant. The nanofluids were prepared by a two-step method. They found that surfactant had negative effect on the thermal conductivity of base fluid. They observed lower thermal conductivity for longer alkyl chain length using surfactants. However, the addition of surfactants significantly improves the stability of Al_2O_3/de-ionized water nanofluids.

They found that the highest thermal conductivity occurs at an optimal concentration of surfactant and particles. The optimal concentration of SDS-surfactant and particle were approximately 2/1, 1/1, 1/2, 3/5 when the particle concentrations were 0.1%, 0.5%, 1.0%, 2.5% (v/v) in water. The ratio corresponding to the highest thermal conductivity of Al_2O_3/de-ionized water nanofluids and de-ionized water decreases with the increase in particle concentration. Furthermore, they suggested that nanofluids with larger particle

size need higher concentrations of surfactant to get increased thermal conductivity.

Mostafizur (2014) measured thermal conductivity for three types of nanoparticles, namely Al_2O_3, SiO_2 and TiO_2 suspended in methanol solution at five different volume fractions (0.005%, 0.01%, 0.05%, 0.1% and 0.15%) and at five different temperatures (1, 5, 10, 15 and 20°C) using a KD2 pro thermal conductivity meter. They found that the thermal conductivity of methanol-based nanofluids increased with the increase of nanoparticle volume fraction and temperature. The maximum increase in thermal conductivity was about 29.41%, 23.03% and 24.51% for Al_2O_3/methanol nanofluids, SiO_2/methanol nanofluids and TiO_2/methanol nanofluids respectively, at 0.15% (v/v) and temperature of 20°C. They also found that the values of thermal conductivity enhancement of Al_2O_3/methanol were approximately 6% and 5% higher compared to SiO_2/methanol and TiO_2/methanol nanofluids for the same volume concentration and operating temperature.

2.2 Convective heat transfer for nanofluids

Research on convective heat transfer in nanofluids has become more popular in the last ten years, perhaps because of the demand for high rate of cooling of microelectronics components and other critical and compact cooling processes. On the one hand, very few investigations have been carried out in this field while on the other, the conclusions drawn, seem to be controversial.

Lee and Choi (1996) studied the heat transfer behavior in parallel channels using nanofluids and observed increase in thermal conductivity by a factor of 2. Later, Xuan and Li (2003) experimentally investigated convective heat transfer characteristics for Cu-water based nanofluids through a straight tube with constant heat flux at the wall of the tube. They concluded that nanofluids substantially increase the heat transfer rate as compared to that of the pure water. For a constant Reynolds number, the heat transfer coefficient of nanofluids containing 2% volume of Cu nanoparticles was approximately 60% higher than that of the pure water due to the increase in thermal conductivity. They also reported that the

friction factor of the nanofluids did not require extra pumping power at low concentrations of nanofluids.

Chien et al. (2003) investigated thermal conductivity of gold/water nanofluids. They used gold nanoparticles of an average size of 17 nm. The nanofluid was passed through a disk-shaped miniature heat pipe with diameter of 9 mm and height of 2 mm. They found that thermal resistance of the heat pipe fell appreciably with increase in concentration of nanoparticle. Tsai et al. (2004) also used aqueous solutions of various-sized (2-35 nm and 15-75 nm) gold nanoparticles, which were prepared by the reduction of $HAuCl_4$ with tri-sodium citrate and tannic acid. They found large decrease in thermal resistance (0.27°C/W) of the heat pipe with nanofluids as compared with de-ionized water. The thermal resistance of the circular heat pipe ranged from 0.17 to 0.215 °C/W with different nanoparticle solutions. For decreased thermal resistance, they reasoned that a major thermal resistance of heat pipe is caused by the formation of vapor bubble at the liquid-solid interface. A larger bubble nucleation size creates a higher thermal resistance that prevents the transfer of heat from the solid surface to the liquid (Thome et al. (1996)). The suspended nanoparticles tend to bombard the vapor bubble during the bubble formation. It was also expected that the nucleation size of vapor bubble was much smaller for fluid with suspended nanoparticles than that without them.

Khanafer et al. (2003) numerically investigated the heat transfer behavior of nanofluids in a two-dimensional horizontal enclosure. The nanofluid was assumed to be in single phase and in thermal equilibrium with was no velocity slip between the base fluid and the nanoparticles. It was found that the heat transfer rate increased with the particle concentration at any given Grashof number.

Putra et al. (2003) presented their experimental observations on natural convection of Al_2O_3 and CuO-water nanofluids inside a horizontal cylinder heated from one end and cooled from the other. Unlike for the forced convection, they found linear deterioration in natural convective heat transfer with concentration of nanoparticles. They also observed that the natural convective heat transfer was dependent on the particle density, concentration and the aspect ratio of the cylinder. The deterioration increased with particle concentration and was more

significant for CuO nanofluids. At a Rayleigh number of 535; 300% and 150% decrease in the Nusselt number was found for 4% (w/w) of CuO-water and Al_2O_3-water nanofluids respectively. Their results were different from the numerical results of Khanafer et al. (2003) and the experimental data of Putra et al. (2003). They found that some important factors were not included in the numerical study presented by Khanafer et al. (2003). These factors are particle size, particle shape and particle distribution, which could significantly influence the flow and heat transfer characteristics of nanofluids.

Wen and Ding (2004b) reported experimental results for the convective heat transfer of γ - Al_2O_3 (27-56 nm)/water based nanofluids flowing through a copper tube (D = 4.5 mm, L = 970 mm) in the laminar regime. They found that the inclusion of Al_2O_3 particles can significantly enhance the convective heat transfer coefficient with increase in Reynolds number and particle concentrations. Furthermore, the improvement of the heat transfer coefficient was particularly large at the entrance region and it decreased with the axial distance.

Wen and Ding (2005) also studied the problem of natural convective heat transfer of TiO_2 (30-40 nm)/water nanofluids in a vessel which was composed of two horizontal aluminum discs of diameter 240 mm and thickness 10 mm separated by a gap of 10 mm. They investigated both the transient and steady-state heat transfer coefficients for various concentrations of nanofluids. Similar to Putra et al. (2003), they found that the natural convective heat transfer coefficient decreased as compared to that of pure water. Further, such deterioration increased with concentration of nanoparticles. They proposed several possible mechanisms for their observations such as the convection caused by concentration difference, particle-fluid and particle-particle interactions and modifications of the dispersion properties.

Ding et al. (2005) investigated the heat transfer performance of CNT (aspect ratio, $\alpha >> 1$) nanofluids in a tube with 4.5 mm inner diameter. They found that increase in heat transfer coefficient was much higher than the increase in the thermal conductivity of the base fluid. They reported that convective heat transfer coefficient increased by over 350% at Re = 800 for 0.5% (w/w) of CNT-water nanofluid. They suggested that the possible reasons for the improved thermal

conductivity are shear-induced enhancement in flow, particle re-arrangement and high aspect ratio of CNTs. The studies with nearly spherical nanoparticles (aspect ratio, $\alpha \approx 1$) by Pak and Cho (1998), Xuan and Li (2003), Wen and Ding, (2004b) showed enhancement of the convective heat transfer of up to 60%. However, Yang et al. (2005) used the disc-shape graphite nanoparticle (with aspect ratio l/d = 0.02) to investigate the convective heat transfer coefficient of the graphite nanofluids in laminar flow through a circular tube with diameter of 4.57 mm and length of 457 mm. They found that the increase in heat transfer coefficient was much lower than the increase in the thermal conductivity. It means that apart from the thermal conductivity, aspect ratio of the nanoparticle should be an important factor in determining the thermal performance of nanofluids. Similar results were also seen in the CNT-based suspensions with very high aspect ratios (Ding et al. 2005) ($\alpha >> 1$). They suggested further investigation to clarify this problem.

Heris et al. (2006) investigated laminar flow of CuO/water and Al_2O_3/water nanofluids between a 1 m long annular tube with inner tube made up of copper, having inner diameter of 6 mm and thickness of 0.5 mm, and an outer tube of stainless steel having inner diameter of 32 mm. The saturated steam was circulated to obtain constant wall temperature. They found that the heat transfer coefficient increases with increase in the volume fraction of nanoparticles as well as with Peclet number. The Al_2O_3/water nanofluids showed more increment in heat transfer coefficient than CuO/water nanofluids.

Ma et al. (2006) combined diamond nanofluids with an oscillating heat pipe (OHP) to develop an ultra-high-performance cooling device. Experiments showed that diamond-water nanofluids could reduce the temperature difference between the evaporator and the condenser. They found that maximum reduction in temperature was from 40.9 to 24.3ºC for a power input of 80 W for 0.01% (v/v) diamond-water nanofluids. Their findings were similar to Yang et al. (2005).

Later, Heris et al. (2007) presented experimental investigations on forced convective heat transfer of Al_2O_3/water nanofluid in laminar flow through a circular tube with constant wall temperature boundary condition. They reported that heat transfer coefficient of nanofluids increased with increase in the Peclet number as well as with the nanoparticle's concentration. The increase in heat

transfer coefficient due to presence of nanoparticles was much higher than the one which was predicted by single phase heat transfer correlation. It was concluded that thermal conductivity increase was not the sole reason for increase in heat transfer coefficient of nanofluids. They assumed that factors such as dispersion and chaotic movement of nanoparticles, Brownian motion and particle migration may play role in increase in heat transfer coefficient due to nanoparticles.

Tiwari and Das (2007) studied about mixed convection in a two sided, lid-driven, differentially heated, square cavity filled with a Cu/water nanofluid. They found that the convective heat transfer performance is better in case of nanofluids. Their results agreed well with previously published work for single phase flow.

He et al. (2007) reported an experimental study on the convective heat transfer behavior of aqueous TiO_2 nanofluids flowing through a straight vertical pipe under laminar as well as turbulent flow conditions. The effect of nanoparticles concentrations, particle size and the Reynolds number were investigated. They reported that the addition of nanoparticles into the base liquid enhances the thermal conduction and that the enhancement increases with increase in particle concentration and decrease in particle size in both, laminar as well as turbulent flow regimes.

The effect of particle concentration was also found to be more in the turbulent flow regime. They also reported that pressure drop for nanofluids were very close to pressure drop for the base liquid at constant Reynolds number.

Duangthongsuk and Wongwises (2009) presented experimental investigations on convective heat transfer performance and flow characteristic of a TiO_2–water nanofluid flowing in a horizontal double tube counter flow heat exchanger. The effect of nanofluids concentration, Reynolds number and temperature of nanofluid was investigated under turbulent flow conditions. They used TiO_2-water nanofluids, which have a significantly higher heat transfer coefficient than that of pure base fluid.

They reported that 0.2% (v/v) of TiO_2-water nanofluid had approximately 6-11% higher heat transfer coefficient as compared to that of water. The heat transfer coefficient increased with increase in Reynolds number and decrease in

temperature of nanofluid due to increase in the heat transfer. A small pressure drop in the nanofluid was also reported and it was approximately same as that for the water under same conditions.

2.3 Boiling heat transfer for nanofluids

Boiling is a mode of heat transfer which occurs when the surface temperature of heater exceeds saturation temperature of fluid. It is accompanied by phase change due to which heat transfer coefficients in boiling are much larger than other modes of heat transfer as shown in the table 2.1 (Incropera 2009).

Table 2.1: Typical heat transfer coefficients.

Process	Heat Transfer Coefficient, h (W/m^2K)
Free Convection	5-25
Forced Convection	25-20,000
Convection with phase change (Boiling)	500-100,000

Boiling heat transfer is classified into Pool boiling and Flow boiling. Its literature is presented here in two sections of pool boiling and flow boiling. Pool boiling with nanofluids is presented first to understand the basic development in boiling. Conflicting results have been reported even for pool boiling. The inconsistencies indicate that our understanding of the thermal behavior for nanofluids related to boiling heat transfer is still poor.

Further detailed and valuable investigations are necessary to understand the phenomenon of boiling of nanofluids. As we know, boiling is affected by surface properties such as surface roughness, surface wettability and surface contamination.

In the reviewed studies, however, usually only the surface roughness was considered. Hence, systematic studies should be carried out to include the relationship between surface properties and nanofluids.

2.3.1 Pool boiling heat transfer

Enhancements of thermal conductivity of nanofluids make them attractive for cooling applications. When using nanofluids for cooling at high heat flux applications, the single phase heat transfer process follows the boiling regime. Many researchers expect that nanofluids would have a reasonable potential to enhance the boiling heat transfer. A systematic review of their work on pool boiling is presented here.

Das et al. (2003) were first to study the pool boiling characteristics of water-based nanofluids containing 1, 2 and 4% (v/v) of Al_2O_3 nanoparticles. They found deterioration in the boiling performance with increase in particle concentration. Later, Das et al. (2003a) carried out an experimental study on pool boiling characteristics of Al_2O_3 nanofluids under atmospheric conditions in a tube having a diameter of 20 mm. They found that the addition of nanoparticles degraded the boiling performance. The deterioration in boiling performance increased with increase in particle concentration. They attributed it to the change in surface roughness during pool boiling of nanofluids. For higher particle concentration and higher surface roughness, the uneven surface can trap the particles more easily and make the surface smoother, which can degrade the performance. Das et al. (2003b) also studied pool boiling in tubes with small diameters (4 and 6.5 mm). They observed that the deterioration in boiling performance in the smaller tubes was lower than the bigger tubes. They concluded that, apart from the increase in thermal conductivity, there should be some other factors that affect the heat transfer coefficient of the nanofluids in boiling.

Witharana (2003) investigated the pool boiling heat transfer coefficients (HTC) of Au/water, SiO_2/water and SiO_2/ethylene glycol nanofluids in a cylindrical vessel with 10 cm diameter and 10 cm height. The average size of the nanoparticles was 30 nm. The vessel was supplied a fixed heat flux at the bottom and the top was kept open to the atmosphere. Results of Au/water nanofluids {ø = 0.0002-0.001% (w/w)} showed that the HTC of nanofluids was higher than that of the pure water, and it escalated with increase in concentration of gold particles. They observed that the increase in HTC was above 11% at intermediate heat flux

of 3 W/cm^2 and as high as 21% at the maximum heat flux of 4 W/cm^2. However, the SiO_2/water and SiO_2/ethylene glycol nanofluids recorded decrease in HTC as compared to the base fluids, which was contrary to the expectations. The author did not explain the strange phenomenon and instead suggested repetition of the experiments.

You et al. (2003) were the first to investigate the Critical heat flux (CHF) of Al_2O_3/water nanofluids in pool boiling. Their boiling apparatus was provided with usual horizontal heater. They found that CHF of Al_2O_3/water nanofluids increased by 50 to 200% compared to that for pool boiling of pure water. They used concentrations up to 0.05 g/l i.e. up to 0.5% (w/w). The CHF increased sharply with concentration, while beyond 0.2 % (w/w) it remained constant at 300% of that for pure water. They also found that the size of the bubbles increased and frequency of bubble departure decreased with the addition of nanoparticles in the water. They opined that there were some unknown key factors responsible for increase in CHF of the nanofluids, which need further investigation.

P. Vassallo et al. (2004) studied the pool boiling characteristics for both SiO_2/water nano-solutions and micro-solutions with horizontal NiCr wire of 0.4 mm diameter instead of a heating surface. The wire was long (~75 mm) and the temperature of the wire was evaluated from the resistance of the wire. They reported that nanoparticles of SiO_2 could not precisely account for the heat transfer enhancement in the nucleate boiling regime, but the CHF increased significantly for both nano and micro-particles. They conjectured that the increase in CHF was due to the surface coating of the silica affecting the density of nucleation sites.

Zhou (2004) investigated the pool boiling heat transfer characteristics of copper/acetone based nanofluids with and without acoustic cavitations. They reported that the copper nanoparticles and acoustic cavitations had significant influence on the heat transfer in the fluid. However, the addition of nanoparticles did not affect the dependence of heat transfer on acoustic cavitation and fluid subcooling. As compared to the experimental results of Das et al. (2003a; 2003b), the pool boiling heat transfer did not decrease with increase in particle volume

fractions in the absence of the acoustic field. While in an acoustic field, the boiling heat transfer of nanofluids increased and the boiling hysteresis disappeared.

Bang and Chang (2005) investigated the effect of Al_2O_3 nanoparticles on heat transfer and bubble formation in a quiescent pool of nanofluids under adiabatic conditions. They used a 100 mm square surface in horizontal and vertical conditions. They observed that after boiling, the surface roughness increased with nanoparticle concentration. However, the critical heat flux (CHF) increased by ~32% and ~13% for both a horizontal flat surface and a vertical flat surface in the pool, respectively. They cautioned that increased roughness caused by the deposition of nanoparticles will cause fouling and lead to deterioration of the boiling heat transfer performance. They also reported that the nanoparticles suspended in the liquid alone could affect bubble formation significantly by modifying bubble dynamics such as bubble departure diameter and frequency.

Later, Bang and Chang (2005a) investigated the effect of Al_2O_3-water nanofluids in pool boiling using an elaborate apparatus with visualization windows. They also carried out visualization study for water and a dilute {0.5% (v/v)} Al_2O_3/water nanofluid, but it could not any insight. They used a much smoother heater, having a surface roughness of approx 37 nm than that was used by Das et al. (2003a). Similar to Das et al. (2003a), they observed that heat transfer coefficient decrease with concentration of Al_2O_3-water nanofluid. They also reported that the rate of change in heat transfer coefficient also decreases with concentration.

Wen and Ding (2005a) conducted experiments on pool boiling heat transfer using γ- Al_2O_3/water nanofluids. γ-Al_2O_3 particles were produced through an electrostatic stabilization method with the aid of a high shear homogenizer. They found that the presence of alumina in the nanofluid can enhance the boiling heat transfer significantly. They found ~40% enhancement in the boiling heat transfer for 1.25% (w/w) concentration of nanoparticles. They suggested extra thermal resistance to the boiling surface caused by the sedimentation of nanoparticles, the effect of surfactant, and the interaction between the boiling surface and the nanofluids as the possible reasons for the controversies that had arisen from the previous studies. They suggested further research on nanofluids to

investigate the important factors affecting the boiling performance. In contrast to the report of Das et al. (2003, 2003a) and Bang and Chang (2005, 2005a), Wen and Ding (2005a) reported increase in pool boiling heat transfer with nanoparticle concentration and heat flux in nanofluids. They found an increment as high as 40% in heat transfer coefficient at the concentration of about 0.3% (v/v). They observed that increase in heat transfer cannot be explained by increase in conductivity alone. They proposed that the concentration of nanoparticles which were used in the said study was lesser than that of nanofluids which were used in previous studies, as a possible reason.

Kim et al. (2006) experimentally investigated CHF in pool boiling on a stainless steel plate for Al_2O_3, ZrO_2 and SiO_2 nanoparticles in water. They found that CHF increases with addition of nanoparticles and opined that the possible reason for the same is that nanoparticles deposited on the heater surface form an irregular porous structure that increases the wettability of the surface.

Later, Kim et al. (2006a) experimentally investigated CHF in pool boiling of TiO_2 nanoparticles in water on Ni-Cr wire. They found that CHF increases up to 200% with the addition of nanoparticles. Further, Kim et al. (2006b) investigated CHF in pool boiling on a Ni-Cr and Ti wires for Al_2O_3 and TiO_2 nanoparticles in water. They found that CHF increases with increase in concentration of nanoparticles. They also reported that the nanoparticles get deposited on the surface of heater. They also measured CHF for pure water for nanoparticle deposited heated wire and found increase in CHF.

Chopkar et al. (2007) performed pool boiling heat transfer on Cu surface for ZrO_2 nanoparticles in water. They found that boiling heat transfer remains unchanged. They also added surfactants to nanofluid as a stabilizer and found that boiling renders heater surface smoother. Further, Ding et al. (2007) studied the pool boiling heat transfer characteristics of Al_2O_3 and TiO_2 nanoparticles in water on stainless steel plate. They found that boiling heat transfer performance increases for both TiO_2 and Al_2O_3 nanoparticle suspensions. The pool boiling heat transfer increased with increase in nanoparticle concentration. The enhancement is more sensitive to TiO_2 than Al_2O_3.

Park and Jung (2007) investigated pool boiling heat transfer performance on a stainless steel tube for carbon nanotubes (CNT) in water and R-22. They found that CNTs improved boiling heat transfer performance by up to 29% for both base fluids. They also observed that there was no surface fouling with CNTs.

Kim et al. (2007) measured CHF for pure de-ionized water as well as for the different nanofluids on a stainless steel thin wire in the pool boiling. The wire had a diameter of 0.381 mm and a length of 120 mm, and was fitted in horizontal condition. They used alumina (Al_2O_3), zirconia (ZrO_2) and silica (SiO_2) nanoparticles in water. They worked on less concentrated nanofluids with volume concentrations of 0.001%, 0.01% and 0.1% for each type of nanoparticle. They observed glowing of the wire and the sudden change in the electrical resistance, defined as CHF. Compared to water, CHF increased for all concentrations and all types of nanofluids. The increase in CHF was between 11.5% and 52% for 0.001% (v/v), between 15% and 75% for 0.01% (v/v), and between 20% and 80% for 0.1% (v/v) concentration of nanoparticles.

Liu et al. (2007) presented experimental study on pool boiling heat transfer characteristics for Al_2O_3/water nanofluids using four different volume concentrations. The pool boiling heat transfer coefficients of nanofluids was measured on a flat surface. These were compared with the heat transfer coefficient of pure water. They found that the addition of alumina nanoparticles caused a decrease in the nucleate pool boiling heat transfer coefficient. A flow pattern characterized by a vapor mushroom in high heat flux boiling phenomena was observed in both pure water and nanofluids. They concluded that the number of active nucleation sites reduced with concentration of nanoparticles. They found that the pool boiling heat transfer is also affected by change in surface roughness. It was found that the change in roughness caused a kind of fouling effect with poor thermal conduction in single phase heat transfer.

Milanova and Kumar (2008) investigated the pool boiling for SiO_2-water nanofluids and salty water. It was found that Critical Heat Flux (CHF) was increased by 50% with no nanoparticle deposition on the wire. The CHF was enhanced by three times when salty water was used.

Trisaksri and Wongwises (2009) studied the pool boiling behaviour for Cu nanoparticles and TiO_2 nanoparticles in refrigerant R-141b on a cylindrical tube. They found that the boiling heat transfer performance deteriorated with an increase in nanoparticle's concentration in both the fluids. But there was no effect on heat transfer coefficient at concentrations lower than 0.01% (v/v) for both nanofluids.

Suriyawong and Wongwises (2010) investigated the heat transfer characteristics for nucleate pool boiling of TiO_2-water nanofluids on Cu and Al plates for two surface roughnesses (0.2 and 4 μm). Concentration of nanoparticles in water was very low, i.e. 0.00005%, 0.0001%, 0.0005%, 0.005%, and 0.01% (v/v). They found that for copper plate with nanofluid's concentrations more than 0.0001%, the heat transfer coefficient was less than that for the base fluid for both surface roughnesses. They reported that for copper at low nanoparticle concentrations boiling heat transfer coefficient increased by 15% for 0.2 μm and by 4% for 4 μm roughness. However, for aluminium surfaces the heat transfer coefficient was found less than that for the base fluid for all the concentrations of nanofluids and surface roughness.

Ahn et al. (2010) performed pool boiling experiments with water at saturated conditions using the zircaloy plates with different topography and wettability. In their study, the boiling heat transfer curves for all the samples were almost identical. However, CHF was higher for the treated samples in comparison to that for the original samples. With decreasing contact angle CHF increased and reached significantly higher values for contact angles below 10°.

Kwark et al. (2010) investigated CHF and pool boiling heat transfer performance on Cu plate for Al_2O_3, CuO and diamond nanoparticles suspended in water. They found that HTC increases with increase in nanoparticle concentration, until CHF is obtained. They also reported that BHT coefficient and CHF remains unchanged after repeated testing.

Heris (2011) investigated pool boiling heat transfer characteristics of CuO/ethylene glycol–water (60/40) nanofluids because he considered that the mixtures of ethylene glycol and water are the most common water-based

antifreeze solutions used in automotive cooling systems. He found considerable increase in heat transfer coefficient with the addition of nanoparticles and increases by up to 55% for 0.5% (v/v) mixture of ethylene glycol and water.

Bolukbasi and Ciloglu (2011) studied pool boiling heat transfer characteristics of vertical cylinder rod quenched by SiO_2-water nanofluids at saturated temperature and atmospheric pressure. Pure water and SiO_2-water nanofluids suspensions at four different concentrations (0.001, 0.01, 0.05 and 0.1% v/v) were selected as the coolants. The test specimen heated at high temperatures was plunged in the cooling fluids at saturated conditions. They found that the pool film boiling heat transfer in nanofluids was identical to that for pure water. Though, by repeating the tests with nanofluids of higher concentrations, the film boiling region disappears and the critical heat flux increases. They also found that the nucleate pool boiling heat transfer coefficient decreased compared to that for the pure water, but a considerable decrease in nucleate pool boiling heat transfer was not observed with re-tests. They also found change in surface characteristics due to the deposition of nanoparticles on the surface, which was considered to be an effect of the quenching process.

Kole and Dey (2012) investigated pool boiling heat transfer and critical heat flux for ZnO-ethylene glycol nanofluids at atmospheric pressure on cylindrical polished copper heater surface. Surfactant free and fairly stable ZnO-ethylene glycol (EG) nanofluids were prepared using prolonged sonication (>60 h). They found that the thermal conductivity of the nanofluid increases up to a maximum of 40% for 3.75% volume fractions of ZnO loading in EG at 30°C. They also found that the boiling heat transfer coefficient increases with increase in ZnO concentration, maximum by 22% as compared to that for the base fluid at 1.6% volume fraction of ZnO. However, further mixing of ZnO nanoparticles in EG decreased the heat transfer coefficient. They also measured CHF on a thin Constantan wire and found that the CHF value increased appreciably with increase in ZnO concentration and displayed a maximum increase of about 117% for the nanofluid containing 2.6% (v/v) of ZnO.

Raveshi et al. (2013) investigated nucleate boiling heat transfer of alumina-water-ethylene glycol (AWEG) nanofluids (up to 1% v/v concentration of

alumina) in water and ethylene glycol in same quantity (WEG50) under atmospheric pressure. They found that the effect of concentration of nanoparticles on heat transfer coefficient was high and the maximum increase in boiling heat transfer coefficient was 64% at 0.75% (v/v) AWEG nanofluid. They considered that in low concentration, the deposited layer was very thin, which modifies the heat transfer surface by multiplying the nucleate site creating cavities that are active, and finally leading to increase in boiling heat transfer. They also reported thicker deposited layer at the end of testing because of the higher concentration of the nanoparticles. Therefore, the nucleation cavities are blocked and an optimum volume concentration for the boiling HTC was observed. The results show the high effectiveness of the nanoparticles on heat transfer coefficient. In addition, the experimental results indicate that there is an optimum volume concentration of nanoparticles, in which the heat transfer coefficient has its maximum value. Furthermore, the optimum observed volume concentration of nanoparticle and the maximum increment of boiling heat transfer coefficient in the study were 0.75% and 64% respectively.

Jung et al. (2013) studied the critical heat flux and pool boiling heat transfer coefficient of binary nanofluids (Al_2O_3-H_2O/LiBr-based binary) on a copper plate heater (10 x 10 mm^2) using the polyvinyl alcohol (PVA) as a stabilizer. Concentration of nanoparticle varied up to 0.1% (v/v) in H_2O/LiBr solutions having 3, 7 and 10% (w/w) of LiBr. They found that the Al_2O_3 nanoparticles could be stably dispersed in H_2O/LiBr. They also found that boiling heat transfer coefficient of the binary nanofluids was lower than that of the base fluid. They reported that the CHF increased with increase in concentration of nanoparticles. They obtained about 48.5% increase in CHF as compared to the base fluid with 0.1% (v/v) of Al_2O_3 in 10% (w/w) of LiBr aqueous solution.

Shahmoradi et al. (2013) investigated pool boiling characteristics of Al_2O_3 based nanofluid {< 0.1% (v/v)} on a flat plate heater surface. They found that the heat transfer coefficient of the nanofluid reduces while critical heat flux (CHF) increases and the rate of increase in CHF increased with increase in volume fraction of nanoparticles. They observed that after the boiling, the surface roughness increases or decreases depending on the initial condition of the heater

surface. They also found that surface topology changes from natural convection boiling to nucleate boiling regime and near CHF. They observed that a porous layer of nanoparticles is formed on boiling surface via boiling of nanofluids, which increases the surface wettability and CHF.

Tang et al. (2014) investigated the pool boiling heat transfer characteristics of γ-Al_2O_3-R141b nanofluids on a horizontal flat square copper surface at 10–200 kW/m^2 heat flux under atmospheric pressure. Before boiling, they maintained surface roughness by using a sandpaper of grade P2000. They prepared nanofluids by suspending γ-Al_2O_3 nanoparticles in refrigerant (R141b) for 0.001%, 0.01% and 0.1% (v/v) concentrations, with and without surfactant sodium dodecyl benzene sulphonate (SDBS).

They observed that the suspended γ-Al_2O_3 nanoparticles enhance the pool boiling heat transfer characteristics for R141b at concentrations of 0.001% and 0.01% (v/v) with and without the surfactant SDBS.

However, the γ-Al_2O_3 nanoparticles deteriorate the pool boiling heat transfer characteristics at 0.1% (v/v) concentration without the surfactant SDBS due to deposition of large number of nanoparticles. When the particle concentration is 0.001% (v/v), increase in boiling heat transfer coefficient decreased with the addition of SDBS and when the particle concentrations are 0.01% and 0.1% (v/v), the increase in boiling heat transfer coefficient increased with the addition of SDBS.

2.3.2 Flow boiling heat transfer

Research in flow boiling heat transfer for nanofluids has become more popular in the past five years because of the recent interest in cooling of nuclear reactors, microelectronics, space components and other compact cooling process.

Mudawar and Anderson (1990) worked on effect of pressure on heat transfer coefficient of water during flow boiling. They reported that nucleate boiling heat transfer increases with increase in pressure and thus critical heat flux also increases.

Chun et al. (2001) performed CHF experiments in an annular test section for a wide range of pressure from 570 to 15010 kPa (5.7-150.1 bar). The mass flux was varied from 200 to 650 kg/m^{2}s and the inlet sub cooling from 85 to 413 kJ/kg. CHF occurrence was detected by continuous temperature increase at one of the embedded thermocouples on the outer surface of the heated tube. CHF always occurred at the top end of the heated section. The authors reported that the CHF increased with pressure, reached a maximum in pressure range of 2000-3000 kPa (20-30 bar), and then decreased with further increase in pressure. However, this effect was particularly observed for CHF at higher mass fluxes (500-650 kg/m^{2}s) and high sub cooling. For the lower mass fluxes 200-500 kg/m^{2}s, increase in the low pressure region was not observed. It was also observed that the vapor mass quality at the CHF depends on pressure. For a low mass flux of 200 kg/m^{2}s the vapor mass quality increased continuously from about 0.2 at 570 kPa to 0.4 at 15010 kPa whereas the vapor mass quality for the high mass flux of 650 kg/m^{2}s remained almost constant between 0.1 and 0.2 over the complete range of pressure.

Qu et al. (2003) reported an experimental study on convective boiling heat transfer of copper/water nanofluids and de-ionized water flowing in vertical micro-channels. They investigated the local heat transfer coefficients and surface temperature for very small nanoparticles concentration. For Cu/water nanofluid, they reported higher local heat transfer coefficient, higher local heat flux, higher pressure drop and lower surface temperature than its base fluid at the same mass flux. The results were somewhat contrary to some previous results obtained on pool boiling heat transfer where the addition of the nanoparticles into the base fluids did not enhance the heat transfer and caused no significant improvement in pressure drop.

Lee and Mudawar (2007) studied the behaviour of alumina (Al_2O_3) nanoparticles in water for micro-channel cooling applications. They found that there was increase in heat transfer coefficient for single phase laminar flow. In the two-phase regime, the nanofluids caused surface deposition in the micro-channels and large clusters of nanoparticles were formed. There was no increase in heat transfer coefficient of the base fluid in two-phase flow at low volume

concentrations of nanoparticles (less than 2%). They assumed that comparatively higher than 2% volume concentrations of nanoparticles were required to alter the heat transfer coefficient of the base fluid.

Liu et al. (2007) investigated the effect of pressure and heat flux on flow boiling of refrigerant R-134a in a narrow vertical duct. They also studied the bubble characteristics of the refrigerant. Refrigerant R-134a was used as the test fluid at different pressures (ranging from 690 to 827 kPa) and different heat fluxes to quantify their influence in bubble characteristics such as bubble nucleation, growth, departure and coalescence. They used two synchronized high resolution and high-speed cameras which capture thermo-chromic liquid crystal (TLC) images and bubbling activities at high frame rates. By altering flow rate and system pressure, the TLC images and bubble images were captured and analyzed. The results showed that the bubble generation frequency and size increased with heat flux. An increase in pressure from 690 to 827 kPa increased the bubble frequency and size to about 32 Hz and 20 mm respectively.

Park et al. (2007) measured the heat transfer coefficient for flow boiling of R22 and water, with and without 1.0% (v/v) of carbon nanotubes. They reported that heat transfer coefficient increases with addition of CNTs. A large increase up to 28.7% was observed when heat fluxes were lower than 30 kW/m^2. However, when the heat flux was increased, the increase in heat transfer was suppressed due to vigorous bubble generation.

Park and Jung (2007) experimentally investigated the flow characteristics of the aqueous suspensions of carbon nanotubes (CNT's). For the pressure drop measurements, stable nanotubes suspensions were made by two different methods. The first method was dispersing nanotubes using a surfactant and the second method was by introducing oxygen-containing functional groups on the CNT surfaces by acid treatment. Pressure drop in the horizontal tube and the viscosity of the nanofluids were measured and the effects of CNT loading and different preparation methods were investigated. Viscosity measurements show that the nanofluids prepared by the acid treatment had much lesser viscosity than the other one (the one made using a surfactant). The nanofluids prepared by the acid treatment have much lesser viscosity than the ones made using surfactant. Under

laminar flow conditions, the friction factor of CNT nanofluids stabilized by adding surfactant is much higher than that for the one made using surfactant, and both nanofluids show higher friction factors than that for distilled water. In contrast to this, under turbulent flow conditions, the friction factor for both the nanofluids was similar to that of the base fluids.

Peng et al. (2007) investigated the influence of nanoparticles on the heat transfer characteristics of a refrigerant-based nanofluid for flow boiling inside a horizontal smooth tube. R113 refrigerant and CuO nanoparticles were used for preparing the refrigerant-based nanofluid. The experimental results show that the heat transfer coefficient of refrigerant-based nanofluid was higher than that for the pure refrigerant and the maximum increase in heat transfer coefficient was 29.7%.

Later, Peng et al. (2009) investigated the effect of increase in concentration of nanoparticles on the frictional pressure drop of refrigerant-based nanofluid and studied it for flow boiling inside a horizontal smooth tube. They presented a correlation for predicting the frictional pressure drop of refrigerant-based nanofluid. They used R113 refrigerant and CuO nanoparticle for preparing refrigerant based nanofluids. They measured the frictional pressure drop for variable mass fluxes from 100 to 200 kg/m^2s, heat fluxes from 3.08 to 6.16 kW/m^2, inlet vapor qualities from 0.2 to 0.7 and mass fractions of nanoparticles from 0 to 0.5% (w/w) in R113. They concluded that the frictional pressure drop of refrigerant-based nanofluid increases with the increase of the mass fraction of nanoparticles, and under variable parameters, the maximum increase in frictional pressure drop was 20.8%. A frictional pressure drop correlation for refrigerant based nanofluid was also proposed, which predicted 92% of the experimental data within the deviation of ±15%.

Kuo et al. (2009) studied the effect of pressure on flow boiling instabilities in micro-channels using water in 223 μm hydraulic diameter micro-channels with pressures ranging from 50 to 205 kPa and mass fluxes ranging from 86 to 520 kg/m^2s. The onset of flow oscillation, critical heat flux (CHF) conditions, local transient temperature measurements and flow boiling visualization were studied. It was observed that system pressure significantly affects flow instabilities and that for high pressures, boiling instabilities were significantly delayed. It was also

observed that the CHF increased with increase in mass flux. Local temperature measurements also revealed lower magnitudes and higher frequencies of oscillations at high system pressure.

Ahn et al. (2010) investigated aqueous nanofluids with a 0.01% concentration of alumina nanoparticles. They found distinct increase in CHF due to forced convective flow conditions compared to that for the pure water. They conducted experiments with varying flow velocities, starting from 0 m/s (pool boiling) to 4 m/s. A 50% increase in CHF was found at 0 m/s, which was consistent with the result, obtained by previous researchers Bang and Chang (2005). They used a scanning electron microscope (SEM) to examine the heater surfaces after the boiling. The contact angle was also measured. They found that the increase in CHF was mainly due to nanoparticle deposition on the heater surface during vigorous boiling. The contact angle decreased with deposition of nanoparticles. They compared the contact angles for a water droplet on the bare surface, water-boiled surface at 3 m/s and Al_2O_3-water nanofluid boiled surfaces with no flow condition. The measured contact angles were 75°, 65° and 12° on the bare surface, water-boiled and Al_2O_3-water nanofluid boiled surfaces respectively. They concluded that the nanoparticle deposited surface have less contact angle which led to significant increase in the wettability of the heater surface.

Henderson et al. (2010) investigated flow boiling heat transfer characteristics of R-134a/POE/CuO nanofluids in a horizontal tube. Test results, at one particle volume fraction of 0.02% showed little effect on the heat transfer coefficient when compared to R-134a/POE mixture. For a 0.04% CuO volume fraction the average heat transfer increased by 52% and with a 0.08% nanoparticle volume fraction, average heat transfer increased by 76%.

Another investigation by Kim et al. (2010a) resulted in a similar deposition on the heater surface after the boiling. They examined subcooled flow boiling using dilute alumina, zinc oxide and diamond water-based nanofluids. They measured both, CHF and heat transfer coefficient during the flow boiling. They found that CHF increased with both mass flux and nanoparticle concentration for all the nanoparticle materials. An increase of up to 53% was observed for CHF. They reported that heat transfer coefficient did not increase for the nanofluids at

low heat fluxes, but a slight increase was seen at higher heat fluxes. As Ahn et al. (2010), they also observed that the nanoparticle deposition on the heater is one of the main contributors for increase in CHF. As to how this nanoparticle deposition can affect heat transfer coefficient, they said: firstly, the deposition of nanoparticles changes the number of micro-cavities on the surface, and secondly the surface wettability is also changed.

They measured the number of micro-cavities on the surface and the contact angle of the fluid on the surface, and hence obtained an estimation of the nucleation site density at the heater surface. However, irrespective of increase or decrease in nucleation site density, heat transfer coefficient remained largely unchanged. They suggested that there must be other mechanisms offsetting the increase in nucleation site density, possibly changes in the bubble departure diameter and/or bubble departure frequency.

K.H. Bang et al. (2011) investigated the effect of pressure on flow boiling heat transfer coefficient for water in mini-channels made up of 1.73 mm inner diameter round tubes. Experimental data for two specific values, 2 bar and 16 bar, were compared. They reported that flow boiling heat transfer coefficient increased with increase in vapor quality, and was in the range of 10,000-35,000 W/m^2K. It was also reported that pressure does not alter heat transfer coefficient significantly. They also stated that the slug flow pattern seemed to be dominant at low vapor quality and heat transfer coefficient was slightly higher at the higher pressures. However, their results have large discrepancies when compared with the existing correlations, implying that these correlations did not correctly account for the variations in pressure.

Lee et al. (2014) investigated the effects of two-phase flow conditions on flow boiling CHF for magnetite-water nanofluids for a wide range of vapour quality at the exit, especially for intermediate and high vapour quality at the exit. They observed that the CHF increased with increase in vapour quality at the exit. They also observed departure from Nucleate Boiling (DNB) like thermal crisis with increase in vapour quality at exit. Their results were consistent with the previous studies reporting delay in DNB when using nanofluids at low vapour quality at exit. Meanwhile, increase in the CHF was not reported for high vapour

quality at the exit. They found that a liquid film dry-out (LFD) type thermal crisis occurred in annular flow using high vapour quality at the exit. This CHF increment was not expected when using a nanofluid under the LFD condition because LFD phenomena is almost unaffected by the surface conditions. As the vapour quality at the exit increased from 0.07 to 0.74, the amount of increase in CHF gradually decreased to zero.

2.4 Visualization of Boiling

The visualization studies are important for nanofluids because it can help to understand the boiling phenomena. It can be used to understand the phenomenon of bubble generation, bubble grow, bubble departure and bubble flow.

Flow visualization studies on nanofluids couldn't be found in the literature. However, studies on bubble parameters and bubble behavior for conventional fluids have been reviewed in the following section.

Gunther et al. (1951) was the first person who studied bubble behavior during flow boiling using high speed visualization techniques. He determined bubble size, bubble lifetime, bubble growth rate and other parameters as functions of system parameters like pressure, amount of sub cooling and bubble velocity. They reported that bubbles were small hemispheres which grow and collapse while sliding along the wall. In their study, bubble size and bubble life time decreased with increase in bubble velocity, sub cooling and heat flux. They also reported that bubble population increased rapidly with increase in heat flux as burnout approached.

Abdelmessiah et al. (1972) used high speed visualization techniques to observe the effect of velocity of the fluid on bubble growth and collapse from an artificial nucleation site and found that an increase in velocity of the fluid resulted in decrease in bubble size and bubble life time. They also reported that the bubble size increased with the increase in heat flux, which was contradictory to Gunther's results.

Akiyama and Tachibana (1974) investigated the bubble growth and collapse mechanism, for water flowing upward through a vertical annulus with inner heating at atmospheric pressure. They found that heat transfer coefficient for the sliding bubbles could be modeled as a rough surface heat transfer problem, where diameter of bubbles is treated as the characteristic length. The heat transfer mechanism in fully developed nucleate boiling was assumed to be dominated by the ejection of bubbles agitating the subcooled liquid and the thermal layer.

Valle and Kenning (1985) investigated the effect of heat flux on bubble size, life span and bubble frequency on the nucleation sites of a stainless steel plate. Contrary to the Gunther's observations, they found that bubbles collapsed on their nucleation sites without sliding along the wall. They also observed that bubble size, life span and bubbles frequency increased with increase in heat flux at the nucleation sites. However the life span increased at low heat fluxes, got saturated and decreased further with increase in high heat fluxes. They also reported that heat transfer occurs primarily by bubble induced quenching of the wall by cold liquid.

Bibeau and Salcudean (1991) investigated the effect of upward and downward flow in a vertical rectangular narrow channel on subcooled void fraction. They used water as the working fluid. They varied the system pressure from 0.1 to 1.0 MPa, sub cooling from 20 to 36 K and heat flux from 50 to 348 kW/m^2. Bubble behavior under different working conditions were recorded by a high speed camera at a speed of 10,000 fps (frame per second). They found that the system pressure has a significant effect on the bubble growth and the bubble detachment. At lower pressure, bubbles grow up at nucleate sites and then collapse without sliding. However, at higher pressure, bubbles keep growing without collapsing as they slide along the heating wall. They assumed that the growth rate of sliding bubble affects the sliding velocity of bubble and distance between corresponding bubbles ahead. They observed that at the beginning of bubbles, bubble sliding velocity was lower than the bulk fluid velocity.

Zeitoun and Shoukri (1996) studied the effect of departure of bubbles on the phenomenon of net vapour generation (NVG). They observed that there was no effect of departure of bubbles on the phenomenon of net vapour generation

(NVG). They reported that increase in bubble size is due to decrease in condensation and that bubble coalescence was the main reason for significant increase in void fraction along the length of the channel. They found that bubble growth-collapse cycle was similar for the parallel and the normal flow after the detachment of bubbles in subcooled flow boiling regions. The bubble size and bubble life increased as sub cooling decreased.

Kandlikar and Spiesman (1997) performed visualization studies using a hydrophilic heated surface. Filtered and de-ionized water was used as the working fluid and the flow direction was vertically upward. Observation of the bubble behavior at the onset of nucleate boiling (ONB) revealed that at elevated pressures, bubbles slide along the heated surface after they leave the nucleation site under the influence of the shear-induced lift forces. At low pressures (close to the atmospheric pressure) they were lifted off the vertical heated surface immediately after nucleation and collapsed in the subcooled liquid due to condensation. Consequently, bubble life-time at ONB was remarkably shorter in the low pressure experiments. It was discussed that the lift-off limit can be expressed in terms of the Jakob number since the distinct difference in the bubble behavior is mainly caused by the bubble growth rate after the nucleation.

Similarly, Thome et al. (1998) conducted experiments to explore the important mechanisms causing net vapour generation (NVG) in subcooled flow boiling under elevated pressure conditions. It was found that at low pressures, all the bubbles collapsed in the subcooled bulk at onset of nucleate boiling (ONB) but some bubbles reattached to the heated surface when sub cooling was low enough. Since the bubbles slide along the heated surface for a long distance after reattachment, the bubble life-time was significantly higher and consequently, the vaporization rate was noticeably greater than the condensation rate.

It was concluded that the bubble reattachment to the heated surface is a key phenomenon that causes NVG at low pressures. Under the moderate pressure conditions, however, it was believed that different mechanisms are responsible for the onset of NVG since the bubbles are not lifted off the surface even at ONB. The mechanisms of NVG at elevated pressures are obviously of great importance from

the engineering standpoint since most power plants are operated in high pressure conditions.

Thorncroft et al. (1998) investigated bubble growth and bubble departure in vertical up-flow and down-flow conditions in a 12.7 mm square duct, which was 30 cm long and had a ni-chrome heater strip attached to one side of the test section. They used FC-87, a perfluorocarbon fluid at velocities ranging from 0.11 to 0.38 m/s, liquid sub cooling ranging from 1°C to 5°C and wall superheat ranging up to 7°C. In up-flow bubbles remained attached to heating surface assuming a cap like shape. Nucleation site density increased with heat flux. However, in down-flow they observed three regimes of bubble detachment. At velocities around 0.11 m/s, the bubbles departed in upward direction against the bulk fluid velocity. At slightly higher velocities around 0.18 m/s, bubbles lifted off directly above the nucleation sites without sliding. At still higher velocities, around 0.38 m/s, the bubbles slid downwards but the sliding distance was not as long as that in the up-flow. Lift off was very regular and heat transfer coefficient was calculated to be lower than that in the up-flow. They attributed higher heat transfer in up-flow conditions to vapor bubble sliding.

Klausner (2000) studied the vapour bubble departure in a 25 x 25 mm^2 horizontal test section which had a ni-chrome heater surface that was 457 mm long. They conducted experiments with R-113, with flow velocities up to 1 m/s and wall superheat ranging from 10°C to 21°C. They found upstream and downstream contact angles to be around 45° and 36° respectively for a typical bubble. They concluded that surface tension alone is not able to stop vapor bubble departure. They reported that the liquid drag acts opposite to the direction of the liquid flow and plays an important role in holding the bubble to its nucleation site prior to its departure.

Prodanovic et al. (2002) conducted experiments on flow boiling in a vertical tube which was heated on the inside. Through photographic studies they identified three separate regions between ONB (Onset of Nucleate Boiling) and OSV (Onset of Significant Void) with respect to heat flux. The regions were low heat flux region, isolated bubble region and region of significant coalescence. Bubble behavior varies from one region to another. They also varied pressure

from 1 to 3 bar and found that pressure affects bubble behavior significantly. They reported that bubble diameter decreases with the increase in pressure.

Chang et al. (2002) performed visualization studies at atmospheric pressure in a vertical rectangular channel and observed that the number of near-wall bubbles increased with the increase in heat flux. At sufficiently high heat fluxes, they observed three characteristic layers in the heated channel. The three layers were: (a) a superheated liquid layer with small bubbles attached on the heated wall, (b) a flowing bubble layer consisting of large coalesced bubbles over the superheated liquid layer, and (c) the liquid core over the flowing bubble layer. In addition, the existence of a liquid sub-layer under coalesced bubbles was identified photographically. They used high speed video cameras as well as digital cameras for recording the near wall bubble phenomenon. They opined that formation of large vapour clots resulting from coalescence of bubbles and evaporation of superheated liquid layer beneath the vapour clots might be the reason for CHF, because cooling is not possible beneath the vapour clots at high heat fluxes.

Shedd and Rodriguez (2004) used backlight imaging technique to obtain images of bubbles within the liquid film of adiabatic air-water horizontal annular flow. The bubble statistics concluded that the bubble size distribution within the liquid film increased exponentially. The parameters of the distribution were observed to be dependent on the air flow rate and essentially independent of the liquid flow rate. The bubble data, together with fluorescent imaging of waves on the liquid film, indicated that gas entrainment in the film was primarily controlled by air flow rate and wave behaviour. This was confirmed by the existence of a consistent Weber number based on the maximum observed bubble diameter and disturbance wave velocity.

Situ et al. (2004) conducted subcooled flow boiling experiments in a vertical annulus and studied the phenomenon with high speed videography. A high-speed digital video camera (5000 fps) was used to record the dynamics of the subcooled ebullition process. The video images were compared which defines that the bubble waiting period depends on nucleus cavities and different experimental conditions, while the bubble growth period is relatively stable and short, i.e., less

than 3 ms. They reported that the bubble departure frequency increases as heat flux increases. Bubble coalescence occurred at the nucleation site when the bubble frequency was higher than 500 bubbles/s. They also found that, for some cases, the departure frequency reaches asymptotically up to 1000 bubbles/s.

By using three different methods, Soria et al. (2005) measured the volume and the equivalent radius of air bubbles at detachment from the tip of different capillary tubes in quiescent water. The intention was to provide an accurate cross-calibration of two of the methods against a standard laboratory method. The inverted funnel method is a laboratory standard and was performed within a 0.5% repeatability error for 50 bubble sets. The passive acoustic method was performed with an accuracy of 97% to 99% with respect to the inverted funnel method. The photographic method gave accuracy of 88% to 96%. After improvement of the photographic method by an empirical cutting edge criterion, its accuracy was raised from 95% to 99%.

Maurus and Sattelmayer (2006) conducted experiments in subcooled flow boiling of water circulating in a closed loop at atmospheric pressure. The horizontally oriented test-section consisted of a rectangular channel with a copper strip heated on one side and good optical access. Various optical observation techniques were used to study the bubble behavior and the characteristics of the fluid phase. The bubble behavior was recorded by high-speed cinematography and by a digital high resolution camera. Automated image processing and analysis algorithms developed by the authors were applied for a wide range of mass flow rates and heat fluxes in order to extract characteristic length and time scales of the bubbly layer during the boiling process. Using this methodology, the bubble size, the bubble lifetime, the time of generation of new bubble at the same nucleation site were studied. They reported that the void fraction increases with increase in heat flux and decreases with the mass flux. They also reported that bubble spacing increases with increase in mass flux and decrease in heat flux.

Celata et al. (2007) conducted visualization experiments in a vertically oriented square duct and observed the heater burnout. Distilled water was used as the working fluid with velocity varying from 3 to 10 m/s, pressure varying from 5 to 30 bar and with sub cooling of 10 to 30° C. High speed videos of the flow

pattern in the subcooled flow boiling of water from the onset of nucleate boiling up to physical burnout of the heater were recorded. They analyzed the video and discerned that, when the rate of bubble generation is increasing with bubbles growing in the superheated layer close to the heating wall, their coalescence produces a type of elongated bubble called vapour blanket. Various bubble parameters were measured by using image processing. It was found that bubble size was a function of pressure and velocity of the fluid. Bubble size increases with increase in heat flux and decreases with the increase in the degree of sub cooling, pressure and velocity. It was also observed that surface finish of heater was one of the important parameters which affect CHF. The bubbles were larger for a surface with greater number of cavities. Smoother wire exhibited premature burnout with respect to the normal wire due to drastic reduction of bubbles generation at the wall. A threaded wire shows premature burnout with respect to the normal wire.

Mudawar et al. (2007) conducted flow boiling experiments in a channel with FC-72 as the working fluid. Fluid velocity varied from 0.5 to 1.2 m/s at 20°C to 40°C sub cooling. They found that CHF increases monotonically with increase in velocity and sub cooling. High speed video imaging revealed the sequence of events leading to CHF. The study of these events was helpful in explaining the CHF. While some bubbles detached from the wall and entrained in the bulk liquid flow, the most of the vapours remains in close proximity to the wall, especially at high flow velocities. Bubbles first slide along the heated wall and then coalesce with other bubbles to form elongated vapour bubbles (vapour patches). These elongated vapour bubbles (vapour patches) propagate along the heated wall and grow in size.

As a result cooling of heating surface is retarded leading to CHF. Just before CHF, the series of vapour patches form a fairly continuous vapour layer that permits liquid contact with the heated wall only in the wave troughs and wetting fronts between the vapour patches. At CHF, these wetting fronts vanish from the heating surface. These findings prove that the CHF mechanism for subcooled flow boiling is identical to the interfacial lift-off mechanism proposed previously for saturated flow boiling.

Vasiliev et al. (2009) reported experimental investigations of a transparent flat mini evaporator heated by a laser beam. The influence of non-absorbing and absorbing nanoparticles immersed in pure water and heat absorbing fluid on heat transfer intensification were studied. They found that nanoparticles may initiate vaporization and boiling of fluid at low heat input. For specific tasks and conditions, the nanoparticles may work in passive or active modes. They assumed that in passive mode, nanoparticles do not generate thermal energy and improve bubble nucleation conditions due to additional nucleation of the fluid, thus decreasing boiling/vaporization temperature thresholds. In active mode, nanoparticles convert optical energy into thermal energy and decrease boiling energy threshold by 10–100 times relative to that of the pure fluid. In both the modes actual thresholds depend upon the size and concentration of the nanoparticles.

2.5 Summary of literature review and scope for present work

The thermal conductivity of many base fluids were reviewed and studied broadly and it was found to be increase with the addition of nanoparticles in the base fluids. Substantial work has been carried out on different methods of preparation of nanofluids but limited data is available on sonication method and the effect of sonication time on thermal conductivity. There were discrepancies in the findings of some of the researchers. For example, one researcher claims that 50 minutes sonication is adequate while others report that 3 to 6 hours are required for the same. This means that a more focused research on sonication is needed.

Several researchers have carried out extensive work on convective heat transfer for nanofluids in last ten years. They established that principle factors influencing the heat transfer characteristics of the nanofluids in the convective flow are:

1. The type of nanoparticles,
2. The concentration of nanoparticles in the nanofluid,
3. The heat flux and
4. The topology of the heating surface.

It is reported that the convective boiling heat transfer has immense potential in enhancing the critical heat flux (CHF). However, reported data on heat transfer coefficients are contradictory. Thus, more experiments are required to establish the most effective convective heat transfer coefficient value for the selected nanofluids.

Relatively less work has been done on flow boiling heat transfer characteristics of the nanofluids. But considering the desperate demand by today's thermal process industries to reduce operational cost and provide better system component protection, more meaningful research is called for. This demands research on the influence of pressure, types of nanoparticles, concentration of nanoparticles and heat flux on flow boiling heat transfer coefficient.

Currently, there is no universal mechanism which explains the hydrodynamic behaviour of the bubbles in flow boiling heat transfer process. This research gap essentially calls for modern flow pattern analysis techniques such as finite element fluid dynamic analysis, visualization techniques, etc. The mechanism of flow boiling heat transfer in practice may be better explained on basis of the hydrodynamic behaviour of the bubbles. In the present work, the bubbles behaviour has been investigated by using high speed visualization techniques.

Themes discussed in this chapter highlight the interesting and often, contradictory nature of the effects of the flow parameters on boiling heat transfer in nanofluids. The work on flow boiling heat transfer of nanofluids is scarce and literature on visualization study of bubble behavior for nanofluids is not available. Hence, the present work attempts to fill the study heat transfer in nanofluids by studying the effect of principle parameters like pressure, concentration and heat flux.

3.

EXPERIMENTAL FACILITY

This Chapter describes the experimental setup, gives details of the instruments used and the experimental procedure. The fabrication and commissioning of the test section and various devices used in setup have also been discussed.

The existing test facility at Malaviya National Institute of Technology (MNIT), Jaipur, India which was designed and fabricated under the sponsorship of Indian Space Research Organization (ISRO), India, has been redesigned for the present research work. The main modifications made in the existing experimental setup are:

- The filter which was earlier placed between the pump and the flow meter has been removed to avoid loss of nanoparticles.
- The old rusted piping has been replaced with smooth stainless steel (SS) pipes in the primary loop that would have caused scaling and rust problem.
- The extra length of the connecting copper rod of the test section has been reduced to minimize the heat loss.
- An ultrasonic vibration machine (UVM) has been added to prepare nanofluids.

The schematic diagram of the experimental setup is shown in Fig. 3.1. The closed loop test facility consists of a 10 liter storage reservoir, a circulating pump, a flow meter, an electrically heated horizontal annular test section, a condenser and a heat exchanger. The working fluid was prepared in the UVM and stored in the reservoir from where it was pumped to the test section through a flow meter. The fluid was boiled in the test section by an electrical heater made up of SS rod. The mixture of the steam and the fluid were passed through a condenser and a heat exchanger before returning it to the storage reservoir.

3.1 Development of the Test Section

Most of the boiling applications in the industries make use of stainless steels. Therefore, the heating element in the test section was made of stainless steel. The test section was covered with a borosilicate glass tube to facilitate flow visualization.

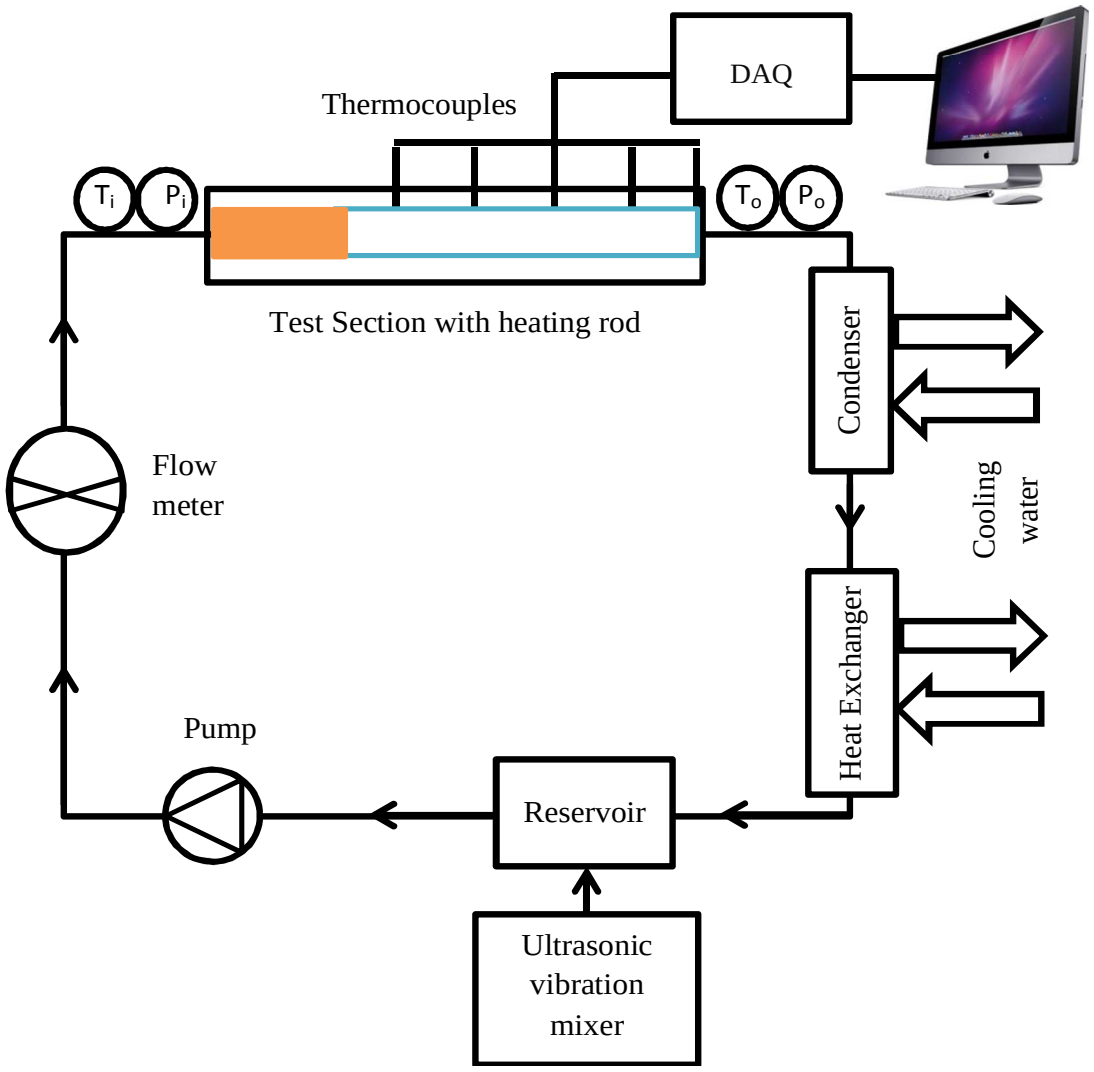

Figure 3.1. Schematic of Experimental Setup.

3.1.1 Test Section Design

The test section consists of a horizontal heat exchanger mounted on a concrete platform. The test section is 780 mm long. The annulus through which fluid flows, consists of an electrically heated SS pipe mounted inside the borosilicate glass tube. DC current was supplied through copper leads to heat the SS rod. The heated length of 500 mm is located as per design consideration of Thome et al. (2004), which is located at 230 mm downstream of the inlet plenum, thus allowing the flow to develop fully. The test section is shown in Fig. 3.2. The photograph of test section is shown in Fig. 3.3.

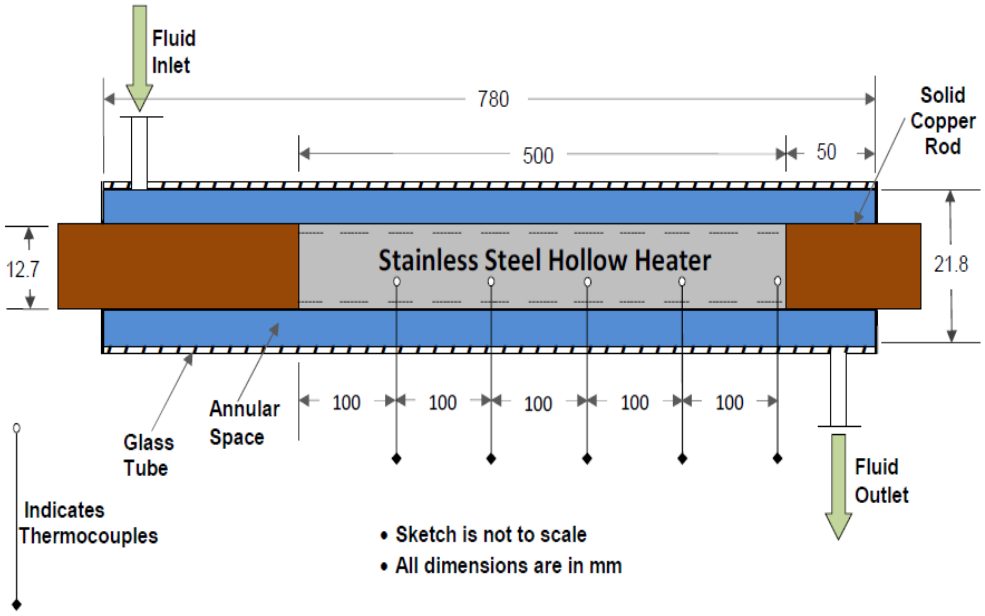

Figure 3.2. Test Section.

The specifications of the test section are given in Appendix A.

Figure 3.3. Photograph of the test section.

A heat exchanger is provided between the condenser and SS storage reservoir in order to bring down the temperature of the working fluid. The mixture of the working fluid and the steam from the exit of the test section enter the horizontal condenser where steam is condensed. The condenser and heat exchanger are made of SS tubes.

3.1.2 Fabrication of Test Section

The test section was fabricated by assembling SS pipe, solid copper rod, the borosilicate glass tube and the Teflon cork. Following steps were performed in sequence to assemble the test section.

1. The required length of SS pipe (SS310) (500 mm length, 12.7 mm outer diameter and 1 mm thickness) was cut off.
2. Two copper pieces of diameter (12.7 mm) were cut to desired lengths of 355 mm and 175 mm for inlet and outlet connections respectively.
3. 25 mm of the longer copper bar having a length of 355 mm was inserted into the SS pipe at the inlet side after reducing its diameter to 11.7 mm.
4. Again 25 mm of the longer copper bar having a length of 175 mm was inserted into the SS pipe at the exit side after reducing its diameter to 11.7 mm.
5. The copper bar also provided support to the hollow SS rod at the entry and the exit. 100 mm length was left on both the copper bars for electrical connection.
6. Five indentations were made to locate the positions of the J-type thermocouples on the SS hollow heater rod.
7. Five J-type thermocouples were inserted in the borosilicate glass tube through designed passes for thermocouples and soldered at the corresponding indentations on the SS heater rod.
8. Finally the borosilicate glass tube and the solid copper rods were connected using Teflon tape and Teflon cork. Adhesive was also applied at both the ends to prevent any leakage from the test section.

3.2 Fluid Flow System

The experimental setup consisted of three separate loops. The primary loop was a closed loop and contained nanofluid. The secondary and the tertiary loops were open loops and contained normal water. The working fluid flowed through the primary loop, cooling water for condenser and heat exchanger flowed through the secondary loop and the cooling water for the transformer flowed through the tertiary loop.

3.3 Ultrasonic Vibration Machine

An Ultrasonic Vibration Machine (UVM) was used to prepare the nanofluid. UVM helps to disperse the nanoparticles in base fluids. The time for mixing the nanoparticles in the base fluid varies according to type of nanoparticle and required concentration.The ultrasonic energy is produced by converting electrical energy into mechanical vibrations by using a generator and piezo-electric transducers. Whenever this ultrasonic vibration is transferred to the nanofluid, rapid formation and collapse of millions of microscopic bubbles produce intense scrubbing effect. This phenomenon is called cavitation. It separates all the nanoparticles and disperses them in the base fluid, in a very short time. Figure 3.4 shows the UVM manufactured by Toshcon, having a capacity of 24 liters, which was used for making nanofluids. The specifications of UVM "Deep Drawn Tanks model SW 24" are given in Appendix B.

Figure 3.4. Photograph of Ultrasonic Vibration Mixer Machine Outer shell and prepared Al_2O_3-water nanofluids in UVM.

The nanoparticles were mixed in distilled water using UVM. The quantity of nanoparticles was calculated as per the concentration required. TiO_2, ZnO,

Al_2O_3 and MWCNT nanoparticles were used for preparing the nanofluids. This mixture was vibrated for achieving maximum thermal conductivity of nanofluid for 1 to 3 hours, 5 to 6 hours, 8 to 10 hours and 10 to 12 hours for TiO_2, ZnO, Al_2O_3 and MWCNT nanoparticles respectively. Each of the prepared nanofluid was collected in the reservoir and circulated in the primary closed loop.

3.4 Imaging Facility

An XCAP SV-642 camera (EPIX) and XCAP – Std. software containing driver of SV642C was used for bubble visualization. The high speed camera was connected to a PIXCI imaging board installed on the computer. It can capture images at the rate of 19,600 fps at reduced resolutions and it has a shutter speed of 20 microseconds. This resolution is good enough for the proposed work.

The camera was placed 400 mm away from the test section to capture length of about 35 mm along the heater surface. A single film could capture about 4.7 ms of boiling process. A CFL lamp with high frequency ballast, which provides flicker free and uniform illumination, was used as the lighting source.

The captured images were analyzed using National Instrument's Labview IMAQ vision builder image processing software. The schematic layout for high speed photography is shown in Fig. 3.5.

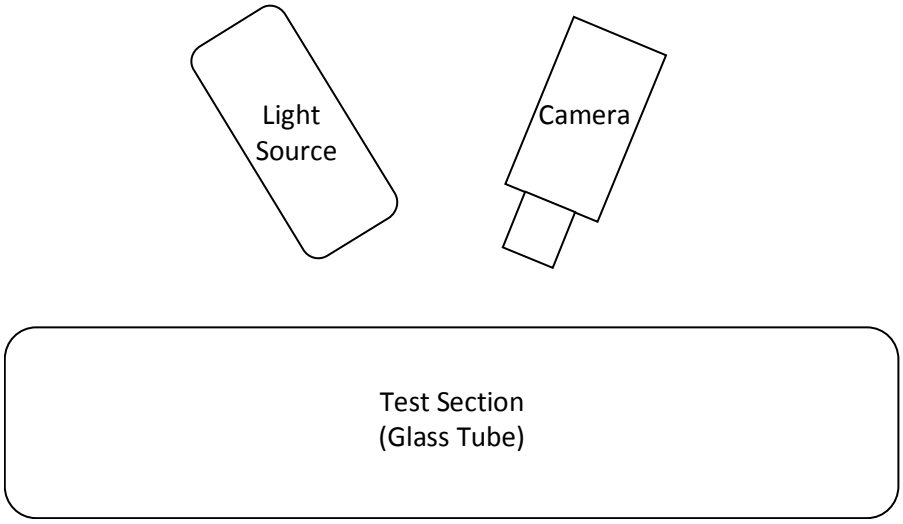

Figure 3.5. Schematic of high speed photography setup.

3.5 Power Supply

The transformer can provide wide range of heat flux to the heating rod. The 415 V three phase power was supplied to the transformer. It was stepped down to 0 to 32 volts using 64 kVA DC regulated power supply. The converted DC was supplied to the SS heater rod through bus bars, shunt and copper rod. Figure 3.6 shows the transformer and bus bars. The rectifier used in transformer for the power supply was cooled by normal water. The bus bars were used in place of normal wire to transmit power to the test section, safely i.e. without any risk of melting.

Figure 3.6. Photograph of 64 kVA Transformer.

3.6 Degassing Valve

Degassing of the working fluid is necessary before the start of experiment to avoid any gas entrapment. Hence two gas release valves were put in the primary loop at high points. The test rig was run with working fluids at high pressure for 3-4 hours and gases were expelled through these gas release valves. The location of gas release valves is at highest point of primary loop as seen in the photograph of

the test section (Fig. 3.3). The degassing process was repeated two to three times before each experiment to ensure that all the entrapped gas is removed.

3.7 Insulation

To minimize the heat loss from the working fluid to the surrounding, the piping section in the primary closed loop was thermally insulated with cotton wool and rubber (SUPERLON rubber). The sizes of two rubber insulations were 1/2" ID, 3/8" TK and 7/8" ID, 3/8" TK for different pipes having OD of 1/2" and 1" respectively.

Since the SS heater rod was completely surrounded by the working fluid in the test section, therefore heat loss from the heater rod to outside environment was not possible, refer Fig. 3.7. However the maximum heat loss from the working fluid to the surrounding through the glass tube was 7%.

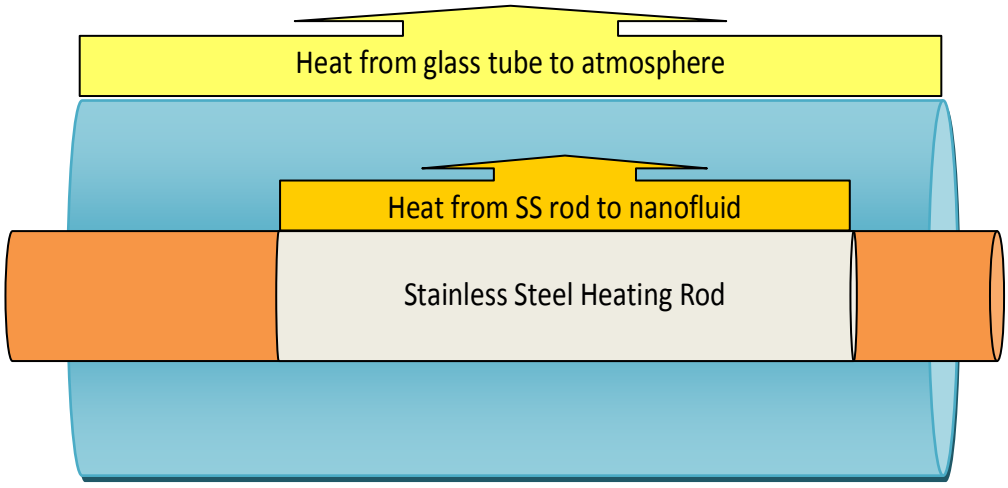

Figure 3.7. Representing heat loss from the test section.

3.8 Instrumentation

The loop allows for varying power input, pressure, inlet temperature and flow rate. All the instruments were calibrated and error analysis was carried out for each instrument. The error analyses of the instruments are given in Appendix C.

3.8.1 Thermal Property Analyzer

It is a device which measures the thermal properties of fluids and solids. It can measure thermal properties of nanofluids and a variety of other materials including granules, rocks, etc. It uses 3 different thermal sensors i.e. KS-1, TR-1 and SH-1 to measure thermal diffusivity, specific heat, thermal conductivity and thermal resistivity of fluids and many other solid materials.

The KD2 Pro sensor uses transient hot wire technique to measure the thermal conductivity of fluids. It consists of a very long and thin continuous heat generating source which dissipates heat into the test medium. When electrical energy is supplied to the source, its temperature changes which results into change of the resistance of Wheatstone bridge circuit. This is measured using a data acquisition system. The thermal conductivity of the sample is determined from the heating power and the slope of temperature change in logarithmic time.

The thermal property analyzer measures thermal conductivity in a time span of 90 sec. A measurement cycle consists of a 30 sec of heating period, a 30 sec of equilibrium period and a 30 sec of cooling period. Temperature measurements are made at 1 sec intervals during heating and cooling. Measurements are then fit into exponential integral functions using a nonlinear least squares procedure. A linear drift term corrects for the temperature changes of the sample during the measurement to optimize the accuracy of the readings. Figure 3.8 shows the Thermal Property Analyzer (KD2 Pro). The specifications of the KD2 Pro are given in Appendix D.

Sensors of KD2 Pro

The thermal property analyzer uses three sensors which measure thermal properties, but they differ with each other in use. These sensors are KS-1, KS-2 and KS-3. The KS-1 sensor can be used to measure the thermal conductivity of fluids.

The KS-1 sensor has a single needle element (60 mm long, 1.3 mm diameter) which measures thermal conductivity and thermal resistivity. It is designed primarily for liquid samples and insulating materials having thermal

conductivity < 0.1 W/mK. This sensor supplies a very small amount of heat to the needle. The negligible heat helps to prevent free convection in liquid samples.

In this study KS-1 was used for measuring thermal conductivity of nanofluids. Appendix E gives the parameters of KS-1 probe which was used to measure thermal conductivity of the nanofluids.

Figure 3.8. Thermal Property Analyzer (KD2 Pro).

3.8.2 Flow Meter

FL-204, 4-wire turbine type flow meter manufactured by Electronet, having a range of 0.02 to 0.3 liters per second was used for measuring the flow rate in the closed loop, refer Fig. 3.9. It has less than 100 ms response time with repeatability of ± 1% and accuracy of ± 1%. It has a 4 digit, 0.3" LED display for instantaneous flow rate and 8 digit, 0.3" LED display for total flow.

Figure 3.9. Photograph of turbine type flow meter.

3.8.3 Temperature Sensors and Data Acquisition System

Thermocouples were used for measuring inlet and outlet temperatures of the working fluid in the test section. Five thermocouples were soldered on SS rod at equidistant locations to measure local surface temperatures. The thermocouples were located at five different locations on the surface of the test section at an interval of 100 mm for analyzing and verifying the visualization results with high speed photography. Apart from these five thermocouples, two more thermocouples were used for measuring the inlet-outlet bulk temperature of the working fluid. All these thermocouples (JMQSS-IM050U-300) are of 1 mm wire diameter, J-type, ungrounded and manufactured by Omega. The location of all the thermocouples is shown in Fig. 3.3. A Data Acquisition System, OMB-DAQ-55, manufactured by Omega, was used for recording the temperatures in the computer during the experiment.

3.8.4 Pressure Sensors

Figure 3.10 shows pressure indicator with pressure transducer, manufactured by Keller. Two pressure sensors were used to measure static pressure at the inlet and outlet of the test section. Both pressure sensors have a range of 1 to 10 bar with an accuracy of ±0.1%. Pressure drop was measured with two pressure indicators at inlet and outlet of the glass tube.

Figure 3.10. Photograph of pressure sensor and digital pressure indicator.

3.8.5 Surface Roughness Tester

Surtronic 25 surface roughness tester, manufactured by Taylor Hobson, having ±2% accuracy, was used to measure the surface roughness of the heater surface before and after the boiling. The Surtronic 25 surface roughness tester works on inductance principle.

3.8.6 Voltmeter and Ammeter

The voltage across SS heater rod was obtained by a voltmeter (VM1606). It is manufactured by Meco and has an accuracy of ±0.1%.

The current through the SS heater rod was measured by an ammeter (AM1004). It is also manufactured by Meco and has an accuracy of ±0.1%. It has an induction coil which generates an A.C. signal (0 to 75 mV) proportional to the current. Figure 3.11 shows the ammeter and the voltmeter.

Figure 3.11. Photograph of Ammeter and Voltmeter.

3.8.7 Other Accessories

A **desktop computer** (Lenovo) having Intel Dual-Core processor, 160 GB HDD, 2 GB RAM was used to store the data. The images of flow process were visualized at the desktop screen with high speed camera and XCAP standard software. The DAQ system was also connected to the computer by using the "Personal DAQ View Plus" software.

An **electrical heater** was provided in the storage reservoir to regulate the temperature of the base fluid. It was controlled by a temperature control device. It was also provided with a temperature indicator to display the temperature of the nanofluids in the reservoir. The reservoir was made of SS sheets. Figure 3.12 shows the reservoir containing nanofluid after the experimentation.

A **centrifugal pump** made of SS was used for circulating the working fluid in the apparatus. It can develop 4 bar pressure at a flow rate of 20 liters per minute. Figure 3.13 shows the centrifugal pump that was used for the experiment.

Figure 3.12. SS sheet made storage reservoir.

Figure 3.13. Centrifugal pump.

3.9 Preparation of Nanofluids

Preparation of nanofluids is an important step in carrying out the experimental study of the nanofluids. Nanofluids cannot be just made by simple mixing. Following conditions must be satisfied before a nanofluid can be used for the experimentation.

- The nanofluid must be stable.
- There should be no agglomeration of the nanoparticles.

Al_2O_3, TiO_2 and ZnO nanoparticles are selected as they have good thermal conductivity, are easily available and a number of studies done on them are available in the literature. Additionally MWCNT has been included because of its high thermal conductivity.

For the preparation of the nanofluids, mass of the nanoparticles was calculated depending upon concentration of nanoparticles selected. The required mass of the nanoparticles was then dispersed in 10 liter of distilled water in a UVM tub. The UVM was used to mix the nanoparticles in distilled water. Thermal conductivity of the nanofluid was measured at 30 minutes interval as follows.

- A 25 ml Sample of nanofluids was taken in a narrow necked small bottle.
- KS-1 sensor of the KD2-Pro was inserted in the bottle.
- The sensor was positioned vertically in the center of the bottle before recording the reading.

The sonication time at which nanofluid was found to have the maximum thermal conductivity was noted. Now a fresh sample of nanofluid was prepared by running the UVM for the time at which maximum thermal conductivity was observed. Table 3.1 gives the sonication times at which thermal conductivity of different nanofluids were maximum.

As per the specifications of thermal property analyzer KD2-Pro, accuracy of measurement of thermal conductivity was 5% and its repeatability was within 2%. The graphs between thermal conductivity ‘k’ and sonication time are presented in chapter 5.

Table 3.1: Sonication time of UVM to achieve maximum thermal conductivity.

Nanoparticles	Concentration (%)	Sonication Time (in hour)
Al_2O_3	0.0001	5.0
	0.0010	6.0
	0.0100	6.0
	0.1000	6.0
TiO_2	0.0001	2.5
	0.0010	2.5
	0.0100	2.5
	0.1000	3.0
ZnO	0.0001	4.0
	0.0010	4.0
	0.0100	4.0
	0.1000	4.0
MWCNT	0.0001	3.5
	0.0010	4.5
	0.0100	5.5
	0.1000	6.0

3.10 Experimental Procedure

After the setup of the experimental facility was completed, following steps were followed to obtain the readings:

i. The required concentration of nanoparticles was prepared by mixing of calculated mass of nanoparticles in the base fluid, i.e. distilled water in the UVM and stored in the reservoir.

ii. The test section and heater surface were cleaned with 13.88 normal H_2SO_4 in distilled water before final cleaning by distilled water at 90°C and atmospheric pressure to remove oxides and other residues.

iii. The reservoir and the loop were filled with the working fluid, i.e. distilled water or nanofluids.

iv. The working fluid pumped to the test section through a flow meter.

v. The working fluid was circulated in the primary closed loop and parameters like pressure, flow rate and temperatures were set.

vi. The required current was supplied in steps of approx 40 A to the heater rod. The fluid was boiled in the test section by an electrical heater made up

of SS rod. The mixture of the steam and the fluid were passed through a condenser and a heat exchanger before returning it to the storage reservoir. The readings were taken after the steady state was achieved.

vii. The parameters during the boiling process were recorded by the data acquisition system (DAQ) and simultaneously the image of the boiling process was captured by a high speed video camera.

viii. Each experiment was repeated three times to verify repeatability of the experiment.

ix. The step iv to viii of experimentation was repeated for each increment of 0.5 bar pressure.

x. The surface roughness of the heating rod was measured with Surtronic 25 surface roughness tester. The measurement procedure for surface roughness is as following:

   a. The test section rod was removed after the experiment and SS rod was separated from it.
   b. A sample piece was cut from the SS rod.
   c. This was fitted on the bench of Surtronic 25 surface roughness tester.
   d. The sensor of the roughness tester was moved to & fro, on the sample and the relevant reading was noted.

xi. Again, a new test section was assembled and fitted in the primary loop.

xii. The reservoir was filled again with the working fluid of increased concentration and the experimental steps i to xiii were repeated for increased pressure and heat flux of the nanofluid using new heater rod.

During the experiment, the boundary conditions were maintained by using controlling devices, such as, temperature controller, power controller, control valves to control the sub-cooling, power input, pressure and mass flux.

3.11 Estimation of Parameters

Pressure and flow rate were measured by pressure sensor and flow meter respectively. Temperatures of the fluid at inlet and outlet of the test section were

measured by thermocouples. Temperatures along the heater rod were recorded by a data acquisition system. Parameters and constants used for following calculations are shown in Appendix-F (Properties of Nanoparticles), Appendix-G (Thermal Properties of Water) and Appendix-H (Thermal Conductivity of Nanoparticles).

Mass of nanoparticles

Mass of nanoparticles mixed in the base fluid is calculated, based on physical principle of the mixture as described by Heris et al. (2007)

(0.1% Al_2O_3, for 10 liter fluid),

$$m_{np} = l * 10^{-3} * \nu * \rho_{np} \quad (3.1)$$

$= 10*10^{-3}$ (m^3) x 0.001 x 3700 (kg/m^3)

= 0.037 (kg)

= 37 (g)

here

m_{np} is mass of nanoparticles in kg,

l is volume in liter

ν is nanoparticle volume fraction and

ρ_{np} is density of nanoparticles in kg/m^3

Heat flux

The heat flux was measured as follows:

$$q = \frac{VI}{A} \quad (3.2)$$

here

q = heat flux (W/m^2)

V = voltage across the heater rod (V)

I = current flowing through the heater rod (A)

A = area of cross-section of the heater rod (m^2).

Figure 3.14 shows the trend of heat flux with current.

Heat transfer coefficient (h)

Heat transfer coefficient used in calculating heat transfer between a fluid and a solid, for convection or phase change is:

$$h = \frac{q}{\Delta T} \tag{3.3}$$

here

q = heat flux (W/m^2)

h = heat transfer coefficient (W/m^{2}K)

ΔT = difference in temperature between the solid surface and surrounding fluid (K)

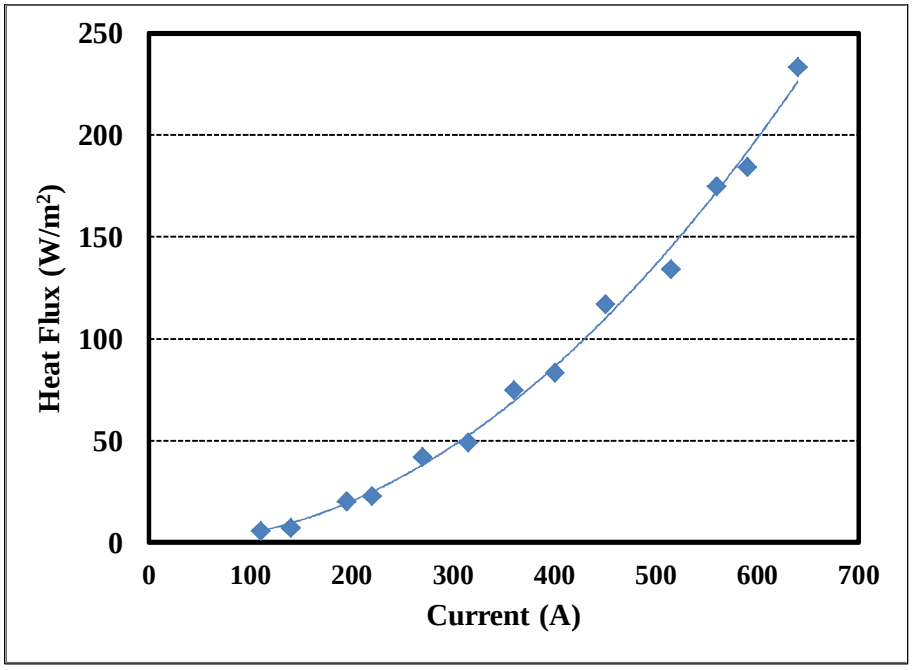

Figure 3.14. Trend of heat flux with current.

3.12 Range of the Parameters

Concentrations of the nanoparticles Al_2O_3, TiO_2, ZnO and MWCNT chosen for the experiment were 0001%, 0.001%, 0.01% and 0.1%. Pressure was varied from 1 to 2.5 bar. The experiments could not be conducted at pressure

above 2.5 bar as that was beyond the permissible limit for bonding of the glass tube with thermocouples and with the heater rod at high heat flux.

Heat flux was varied from 0 to 400 kW/m^2 while the mass flux was kept constant at 400 kg/m^2s. The inlet temperature was set at 80°C and mass flux fixed at 400 kg/m^2s. The range of parameters adopted during the experiments is shown in table 3.2.

Boundary conditions for variable parameters are maintained through controlling instruments. Inlet temperature was controlled with temperature controller in reservoir and cooling in condenser and heat exchanger. Pressure was controlled with controlling valves in pipe flow. Mass flux was controlled with controlling valves in pipe flow and constant flow of pump. The results are limited to possible maximum heat flux to avoid leakage of nanofluid and any accident.

Table 3.2: Range of variable parameters.

S. No.	PARAMETER	RANGE
1	Concentration, (%)	0.0001, 0.001, 0.01 and 0.1
2	Pressure, (bar)	1 to 2.5
3	Heat flux, (kW/m^2)	0 to 400
4	Average nanoparticle size, (nm)	40 for oxides, 20 for MWCNT
5	Nanoparticles	Al_2O_3, TiO_2, ZnO, MWCNT
6	Mass flux, (kg/m^2s) {Reynolds no.}	400 {10000}
7	Inlet Temperature, (°C)	80

3.13 Validation for Heat Transfer Coefficient

Six hour sonicated Al_2O_3-water nanofluid with concentration of 0.0001% was used for validation. The convective and flow boiling procedure was repeated four times as per section 3.10. The readings were taken to determine the optimum heat transfer coefficient at a pressure of 1.0 bar. The readings were interpreted for a decision. Similar trend was observed for all the cases. The results of present

experiment have been plotted in Fig. 3.15. The findings of heat transfer coefficient were compared with data reported by Jabardo et al. (2004) for refrigerant (R11). It is clear from the figure that, the present work compare well with 90% precision. The difference may be due to different environment of present work and the work done by Jabardoet. al (2004) for R11.

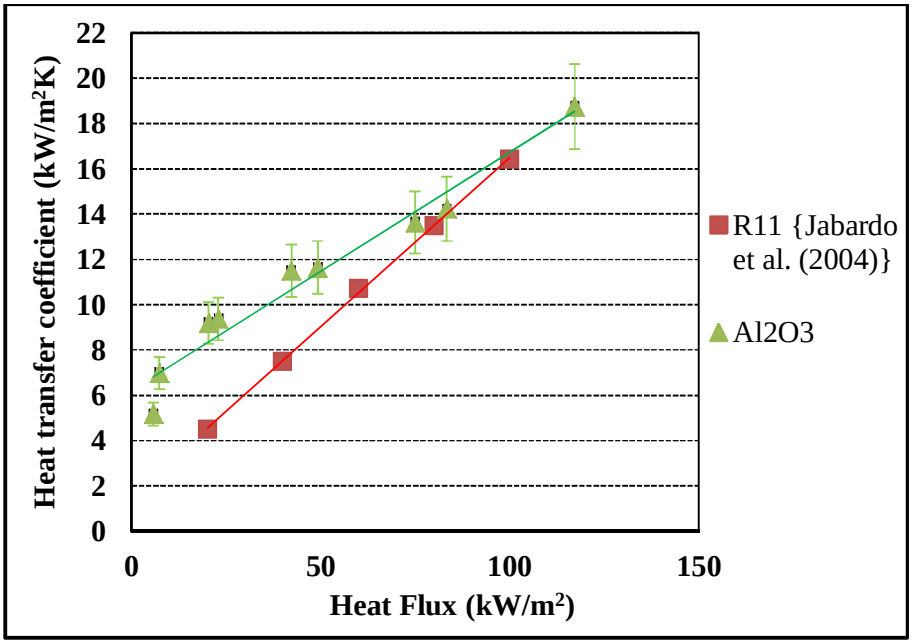

Figure 3.15. Comparison of results of heat transfer coefficient with Jabardo et. al (2004).

4.

BUBBLE ANALYSIS

The bubbles were analyzed using Image Acquisition (IMAQ) vision builder software. It converts the bubble parameters in pixel form which are subsequently converted to get real dimensions of the bubbles. The main steps involved in getting the results in pixel form are:

1. Loading of image
2. Image conversion
3. Image contrast enhancement
4. Image filtering
5. Convolution – highlight details
6. Edge detection
7. Cropping of region of interest
8. Image "Thresholding"
9. Basic morphological operations
10. Advanced morphological operations
11. Particle filtration
12. Particle analysis

4.1 Image Processing for Bubble Parameters

The image processing is very useful due to its non-intrusiveness and its ability to study very short duration phenomenon such as bubble formation, growth and condensation. The analysis of flow boiling can be carried out using this technique.

National Instruments IMAQ Vision Builder 6.1 image processing software was used for the image analysis. The complete procedure consists of 12 steps followed by visual inspection to compare the results with initial image.

Sample outcome for every step of script is shown in the figures from 4.1 to 4.12. Details on standard image processing operations can be found in Gonzalez and Woods (1993).

A set of 100 images was batch processed using National Instruments IMAQ Vision Builder 6.1 image processing software. The main steps involved in image processing are as followings -

Loading of Images

Each frame of the photograph obtained for processing was loaded as 8 bits RGB (Red, Green and Blue) color format. A sample of the photograph after loading is shown in figure 4.1. The size of the raw image processed was 1024 x 768.

Conversion of RGB Image to Gray Scale Image

The loaded image is a colored image. The color images are formed in RGB color space using red, green, and blue component. The loaded RGB image was converted from RGB to gray-scale image by extracting one of the three color planes. The extracted image is a gray-scale image. A sample of the same is shown in figure 4.2. The gray-scale image obtained has 256 gray levels, ranging from 0 (black) to 255 (white).

Enhancing the Contrast of the Image

Due to higher shutter speed and lack of sufficient light, at times an object (a bubble) in the image becomes dull. By increasing the contrast, the bubbles can be made visible. So for better visibility, contrast of the gray–scale image was enhanced. A sample image with enhanced contrast is shown in figure 4.3.

Image Filtration

Filters can smoothen, sharpen, transform and remove noise from an image so that the required information can be extracted. A median filter was applied to the image to remove or attenuate the noise present in the image. Median filter is also useful in preserving edges in an image while reducing random noise. The noise in form of impulsive or salt and pepper can occur due to a random bit error in a communication channel. In a median filter, a window slides along the image, and the median intensity value of the pixels within the window becomes the output intensity of the pixel being processed.

The bubble images in the pixel form, separated considerably from the surrounding ones, are discarded by substituting the median of its neighbor pixel in this operation. The bubble images are discarded to minimize the errors. However as a result of image filtration, sharpness of the image deteriorates slightly. A sample of the filtered image is shown in figure 4.4.

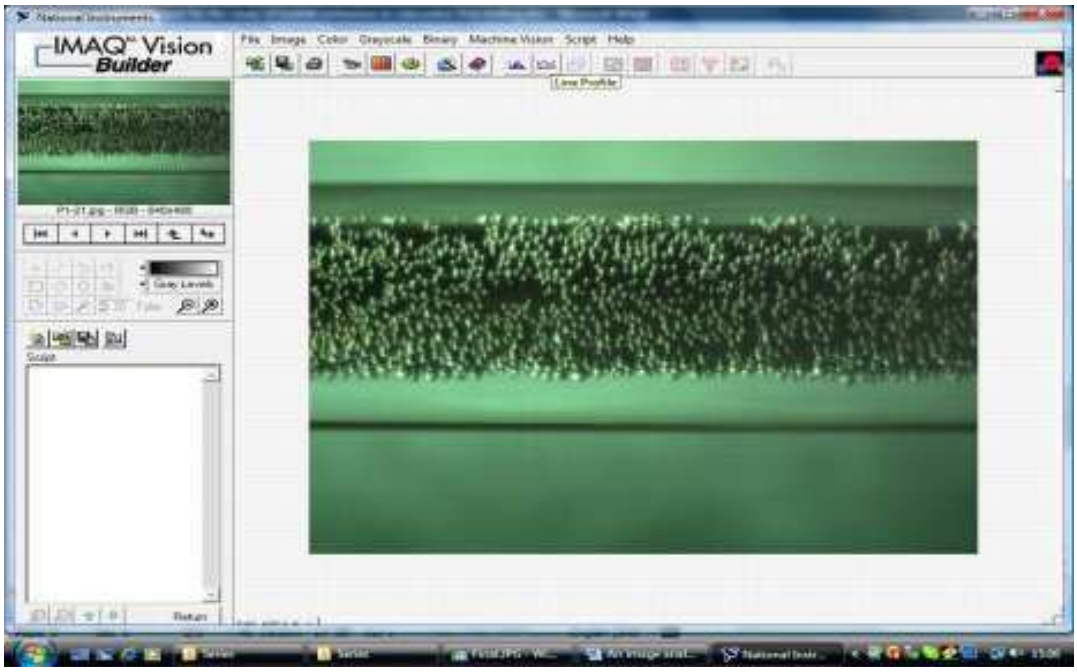

Figure 4.1. Loaded image in IMAQ Vision Builder.

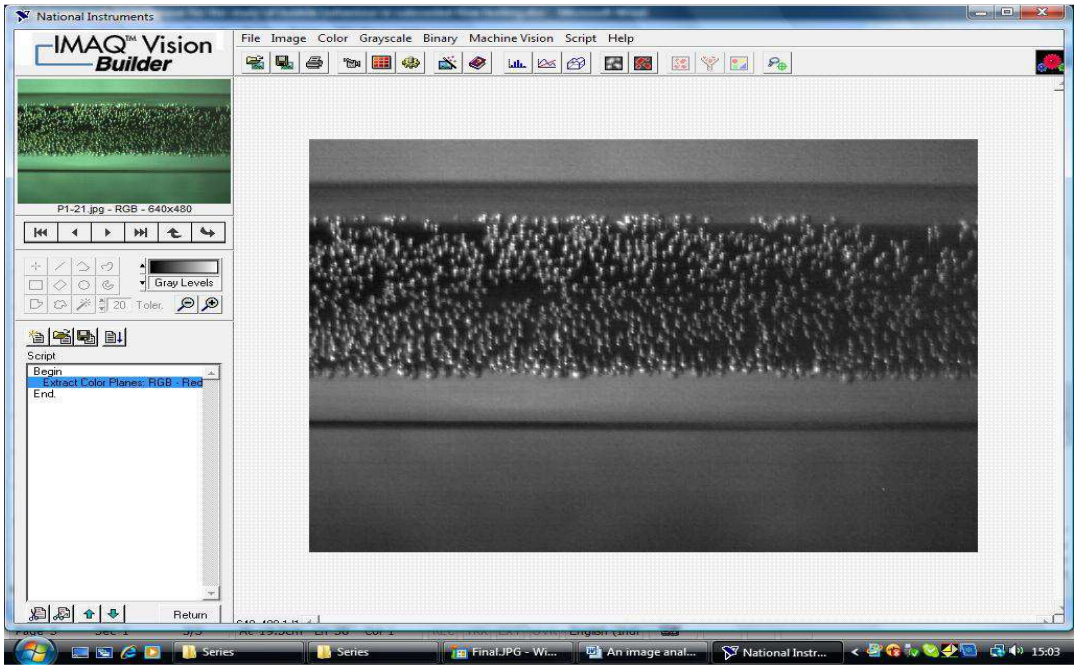

Figure 4.2. Conversion of raw image into gray scale image.

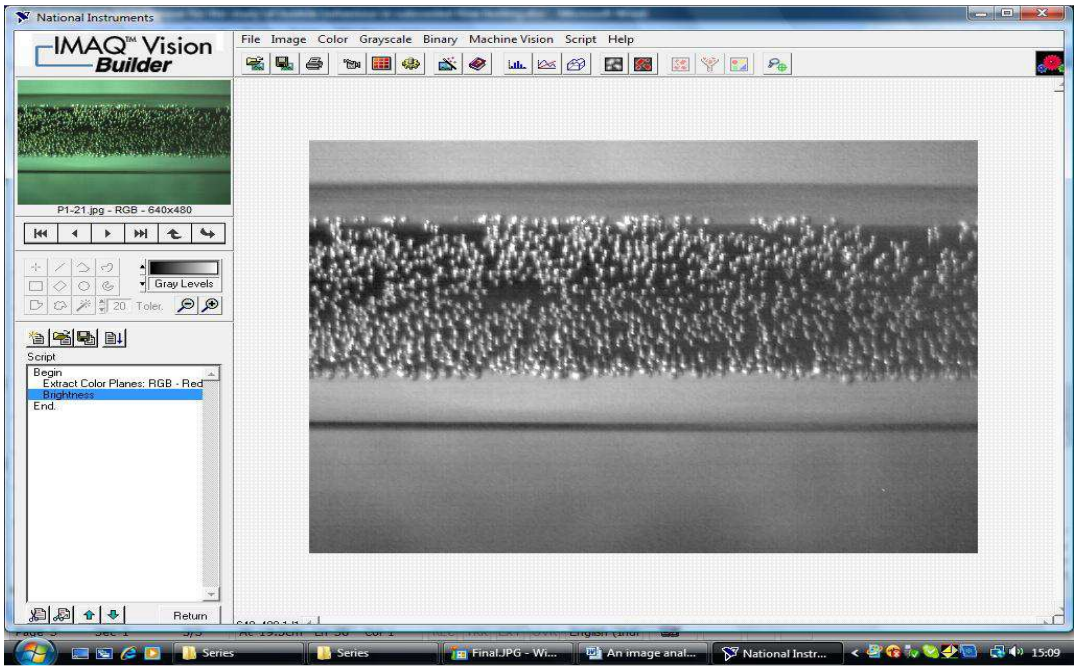

Figure 4.3. Image of Enhanced Contrast.

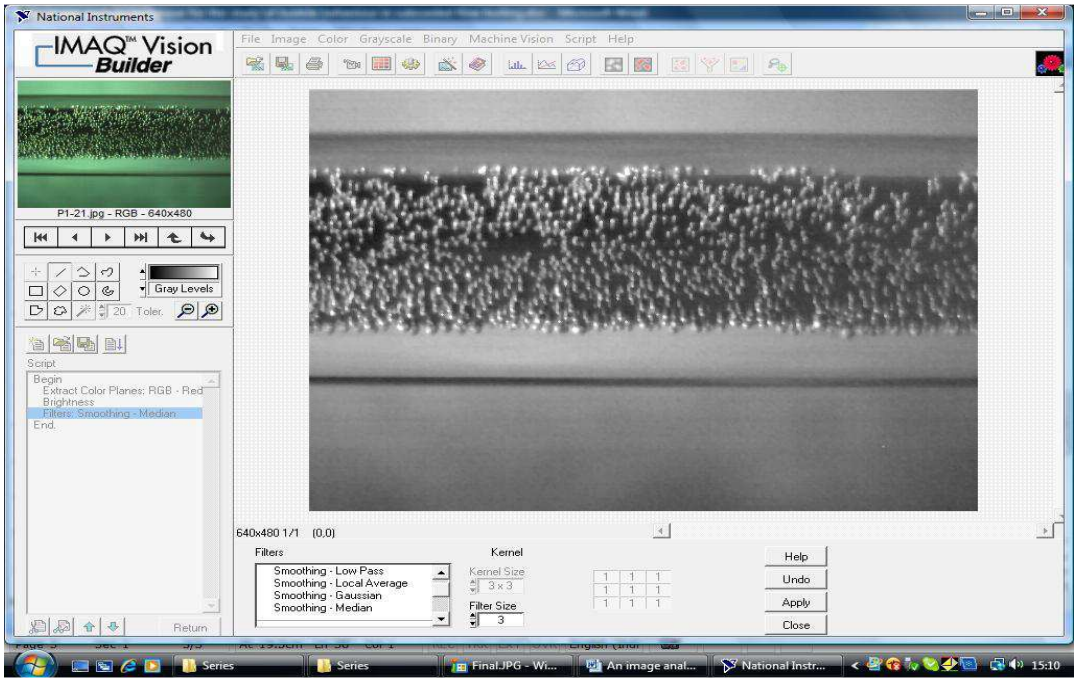

Figure 4.4. Filtered Image.

Convolution – Highlighting Details

A kernel represents a pixel and its relationship to neighboring pixels. In image processing, a kernel or mask is a small matrix useful for blurring, sharpening, embossing, edge-detection etc. This is accomplished by means of

convolution between the image and its kernel. In this operation, intended objects (bubbles) were highlighted from the background, by applying 7 x 7 kernel across the image. This is better than 5 x 5 kernel and 3 x 3 kernel options. Only these three options were available in Image Acquisition (IMAQ) vision builder software. The processed image is shown in figure 4.5.

Edge Detection

This operation was employed to locate the intersection points between a set of search lines within an image area. Circular edge of bubble can be identified by Roberts's edge detection algorithm, available in the software. Roberts's edge detection operation was performed to select the edges of bubbles in the image area. The edges were identified clearly in an annulus area and were highlighted in the image area. The edge detected image is shown in figure 4.6.

Cropping of Image

Region of interest (Heater rod portion) was separated from the image by cropping out the glass tube portion from the image, as shown in figure 4.7.

Image 'Thresholding'

'Thresholding' consists of dividing an image into two regions: a particle region and a background region. This process works by setting to 1 all the pixels that belong to a gray-level interval, called the threshold interval and setting all other pixels in the image to 0.

The 'thresholding' was used to isolate the objects of interest in an image. 'thresholding' converts the image from a grayscale image, with pixel values ranging from 0 to 255, to a binary image, with pixel values of 0 or 1. The range of pixel values in gray-scale image and color images can be selected by 'thresholding' that separate the objects with consideration of the background.

The conversion of a gray image to binary image consist of reduction of grey levels of the original image to one corresponding to black (0) and another corresponding to red (1). This is accomplished by means of a threshold value, i.e., a pixel value defining the transition between black and red colors. Once the

threshold value is defined, image simplification takes place - all pixels with luminosity values lower than the threshold value are considered black, while the remaining pixels are considered red. This operation creates images like the one depicted in figure 4.8.

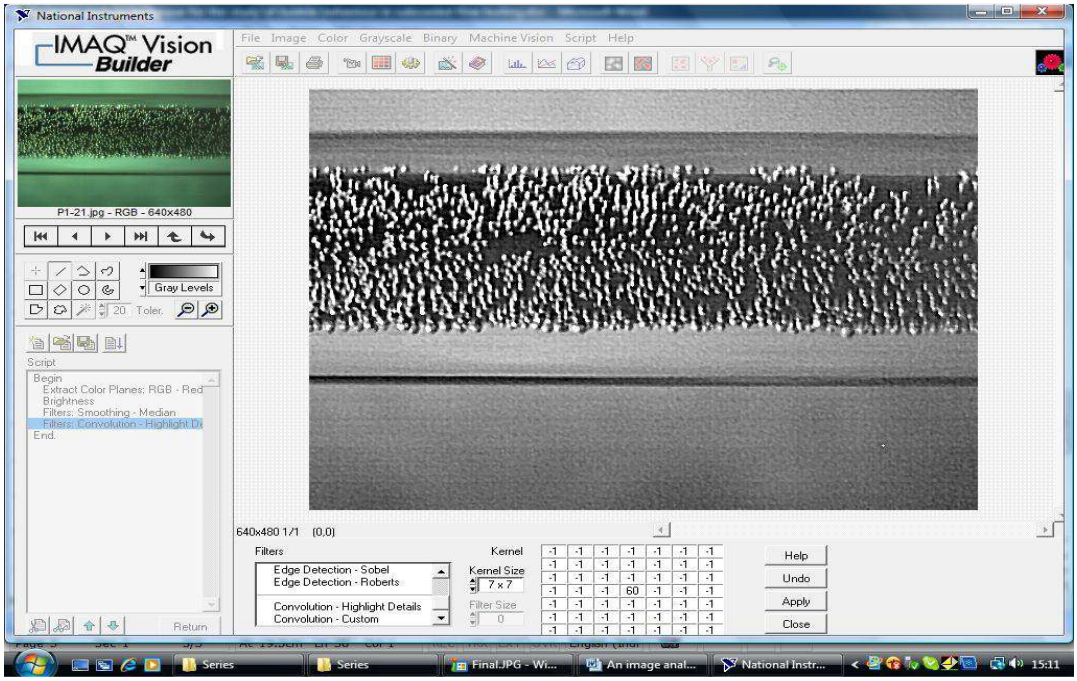

Figure 4.5. Image of Convolution - Highlighting the details.

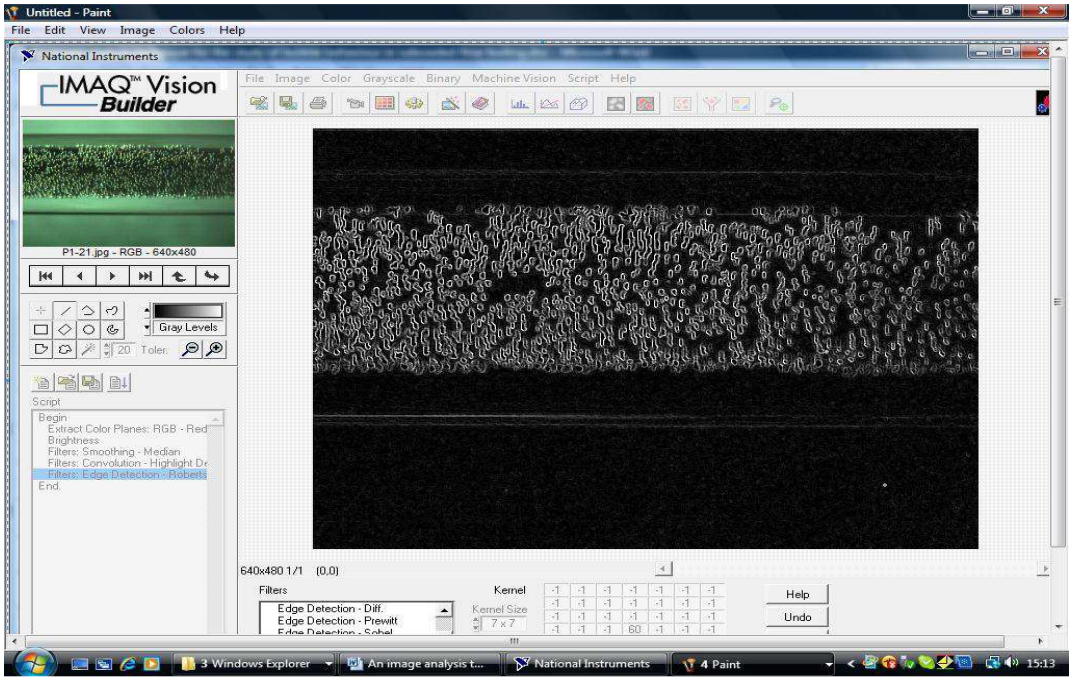

Figure 4.6. Edge detected image.

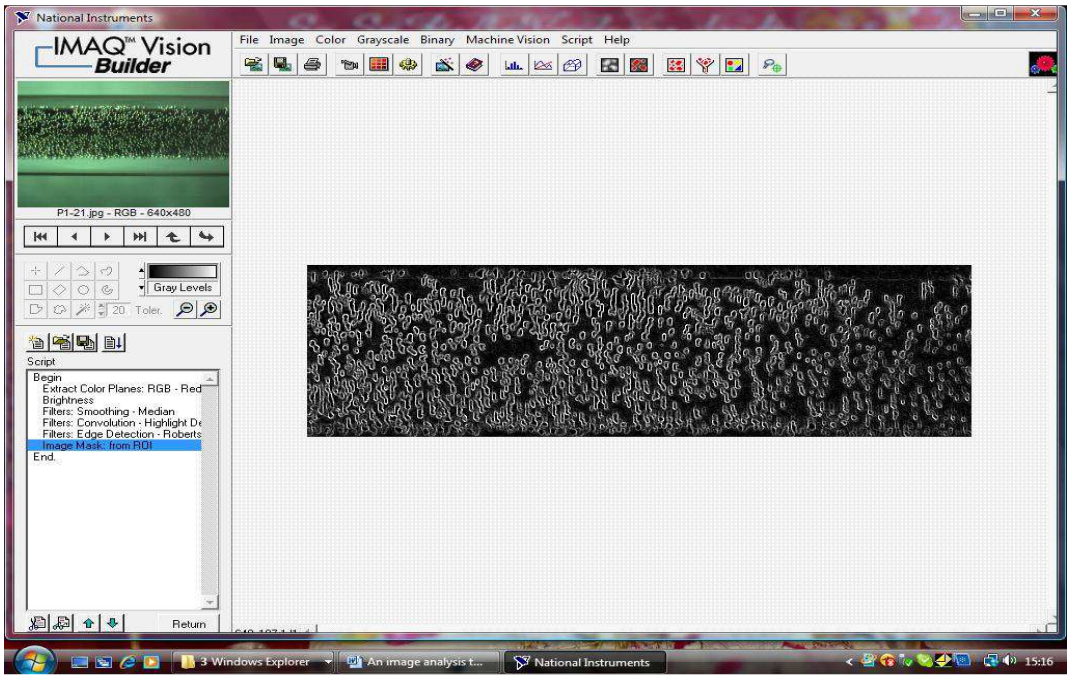

Figure 4.7. Cropped up image showing ROI.

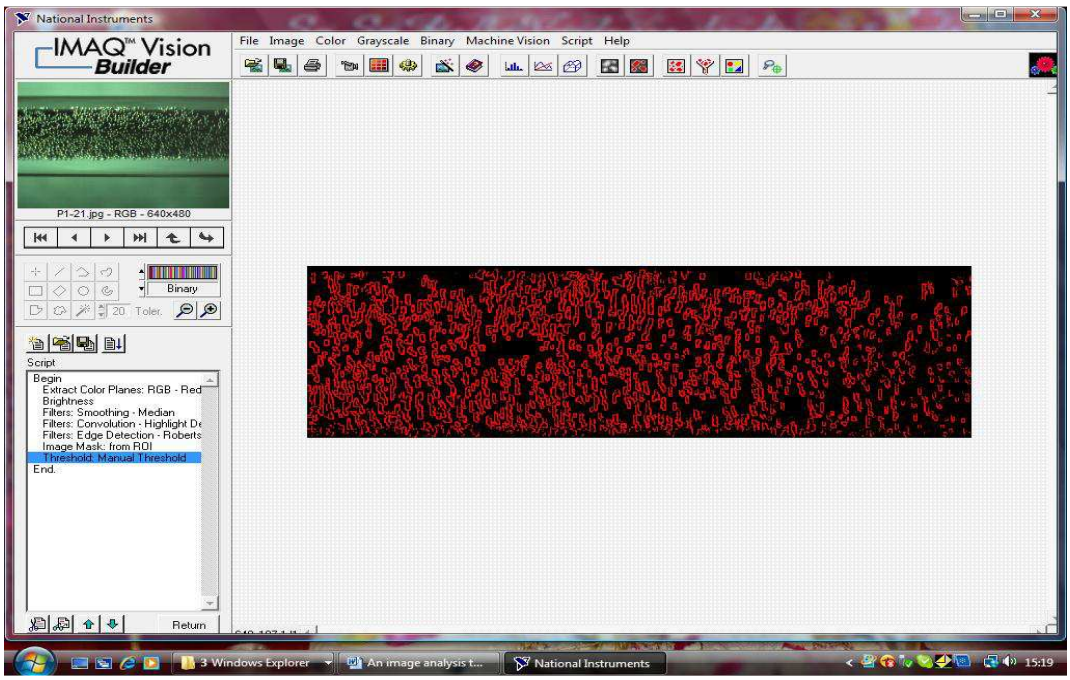

Figure 4.8. Image after 'thresholding'.

Basic Morphological Operations

Morphological functions affect the shape of particles on an individual basis. Morphological operations find shapes in the image for quantitative analysis

such as finding the area, perimeter, or orientation. It affects the shape of particles in binary images. Each particle or region can be affected separately in this step. The functions in this step can be used for tasks such as expanding or reducing objects, filling holes, closing particles, smoothing boundaries to describe objects, prepare images for quantitative analysis, etc. Based on the structure of the bubbles, proper closeness of bubbles fills tiny holes and smoothes inner contours of objects. Proper closeness of bubbles provides a finite and dual combination of closings and openings of selected region of bubbles in the image. Erosion, dilation and proper closing operations were performed here on the selected binary image. These operations creates image like the one depicted in figure 4.9.

Advanced Morphological Operations

This step can be used for removal of small particles from an image, filling of gaps between two particles or bubbles, separation of objects neighboring bordering, labeling particles in an image, etc. The border objects can be removed to eliminate particles that touch the borders of an image. Operations like filling of gaps, removal of small objects and separation of border objects were performed on binary images. This operation creates images like the one depicted in figure 4.10.

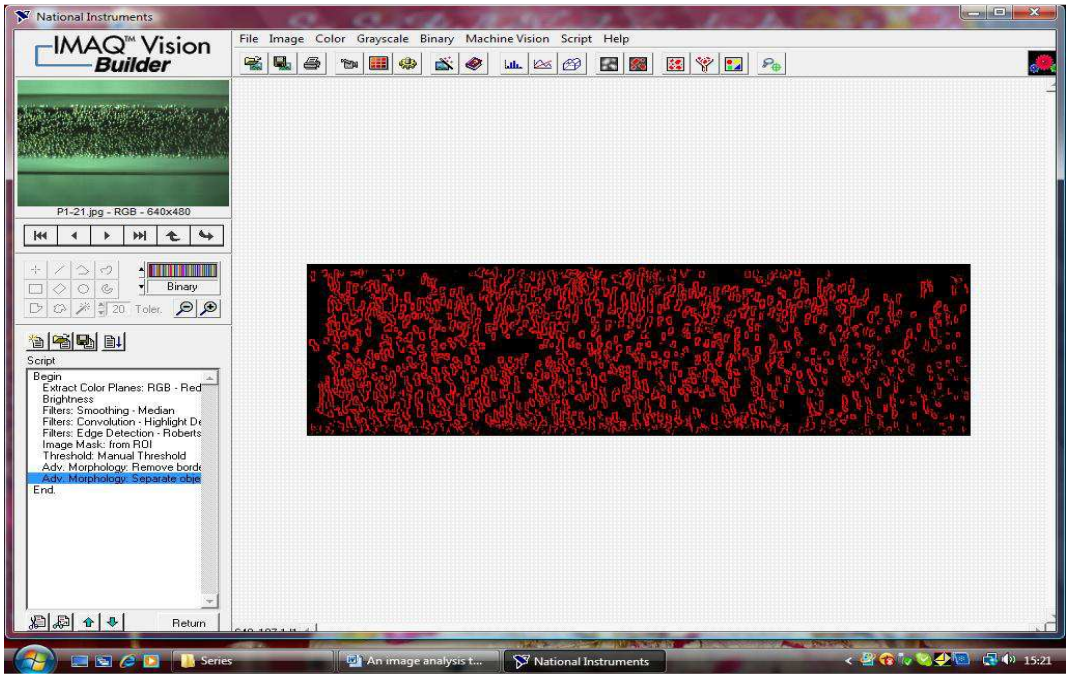

Figure 4.9. Image after basic morphological operations.

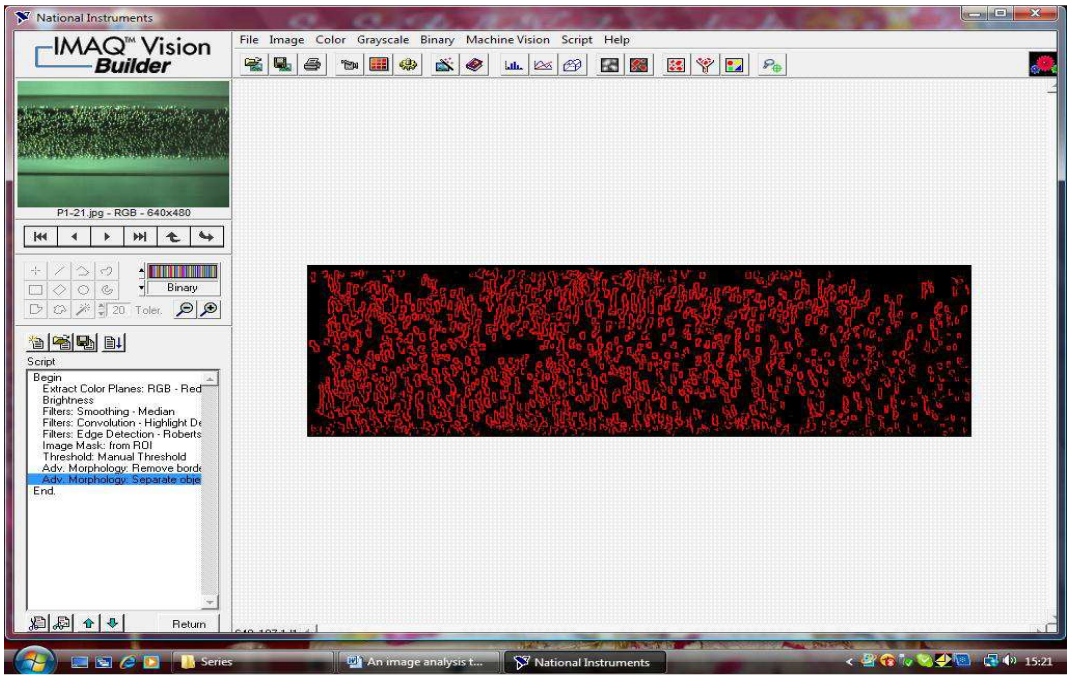

Figure 4.10. Image after advanced morphological operations.

Particle Filtration

Circular or nearly circular objects can be identified in this operation by using Heywood circularity factor. This factor is the ratio of object perimeter to the perimeter of a circle within the same area. Contours with a Heywood circularity factor ranging from 1 to 1.06 were accepted as bubbles and other non-circular objects were filtered and removed as shown in figure 4.11.

Particle Analysis.

Particle analysis comprises of a series of processing operations using suitable functions that gives information about the particle's shape in an image. Particle analysis was performed to detect connected regions of bubbles or groupings of pixels in an image and then to take selected measurements of those regions of bubbles. Using particle analysis, one can detect and analyze any two-dimensional shape in an image. This operation is also used to find statistical information about the particles (bubble), such as their size, number and relative ratios of located areas. By using this operation, bubble size and image area were obtained in terms of pixels. All bubbles were numbered and measurement of bubbles were stored in an excel data sheet. The bubble diameter, bubble density and void fraction were measured in the image. The processed image and

corresponding data are shown in figure 4.12. The results, pixels, area (unit) and image are (unit) in figure represents the no. of counted bubbles, pixels of respective bubbles, area of respective bubbles (in pixels) and image area (in pixels) respectively.

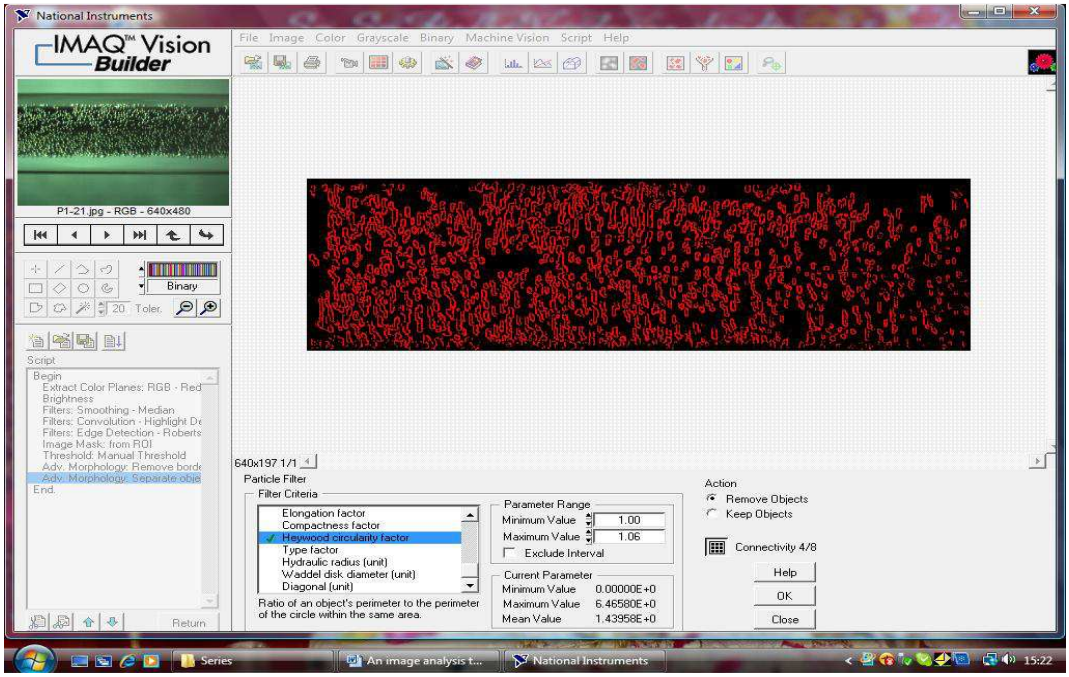

Figure 4.11. Image after particle filtration using Heywood circularity factor.

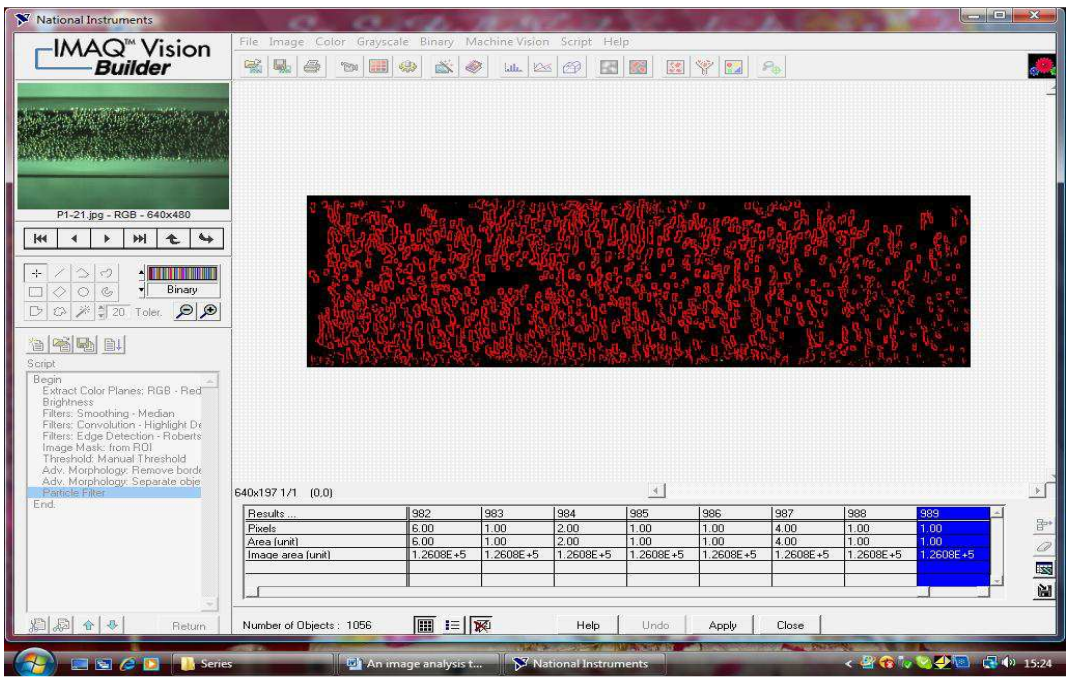

Figure 4.12. Image after particle analysis.

4.2 Visual Inspection and Validation

Despite these entire image processing operations, there is still a chance of bubble coalescence. Even though, there are various operations like pattern recognition and geometric matching by which bubbles coalescence can be identified, it is not possible to get 100% satisfactory results. As a result, a decision was taken to compare the original image with the processed image to identify bubble coalescence and separate the connected bubbles manually. Though this method is not widely used, still it was used to reduce the error. There is 5% error in measurement of bubble parameters.

4.3 Calculations for Bubble Diameter and Bubble Density

The result obtained after image processing operations is in terms of pixels. These pixel values are converted into geometrical dimensions using the following formulae:

Area of bubble, Ab (mm^2) =

$$A_b = \frac{A_p \, X \, A_f}{A_I} \tag{4.1}$$

where

Ap = Area of bubbles, (pixels)

Af = Focused area of image, (mm2)

AI = Image Area, (pixels)

Diameter of bubble, D (mm) =

$$D = \sqrt{\frac{4A_b}{\pi}} \tag{4.2}$$

Number of bubbles can be obtained at the end of image processing operation, using IMAQ vision builder software. Bubble density can be calculated as

Bubble density ($1/m^2$) =

$$\rho = \frac{N}{A_f} \tag{4.3}$$

where,

N = number of bubbles

Af = Focused Area (m2)

4.4 Calculation for Void Fraction

Void Fraction is an important parameter in multiphase flows, and in particular in two-phase gas-liquid flows. Void fraction is the ratio of bubbles area in the unit image area of the heater surface. Void fraction is calculated as:

Void fraction, ε_g =

$$\varepsilon_g = \frac{N_{pv}}{T_{pvl}} \tag{4.4}$$

where,

N_{pv} = No. of pixels occupied by vapour

T_{pvl} = Total No. of Pixels occupied by vapour and liquid

5.

RESULTS AND DISCUSSION

In this chapter, the findings are discussed which obtained from experimental observations. The heat flux, pressure, different nanoparticles like: Al_2O_3, TiO_2, ZnO and MWCNT, concentration of different nanoparticles in the base fluid (water) are considered as variable parameter whereas thermal conductivity, heat transfer coefficient, pressure drop in test section and bubble parameters like: bubble diameter, bubble density and void fraction are considered as results obtained from experiments. The surface roughness of heater rod is also measured for different concentrations of nanofluids, before and after each set of experiments for increased concentration of nanoparticles in water. The range of variable parameters is shown in table 3.2.

5.1 Thermal Conductivity

Results of thermal conductivity with sonication time are presented here for different nanoparticles like: Al_2O_3, TiO_2, ZnO and MWCNT in water.

5.1.1 Thermal Conductivity of Al_2O_3-Water Nanofluids

Thermal conductivity changes with sonication time because of greater mixing of nanoparticles. Similar observations were found by Murshed et al. (2005) & Hays et al. (2006). After reaching a saturation limit, it decreases because of coagulation. Pal et al. (2015) has also reported similar observations.

Its accuracy is 5% and repeatability is 2%. To assess the repeatability of the tests, the experimental thermal conductivity tested four times. Figure 5.1 shows the repeatability plots for thermal conductivity of 0.0001% Al_2O_3-water nanofluids. Thermal conductivity is plotted on the y-axis whereas sonication time is plotted on the x-axis. The four plots presented herein show that the thermal conductivity values show good repeatability in the experiments conducted.

Figure 5.2 shows the variation of thermal conductivity of Al_2O_3-water nanofluids with sonication time for different concentrations of nanoparticles in water. Initially the thermal conductivity of nanofluid increases with increase in

sonication time, reaches a maximum value and then decreases. From the graph it is observed that thermal conductivity is maximum for sonication time of about 6 hrs for all concentrations of Al_2O_3-water nanofluid. Heat transfer coefficient was measured for the nanofluids having maximum thermal conductivity. Hence subsequently heat transfer coefficient is measured for sonication time of 6 hrs for Al_2O_3-water nanofluid. With extensive sonication (after 6 hrs), thermal conductivity is decreased up to minimum level of thermal conductivity of base fluid (water), as shown by 0.0001% Al_2O_3-water nanofluid in Fig. 5.2. So the sonication time of maximum thermal conductivity of Al_2O_3-water nanofluid, considered as sonication time for Al_2O_3-water nanofluid. The Al_2O_3-water nanofluid of maximum thermal conductivity is selected to investigate heat transfer coefficient of Al_2O_3-water nanofluid.

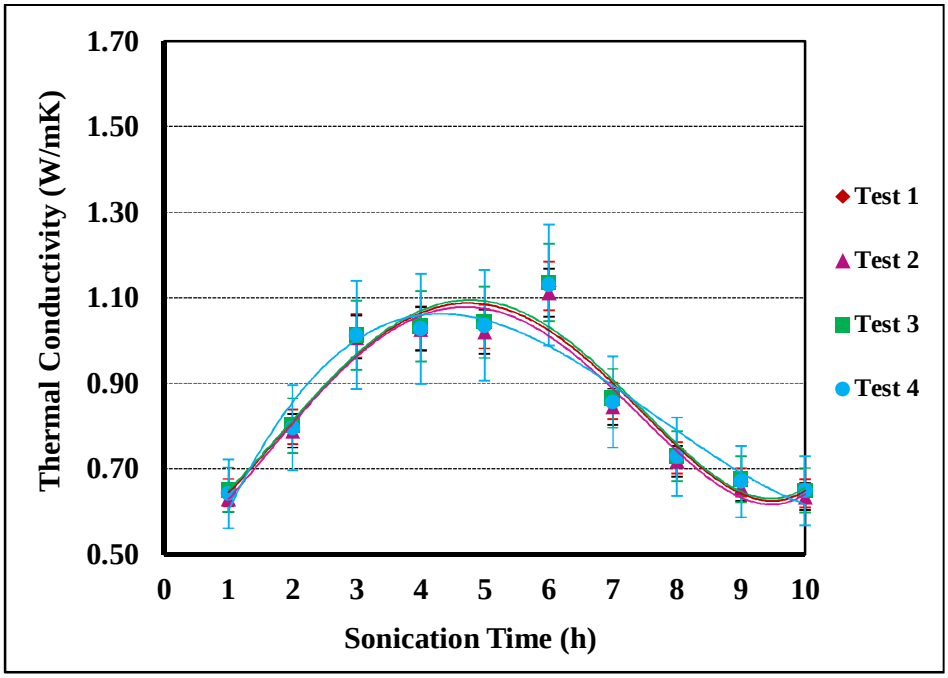

Figure 5.1. Repeatability test for thermal conductivity of 0.0001% Al_2O_3-water nanofluid.

Initially at 1 hrs, thermal conductivity of 0.1% Al_2O_3-water nanofluid is observed to be less than thermal conductivity of 0.01% Al_2O_3-water nanofluid. This is probably because 0.1% Al_2O_3-water nanofluid was not fully prepared initially due to high concentration of nanoparticles.

Fresh Al_2O_3-water nanofluid of each concentration prepared again to obtain maximum thermal conductivity and to investigate heat transfer coefficient. The thermal conductivity of prepared (containing maximum thermal conductivity) Al_2O_3-water nanofluid remains constant for about 16-18 hours after sonication. Hence, heat transfer coefficient of Al_2O_3-water nanofluid is measured within this window of 16 hrs.

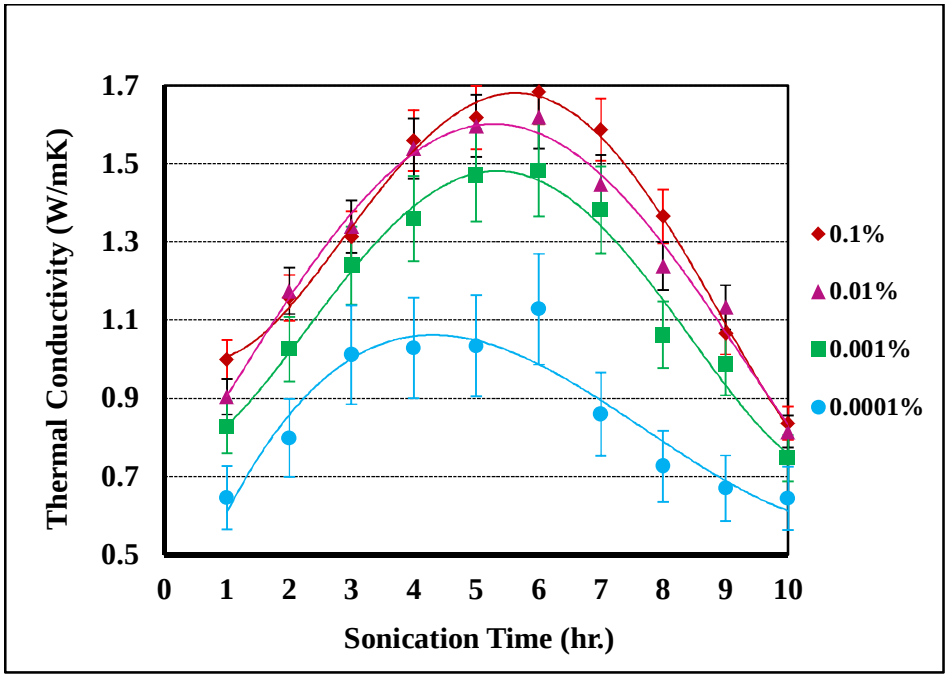

Figure 5.2. Thermal conductivity of Al_2O_3-water nanofluids with sonication time.

5.1.2 Thermal Conductivity of TiO_2-Water Nanofluids

Figure 5.3 shows variation of thermal conductivity of TiO_2-water nanofluid with sonication time. Thermal conductivity of TiO_2-water nanofluid increases with increase in sonication time in the beginning until it reaches a maximum value and then decreases.

Based on concentration of nanoparticles, the sonication time from 2.5 hrs to 3 hrs is considered to prepare the TiO_2-water nanofluid. The thermal conductivity of TiO_2-water nanofluid is almost constant for 24 hours and then

reduces due to variation in surrounding temperature and sedimentation of nano-particles.

Similar to Al_2O_3-water nanofluid, initially the thermal conductivity of 0.1% TiO_2-water nanofluid is observed less than the thermal conductivity of 0.01% TiO_2-water nanofluid possibly due to non-homogenous mixture or not fully prepared nanofluid. For step increased concentration from 0.001% to concentration 0.01%, an increment in thermal conductivity of the TiO_2-water nanofluid is relatively higher, possible reasons need to investigate more. Similar to Al_2O_3-water nanofluid, it is observed that thermal conductivity increases with increase in concentration of nanoparticles.

Fresh TiO_2-water nanofluid of each concentration prepared again to obtain maximum thermal conductivity and to investigate heat transfer coefficient. The thermal conductivity of prepared (containing maximum thermal conductivity) TiO_2-water nanofluid remains constant for about 24 hours after sonication. Hence, heat transfer coefficient of TiO_2-water nanofluid is measured within this window of 24 hrs.

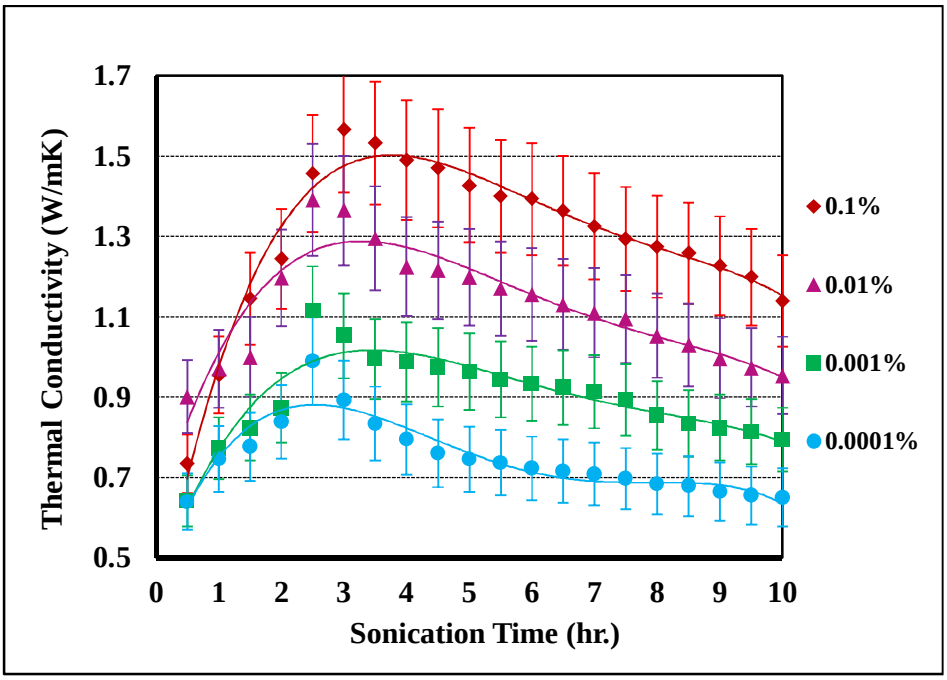

Figure 5.3. Thermal conductivity of TiO_2-water nanofluids with Sonication Time.

5.1.3 Thermal Conductivity of ZnO-Water Nanofluids

Figure 5.4 shows the variation of thermal conductivity of ZnO-water nanofluid with sonication time. Thermal conductivity of ZnO-water nanofluid increases with increase in sonication time in the beginning until it reaches a maximum value and then decreases. Similar to above-selected nanofluids, the sonication time at which the thermal conductivity is maximum, is considered as the optimum sonication time to prepare the ZnO-water nanofluid.

From the graph, it is observed that thermal conductivity is maximum for sonication time of 4 hrs for all the concentrations of ZnO-water nanofluid. The thermal conductivity of ZnO-water nanofluid remains almost constant for 16-20 hours and then reduces due to variation in surrounding temperature and sedimentation of particles. Similar to Al_2O_3-water nanofluids and TiO_2-water nanofluid, it is observed that thermal conductivity increases with increase in concentration of nanoparticles in water.

Fresh ZnO-water nanofluid of each concentration prepared again to obtain maximum thermal conductivity of the ZnO-water nanofluid and to investigate heat transfer coefficient of ZnO-water nanofluid. The thermal conductivity of prepared (containing maximum thermal conductivity) ZnO-water nanofluid remains constant for about 16-20 hours after sonication. Hence, heat transfer coefficient of ZnO-water nanofluid is measured within this window of 16 hrs.

5.1.4 Thermal Conductivity of MWCNT-Water Nanofluids

Figure 5.5 shows variation of thermal conductivity of MWCNT-water nanofluid with sonication time. Thermal conductivity of MWCNT-water nanofluid increases with increase in sonication time in the beginning until it reaches a maximum value and then decreases. Similar to Al_2O_3-water nanofluid, TiO_2-water nanofluid and Zno-water nanofluid, the sonication time at which the thermal conductivity is maximum, is considered as the optimum sonication time to prepare the MWCNT-water nanofluid.

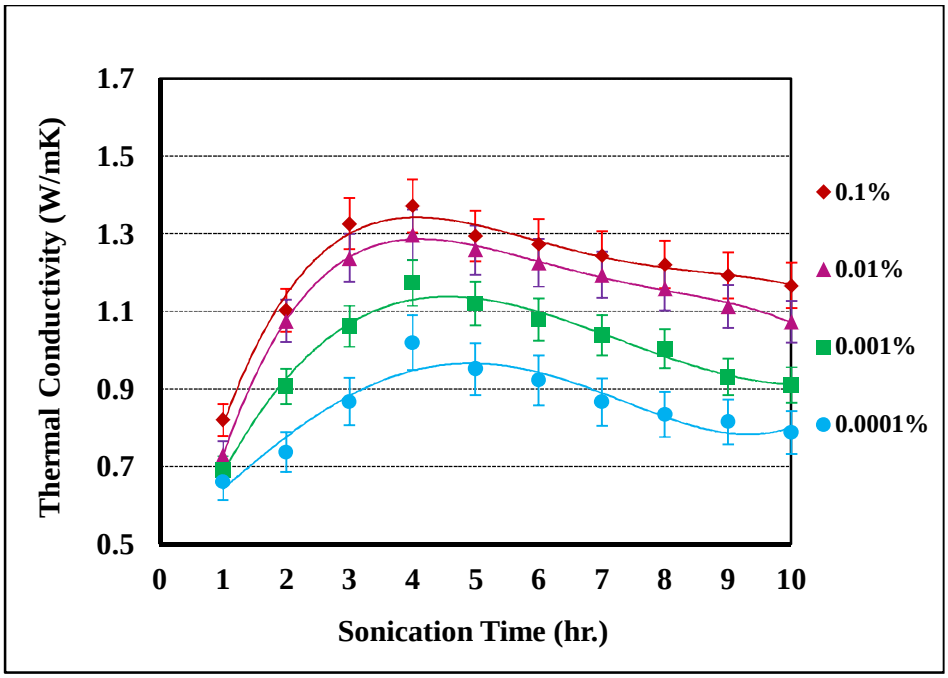

Figure 5.4. Thermal conductivity of ZnO-water nanofluids with sonication time.

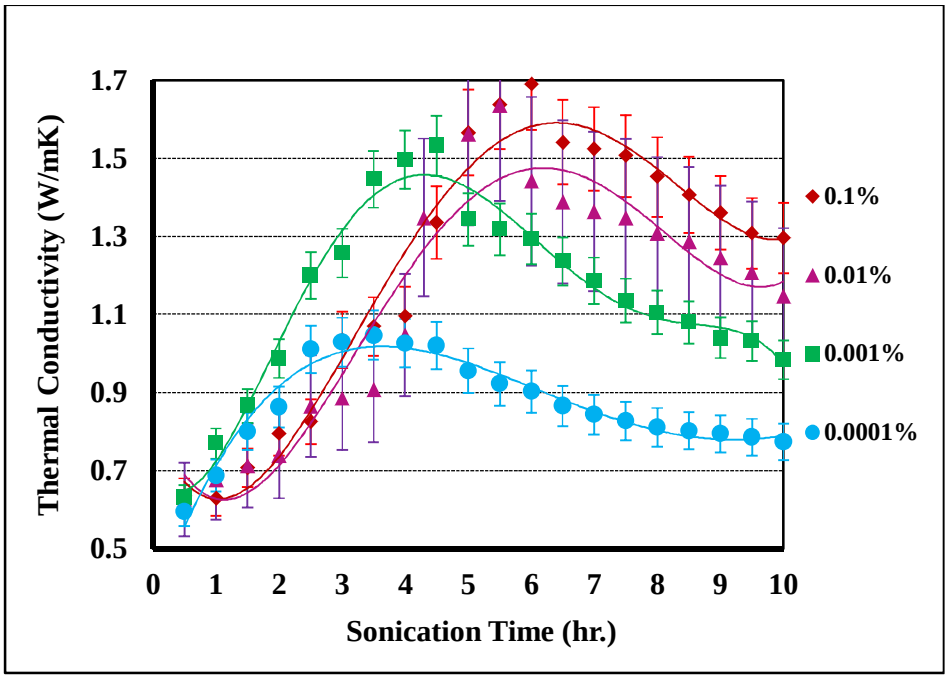

Figure 5.5. Thermal conductivity of MWCNT-water nanofluids with sonication time.

Based on concentration of nanoparticle, the sonication time from 3.5 hrs to 6 hrs is considered to prepare the MWCNT-water nanofluid. The thermal conductivity of MWCNT-water nanofluid remains almost constant for 12-16 hours and then reduces due to variation in surrounding temperature and sedimentation of particles. The initial thermal conductivity of 0.01% MWCNT-water nanofluid and 0.1% MWCNT-water nanofluid is less than 0.001% MWCNT-water nanofluid and 0.0001% MWCNT-water nanofluid possibly due to non-homogenous mixture or not fully prepared nanofluid. However maximum thermal conductivity is higher for higher concentrated nanofluid. Similar to other nanofluids, it is also observed that thermal conductivity increases with increase in concentration of nanoparticles in water.

Fresh MWCNT-water nanofluid of each concentration prepared again to obtain maximum thermal conductivity and to investigate heat transfer coefficient. Thermal conductivity of prepared (containing maximum thermal conductivity) MWCNT-water nanofluid remains constant for about 12-16 hours after sonication. Hence, heat transfer coefficient of MWCNT-water nanofluid is measured within this window of 12 hrs.

5.2 Heat Transfer Coefficient

Convective (single phase) and flow boiling (two phase) study was conducted for measurement of Heat Transfer Coefficient (HTC). The experiment was stopped at starting of film boiling to avoid leakage of nanofluid and accidental by breaking of the glass tube. Experimental data for convective and boiling HTC is represented in this section.

5.2.1 Heat Transfer Coefficient of Water

To assess the repeatability of the tests, the experimental heat transfer coefficient of distilled water tested four times. Figure 5.6 shows the repeatability plots for heat transfer coefficient of distilled water. Heat transfer coefficient of distilled water is plotted on the y-axis whereas heat flux is plotted on the x-axis.

The four plots presented herein show that the values of heat transfer coefficient show good repeatability in the experiments conducted.

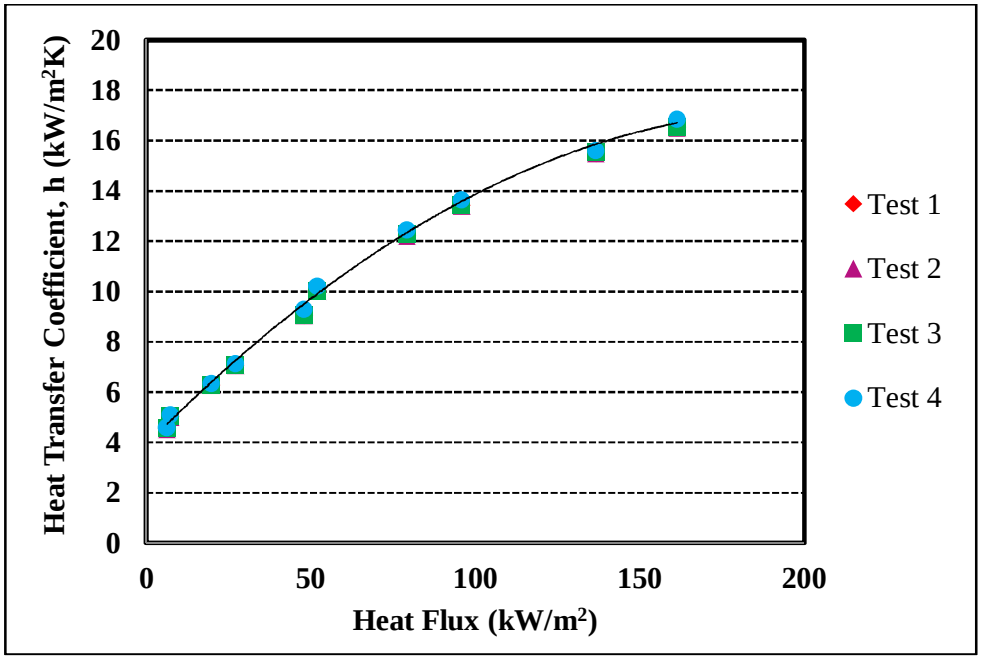

Figure 5.6. Results of repeatability test for water at a pressure of 1 bar, sub cooling of 20°C and mass flux of 400 kg/m^{2}s.

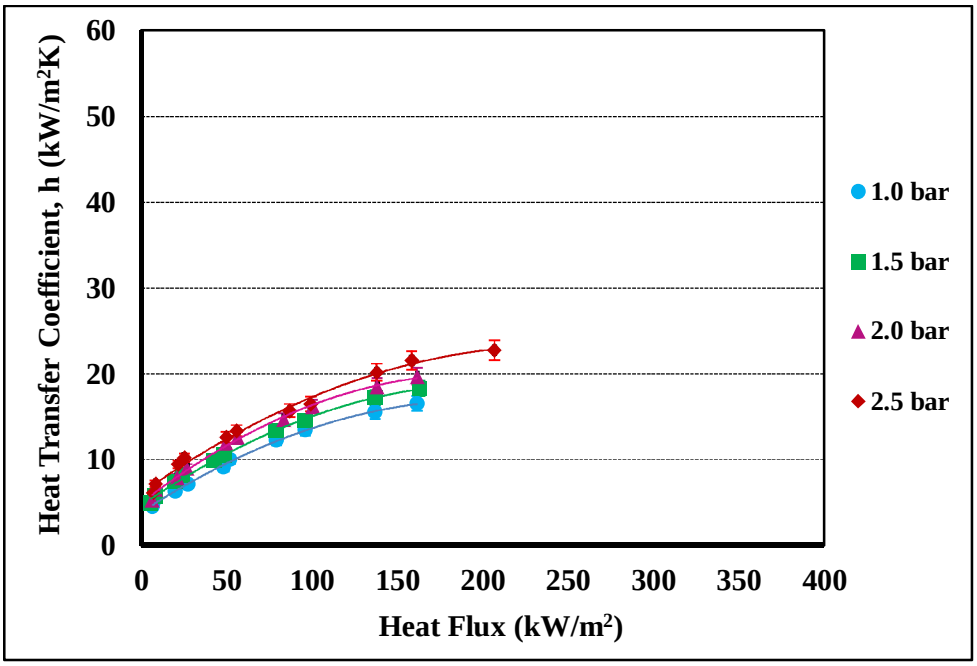

Figure 5.7. Variation of HTC of water with heat flux at a sub cooling of 20°C and mass flux of 400 kg/m^{2}s.

Experimental data in Fig. 5.7 shows variation of heat transfer coefficient (HTC) of distilled water with heat fluxes in single phase followed by boiling. It was nucleate boiling followed by film boiling; the experiment was stopped at starting of film boiling to avoid leakage of nanofluid and any accident by the back pressure (shock) of the steam at high heat flux. The experimental results show that heat transfer coefficient increases with increase in heat flux. It is also shown in same figure that heat transfer coefficient increases with increase in pressure in designed test section at all heat fluxes. The increase in heat transfer coefficient is 23.81% at 2.5 bar over 1.0 bar at 165 kW/m^2 heat flux, 20ºC inlet sub cooling of distilled water and mass flux of 400 kg/m^2s (Re=10000).

5.2.2 Heat Transfer Coefficient of Al_2O_3-Water Nanofluid

To assess the repeatability of the tests, the experimental heat transfer coefficient of 0.0001% Al_2O_3-water nanofluids tested four times. Figure 5.8 shows the repeatability plots for heat transfer coefficient of 0.0001% Al_2O_3-water nanofluids. Heat transfer coefficient of 0.0001% Al_2O_3-water nanofluids is plotted on the y-axis whereas heat flux is plotted on the x-axis. The four plots presented herein show that the values of heat transfer coefficient of 0.0001% Al_2O_3-water nanofluids show good repeatability in the experiments conducted.

Experimental data in Fig. 5.9, Fig. 5.10, Fig. 5.11 and Fig. 5.12 show variation of heat transfer coefficient of Al_2O_3-water nanofluid with heat flux and pressure for different concentrations of nanofluid at a mass flux of 400 kg/m^2s. The experimental results show that HTC increases with increase in heat flux for all concentrations of nanofluid.

Experimental data also shows that HTC increases with increase in pressure at a mass flux of 400 kg/m^2s and at all heat fluxes. The appeared values of heat transfer coefficient are at low concentrations. Low concentration for the nanofluids is used to facilitate the visualization studies and the appeared bubbles during boiling may affect the value of HTC. The values of HTC are similar to Manca et al. (2011) for Al_2O_3-water nanofluid.

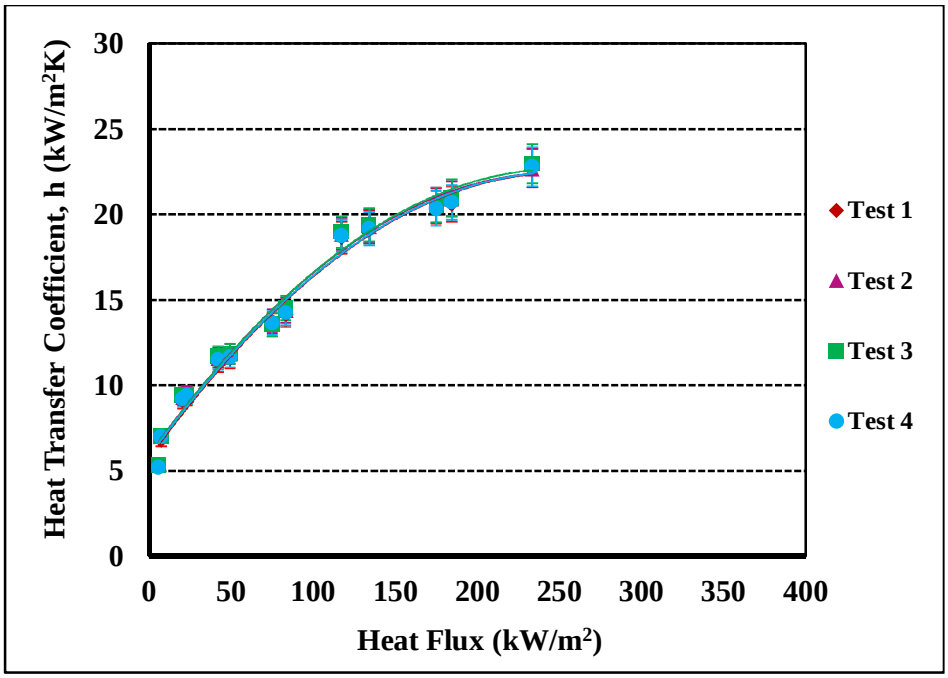

Figure 5.8. Results of repeatability test for 0.0001% Al_2O_3-water nanofluid at a pressure of 1 bar, sub cooling of 20°C and mass flux of 400 kg/m^{2}s.

The maximum increase in HTC due to increase in pressure for 0.0001% Al_2O_3-water nanofluid at 2.5 bar and heat flux of about 230 kW/m^2 and mass flux of 400 kg/m^{2}s with respect to that at 1.0 bar is about 30% (refer Fig. 5.9).

The maximum increase in HTC due to increase in pressure for 0.001% Al_2O_3-water nanofluid at 2.5 bar and heat flux of about 180 kW/m^2 and mass flux of 400 kg/m^{2}s with respect to that at 1.0 bar is about 34% (refer Fig. 5.10).

The maximum increase in HTC due to increase in pressure for 0.01% Al_2O_3-water nanofluid at 2.5 bar and heat flux of about 185 kW/m^2 and mass flux of 400 kg/m^{2}s with respect to that at 1.0 bar is about 32% (refer Fig. 5.11).

The maximum increase in HTC due to increase in pressure for 0.1% Al_2O_3-water nanofluid at 2.5 bar and heat flux of about 180 kW/m^2 and mass flux of 400 kg/m^{2}s with respect to that at 1.0 bar is about 68% (refer Fig. 5.12). It is found that maximum increase in HTC is with added 0.1% Al_2O_3 (maximum concentration) compared to water.

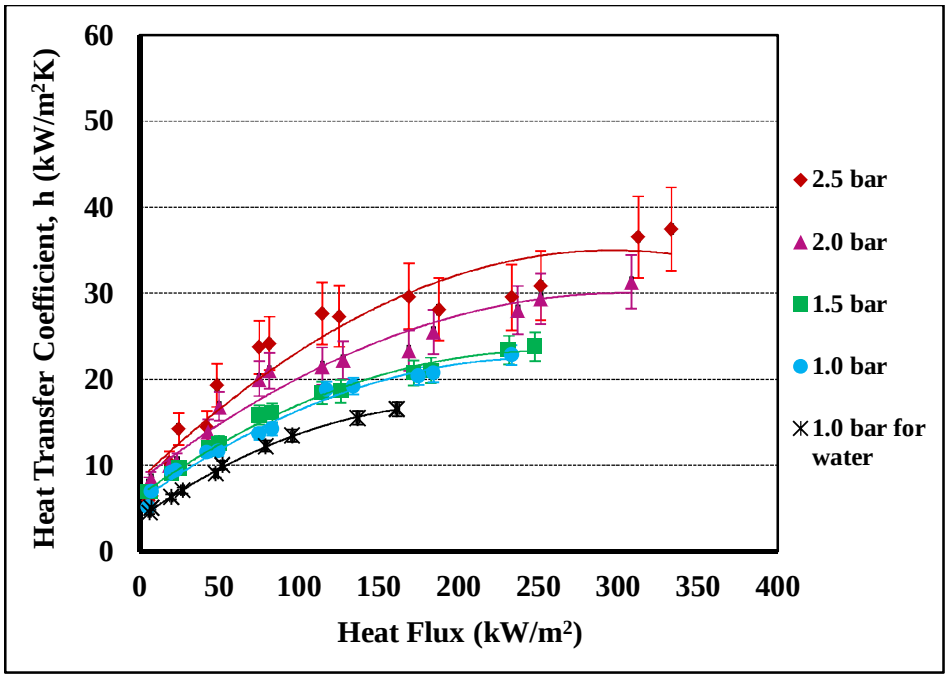

Figure 5.9. Variation of HTC of 0.0001% Al_2O_3-water nanofluid with heat flux at a sub cooling of 20°C and mass flux of 400 kg/m^{2}s.

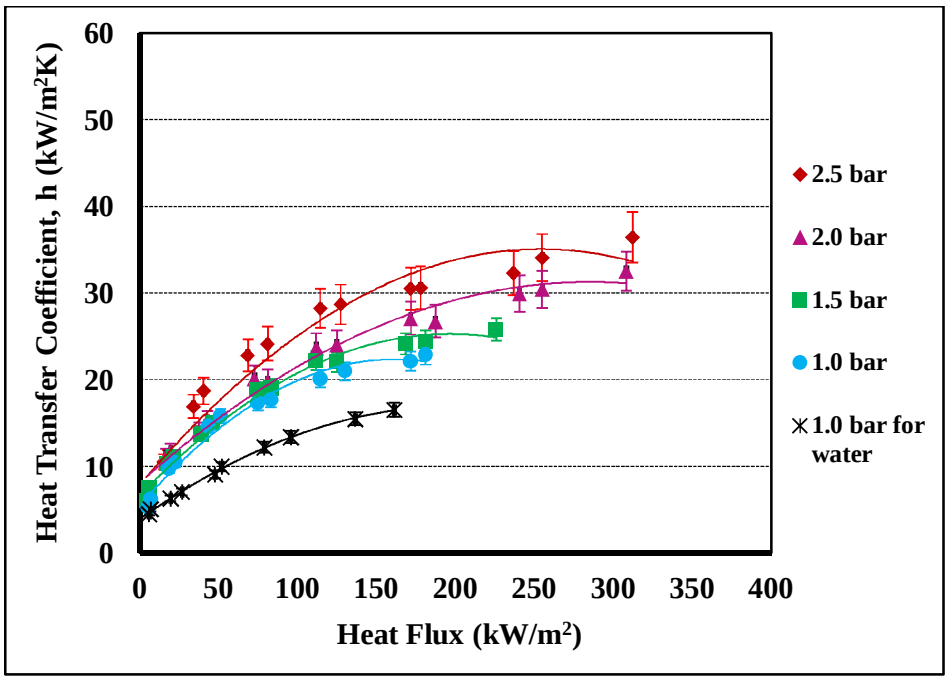

Figure 5.10. Variation of HTC of 0.001% Al_2O_3-water nanofluid with heat flux at a sub cooling of 20°C and mass flux of 400 kg/m^{2}s.

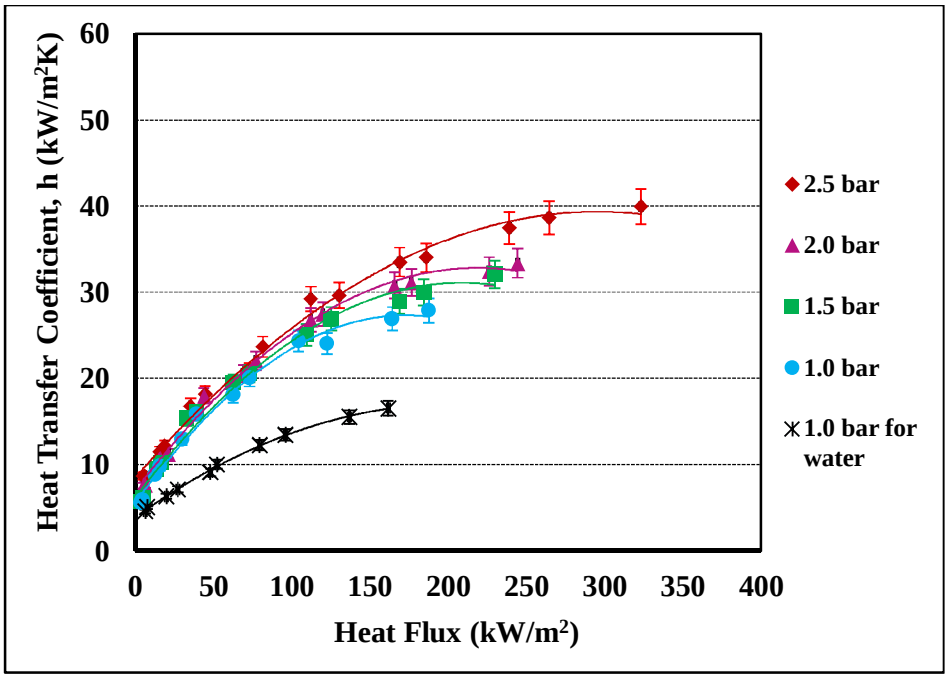

Figure 5.11. Variation of HTC of 0.01% Al_2O_3-water nanofluid with heat flux at a sub cooling of 20°C and mass flux of 400 kg/m^{2}s.

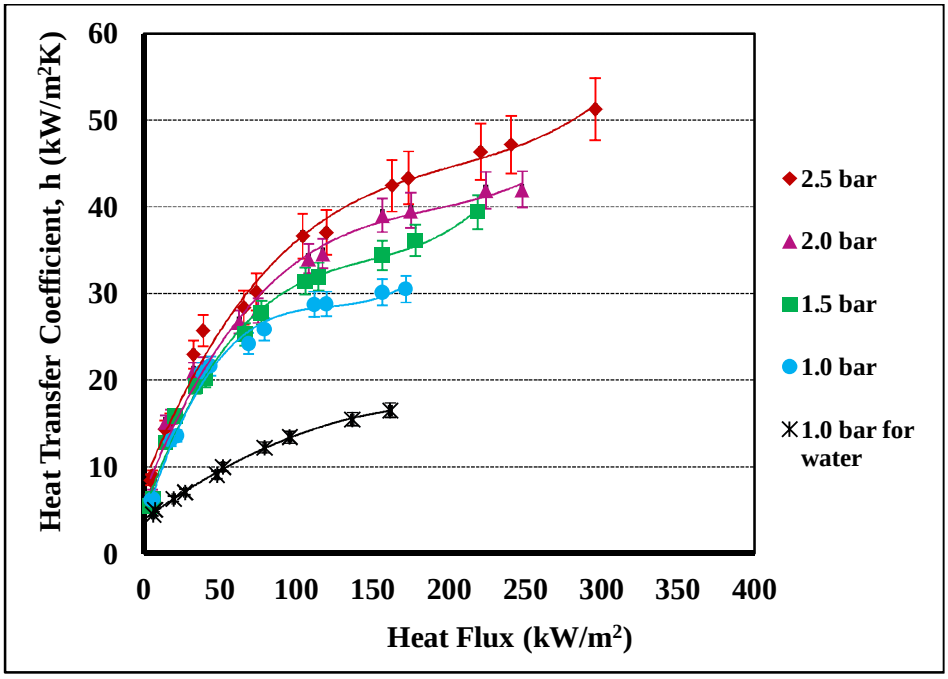

Figure 5.12. Variation of HTC of 0.1% Al_2O_3-water nanofluid with heat flux and pressure at 0.1% Al_2O_3 nanoparticle volume fraction, sub cooling of 20°C and mass flux of 400 kg/m^{2}s.

Figure 5.13 shows variation of heat transfer coefficient (HTC) of Al_2O_3-water nanofluid with heat flux for different concentrations of nanoparticles at a pressure of 1.0 bar and mass flux of 400 kg/m^{2}s.The experimental results show that in the convective region, i.e. at low heat flux, HTC of the nanofluid tested increases rapidly with increase in heat flux for all the concentrations of the nanofluid.

However this rate of increase in HTC does not continue in the boiling region i.e. at higher heat flux (i.e. heat flux > 120 kW/m^2), HTC increases marginally with increase in heat flux for all the concentrations of the nanofluid. It is also observed that HTC increases with increase in concentration of nanoparticles at all the heat fluxes.

Figure 5.14, Fig. 5.15 and Fig. 5.16 show similar behaviors for HTC at different pressures, i.e. 1.5, 2.0 and 2.5 bar respectively and a mass flux of 400 kg/m^{2}s.

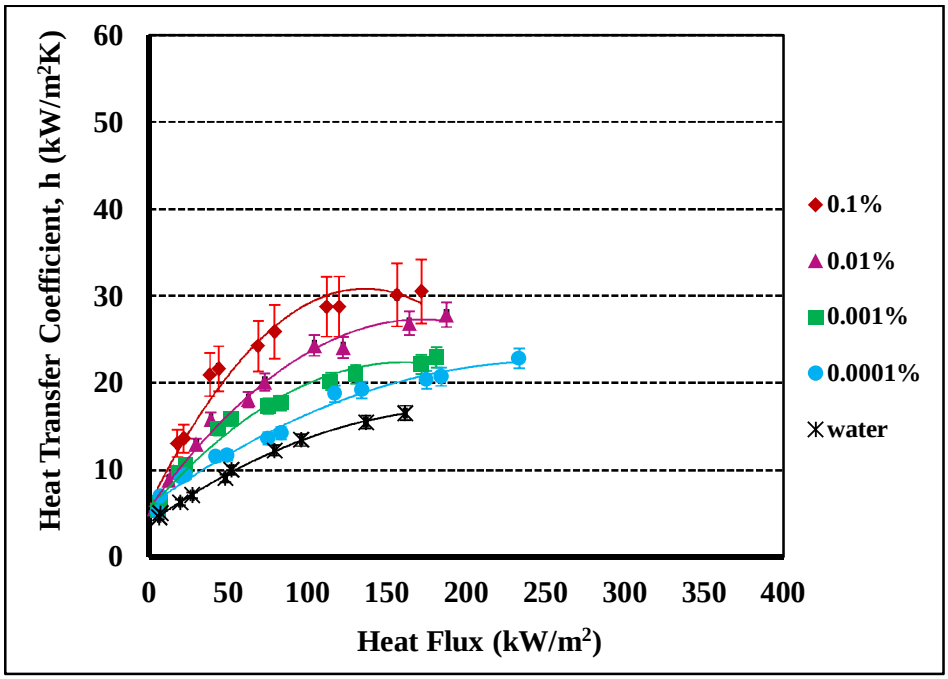

Figure 5.13. Variation of HTC of Al_2O_3-water nanofluids with heat flux at a pressure of 1.0 bar, sub cooling of 20°C and mass flux of 400 kg/m^{2}s.

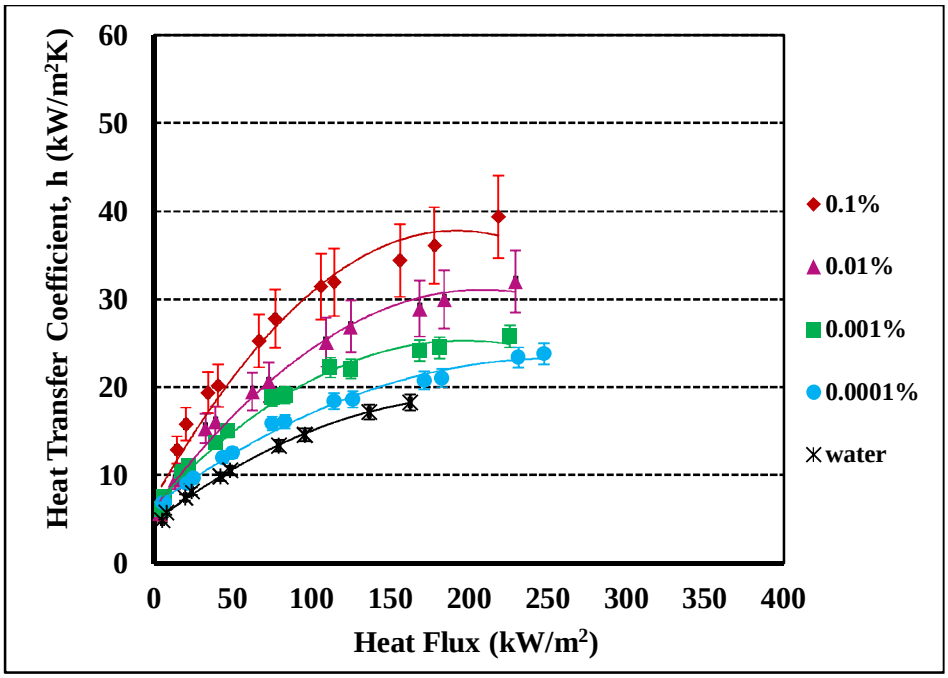

Figure 5.14. Variation of HTC of Al_2O_3-water nanofluids with heat flux at a pressure of 1.5 bar, sub cooling of 20°C and mass flux of 400 kg/m^{2}s.

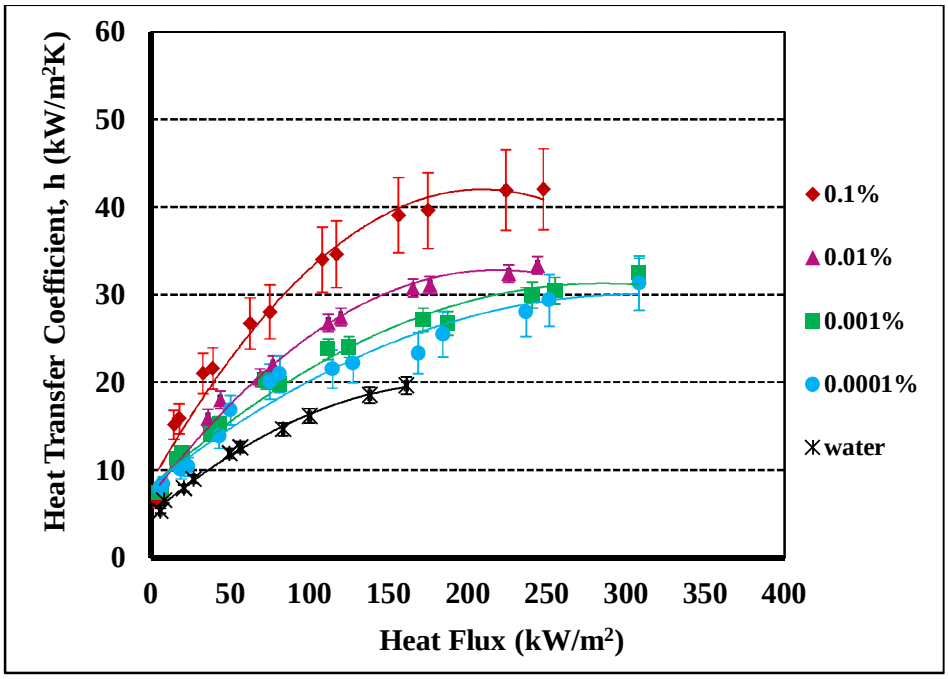

Figure 5.15. Variation of HTC of Al_2O_3-water nanofluids with heat flux at a pressure of 2.0 bar, sub cooling of 20°C and mass flux of 400 kg/m^{2}s.

The maximum increase in HTC with respect to water at 1.0 bar and mass flux of 400 kg/m^{2}s at heat flux of about 160 kW/m^2 is 23% for 0.0001% Al_2O_3-water nanofluid, 34% for 0.001% Al_2O_3-water nanofluid, 63% for 0.01% Al_2O_3-water nanofluid and 84% for 0.1% Al_2O_3-water nanofluid (refer Fig. 5.13).

The maximum increase in HTC with respect to water at 1.5 bar and mass flux of 400 kg/m^{2}s at heat flux of about 160 kW/m^2 is 14% for 0.0001% Al_2O_3-water nanofluid, 32% for 0.001% Al_2O_3-water nanofluid, 58% for 0.01% Al_2O_3-water nanofluid and 89% for 0.1% Al_2O_3-water nanofluid (refer Fig. 5.14).

The maximum increase in HTC with respect to water at 2.0 bar and mass flux of 400 kg/m^{2}s at heat flux of about 160 kW/m^2 is 19% for 0.0001% Al_2O_3-water nanofluid, 38% for 0.001% Al_2O_3-water nanofluid, 56% for 0.01% Al_2O_3-water nanofluid and 99% for 0.1% Al_2O_3-water nanofluid (refer Fig. 5.15).

The maximum increase in HTC with respect to water at 2.5 bar and mass flux of 400 kg/m^{2}s at heat flux of about 210 kW/m^2 is 30% for 0.0001% Al_2O_3-water nanofluid, 42% for 0.001% Al_2O_3-water nanofluid, 65% for 0.01% Al_2O_3-water nanofluid and 104% for 0.1% Al_2O_3-water nanofluid (refer Fig. 5.16).

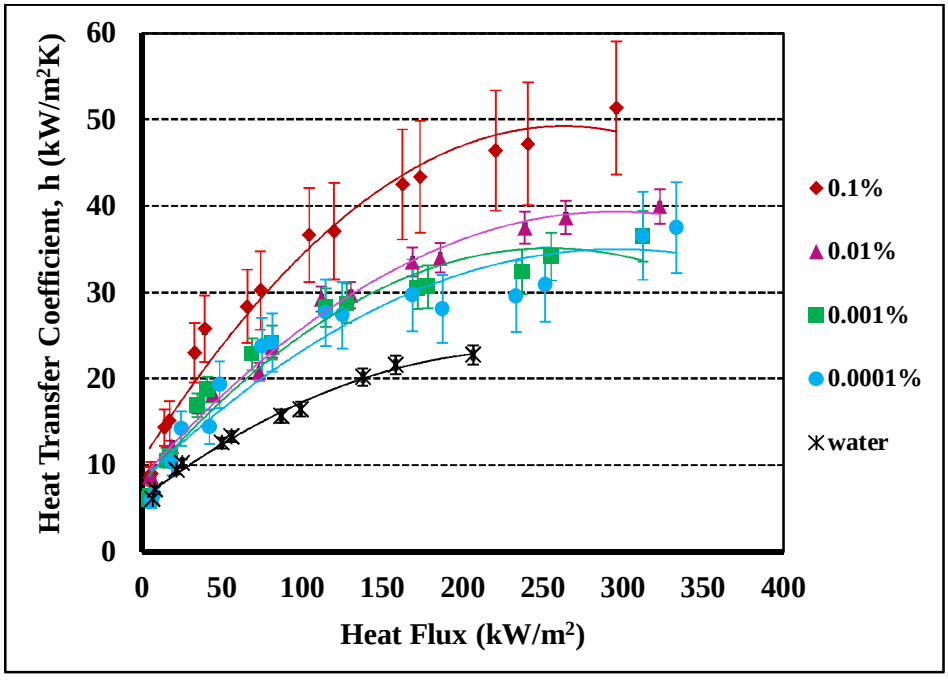

Figure 5.16. Variation of HTC of Al_2O_3-water nanofluids with heat flux at a pressure of 2.5 bar, sub cooling of 20°C and mass flux of 400 kg/m^{2}s.

5.2.3 Heat Transfer Coefficient of TiO_2-Water Nanofluid

Experimental data in Fig. 5.17, Fig. 5.18, Fig. 5.19 and Fig. 5.20 show heat transfer coefficient (HTC) of TiO_2-water nanofluid for concentrations of 0.0001%, 0.001%, 0.01% and 0.1% respectively.

The experimental results show that similar to Al_2O_3-water nanofluid heat transfer increases with increase in heat flux. It is also shown in same figure that heat transfer coefficient increases with increase in pressure at all heat fluxes.

It is also observed that increase in heat transfer coefficient is significant in flow boiling (i.e. heat flux > 150 kW/m^2) compared to convective boiling. Heat flux for the test section increases with increase in pressure as well as with the increase in concentration of the nanofluid.

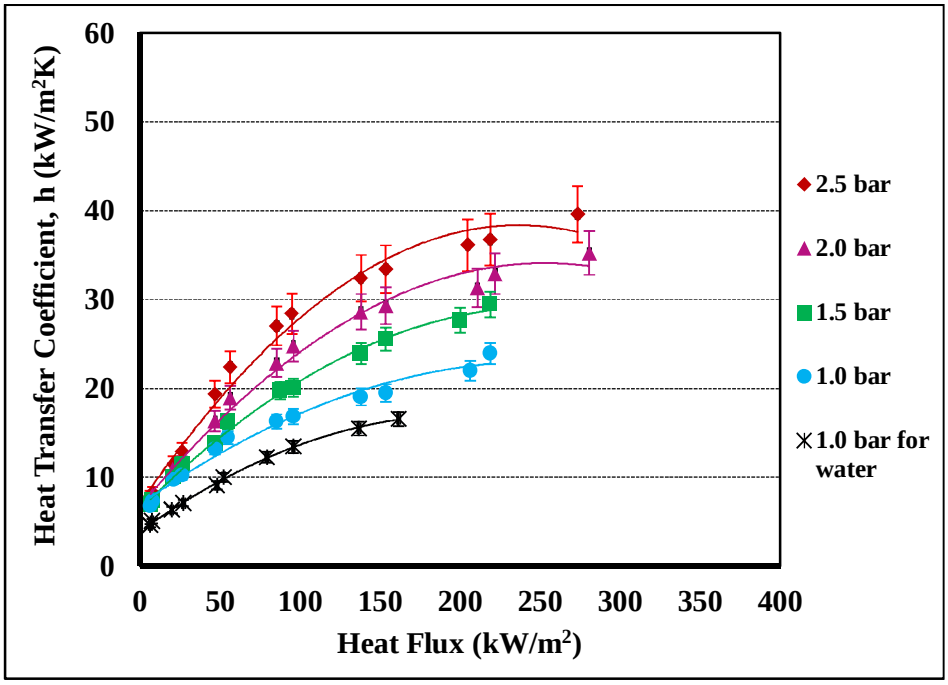

Figure 5.17. Variation of HTC of 0.0001% TiO_2-water nanofluid with heat flux at a sub cooling of 20°C and mass flux of 400 kg/m^{2}s.

The maximum increase in HTC due to increase in pressure for 0.0001% TiO_2-water nanofluid at 2.5 bar and heat flux of about 220 kW/m^2 and mass flux of 400 kg/m^{2}s with respect to that at 1.0 bar is about 54% (refer Fig. 5.17).

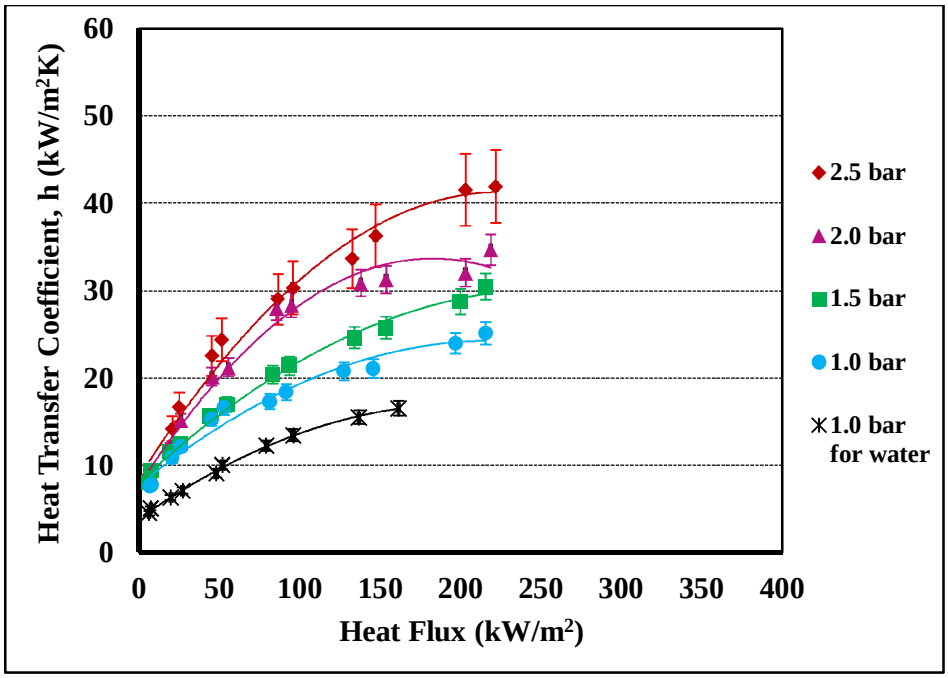

Figure 5.18. Variation of HTC of 0.001% TiO_2-water nanofluid with heat flux at a sub cooling of 20°C and mass flux of 400 kg/m^{2}s.

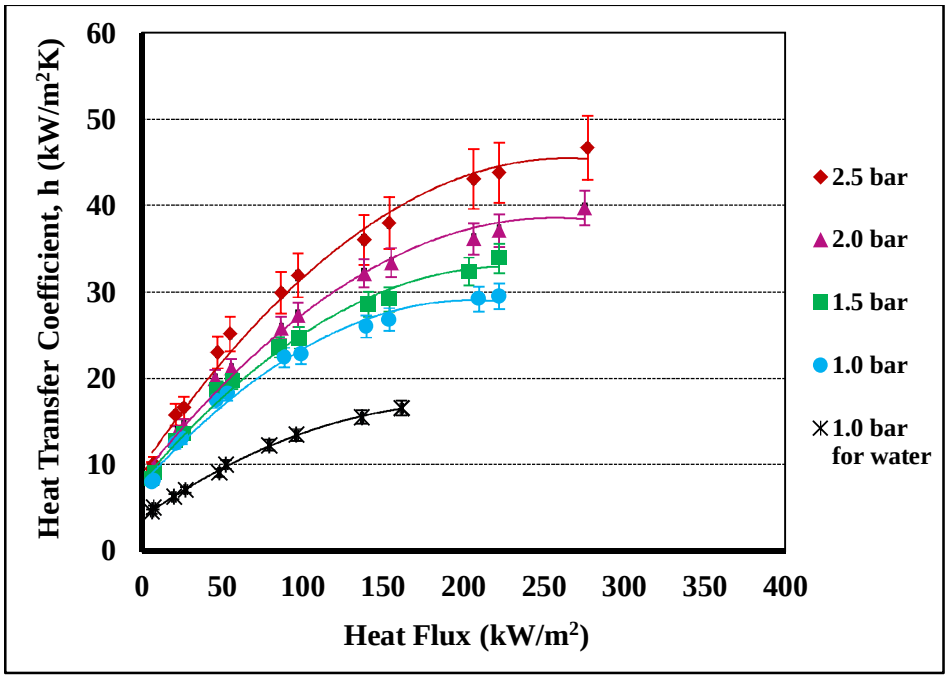

Figure 5.19. Variation of HTC of 0.01% TiO_2-water nanofluid with heat flux at a sub cooling of 20°C and mass flux of 400 kg/m^{2}s.

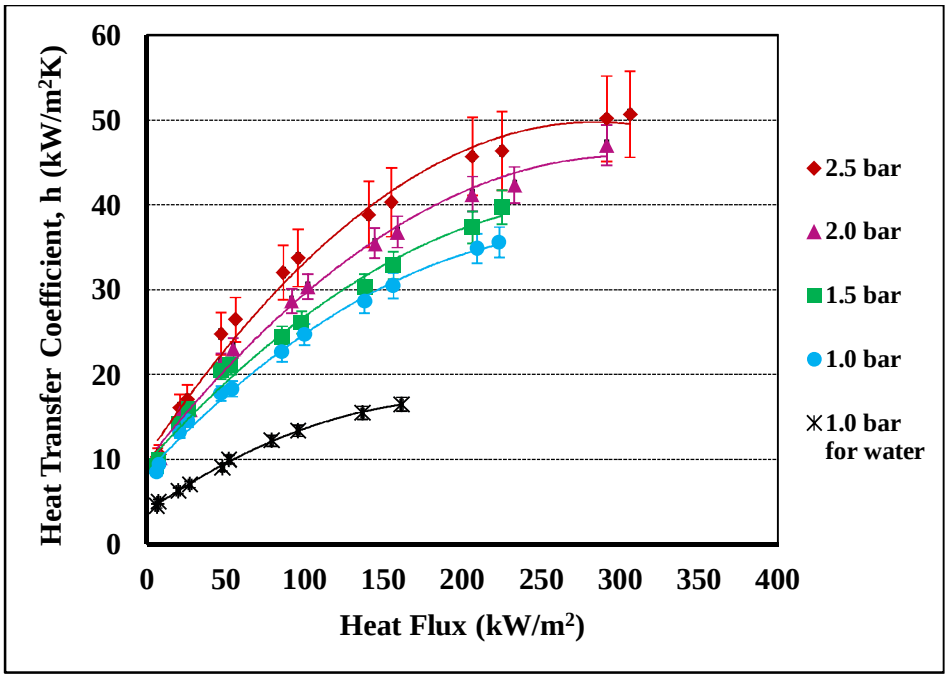

Figure 5.20. Variation of HTC of 0.1% TiO_2-water nanofluid with heat flux at a sub cooling of 20°C and mass flux of 400 kg/m^{2}s.

The maximum increase in HTC due to increase in pressure for 0.001% TiO_2-water nanofluid at 2.5 bar and heat flux of about 220 kW/m^2 and mass flux of 400 kg/m^{2}s with respect to that at 1.0 bar is about 67% (refer Fig. 5.18). The maximum increase in HTC due to increase in pressure for 0.01% TiO_2-water nanofluid at 2.5 bar and heat flux of about 220 kW/m^2 and mass flux of 400 kg/m^{2}s with respect to that at 1.0 bar is about 49% (refer Fig. 5.19). The maximum increase in HTC due to increase in pressure for 0.1% TiO_2-water nanofluid at 2.5 bar and heat flux of about 220 kW/m^2 and mass flux of 400 kg/m^{2}s with respect to that at 1.0 bar is about 30% (refer Fig. 5.20).

Fig. 5.21 shows variation of heat transfer coefficient (HTC) of TiO_2-water nanofluid with heat flux for different concentrations of TiO_2-water nanofluid at a pressure of 1.0 bar and mass flux of 400 kg/m^{2}s. The experimental results show that in the convective region, i.e. at low heat flux HTC of the TiO_2-water nanofluid tested increases rapidly with increase in heat flux for all the concentrations of the TiO_2-water nanofluid. However this rate of increase in HTC does not continue in the boiling region i.e. at higher heat flux HTC increases

marginally with increase in heat flux for all the concentrations of the TiO_2-water nanofluid. It is also observed that HTC increases with increase in concentration of TiO_2-water nanofluid at all the heat fluxes.

Figure 5.22, Fig. 5.23 and Fig. 5.24 show similar behavior for HTC at different pressures, i.e. 1.5, 2.0 and 2.5 bar respectively and a mass flux of 400 kg/m^{2}s. The maximum increase in HTC of TiO_2-water nanofluid with respect to water at 1.0 bar and mass flux of 400 kg/m^{2}s at heat flux of about 160 kW/m^2 is 18% for 0.0001% TiO_2-water nanofluid, 27% for 0.0001% TiO_2-water nanofluid, 62% for 0.0001% TiO_2-water nanofluid and 84% for 0.0001% TiO_2-water nanofluid for 0.0001%, 0.001%, 0.01% and 0.1% concentrations of the nanofluid respectively (refer Fig. 5.21).

The maximum increase in HTC of TiO_2-water nanofluid with respect to water at 1.5 bar and mass flux of 400 kg/m^{2}s at heat flux of about 160 kW/m^2 is 40% for 0.0001% TiO_2-water nanofluid, 41% for 0.001% TiO_2-water nanofluid, 59% for 0.01% TiO_2-water nanofluid and 80% for 0.1% TiO_2-water nanofluid (refer Fig. 5.22).

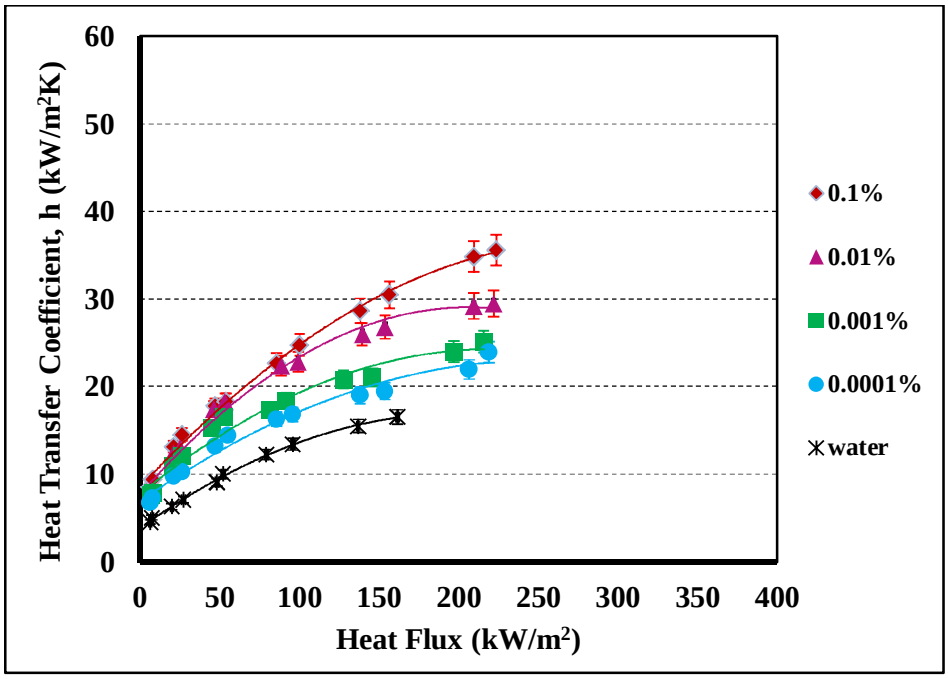

Figure 5.21. Variation of HTC of TiO_2-water nanofluids with heat flux at a pressure of 1.0 bar, sub cooling of 20°C and mass flux of 400 kg/m^{2}s.

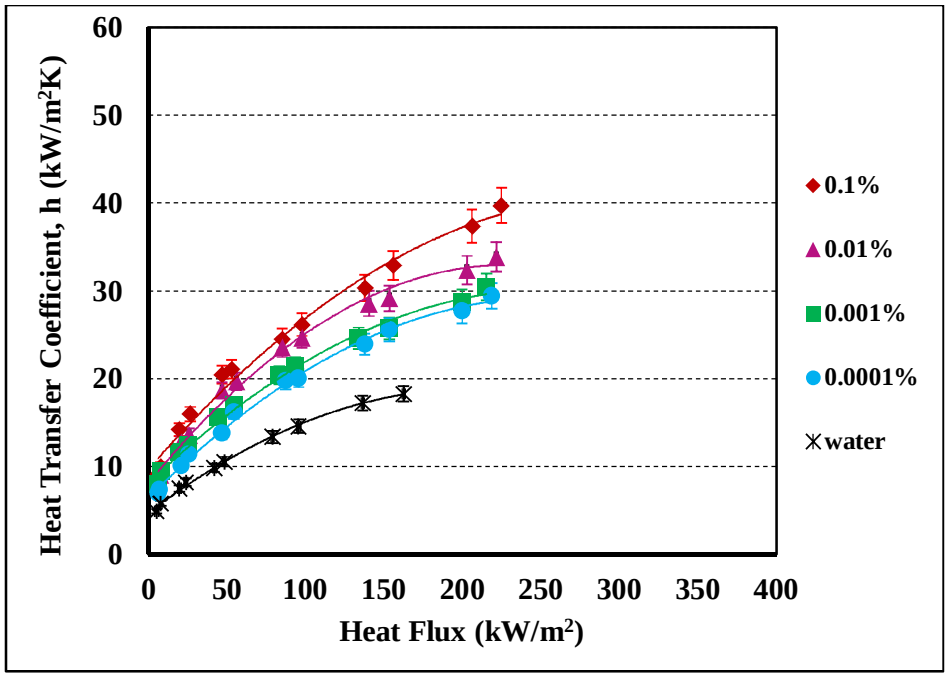

Figure 5.22. Variation of HTC of TiO_2-water nanofluids with heat flux at a pressure of 1.5 bar, sub cooling of 20°C and mass flux of 400 kg/m^{2}s.

The maximum increase in HTC of TiO_2-water nanofluid with respect to water at 2.0 bar and mass flux of 400 kg/m^{2}s at heat flux of about 160 kW/m^2 is 49% for 0.0001% TiO_2-water nanofluid, 59% for 0.001% TiO_2-water nanofluid, 70% for 0.01% TiO_2-water nanofluid and 87% for 0.1% TiO_2-water nanofluid (refer Fig. 5.23).The maximum increase in HTC of TiO_2-water nanofluid with respect to water at 2.5 bar and mass flux of 400 kg/m^{2}s at heat flux of about 210 kW/m^2 is 58% for 0.0001% TiO_2-water nanofluid, 83% for 0.001% TiO_2-water nanofluid, 89% for 0.01% TiO_2-water nanofluid and 101% for 0.1% TiO_2-water nanofluid (refer Fig. 5.24).

It is also found that increase in HTC is significant with 0.0001% TiO_2-water nanofluid compared to water at 2.5 bar. However, heat transfer coefficient doesn't increase with same rate with increase in concentration of nanoparticles as thermal conductivity of the nanofluid also does not increase with the same rate with increase in concentration of nanoparticles. The change in thermal conductivity of nanofluid with increase in concentration of nanoparticles is shown in figure 5.3. Additionally, there is also increase in coating of nanoparticles on the

heater rod with increase in concentration of nanoparticles, which inhibits heat flow.

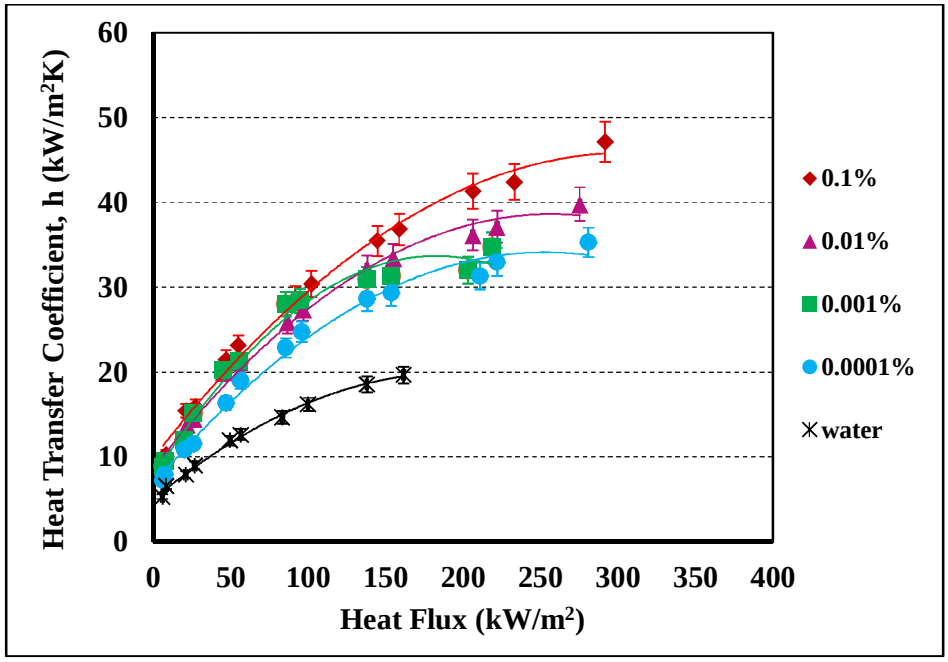

Figure 5.23. Variation of HTC of TiO_2-water nanofluids with heat flux at a pressure of 2.0 bar, sub cooling of 20°C and mass flux of 400 kg/m^{2}s.

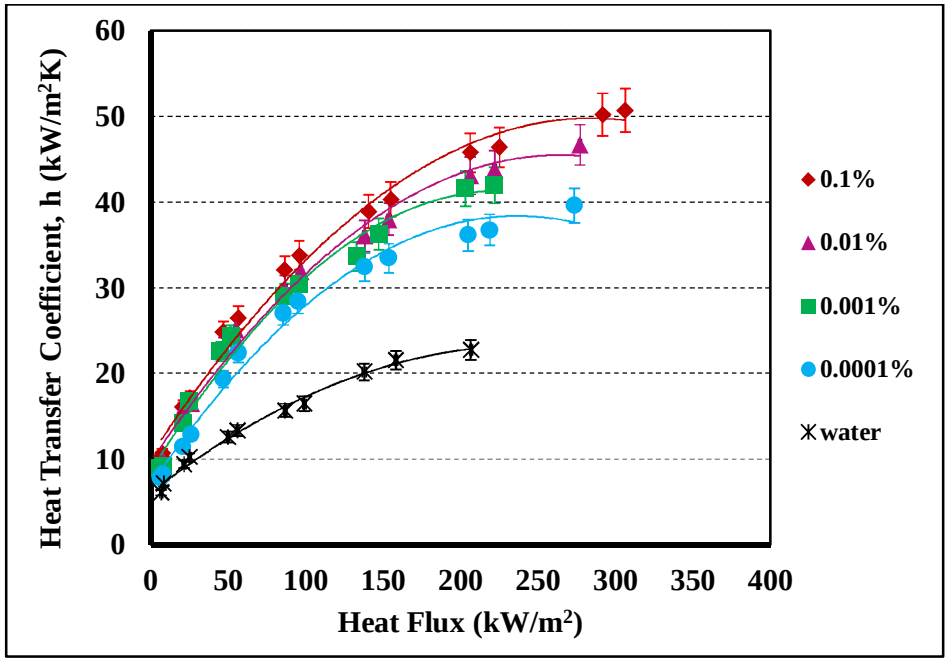

Figure 5.24. Variation of HTC of TiO_2-water nanofluids with heat flux at a pressure of 2.5 bar, sub cooling of 20°C and mass flux of 400 kg/m^{2}s.

5.2.4 Heat Transfer Coefficient of ZnO-Water Nanofluid

Experimental data in Fig. 5.25, Fig. 5.26, Fig. 5.27 and Fig. 5.28 show heat transfer coefficient of ZnO-water nanofluid for concentrations of 0.0001%, 0.001%, 0.01% and 0.1% respectively. The experimental results show that similar to Al_2O_3-water nanofluid and TiO_2-water nanofluid, heat transfer coefficient increases with increase in heat flux. It is also shown in same figure that heat transfer coefficient of ZnO-water nanofluid increases with increase in pressure in designed test section at all heat fluxes. The maximum increase in HTC due to increase in pressure for 0.0001% ZnO-water nanofluid at 2.5 bar and heat flux of about 300 kW/m^2 and mass flux of 400 kg/m^{2}s with respect to that at 1.0 bar is about 53% (refer Fig. 5.25). It is also observed that HTC for convective boiling at 1 bar has lower values than that for water at 1.0 bar. There are two opposite effects that affect HTC, they are thermal conductivity of the fluid and the coating of nanoparticles on the heating surface. It is quite possible that the effect of coating of nanoparticles on the heating surface is more predominant as compared to the effect of concentration of nanoparticles, leading to drop in HTC as compared to that of distilled water.

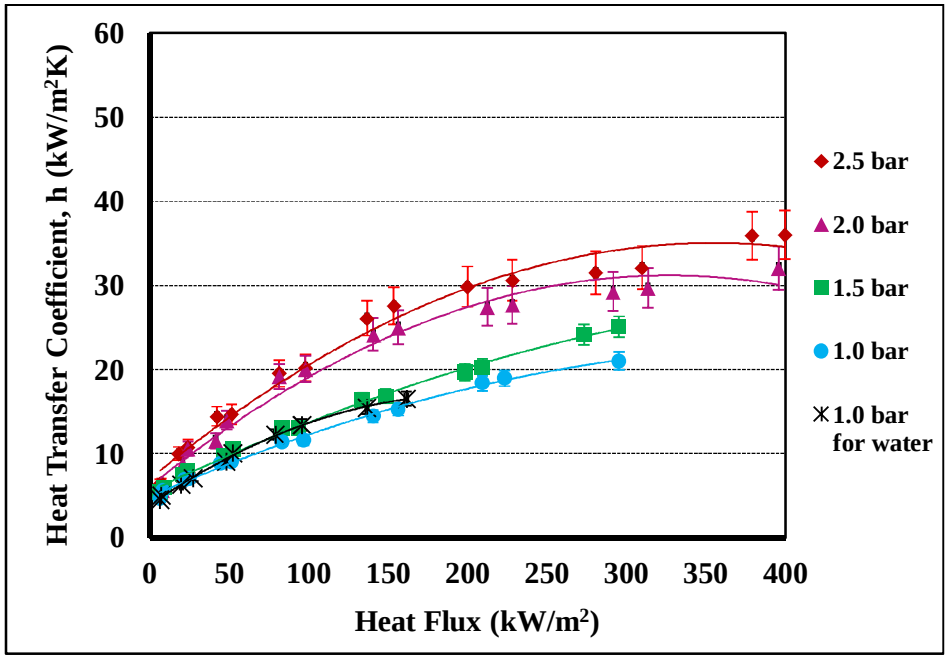

Figure 5.25. Variation of HTC of 0.0001% ZnO-water nanofluid with heat flux at a sub cooling of 20°C and mass flux of 400 kg/m^{2}s.

The maximum increase in HTC due to increase in pressure for 0.001% ZnO-water nanofluid at 2.5 bar and heat flux of about 300 kW/m^2 and mass flux of 400 kg/m^{2}s with respect to that at 1.0 bar is about 49% (refer Fig. 5.26).

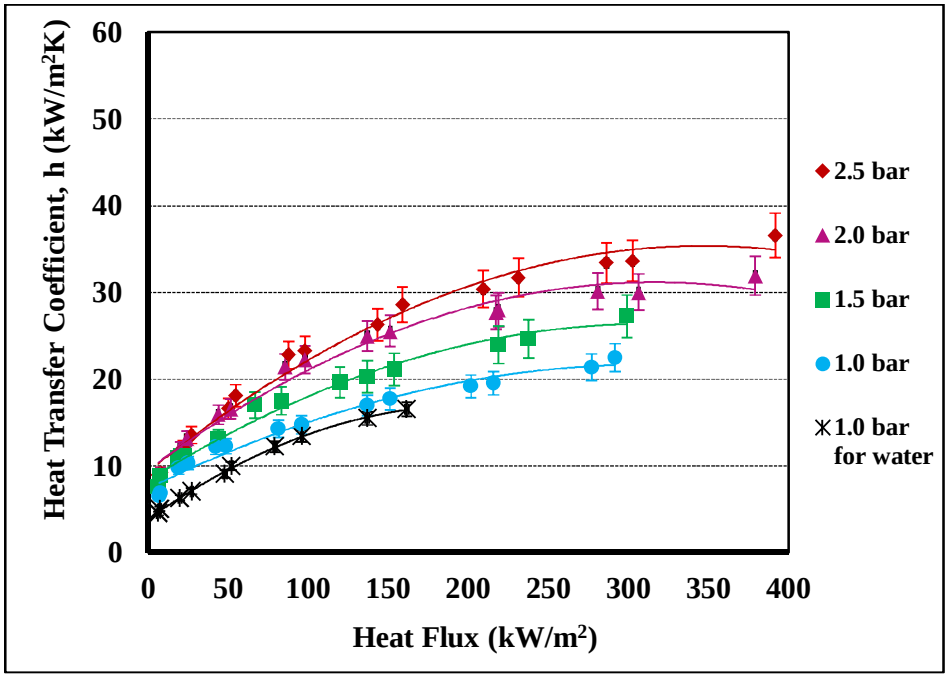

Figure 5.26. Variation of HTC of 0.001% ZnO-water nanofluid with heat flux at a sub cooling of 20°C and mass flux of 400 kg/m^{2}s.

The maximum increase in HTC due to increase in pressure for 0.01% ZnO-water nanofluid at 2.5 bar and heat flux of about 300 kW/m^2 and mass flux of 400 kg/m^{2}s with respect to that at 1.0 bar is about 35% (refer Fig. 5.27). The maximum increase in HTC due to increase in pressure for 0.1% ZnO-water nanofluid at 2.5 bar and heat flux of about 300 kW/m^2 and mass flux of 400 kg/m^{2}s with respect to that at 1.0 bar is about 39% (refer Fig. 5.28).

Figure 5.29 shows variation of heat transfer coefficient (HTC) of ZnO-water nanofluid with heat flux for different concentrations of ZnO-water nanofluid at a pressure of 1.0 bar and mass flux of 400 kg/m^{2}s. In the convective region, i.e. at low heat flux HTC of the ZnO-water nanofluid tested increases rapidly with increase in heat flux for all the concentrations of the ZnO-water nanofluid. However this rate of increase in HTC does not continue in the boiling region i.e. at higher heat flux HTC increases marginally with increase in heat flux for all the

concentrations of the ZnO-water nanofluid. It is also observed that HTC increases with increase in concentration of ZnO-water nanofluid at all the heat fluxes.

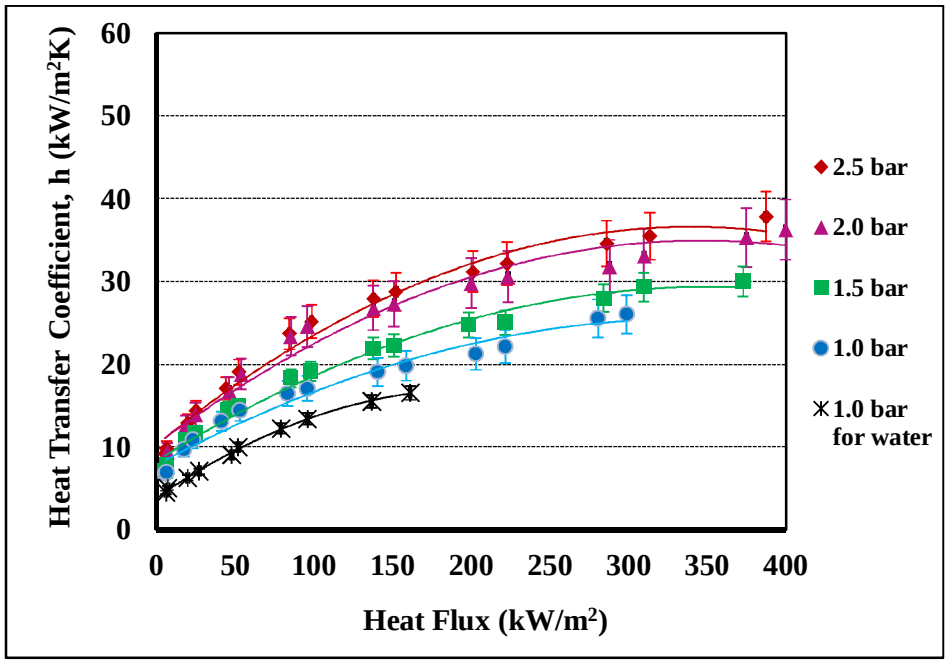

Figure 5.27. Variation of HTC of 0.01% ZnO-water nanofluid with heat flux at a sub cooling of 20°C and mass flux of 400 kg/m^{2}s.

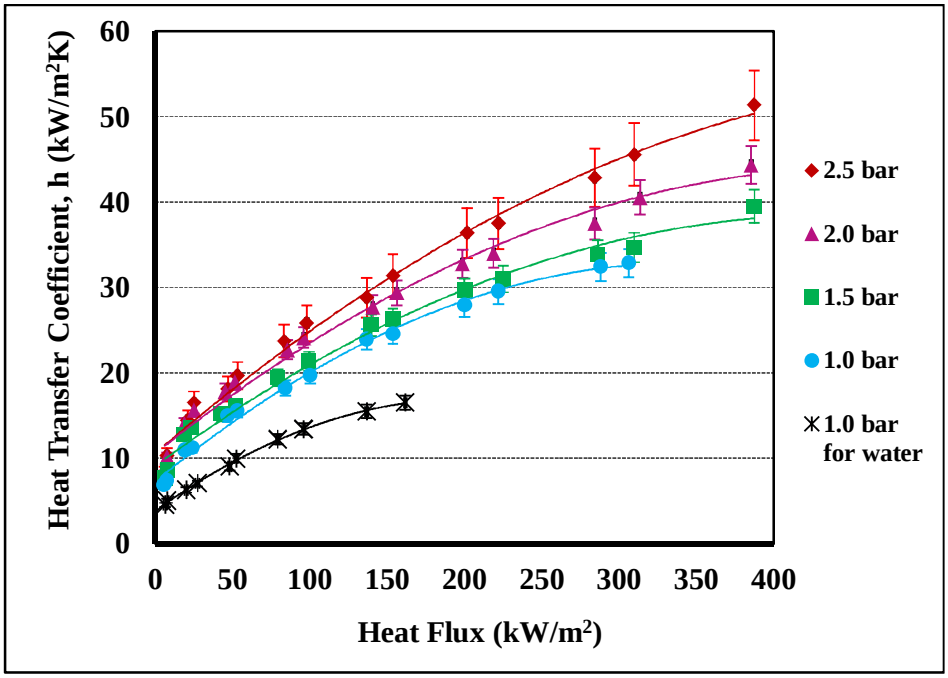

Figure 5.28. Variation of HTC of 0.1% ZnO-water nanofluid with heat flux at a sub cooling of 20°C and mass flux of 400 kg/m^{2}s.

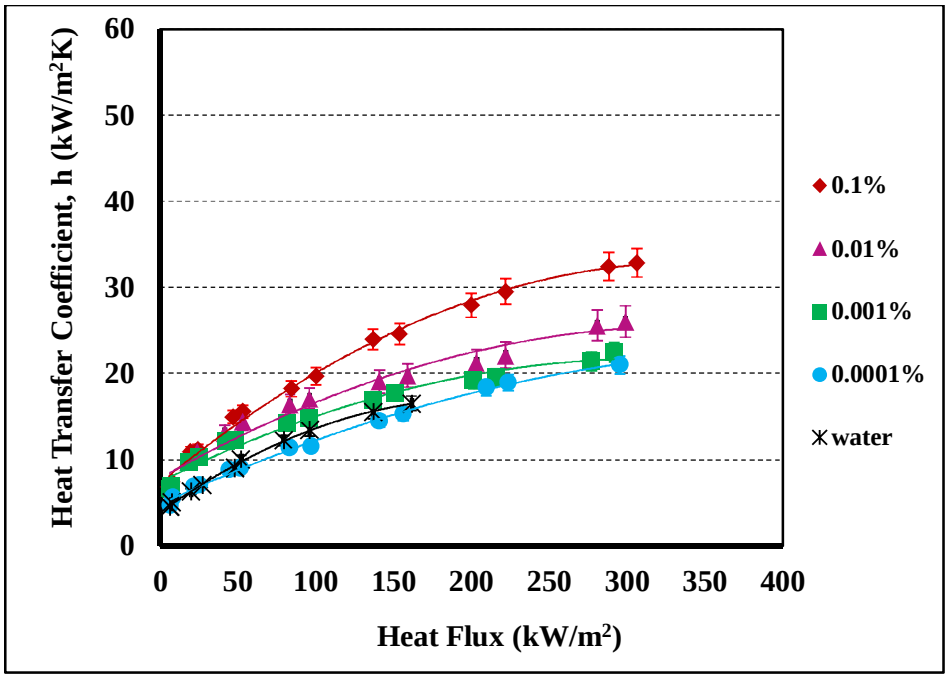

Figure 5.29. Variation of HTC of ZnO-water nanofluids with heat flux at a pressure of 1.0 bar, sub cooling of 20°C and mass flux of 400 kg/m^{2}s.

Figure 5.30, Fig 5.31 and Fig. 5.32 show similar behavior for HTC at different pressures, i.e. 1.5, 2.0 and 2.5 bar respectively and a mass flux of 400 kg/m^{2}s. The maximum increase in HTC of ZnO-water nanofluid with respect to water at 1.0 bar and mass flux of 400 kg/m^{2}s at heat flux of about 160 kW/m^2 is 2% for 0.0001% ZnO-water nanofluid, 7% for 0.001% ZnO-water nanofluid, 20% for 0.01% ZnO-water nanofluid and 49% for 0.1% ZnO-water nanofluid (refer Fig. 5.29).

The maximum increase in HTC of ZnO-water nanofluid with respect to water at 1.5 bar and mass flux of 400 kg/m^{2}s at heat flux of about 160 kW/m^2 is 3% for 0.0001% ZnO-water nanofluid, 16% for 0.001% ZnO-water nanofluid, 22% for 0.01% ZnO-water nanofluid and 44% for 0.1% ZnO-water nanofluid (refer Fig. 5.30). The maximum increase in HTC of ZnO-water nanofluid with respect to water at 2.0 bar and mass flux of 400 kg/m^{2}s at heat flux of about 160 kW/m^2 is 27% for 0.0001% ZnO-water nanofluid, 30% for 0.001% ZnO-water nanofluid, 39% for 0.01% ZnO-water nanofluid and 50% for 0.1% ZnO-water nanofluid (refer Fig. 5.31).

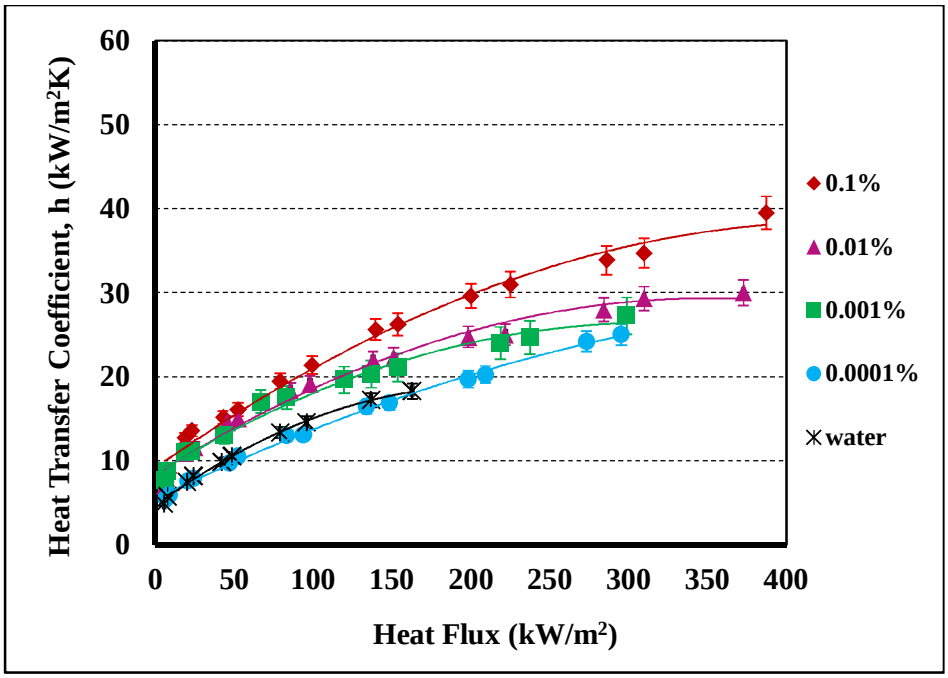

Figure 5.30. Variation of HTC of ZnO-water nanofluids with heat flux at a pressure of 1.5 bar, sub cooling of 20°C and mass flux of 400 kg/m^{2}s.

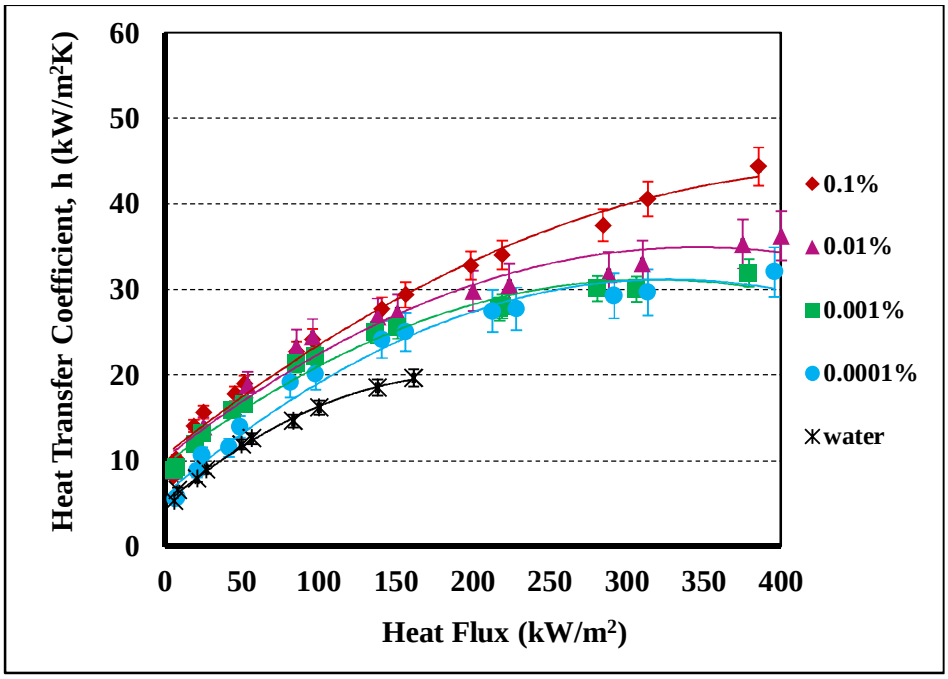

Figure 5.31. Variation of HTC of ZnO-water nanofluids with heat flux at a pressure of 2.0 bar, sub cooling of 20°C and mass flux of 400 kg/m^{2}s.

The maximum increase in HTC of ZnO-water nanofluid with respect to water at 2.5 bar and mass flux of 400 kg/m^{2}s at heat flux of about 210 kW/m^2 is 31% for 0.0001% ZnO-water nanofluid, 34% for 0.001% ZnO-water nanofluid, 37% for 0.01% ZnO-water nanofluid and 60% for 0.1% ZnO-water nanofluid (refer Fig. 5.32).

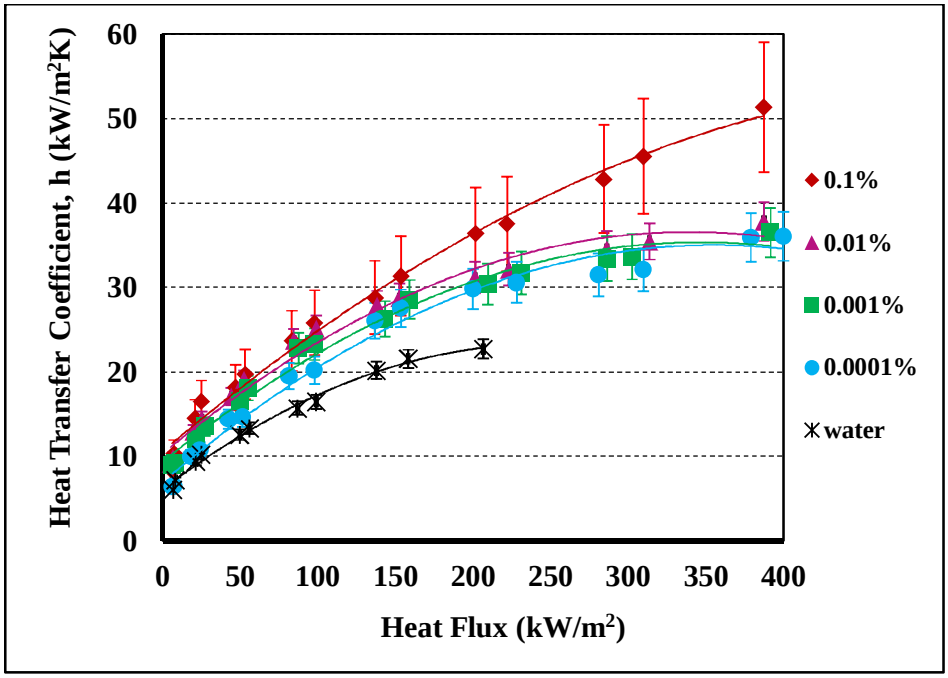

Figure 5.32. Variation of HTC of ZnO-water nanofluids with heat flux at a pressure of 2.5 bar, sub cooling of 20°C and mass flux of 400 kg/m^{2}s.

5.2.5 Heat Transfer Coefficient of MWCNT-Water Nanofluid

Experimental data in Fig. 5.33, Fig. 5.34, Fig. 5.35 and Fig. 5.36 show heat transfer coefficient of MWCNT-water nanofluid for concentrations of 0.0001% MWCNT-water nanofluid, 0.001% MWCNT-water nanofluid, 0.01% MWCNT-water nanofluid and 0.1% MWCNT-water nanofluid respectively.

The experimental results show that similar to above oxide nanofluids, heat transfer coefficient of MWCNT-water nanofluid increases with increase in heat flux. Initially enhancement in heat transfer coefficient is higher in convective range or at low heat flux, but at higher heat flux enhancement in heat transfer

coefficient is not significant. It is also shown in same figure that heat transfer coefficient of MWCNT-water nanofluid increases with increase in pressure in designed test section at all heat fluxes. As shown in Fig. 5.33 at 100 kW/m^2 heat flux, the enhancement in heat transfer coefficient is not significant with pressure, but during phase change process the enhancement in heat transfer coefficient is reasonably higher and then got saturated at higher heat fluxes.

The maximum increase in HTC due to increase in pressure for 0.0001% MWCNT-water nanofluid at 2.5 bar and heat flux of about 165 kW/m^2 and mass flux of 400 kg/m^{2}s with respect to that at 1.0 bar is about 25% (refer Fig. 5.33).

The maximum increase in HTC due to increase in pressure for 0.001% MWCNT-water nanofluid at 2.5 bar and heat flux of about 165 kW/m^2 and mass flux of 400 kg/m^{2}s with respect to that at 1.0 bar is about 39% (refer Fig. 5.34).

The maximum increase in HTC due to increase in pressure for 0.01% MWCNT-water nanofluid at 2.5 bar and heat flux of about 220 kW/m^2 and mass flux of 400 kg/m^{2}s with respect to that at 1.0 bar is about 80% (refer Fig. 5.35).

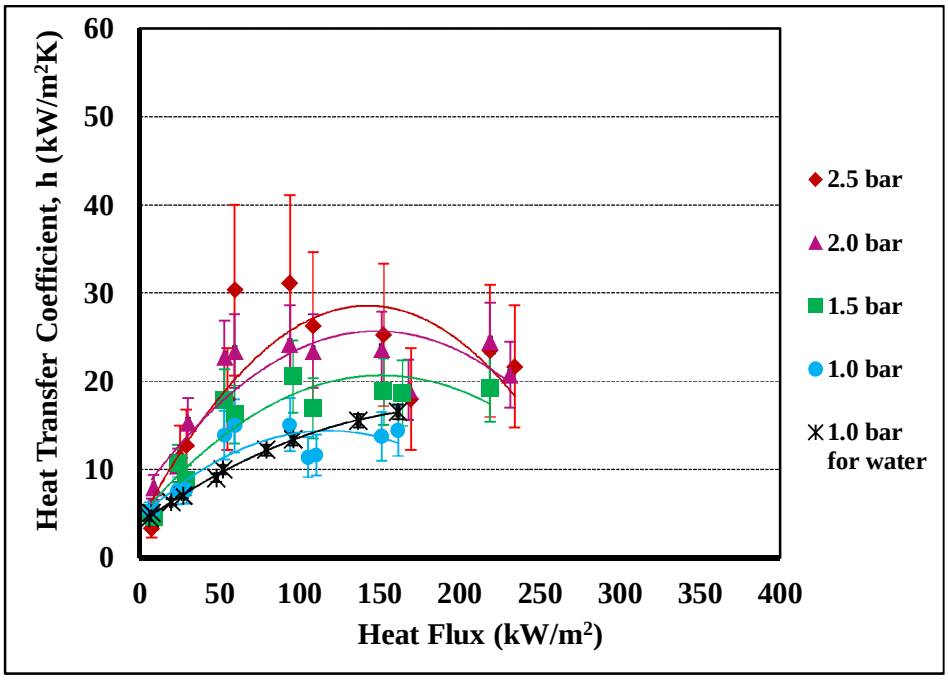

Figure 5.33. Variation of HTC of 0.0001% MWCNT-water nanofluid with heat flux at a sub cooling of 20°C and mass flux of 400 kg/m^{2}s.

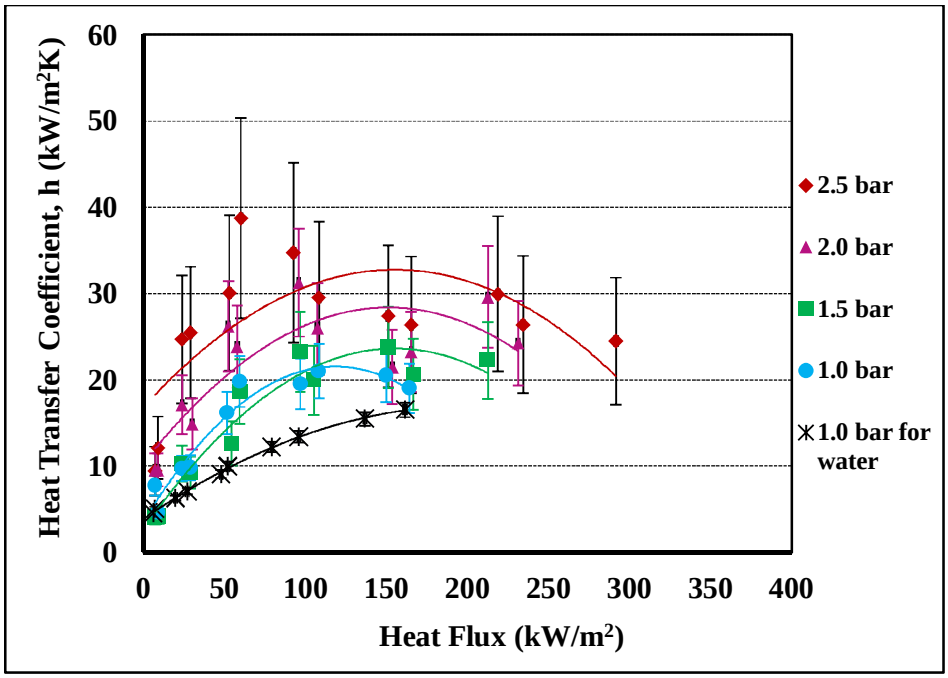

Figure 5.34. Variation of HTC of 0.001% MWCNT-water nanofluid with heat flux at a sub cooling of 20°C and mass flux of 400 kg/m^{2}s.

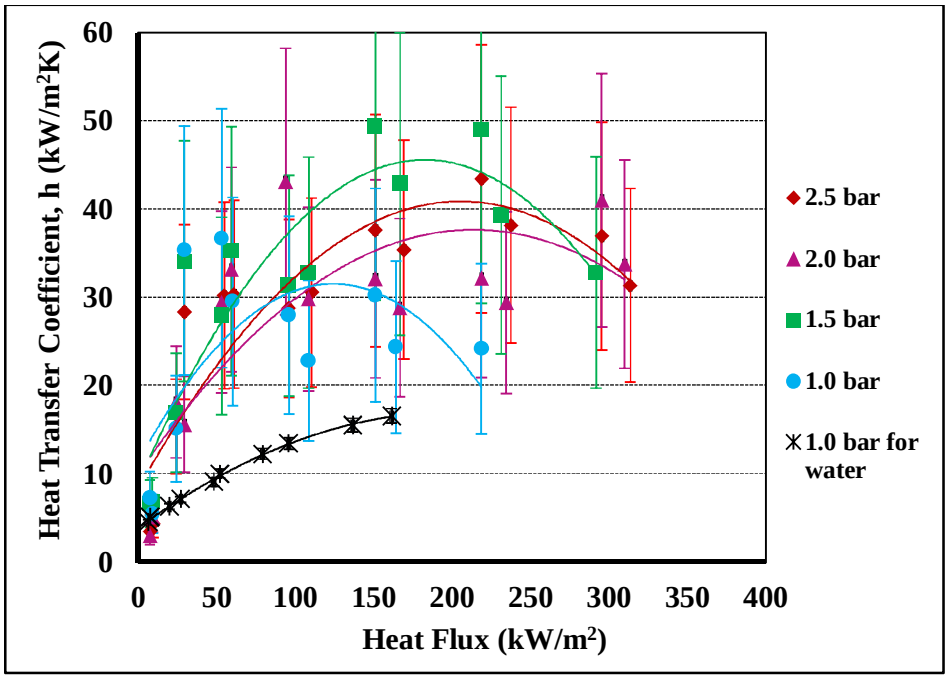

Figure 5.35. Variation of HTC of 0.01% MWCNT-water nanofluid with heat flux at a sub cooling of 20°C and mass flux of 400 kg/m^{2}s.

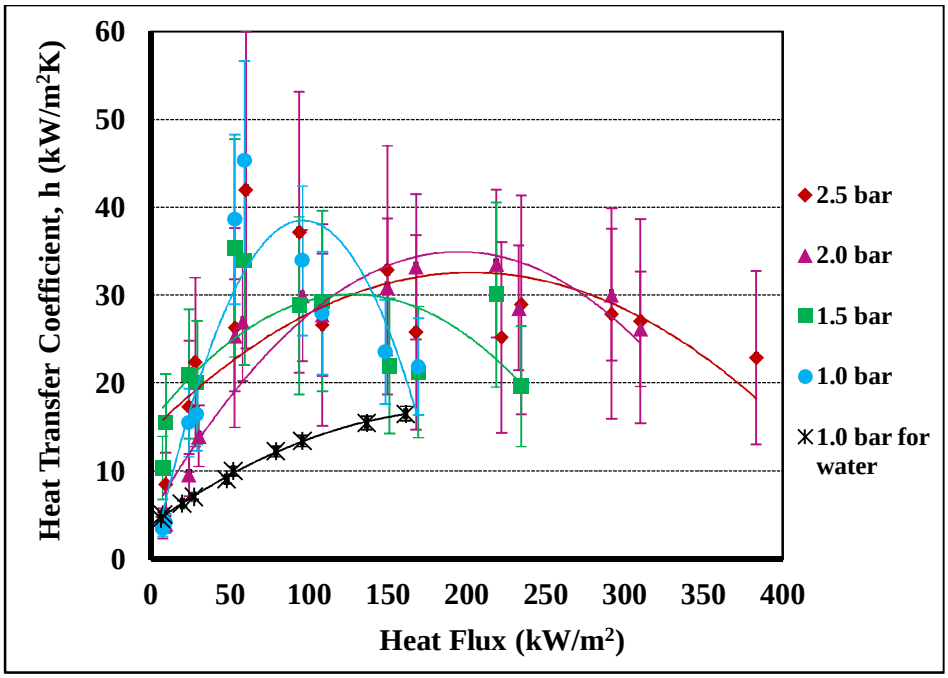

Figure 5.36. Variation of HTC of 0.1% MWCNT-water nanofluid with heat flux at a sub cooling of 20°C and mass flux of 400 kg/m^{2}s.

The maximum increase in HTC due to increase in pressure for 0.1% MWCNT-water nanofluid at 2.5 bar and heat flux of about 165 kW/m^2 and mass flux of 400 kg/m^{2}s with respect to that at 1.0 bar is about 18% (refer Fig. 5.36).

The experimental results shown in Fig 5.33 and Fig. 5.34 show that heat transfer coefficient of 0.0001% MWCNT-water nanofluid and 0.001% MWCNT-water nanofluid increases with increase in heat flux in convective range, than decreases during phase change process and gets saturated with increase in heat flux in boiling range. However for the 2.5 bar, heat transfer coefficient of MWCNT-water nanofluid increased with increase in heat flux in convective range (heat flux about $\leq$ 100 kW/m^2), subsequently it decreased with increase in heat flux in boiling range (heat flux about $\geq$ 100 kW/m^2).

The experimental results shown in Fig 5.35 and Fig. 5.36 show that heat transfer coefficient of 0.01% MWCNT-water nanofluid and 0.1% MWCNT-water nanofluid increases abruptly with increase in heat flux in convective range, than gets saturated with increase in heat flux in boiling range. However for the variable

pressure, no exact trend is observed for heat transfer coefficient of 0.01% MWCNT-water nanofluid and 0.1% MWCNT-water nanofluid.

Fig. 5.37 shows variation of heat transfer coefficient (HTC) of MWCNT-water nanofluid with heat flux for different concentrations of MWCNT-water nanofluid at a pressure of 1.0 bar and mass flux of 400 kg/m^{2}s. In the convective region, i.e. at low heat flux HTC of the MWCNT-water nanofluid tested increases rapidly with increase in heat flux for all the concentrations of the MWCNT-water nanofluid. However this rate of increase in HTC does not continue in the boiling region i.e. at higher heat flux HTC increases marginally with increase in heat flux for all the concentrations of the MWCNT-water nanofluid. It is also observed that HTC increases with increase in concentration of MWCNT-water nanofluid at all the heat fluxes.

Figure 5.38, Fig. 5.39 and Fig. 5.40 show similar behavior for HTC at different pressures, i.e. 1.5, 2.0 and 2.5 bar respectively and a mass flux of 400 kg/m^{2}s.

The maximum increase in HTC of MWCNT-water nanofluid with respect to water at 1.0 bar and mass flux of 400 kg/m^{2}s at heat flux of about 160 kW/m^2 is 5% for 0.0001% MWCNT-water nanofluid, 15% for 0.001% MWCNT-water nanofluid, 47% for 0.01% MWCNT-water nanofluid and 32% for 0.1% MWCNT-water nanofluid (refer Fig. 5.37).

The maximum increase in HTC of MWCNT-water nanofluid with respect to water at 1.5 bar and mass flux of 400 kg/m^{2}s at heat flux of about 160 kW/m^2 is 2% for 0.0001% MWCNT-water nanofluid, 13% for 0.001% MWCNT-water nanofluid, 134% for 0.01% MWCNT-water nanofluid and 16% for 0.1% MWCNT-water nanofluid (refer Fig. 5.38).

The maximum increase in HTC of MWCNT-water nanofluid with respect to water at 2.0 bar and mass flux of 400 kg/m^{2}s at heat flux of about 160 kW/m^2 is 2% for 0.0001% MWCNT-water nanofluid, 18% for 0.001% MWCNT-water nanofluid, 47% for 0.01% MWCNT-water nanofluid and 69% for 0.1% MWCNT-water nanofluid (refer Fig. 5.39).

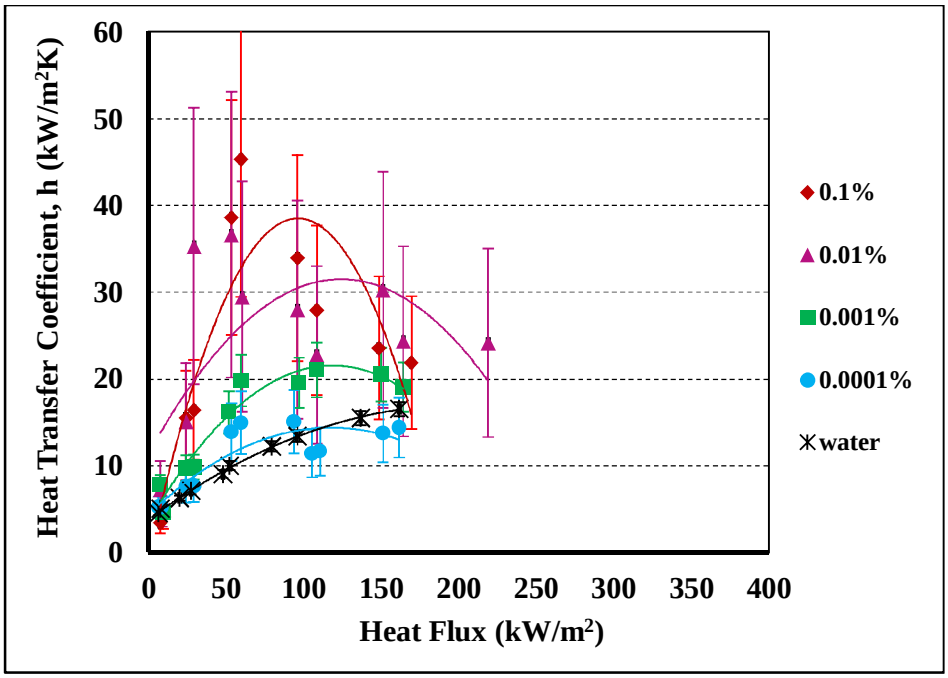

Figure 5.37. Variation of HTC of MWCNT-water nanofluids with heat flux at a pressure of 1.0 bar, sub cooling of 20°C and mass flux of 400 kg/m^{2}s.

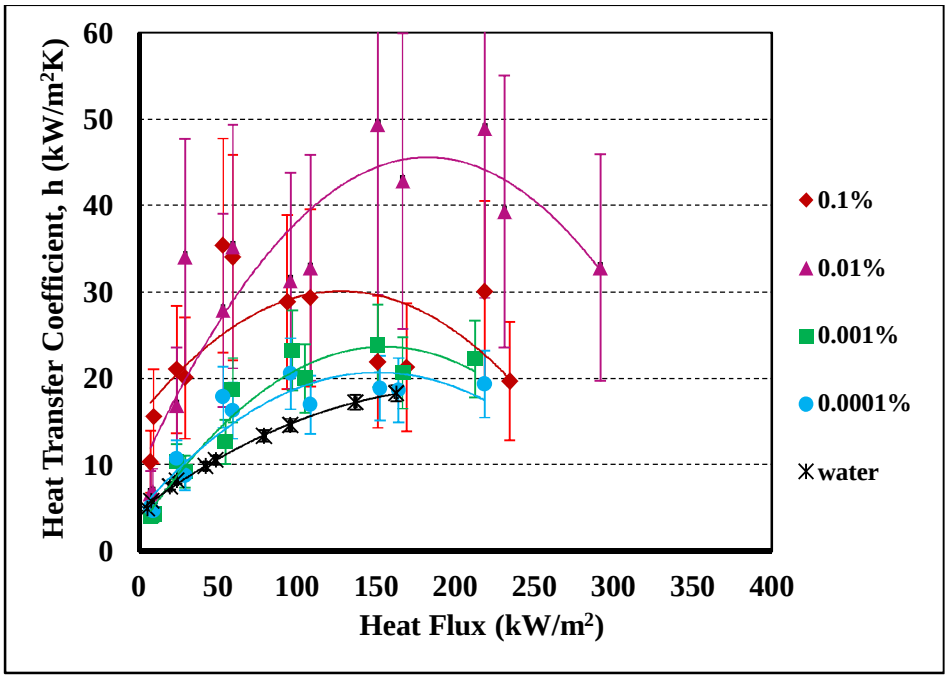

Figure 5.38. Variation of HTC of MWCNT-water nanofluids with heat flux at a pressure of 1.5 bar, sub cooling of 20°C and mass flux of 400 kg/m^{2}s.

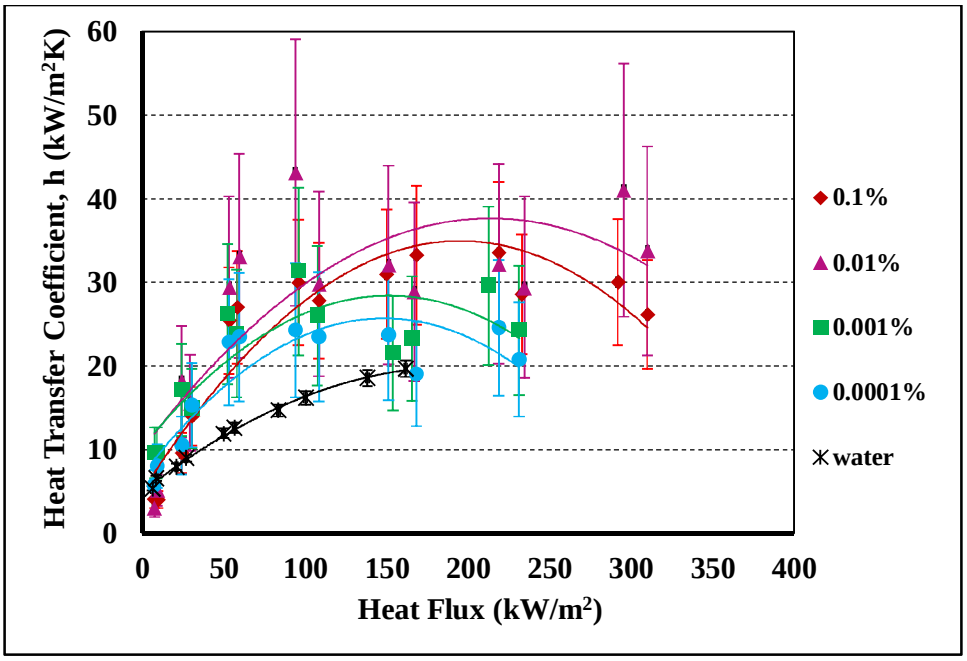

Figure 5.39. Variation of HTC of MWCNT-water nanofluids with heat flux at a pressure of 2.0 bar, sub cooling of 20°C and mass flux of 400 kg/m^{2}s.

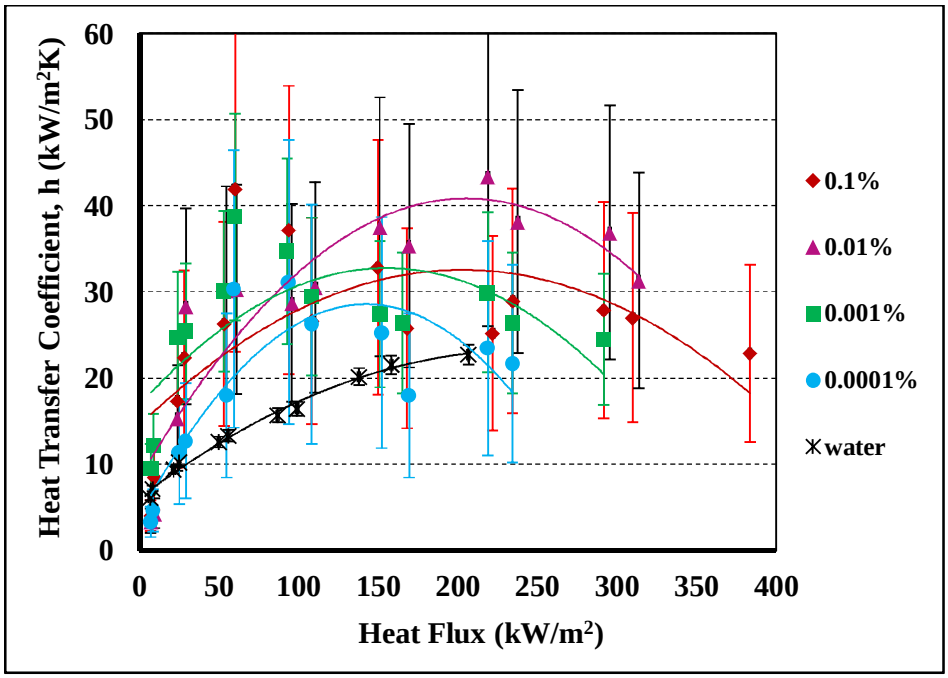

Figure 5.40. Variation of HTC of MWCNT-water nanofluids with heat flux at a pressure of 2.5 bar, sub cooling of 20°C and mass flux of 400 kg/m^{2}s.

The maximum increase in HTC of MWCNT-water nanofluid with respect to water at 2.5 bar and mass flux of 400 kg/m^{2}s at heat flux of about 210 kW/m^2 is 3% for 0.0001% MWCNT-water nanofluid, 32% for 0.001% MWCNT-water nanofluid, 91% for 0.01% MWCNT-water nanofluid and 11% for 0.1% MWCNT-water nanofluid (refer Fig. 5.40).

Figure 5.41 shows variation of heat transfer coefficient with concentrations of nanoparticles in water at a pressure of 1.0 bar, mass flux of 400 kg/m^{2}s and sub cooling of 20ºC.

The experimental results show that HTC of the nanofluid increases with increase in concentrations of nanoparticles in water for all the nanoparticles. The maximum increase in HTC is found for TiO_2-water nanofluids at 1.0 bar.

The increase in HTC s due to increased thermal conductivity of nanofluids and increased surface roughness of heater rod.

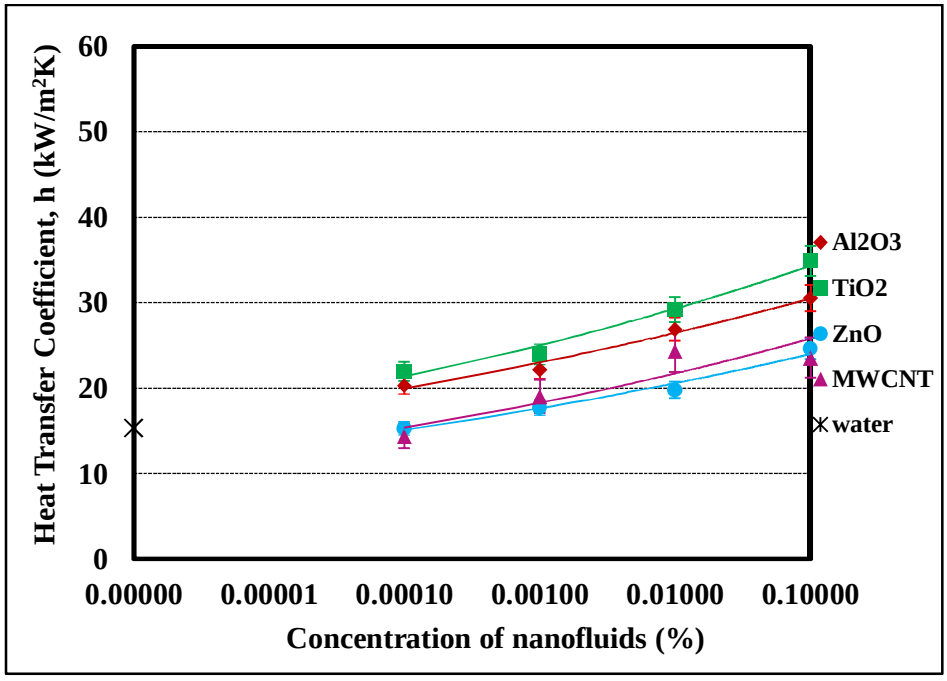

Figure 5.41. Variation of HTC for nanofluids with concentration of nanoparticles in water at a pressure of 1.0 bar, sub cooling of 20ºC and mass flux of 400 kg/m^{2}s.

5.3 Pressure drop

Pressure drop with nanofluids was measured in an annular test section as a function of pressure, concentration of nanoparticles and heat flux. In single and multi-phase flow, instead of variable pressure constant pressure was applied in an annular test section to minimize the fluctuations and flow stabilization time. Heat flux was provided to the test section for continuous heating of heater rod at same pressure. Pressure was increased and experimentation repeated with variable parameters.

5.3.1 Pressure Drop with Water

To assess the repeatability of the tests, the experimental pressure drop in test section was measured four times. Figure 5.42 shows the repeatability plots for pressure drop for water. Averaged pressure drop is plotted on the y-axis whereas pressure is plotted on the x-axis. The four plots presented here show that the measurements of pressure drop show good repeatability.

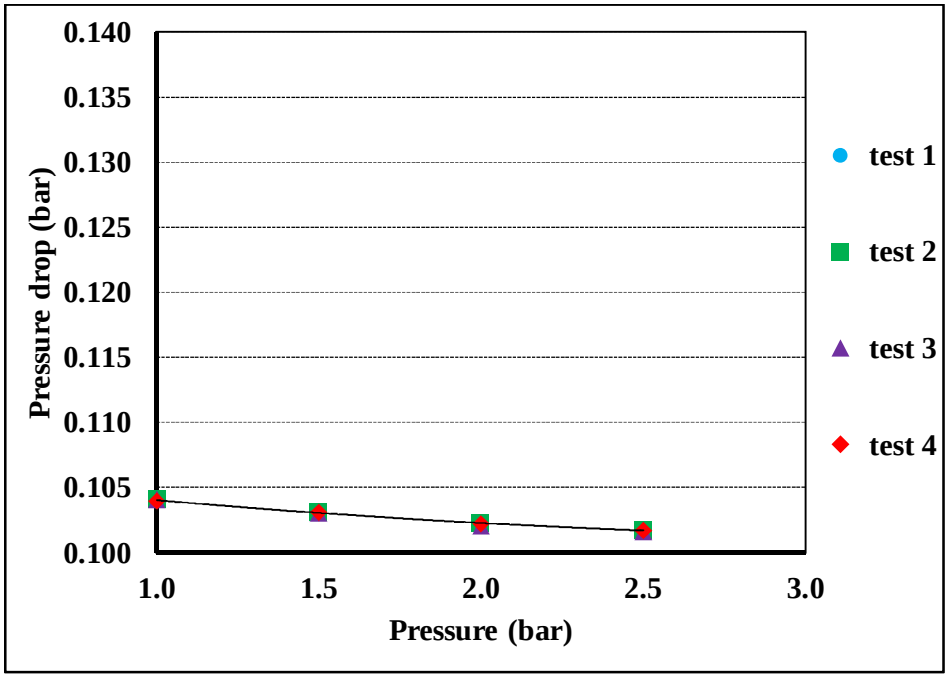

Figure 5.42. Results of repeatability test for water.

Effect of concentration on the pressure drop of Al_2O_3-water nanofluids, TiO_2-water nanofluids, ZnO-water nanofluids and MWCNT-water nanofluids is shown in Fig. 5.43, Fig. 5.44, Fig. 5.45 and Fig. 5.46 respectively.

5.3.2 Pressure Drop with Al_2O_3-Water Nanofluids

Figure 5.43 shows pressure drop (Δp) in an annular test section with pressure for different concentrations of Al_2O_3-water nanofluid. It is observed that pressure drop decreases marginally with an increase in pressure for all the concentrations of the Al_2O_3-water nanofluid.

The decrease in pressure drop with increase in pressure ranges from 13% to 30% as pressure increases from 1.0 bar to 2.5 bar and concentration of Al_2O_3-water nanofluid varies from 0.0001% to 0.1%.

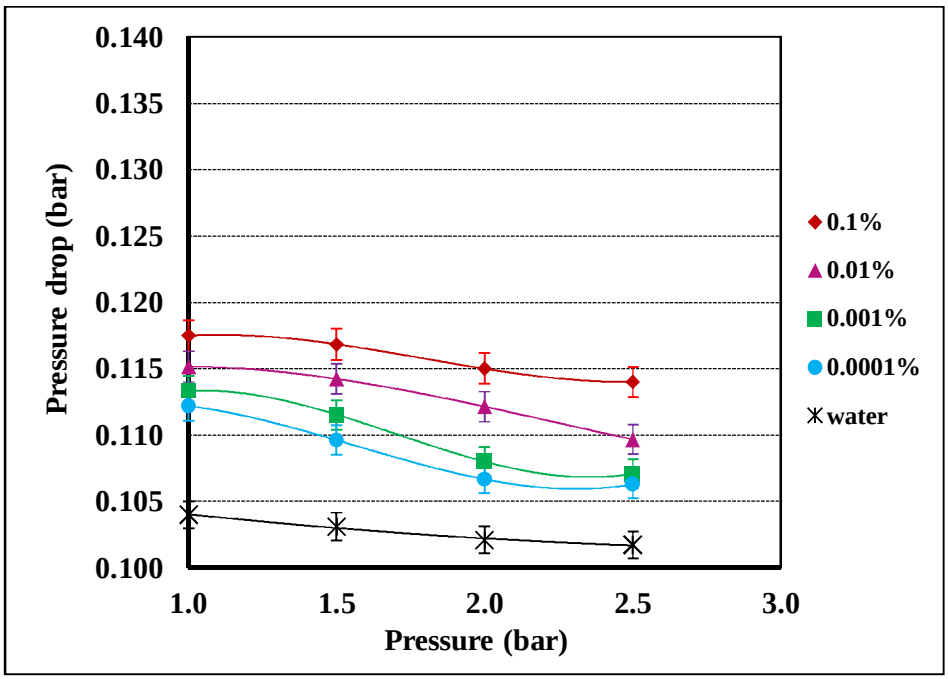

Figure 5.43. Pressure drop in test section with pressure for Al_2O_3-water nanofluids at a sub cooling of 20°C and mass flux of 400 kg/m^{2}s.

It is also observed that for any applied pressure, the pressure drop across the test section increases monotonically with an increase in the concentration of

the Al_2O_3-water nanofluid; it increase from 0.104 bar to 0.118 bar from pure water to Al_2O_3-water nanofluid with a concentration of 0.1% of the Al_2O_3-water nanofluid at a pressure of 1.0 bar. Error for ΔP is 1 % for this case. It increases from 0.104 bar to 0.118 bar from pure water to nanofluid with a concentration of 0.1% of the nanofluid at a pressure of 1.0 bar.

As shown in figure 5.44, it is also observed that pressure drop for Al_2O_3-water nanofluid does not change in convective flow however it increases slightly in boiling flow. It increases in boiling flow due to increase in turbulence through bubble generation.

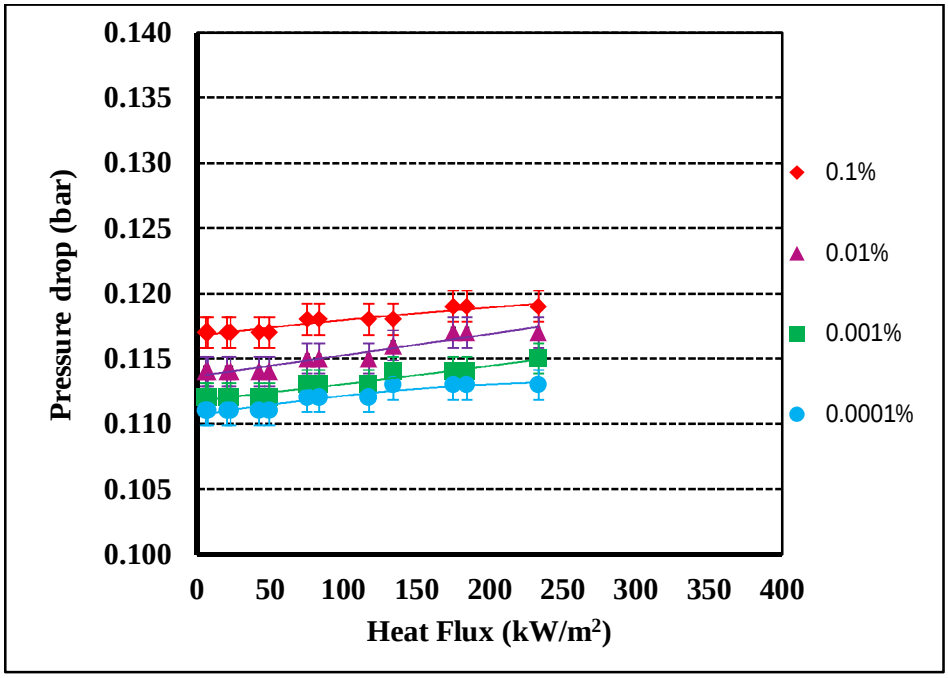

Figure 5.44. Pressure drop in test section with heat flux for Al_2O_3-water nanofluids at a sub cooling of 20°C and mass flux of 400 kg/m^{2}s.

5.3.3 Pressure Drop with TiO_2-Water Nanofluid

Figure 5.45 shows pressure drop (Δp) in an annular test section with pressure for different concentrations of TiO_2-water nanofluid. It is observed that pressure drop decreases marginally with increase in pressure for all the concentrations of the TiO_2-water nanofluid. The decrease in pressure drop with

increase in pressure ranges from 5% to 13% as pressure increases from 1.0 bar to 2.5 bar and concentration of TiO_2-water nanofluid varies from 0.0001% to 0.1%.

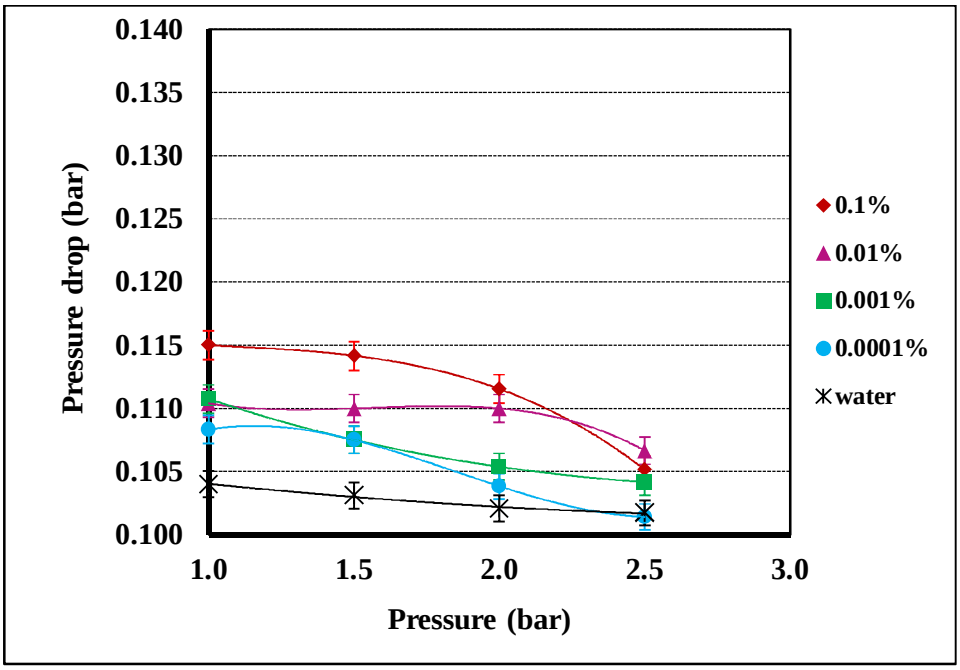

Figure 5.45. Pressure drop in test section with pressure for TiO_2- water nanofluids at a sub cooling of 20°C and mass flux of 400 kg/m^{2}s.

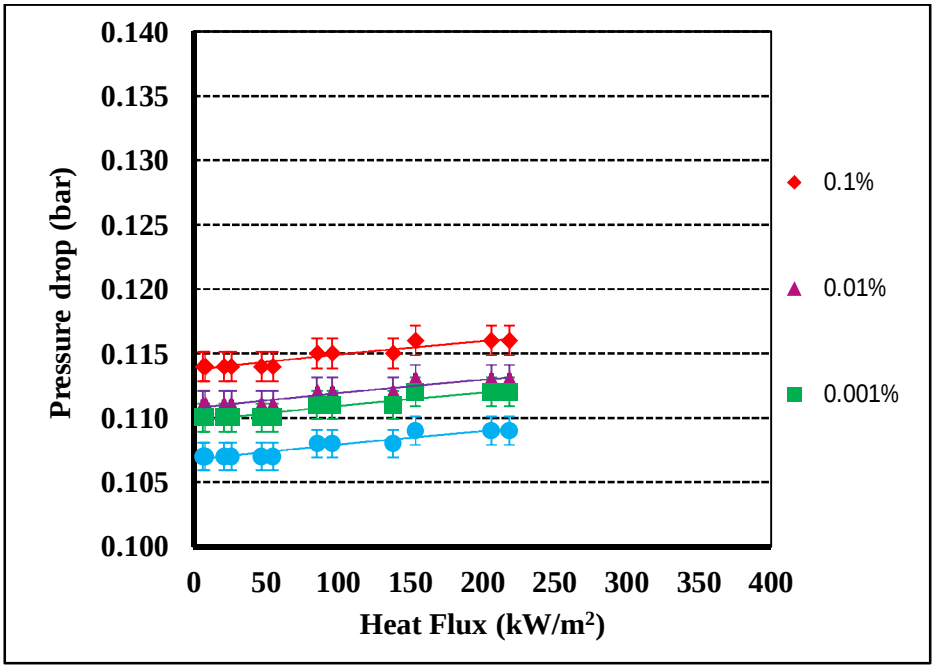

Figure 5.46. Pressure drop in test section with heat flux for TiO_2-water nanofluids at a sub cooling of 20°C and mass flux of 400 kg/m^{2}s.

It is also observed that for any applied pressure, pressure drop across the test section increases monotonically with increase in concentration of the TiO_2-water nanofluid; it increase from 0.104 bar to 0.115 bar from pure water to TiO_2-water nanofluid with concentration of 0.1% of the TiO_2-water nanofluid at a pressure of 1.0 bar.

As shown in figure 5.46, it is also observed that pressure drop for TiO_2-water nanofluid does not change in convective flow however it increases slightly in boiling flow. It increases in boiling flow due to increase in turbulence through bubble generation.

5.3.4 Pressure Drop with ZnO-Water Nanofluid

Figure 5.47 shows pressure drop (Δp) in an annular test section with pressure for different concentrations of ZnO-water nanofluid. It is observed that pressure drop decreases marginally with increase in pressure for all the concentrations of the ZnO-water nanofluid. It is probably due to fewer bubbles generated at same heat flux or probably due to power fluctuations. The decrease in pressure drop with increase in pressure ranges from 2% to 11% as pressure increases from 1.0 bar to 2.5 bar and concentration of ZnO-water nanofluid varies from 0.0001% to 0.1%. It is also observed that for any applied pressure, pressure drop across the test section increases monotonically with increase in concentration of the ZnO-water nanofluid; it increase from 0.104 bar to 0.135 bar from pure water to ZnO-water nanofluid with concentration of 0.1% of the ZnO-water nanofluid at a pressure of 1.0 bar. It is also observed that for an initial concentration of 0.0001% of ZnO-water nanofluid, pressure drop increased at 1.5 bar possibly because of fluctuation by film flow boiling. However for higher concentrations the trend is similar to other nanofluids.

As shown in figure 5.48, it is also observed that pressure drop for ZnO-water nanofluid does not change in convective flow however it increases slightly in boiling flow. It increases in boiling flow due to increase in turbulence through bubble generation.

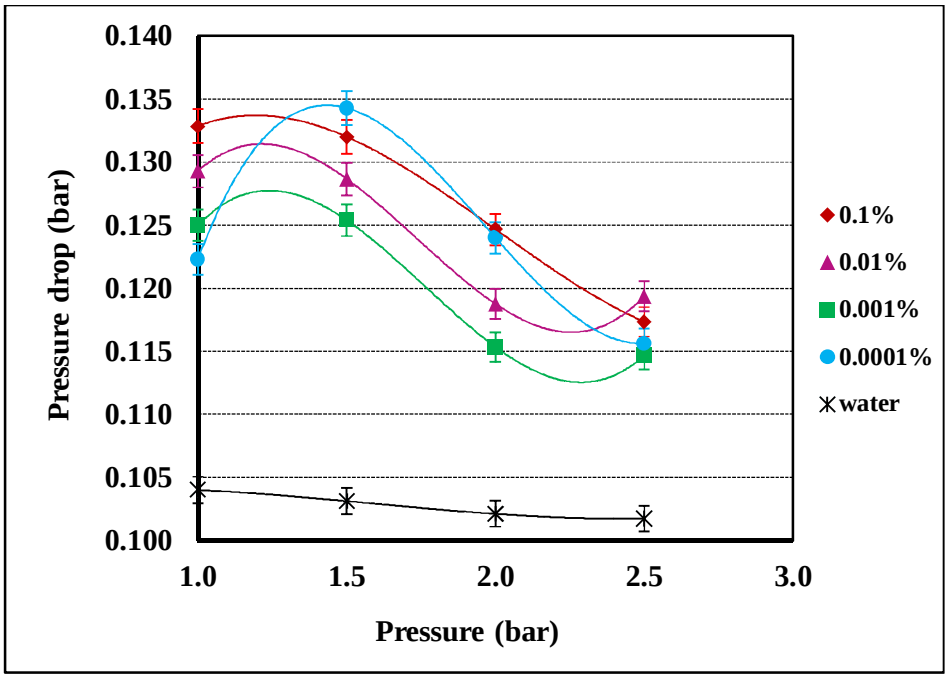

Figure 5.47. Pressure drop in test section with pressure for ZnO- water nanofluids at a sub cooling of 20°C and mass flux of 400 kg/m^{2}s.

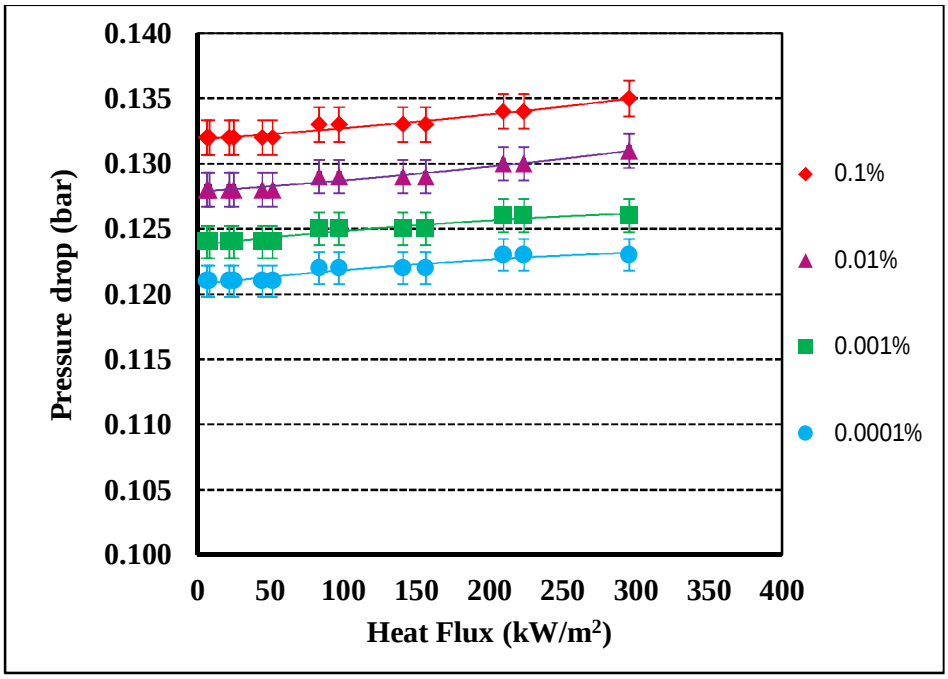

Figure 5.48. Pressure drop in test section with heat flux for ZnO-water nanofluids at a sub cooling of 20°C and mass flux of 400 kg/m^{2}s.

5.3.5 Pressure Drop with MWCNT-Water Nanofluid

Figure 5.49 shows pressure drop (Δp) in an annular test section with pressure for different concentrations of MWCNT-water nanofluid. It is observed that pressure drop decreases marginally with increase in pressure for all the concentrations of the MWCNT-water nanofluid.

The decrease in pressure drop with pressure ranges from 1% to 9% as pressure increases from 1.0 bar to 2.5 bar and concentration of MWCNT-water nanofluid varies from 0.0001% to 0.1%. It is also observed that for any applied pressure, pressure drop across the test section increases monotonically with concentration of the MWCNT-water nanofluid; it increase from 0.104 bar to 0.135 bar from pure water to MWCNT-water nanofluid with concentration of 0.1% of the MWCNT-water nanofluid at a pressure of 1.0 bar.

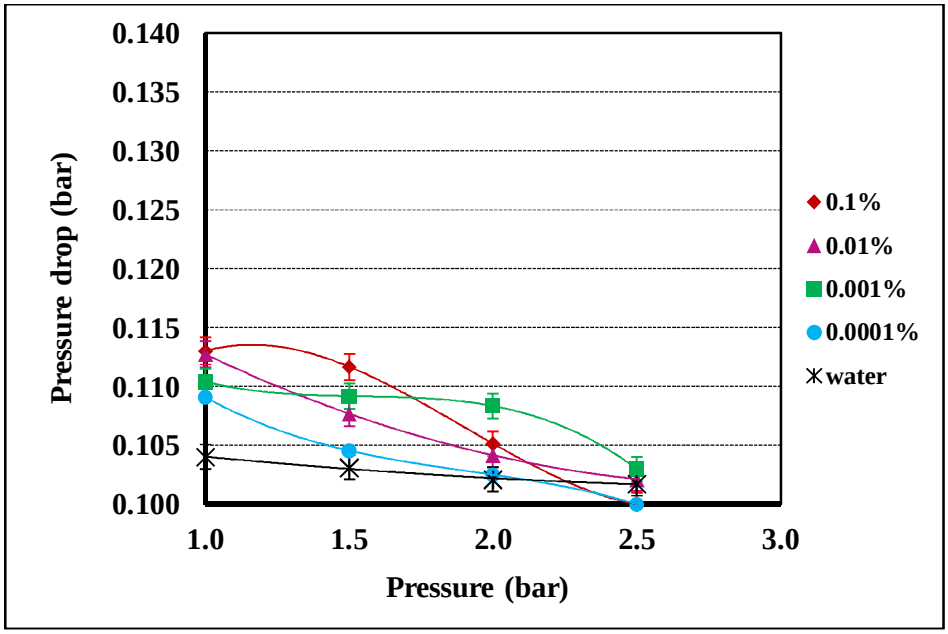

Figure 5.49. Pressure drop in test section with pressure for MWCNT-water nanofluids at a sub cooling of 20°C and mass flux of 400 kg/m^{2}s.

As shown in figure 5.50, it is also observed that pressure drop for MWCNT-water nanofluid does not change in convective flow however it increases slightly in boiling flow. It increases in boiling flow due to increased pressure by an increase in turbulence through bubble generation.

Among all the selected nanofluids, the maximum pressure drop is for ZnO-water nanofluids because of its chemical properties. ZnO nanoparticles also have higher corrosion resistance {Ramezanzadeh et. al (2011)} among selected oxide nanoparticles with containing adhesive properties for the surface.

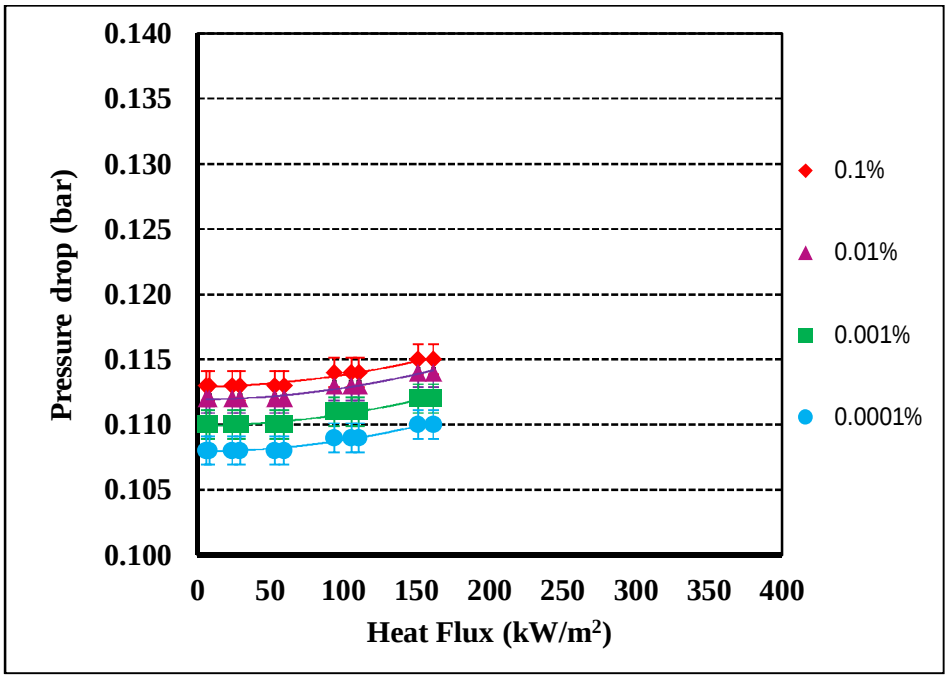

Figure 5.50. Pressure drop in test section with heat flux for MWCNT-water nanofluids at a sub cooling of 20°C and mass flux of 400 kg/m^{2}s.

5.3.6 Pressure Drop with Nanofluids

Effect of concentration on averaged pressure drop with various nanofluids i.e. Al_2O_3-water nanofluid, TiO_2-water nanofluid, ZnO-water nanofluid and MWCNT-water nanofluid is shown in Fig. 5.51 with maximum 3% error.

It is observed that pressure drop increases with increase in concentration of nanofluids. The maximum pressure drop was observed for the ZnO-water nanofluids at its highest concentration.

It is also observed that increase in pressure drop was significant for ZnO-water nanofluid.

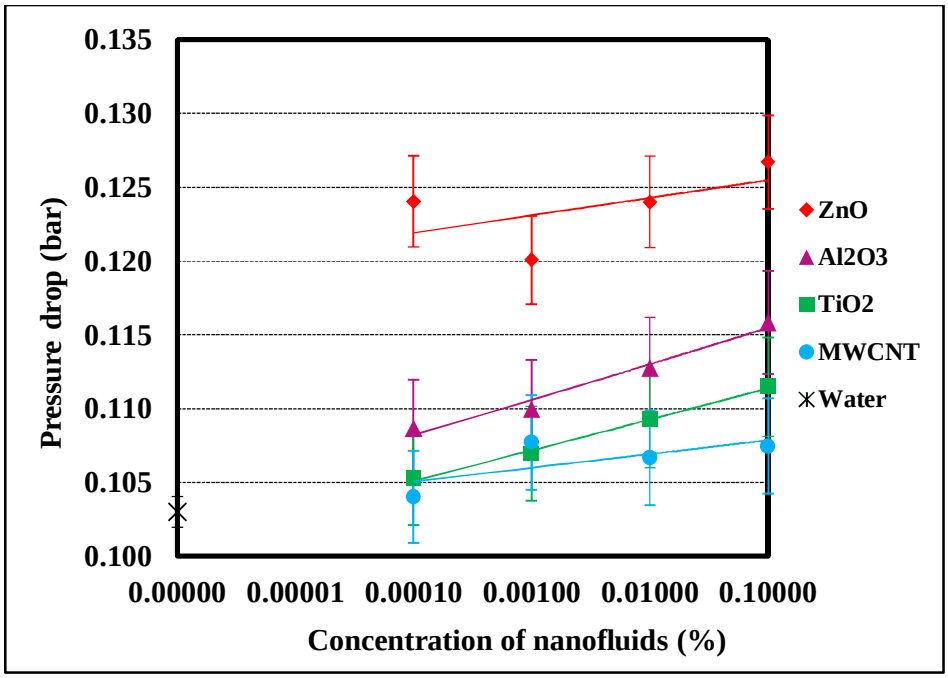

Figure 5.51. Pressure drop in test section with concentration of nanofluids at a pressure of 1 bar, sub cooling of 20°C and mass flux of 400 kg/m^{2}s.

5.4 Bubble Parameters

It is observed from the experimentation that no single model can fully represent the bubble size within the given range of pressures, heat fluxes, concentrations of nanofluids, flow rates and surface characteristics. Nevertheless, the general tendency is discussed in following paragraphs. We need to understand the fundamentals of the role pressure on bubbles, in growth and bubble dynamics by discovering heat transfer and bubble mechanisms at the nano scale.

In following section, effect of pressure, heat flux and concentration of nanofluids is discussed for bubble parameters like: bubble diameter, bubble density and void fraction.

5.4.1 Bubble Diameter

In this section, effect of pressure on bubble diameter studied for water and different nanofluids like: Al_2O_3-water nanofluid, TiO_2-water nanofluid, ZnO-

water nanofluid and MWCNT-water nanofluid, with varying heat flux and concentration of each fluid.

5.4.1.1 Bubble Diameter of Water

Pressure plays very important role in flow boiling heat transfer which affects the bubble parameters significantly during flow boiling process. The experimental results in Fig. 5.52 show the effect of pressure on bubble diameter with variable heat fluxes.

The experimental results of bubble diameter and its dependence on pressure show that pressure acts as a suppressing agent, i.e. with increase in pressure bubble diameter decreases and boiling is delayed in distilled water.

The experimental results in Fig. 5.52 also show the variation of bubble diameter of water with applied heat flux in an annular test section. Results show that bubble diameter increases with increase in heat flux. However, the increase in bubble diameter is more pronounced at lower heat fluxes.

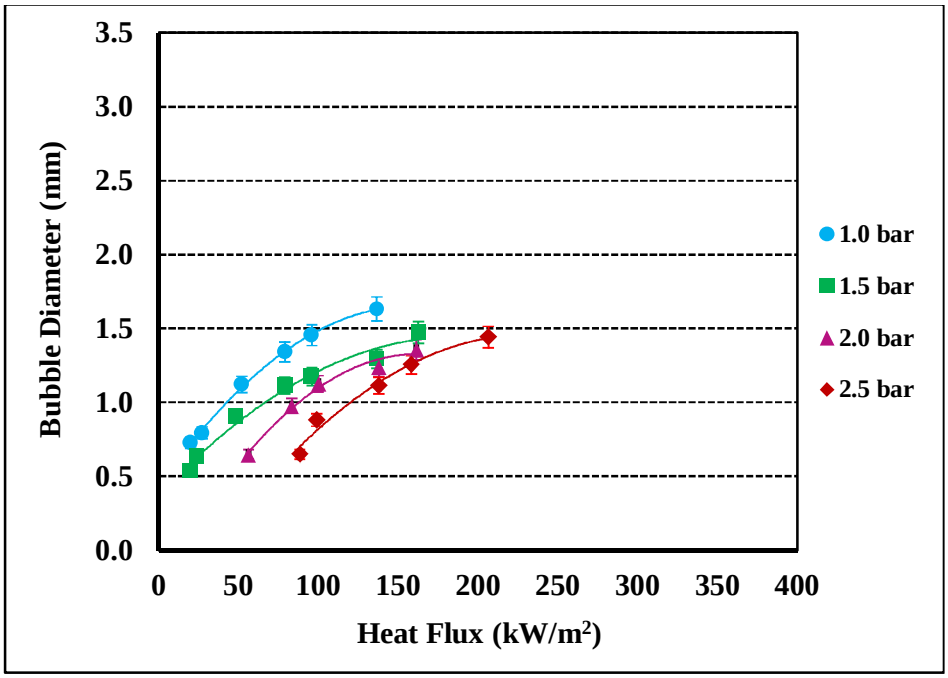

Figure 5.52. Bubble diameters of water with heat flux at a sub cooling of 20°C and mass flux of 400 kg/m^{2}s.

5.4.1.2 Bubble Diameter of Al_2O_3-Water Nanofluid

Variation in bubble diameter of Al_2O_3-water nanofluid with pressure, heat flux and concentration of Al_2O_3 nanoparticles in water has been studied. The visualization and image processing couldn't be done for 0.01% Al_2O_3-water nanofluid and higher concentrations due to the opacity of Al_2O_3-water nanofluid.

To assess the repeatability of the tests, the bubble diameter of 0.0001% Al_2O_3-water nanofluid was measured four times. Figure 5.53 shows the repeatability plots for bubble diameter of 0.0001% Al_2O_3-water nanofluid. The bubble diameter is plotted on the y-axis whereas heat flux is plotted on the x-axis. The four plots presented here, show that the values of bubble diameter show good repeatability.

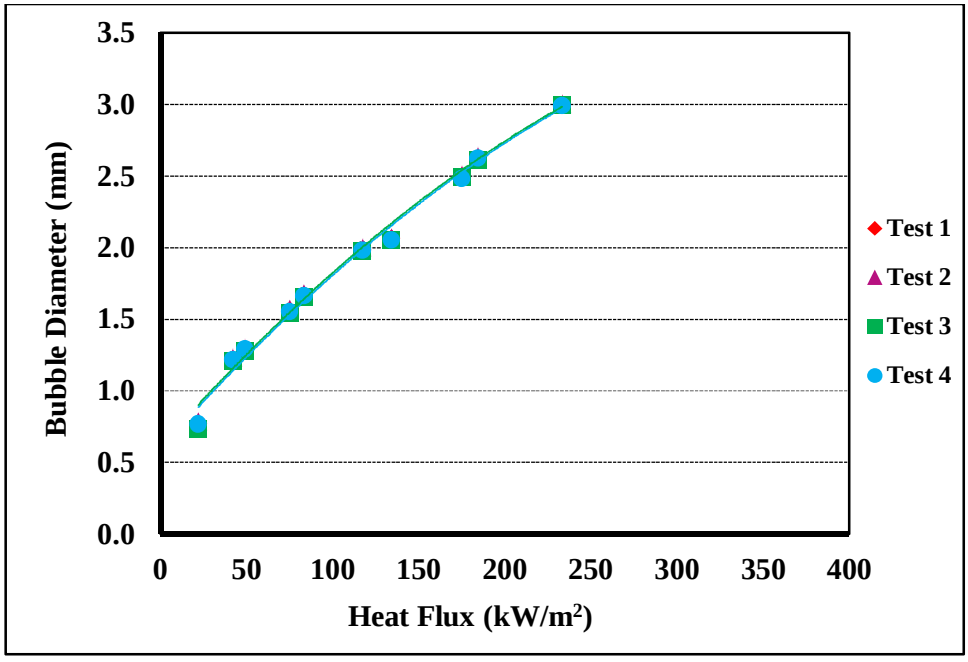

Figure 5.53. Results of repeatability test for bubble diameter for 0.0001% Al_2O_3-water nanofluid at a pressure of 1 bar sub cooling of 20°C and mass flux of 400 kg/m^{2}s.

Fig. 5.54 and Fig. 5.55 show the bubble diameter with pressure and heat flux for 0.0001% and 0.001% Al_2O_3-water nanofluid respectively. The figures show that pressure acts as a suppressing agent, i.e. at any given heat flux bubble

diameter for Al_2O_3-water nanofluids decreases with increase in pressure. It is also observed that the boiling of Al_2O_3-water nanofluids is delayed with pressure, i.e. nucleation of bubble begins at higher heat flux with increase in pressure.

Figure 5.56 and Fig. 5.57 show the bubble diameter for Al_2O_3-water nanofluids with concentrations and heat flux at a pressure for 1.0 bar and 2.5 bar respectively. In figure 5.56, the bubble diameter increases with increase in heat flux and with increase in concentration of Al_2O_3-water nanoparticles. The bubble diameter increased with increase in **heat flux** because bubble takes more heat before the departure from the nucleation site due to high heat flux. The bubble diameter also increases with increase in **concentration** of Al_2O_3-water nanoparticles due to increase in surface tension with increase in concentration of nanoparticles.

It is also observed that at 1.0 bar bubble nucleation starts at same heat flux for both distilled water and Al_2O_3-water nanofluids. However, for a pressure of 2.5 bar the bubble nucleation is delayed (Fig. 5.57) and begins at higher heat flux as compared to distilled water.

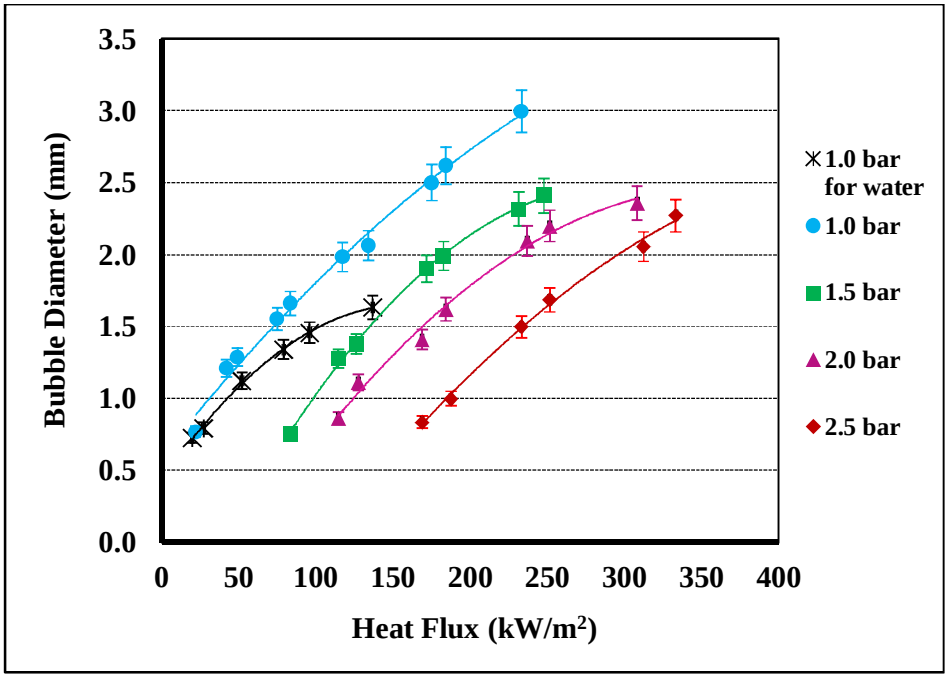

Figure 5.54. Bubble diameters of 0.0001% Al_2O_3-water nanofluid with heat flux at a sub cooling of 20°C and mass flux of 400 kg/m^{2}s.

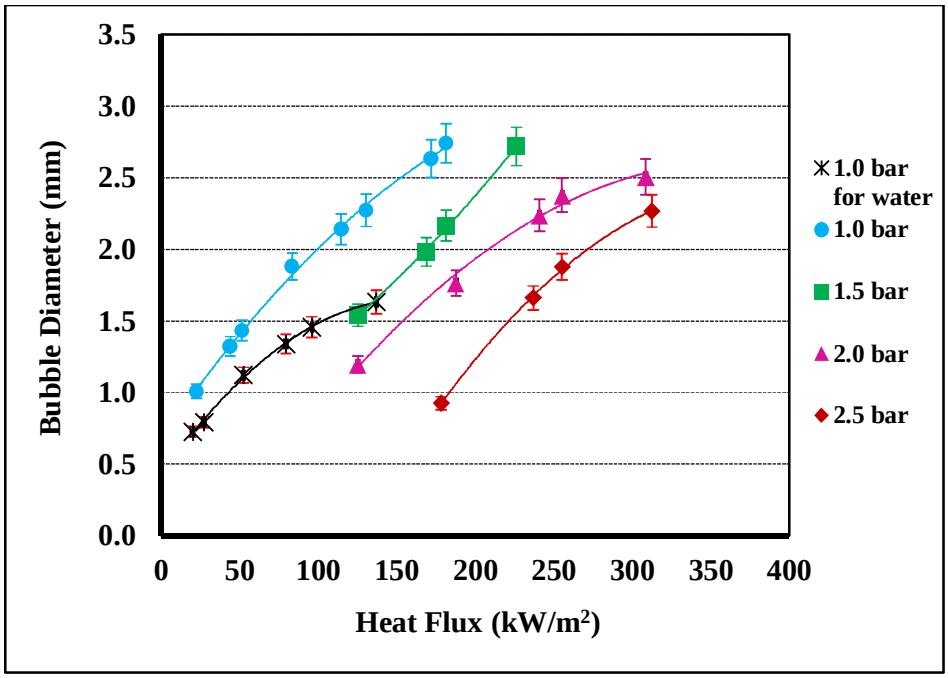

Figure 5.55. Bubble diameters of 0.001% Al_2O_3-water nanofluid with heat flux at a sub cooling of 20°C and mass flux of 400 kg/m^{2}s.

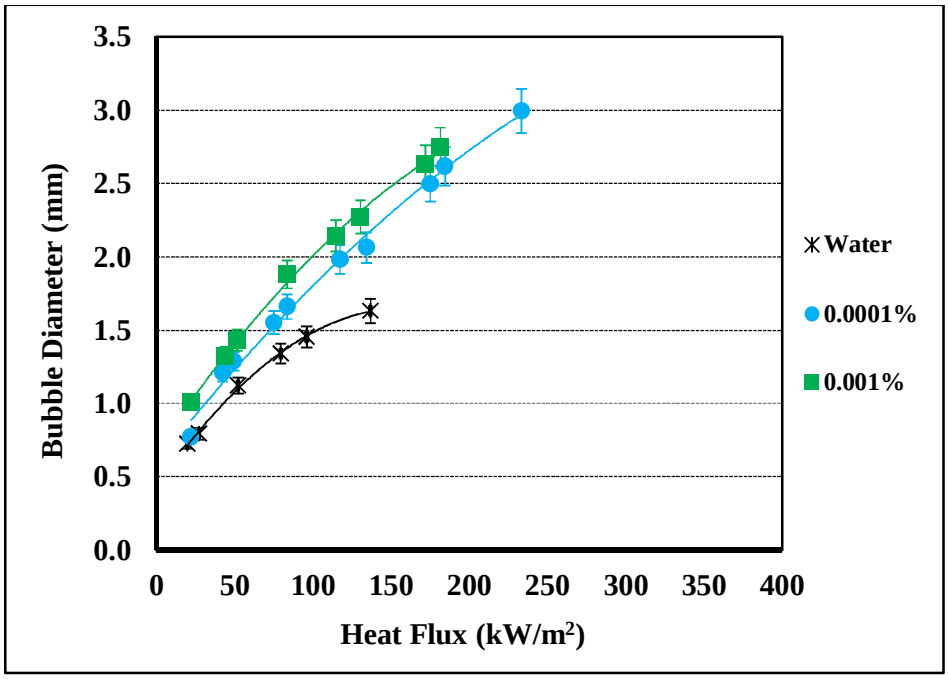

Figure 5.56. Bubble diameters of Al_2O_3-water nanofluid with heat flux at a pressure of 1.0 bar, sub cooling of 20°C and mass flux of 400 kg/m^{2}s.

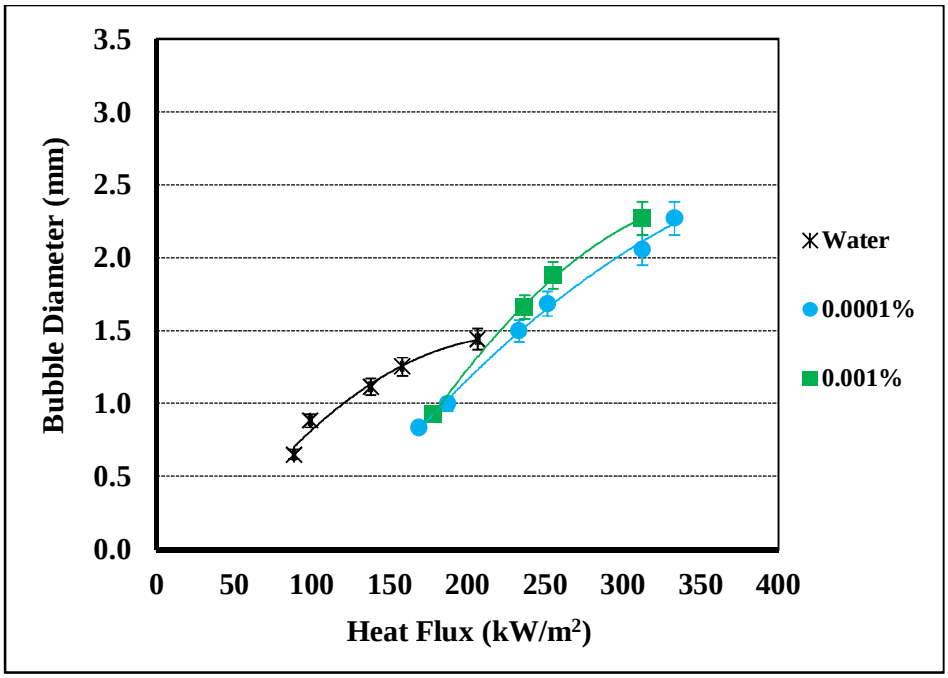

Figure 5.57. Bubble diameters of Al_2O_3-water nanofluid with heat flux at a pressure of 2.5 bar, sub cooling of 20°C and mass flux of 400 kg/m^{2}s.

5.4.1.3 Bubble Diameter of TiO_2-Water Nanofluid

The variation in bubble diameter of TiO_2-water nanofluid with pressure, heat flux and TiO_2 nanoparticle concentration is observed in the present study. The experimental results in Fig. 5.58 and Fig. 5.59 show bubble diameter of 0.0001% TiO_2-water nanofluid and 0.001% TiO_2-water nanofluid with pressure and heat flux in an annular test section.

The visualization and image processing is not possible at 0.01% TiO_2-water nanofluid and higher concentration due to opacity of TiO_2-water nanofluid at higher concentrations.

The experimental results with respect to bubble diameter of TiO_2-water nanofluid and its dependence on pressure show that pressure acts as a suppressing agent, i.e. with increase in pressure bubble diameter decreases and boiling is delayed in TiO_2-water nanofluids. Results show that bubble diameter of TiO_2-water nanofluid increases with increase in heat flux. Bubble diameter also

increases with increase in concentration of TiO_2-water nanofluid at all variable pressure.

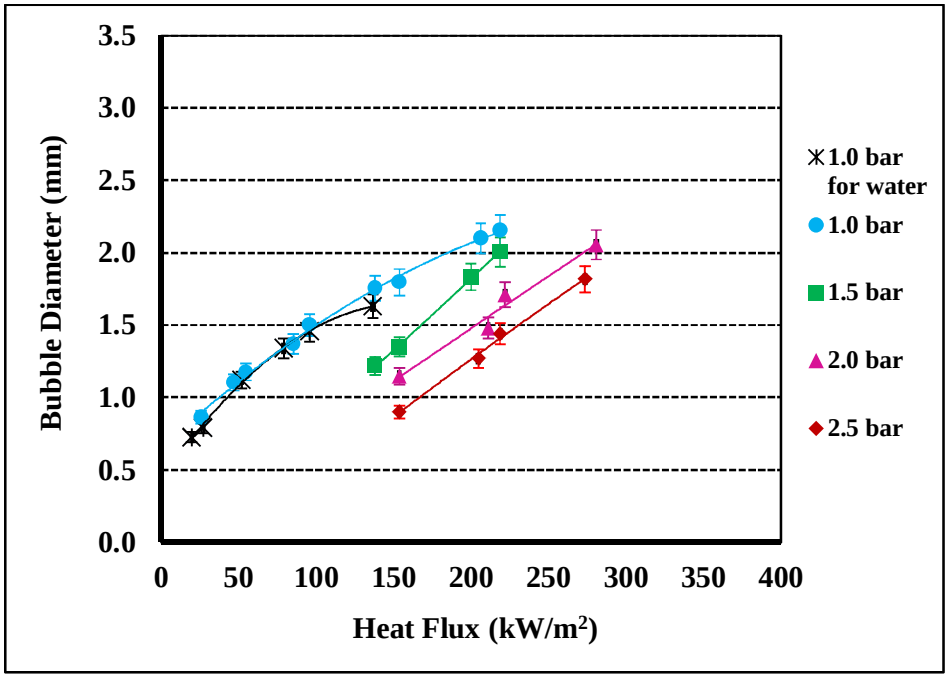

Figure 5.58. Bubble diameters of 0.0001% TiO_2-water nanofluid with heat flux at a sub cooling of 20°C and mass flux of 400 kg/m^{2}s.

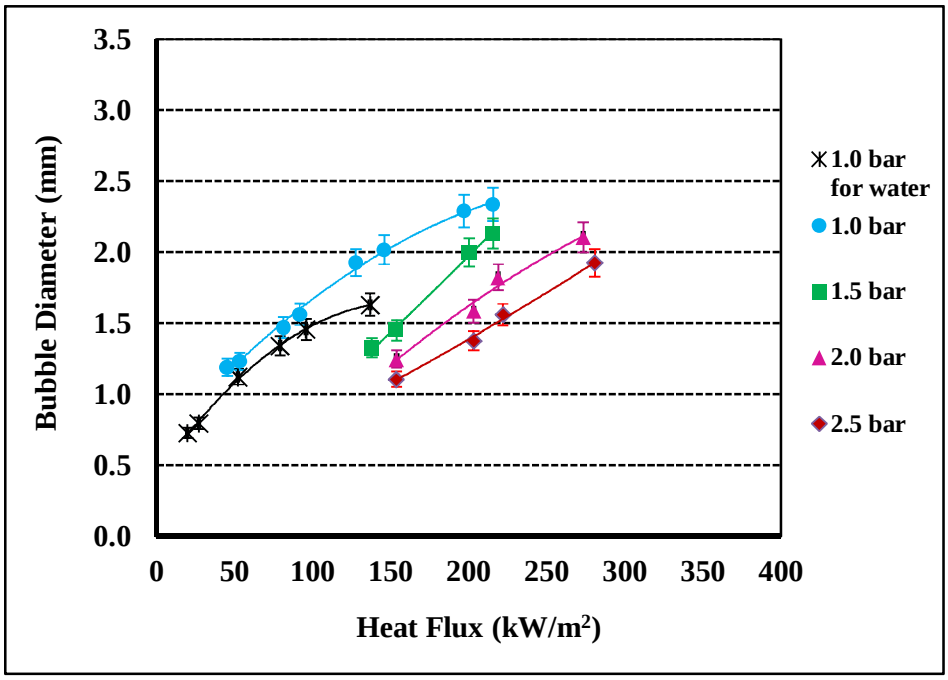

Figure 5.59. Bubble diameters of 0.001% TiO_2-water nanofluid with heat flux at a sub cooling of 20°C and mass flux of 400 kg/m^{2}s.

Figure 5.60 and Fig. 5.61 show the bubble diameter for TiO_2-water nanofluids with concentrations and heat flux for a pressure of 1.0 bar and 2.5 bar respectively.

Figure 5.60 shows that the bubble diameter increases marginally with concentration of TiO_2-water nanofluid. It is also observed that at 1.0 bar bubble nucleation starts at same heat flux for both distilled water and TiO_2-water nanofluids.

However, for 2.5 bar the bubble nucleation is delayed (Fig 5.61) and begins at higher heat flux and size reduces at same heat flux as compared to distilled water.

The bubble diameter decreases as increase in external pressure, bubbles size reduces. The decrease in bubble diameter with increase in pressure is similar to the results obtained by previous researchers like Tolubinsky and Kostanchuk (1970), Bibeau and Salcudean (1991), Prodanovic et al. (2002), Klausner (2000), Celata et al. (2007), Razi et al. (2011), Hashemi et al. (2012), Arani and Amani (2012).

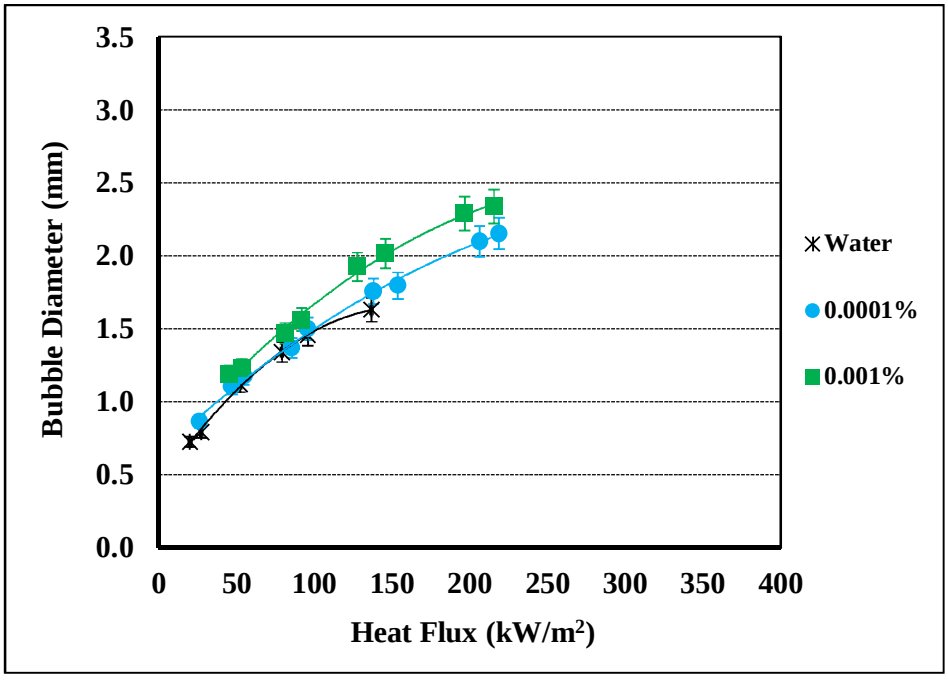

Figure 5.60. Bubble diameters of TiO_2-water nanofluid with heat flux at a pressure of 1.0 bar, sub cooling of 20°C and mass flux of 400 kg/m^{2}s.

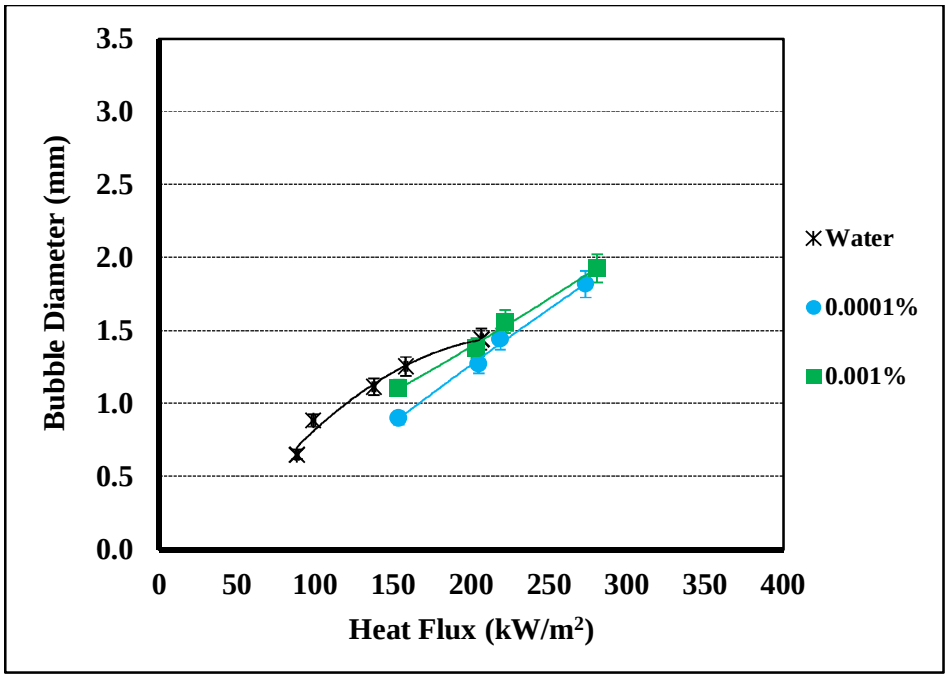

Figure 5.61. Bubble diameters of TiO_2-water nanofluid with heat flux at a pressure of 2.5 bar, sub cooling of 20°C and mass flux of 400 kg/m^{2}s.

5.4.1.4 Bubble Diameter of ZnO-Water Nanofluid

The variation in bubble diameter of ZnO-water nanofluid with pressure, heat flux and ZnO nanoparticle concentration is observed in the present study. The experimental results in Fig. 5.62 and Fig. 5.63 show bubble diameter of 0.0001% ZnO-water nanofluid and 0.001% ZnO-water nanofluid with pressure and heat flux in an annular test section.

The visualization and image processing couldn't be done for 0.01% ZnO-water nanofluid and higher concentrations due to opacity of ZnO-water nanofluid.

The experimental results with respect to bubble diameter of ZnO-water nanofluid and its dependence on pressure show that pressure acts as a suppressing agent, i.e. with increase in pressure bubble diameter decreases and boiling is delayed in ZnO-water nanofluids. Results show that bubble diameter of ZnO-water nanofluid increases with increase in heat flux. Bubble diameter also increases with increase in concentration of ZnO-water nanofluid at all variable pressure.

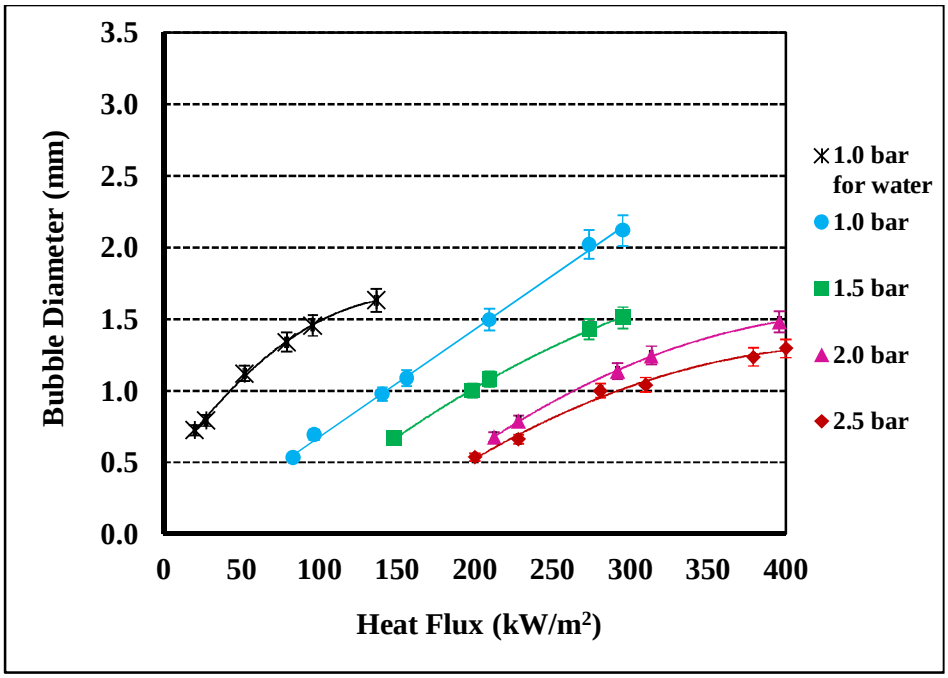

Figure 5.62. Bubble diameters of 0.0001% ZnO-water nanofluid with heat flux at a sub cooling of 20°C and mass flux of 400 kg/m^{2}s.

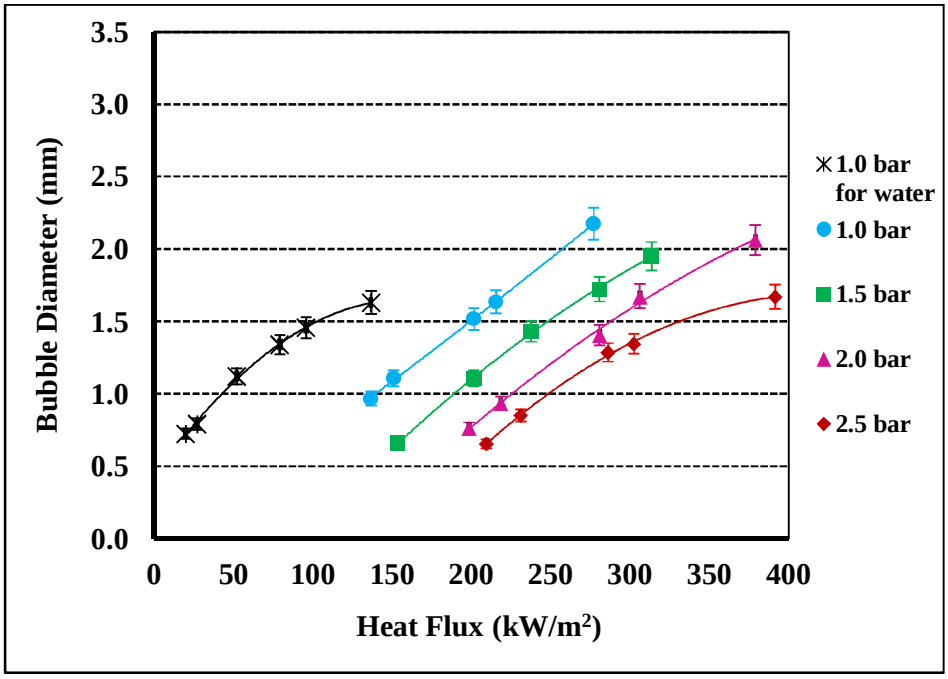

Figure 5.63. Bubble diameters of 0.001% ZnO-water nanofluid with heat flux at a sub cooling of 20°C and mass flux of 400 kg/m^{2}s.

Figure 5.64 and Fig. 5.65 show the bubble diameter for ZnO-water nanofluids with concentrations and heat flux for 1.0 bar and 2.5 bar respectively.

Figure 5.64 shows that the bubble diameter increases marginally with increase in concentration of ZnO-water nanofluid. It is also observed that at 1.0 bar bubble nucleation starts at same heat flux for both distilled water and ZnO-water nanofluids. However, for 2.5 bar the bubble nucleation is delayed (Fig. 5.65) and begins at higher heat flux and size reduces at same heat flux as compared to distilled water.

5.4.1.5 Bubble Diameter of MWCNT-Water Nanofluid

The variation in bubble diameter of MWCNT-water nanofluid with pressure, heat flux and MWCNT nanoparticle concentration is observed in the present study. The experimental results in Fig. 5.66 and Fig. 5.67 show bubble diameter of 0.0001% MWCNT-water nanofluid and 0.001% MWCNT-water nanofluid with pressure and heat flux in an annular test section.

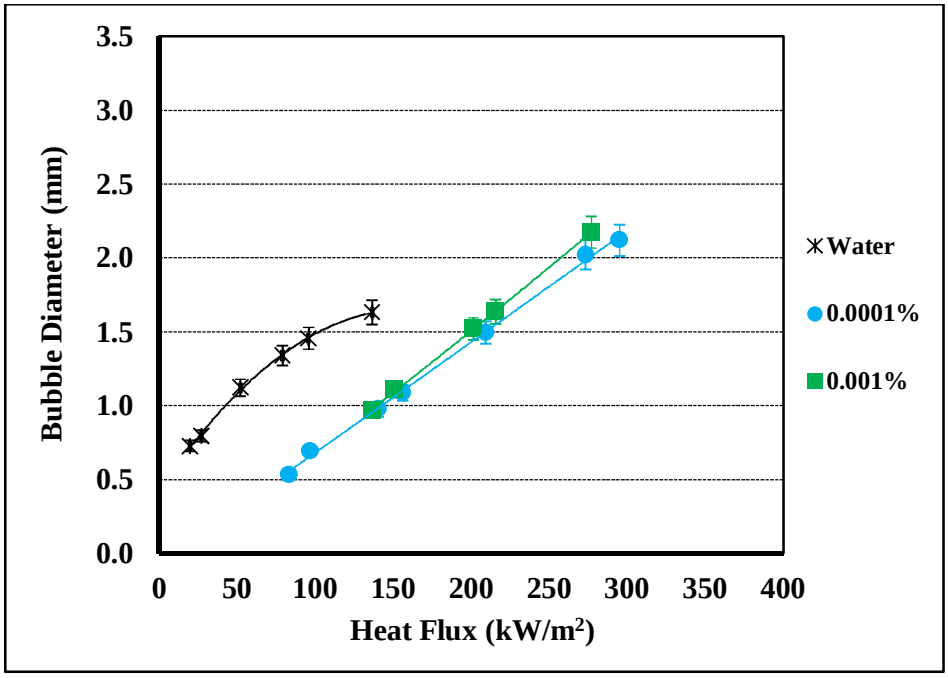

Figure 5.64. Bubble diameters of ZnO-water nanofluid with heat flux at a pressure of 1.0 bar, sub cooling of 20°C and mass flux of 400 kg/m^{2}s.

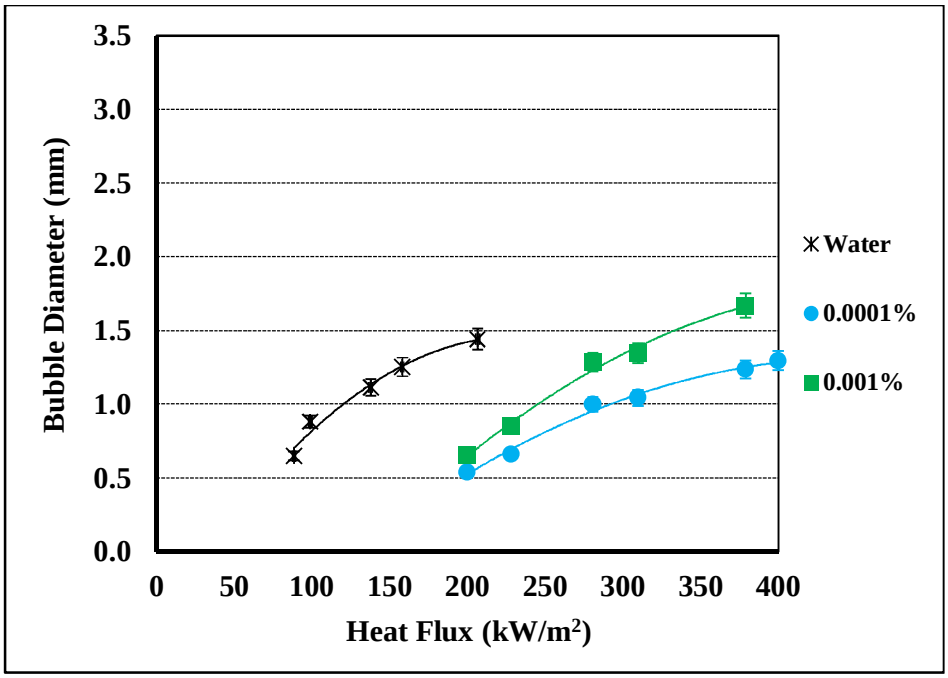

Figure 5.65. Bubble diameters of ZnO-water nanofluid with heat flux at a pressure of 2.5 bar, sub cooling of 20°C and mass flux of 400 kg/m^{2}s.

The visualization and image processing couldn't be done for 0.01% MWCNT-water nanofluid and higher concentrations due to opacity of MWCNT-water nanofluid. The experimental results with respect to bubble diameter of MWCNT-water nanofluid and its dependence on pressure show that pressure acts as a suppressing agent, i.e. with increase in pressure bubble diameter decreases and boiling is delayed in MWCNT-water nanofluids. Results show that bubble diameter of MWCNT-water nanofluid increases with increase in heat flux. Bubble diameter also increases with increase in concentration of MWCNT-water nanofluid at all variable pressure.

Figure 5.68 and Fig. 5.69 show the bubble diameter for MWCNT-water nanofluids with concentrations and heat flux for 1.0 bar and 2.5 bar respectively. Figure 5.68 shows that the bubble diameter increases marginally with increase in concentration of MWCNT-water nanofluid. It is also observed that at 1.0 bar bubble nucleation starts at same heat flux for both distilled water and MWCNT-water nanofluids. However, for 2.5 bar the bubble nucleation is delayed (Fig. 5.69) and begins at higher heat flux and size reduces at same heat flux as compared to distilled water.

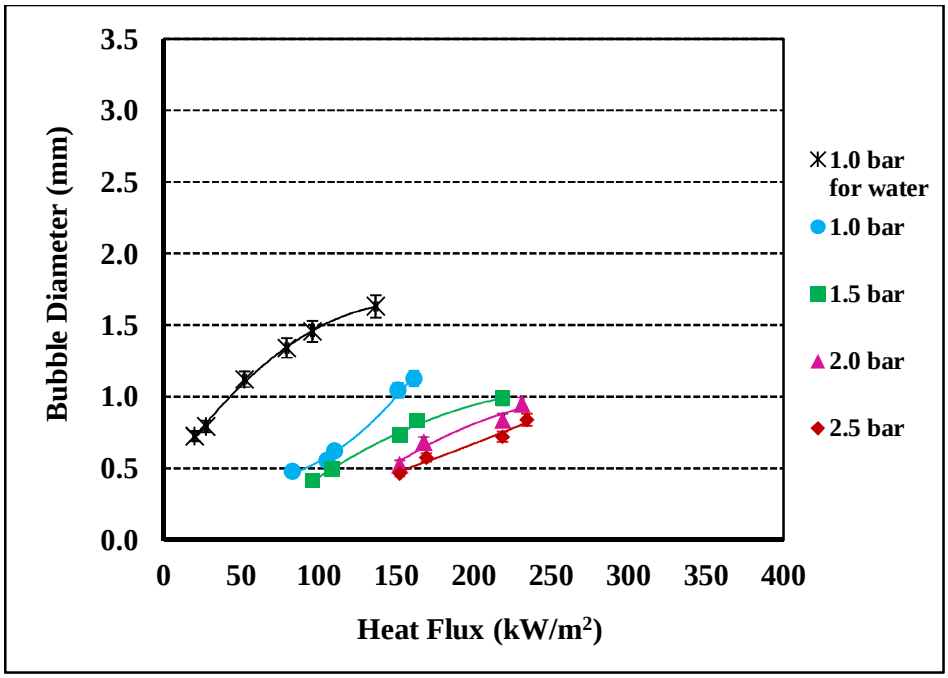

Figure 5.66. Bubble diameters of 0.0001% MWCNT-water nanofluid with heat flux at a sub cooling of 20°C and mass flux of 400 kg/m^{2}s.

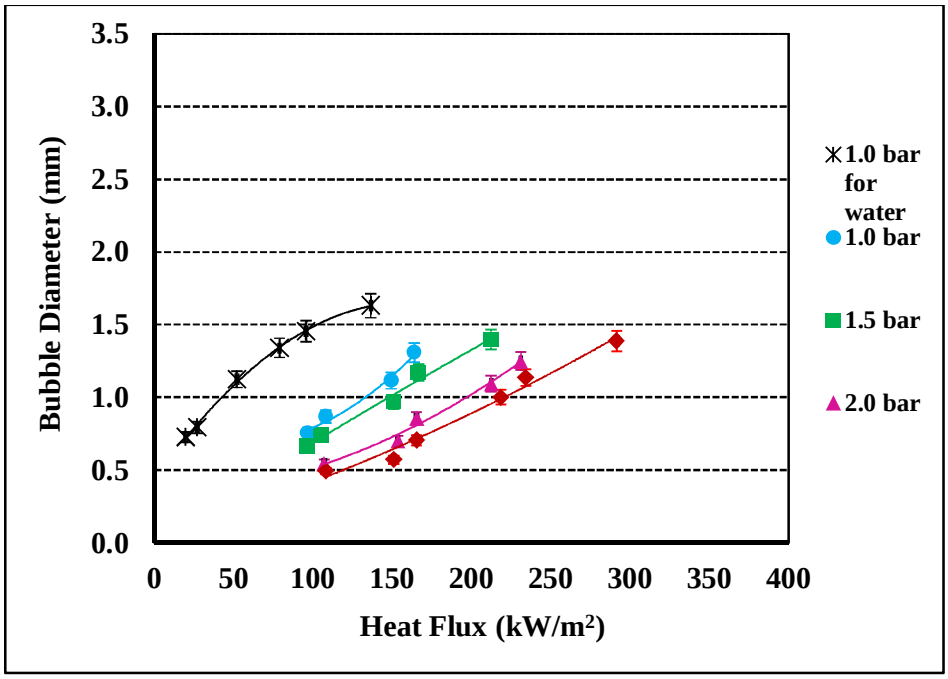

Figure 5.67. Bubble diameters of 0.001% MWCNT-water nanofluid with heat flux at a sub cooling of 20°C and mass flux of 400 kg/m^{2}s.

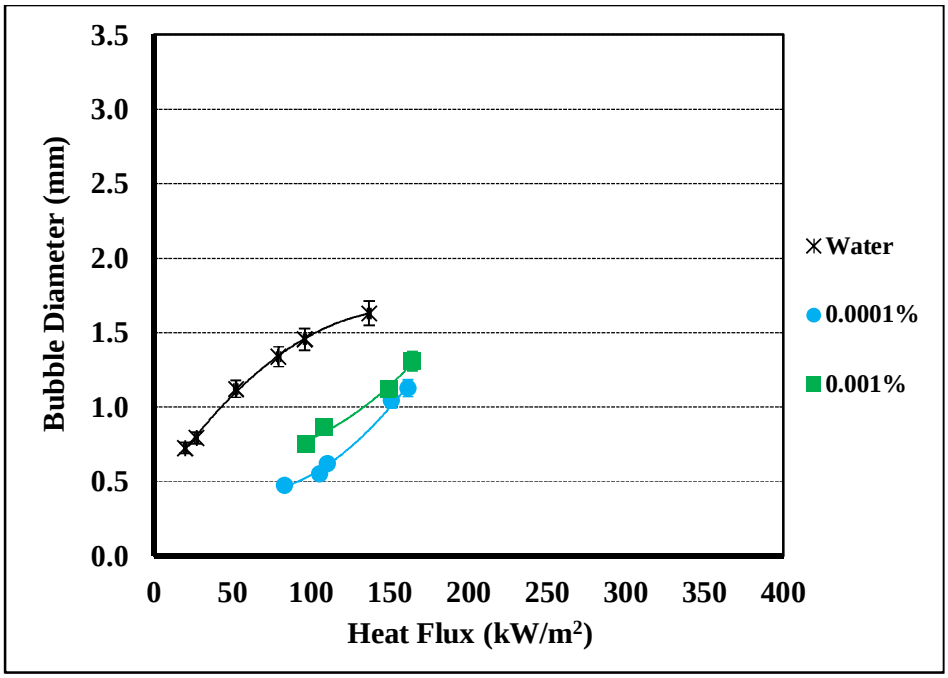

Figure 5.68. Bubble diameters of MWCNT-water nanofluid with heat flux at a pressure of 1.0 bar, sub cooling of 20°C and mass flux of 400 kg/m^{2}s.

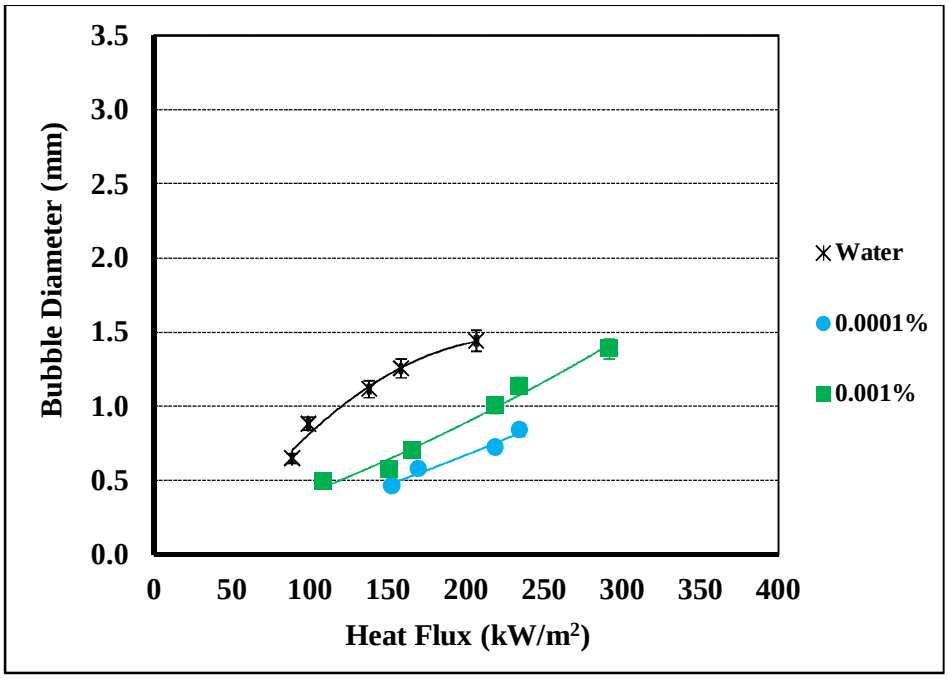

Figure 5.69. Bubble diameters of MWCNT-water nanofluid with heat flux at a pressure of 2.5 bar, sub cooling of 20°C and mass flux of 400 kg/m^{2}s.

5.4.2 Bubble Density

Bubble density is number of bubbles in the observed region per unit image area of the heater surface. In this section, effect of pressure on bubble density studied for water and different nanofluids like: Al_2O_3-water nanofluid, TiO_2-water nanofluid, ZnO-water nanofluid and MWCNT-water nanofluid with varying heat flux and concentration of fluids.

5.4.2.1 Bubble Density of Water

The variation of bubble density of water with pressure and heat flux is observed in the present study. The experimental results in Fig. 5.70 show bubble density of water with pressure and heat flux in an annular test section. The experimental results of bubble density and its dependence on pressure show that pressure acts as a suppressing agent, i.e. with increase in pressure, bubble density decreases. Results show that bubble density of water increases with increase in heat flux. It is observed that bubble density decreases with increasing bubble diameter at constant heat flux and pressure.

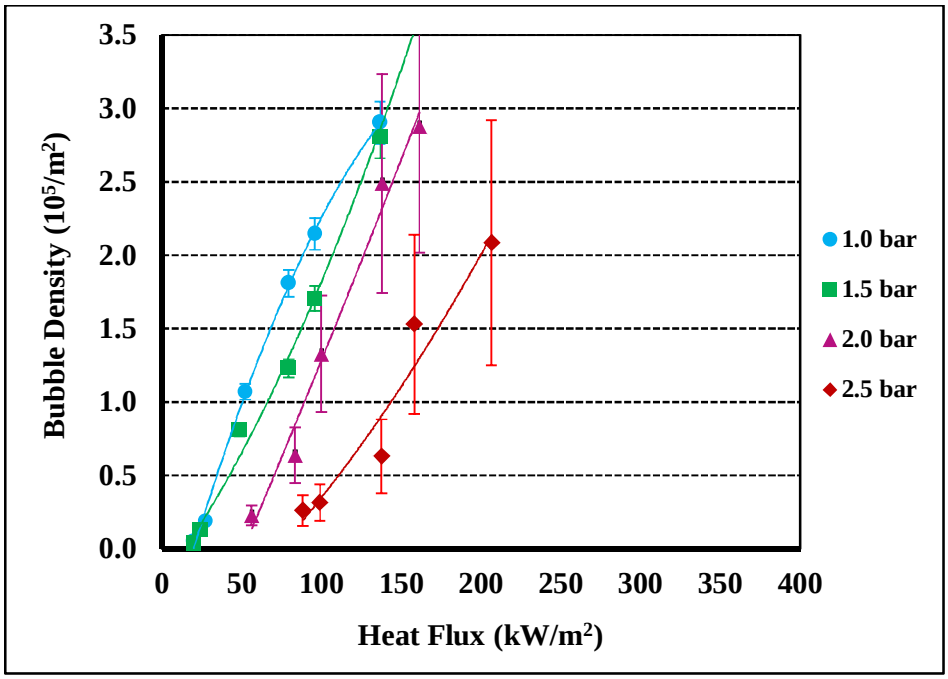

Figure 5.70. Bubble density of water with heat flux at a sub cooling of 20°C, mass flux of 400 kg/m^{2}s.

5.4.2.2 Bubble Density of Al_2O_3-Water Nanofluid

Variation in bubble density of Al_2O_3-water nanofluid with pressure, heat flux and concentration of Al_2O_3 nanoparticles in water has been studied.

To assess the repeatability of the tests, the bubble density of 0.0001% Al_2O_3-water nanofluid tested four times. Figure 5.71 shows the repeatability plots for bubble density of 0.0001% Al_2O_3-water nanofluid. The bubble density is plotted on the y-axis whereas heat flux is plotted on the x-axis. The four plots presented herein show that the values of bubble density show good repeatability in the experiments conducted.

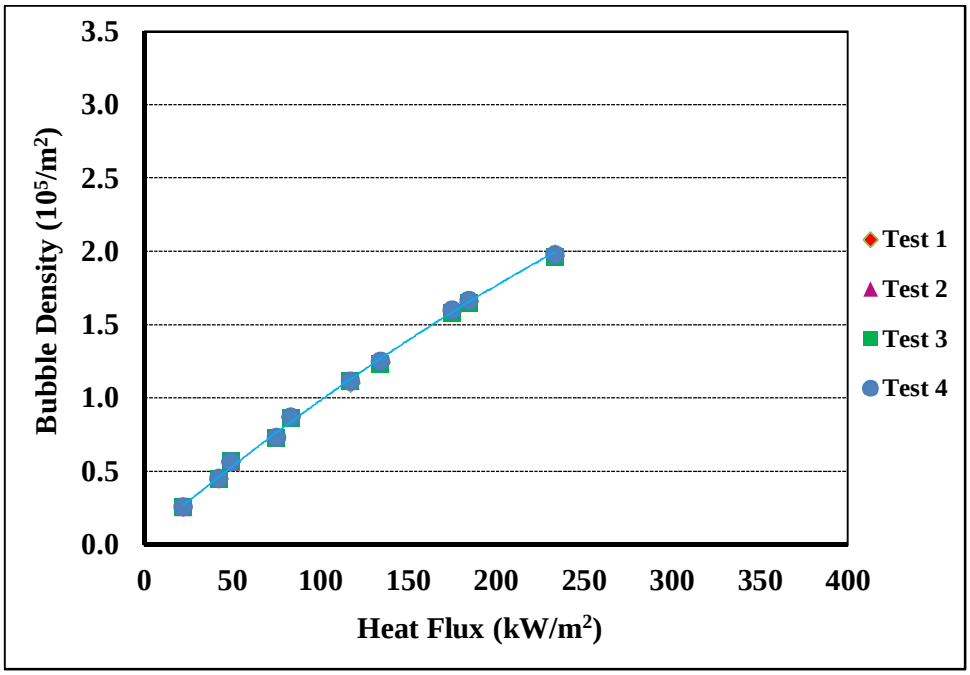

Figure 5.71. Results of repeatability test for bubble density of 0.0001% Al_2O_3-water nanofluid at a pressure of 1 bar, sub cooling of 20°C and mass flux of 400 kg/m^{2}s.

The change in bubble density of Al_2O_3-water nanofluid with pressure, heat flux and Al_2O_3 nanoparticle concentration is shown in Fig. 5.72 and Fig. 5.73. The figures show the bubble density for 0.0001% Al_2O_3-water nanofluid and 0.001% Al_2O_3-water nanofluid with pressure and heat flux respectively. The figures show that pressure acts as a suppressing agent, i.e. at same heat flux bubble density for Al_2O_3-water nanofluids decreases with increase in pressure. While the bubble

density observed less for Al_2O_3-water nanofluids at lower pressure, i.e. higher heat flux is required for higher bubble density of Al_2O_3-water nanofluids.

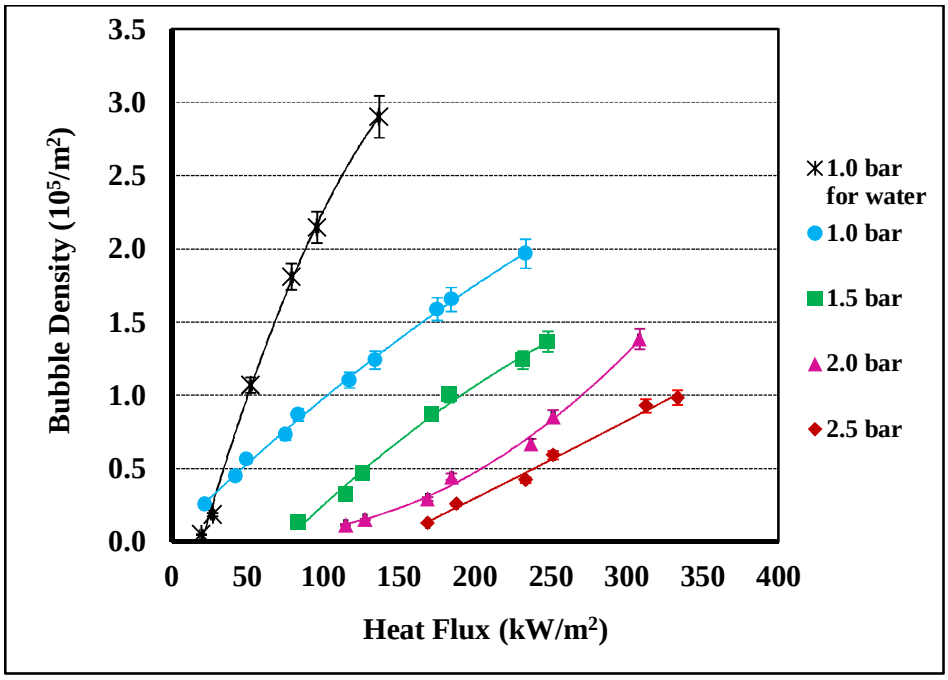

Figure 5.72. Bubble density of 0.0001% Al_2O_3-water nanofluid with heat flux at a sub cooling of 20°C and mass flux of 400 kg/m^{2}s.

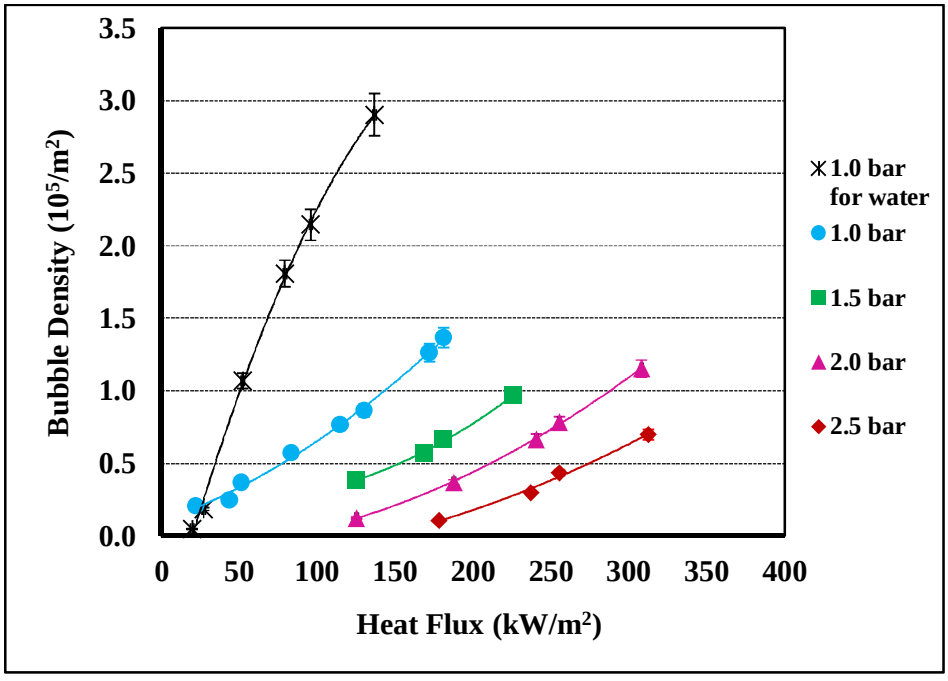

Figure 5.73. Bubble density of 0.001% Al_2O_3-water nanofluid with heat flux at a sub cooling of 20°C and mass flux of 400 kg/m^{2}s.

Figure 5.74 and Fig. 5.75 show the bubble density of for Al_2O_3-water nanofluids with concentration and heat flux for 1.0 bar and 2.5 bar respectively.

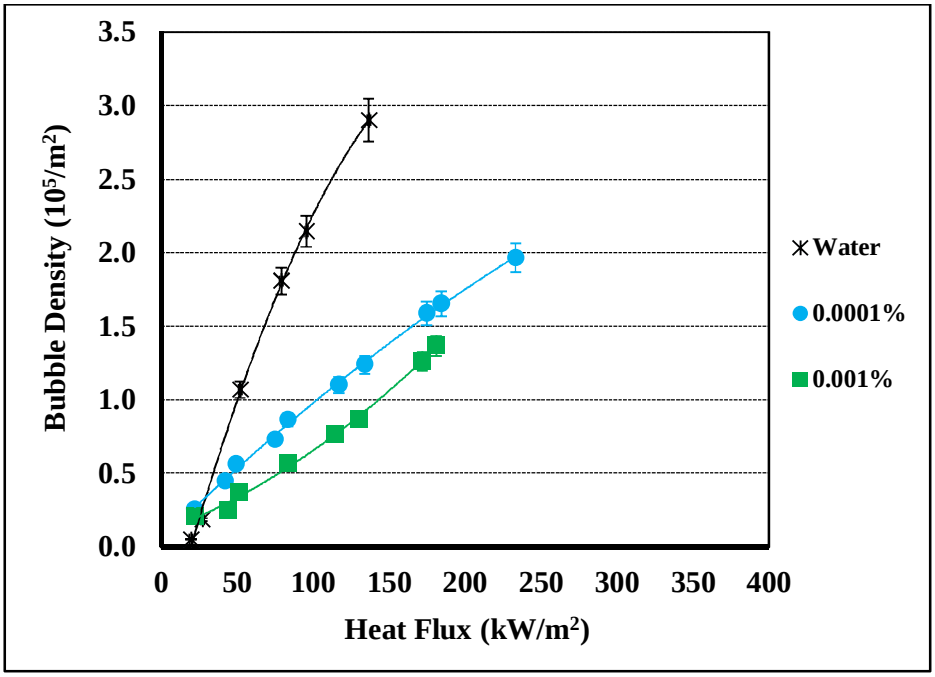

Figure 5.74. Bubble density of Al_2O_3-water nanofluid with heat flux at a pressure of 1.0 bar, sub cooling of 20°C and mass flux of 400 kg/m^{2}s.

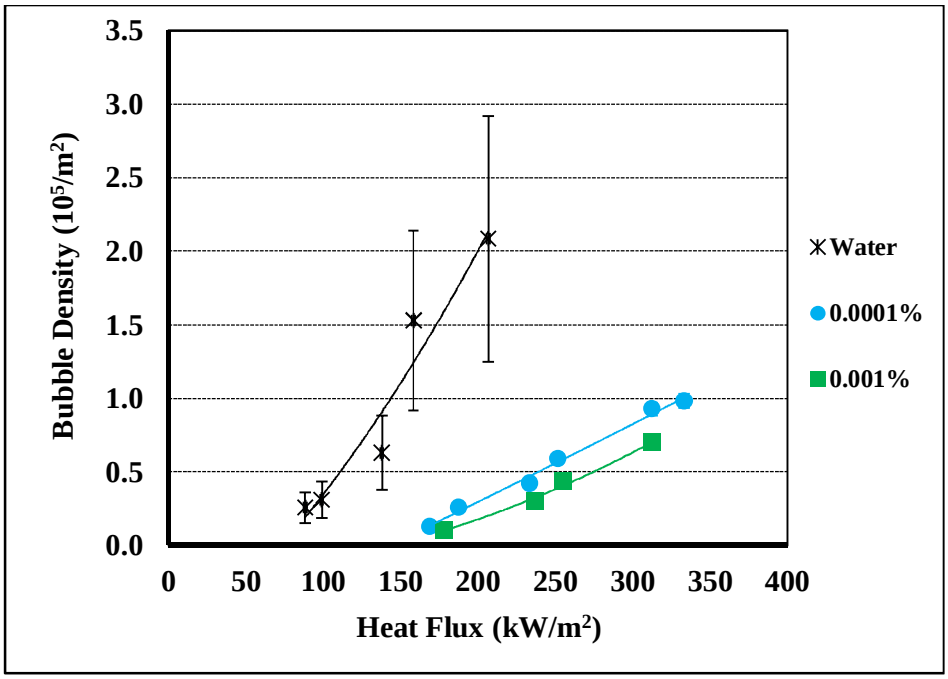

Figure 5.75. Bubble density of Al_2O_3-water nanofluid with heat flux at a pressure of 2.5 bar, sub cooling of 20°C and mass flux of 400 kg/m^{2}s.

Figure 5.74 shows that the bubble density increases with increase in heat flux but decreases with increase in concentration for Al_2O_3-water nanofluid. It is also observed that at 1.0 bar bubble nucleation starts at same heat flux for both water and Al_2O_3-water nanofluids.

But as shown in Fig. 5.75 for 2.5 bar the bubble density is less even at higher heat flux for higher concentration of Al_2O_3-water nanofluids over distilled water.

5.4.2.3 Bubble Density of TiO_2-Water Nanofluid

The variation in bubble density of TiO_2-water nanofluid with pressure, heat flux and TiO_2 nanoparticle concentration is observed here. The experimental results in Fig. 5.76 and Fig. 5.77 show bubble density of 0.0001% TiO_2-water nanofluid and 0.001% TiO_2-water nanofluid with pressure and heat flux in an annular test section.

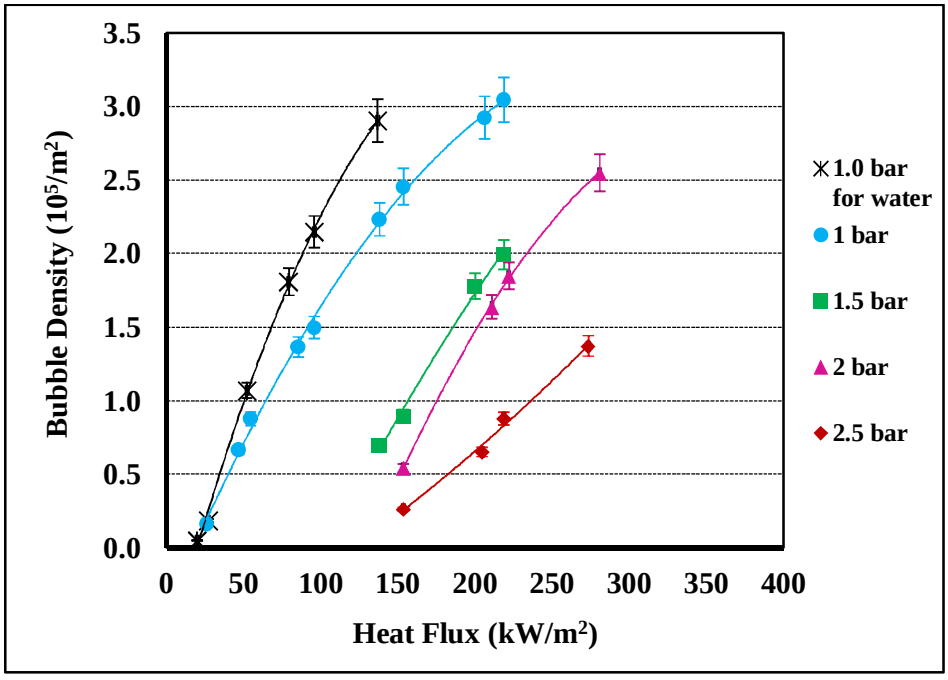

Figure 5.76. Bubble density of 0.0001% TiO_2-water nanofluid with heat flux at a sub cooling of 20°C and mass flux of 400 kg/m^{2}s.

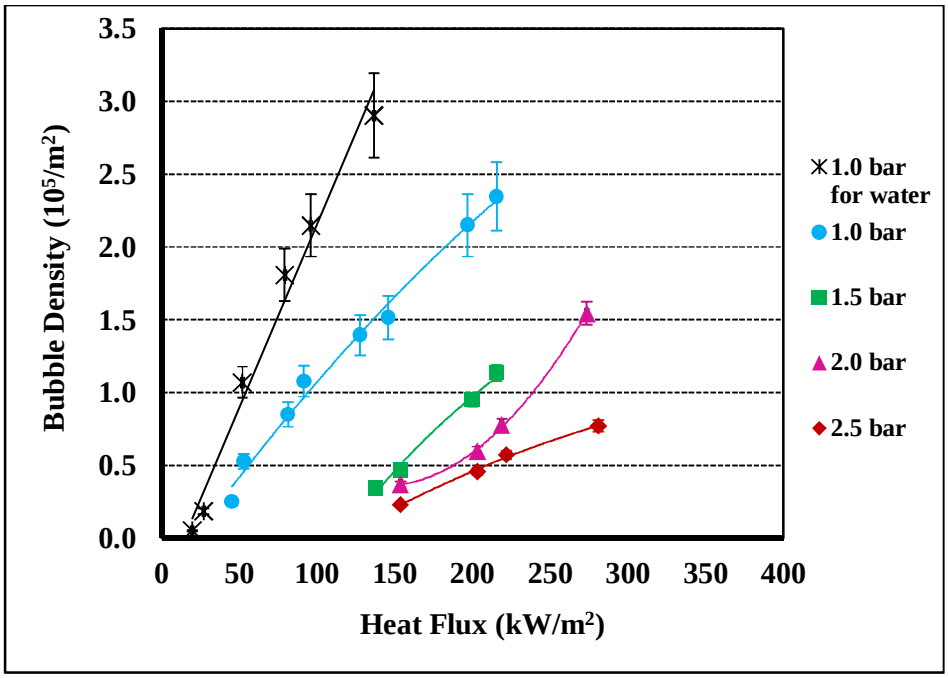

Figure 5.77. Bubble density of 0.001% TiO_2-water nanofluid with heat flux at a sub cooling of 20°C and mass flux of 400 kg/m^{2}s.

The experimental results of bubble density and its dependence on pressure show that similar to water, pressure acts as a suppressing agent for TiO_2-water nanofluid, i.e. with increase in pressure, bubble density of TiO_2-water nanofluids decreases.

Results show that bubble density increases with increase in heat flux. Bubble density decreased with concentration of TiO_2-water nanofluid.

Figure 5.78 and Fig. 5.79 show the bubble density of for TiO_2-water nanofluids with concentration and heat flux for 1.0 bar and 2.5 bar respectively.

Figure 5.78 shows that the bubble density increases with increase in heat flux but decreases with increase in concentration for TiO_2-water nanofluid. It is also observed that at 1.0 bar bubble nucleation starts at same heat flux for both water and TiO_2-water nanofluids. But as shown in Fig. 5.79 for 2.5 bar the bubble density is less even at higher heat flux for higher concentration of TiO_2-water nanofluids over distilled water.

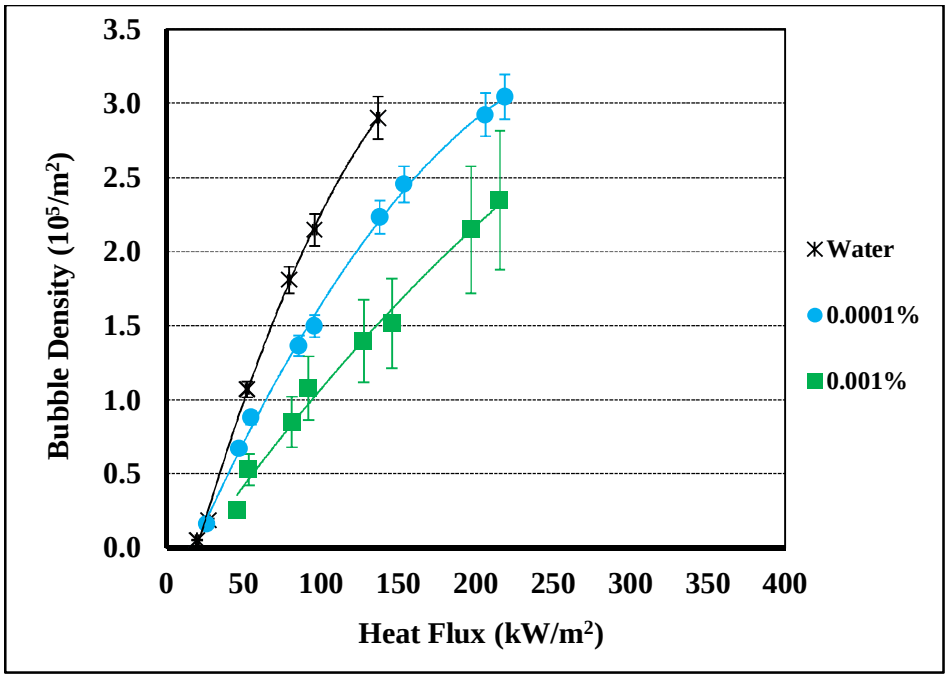

Figure 5.78. Bubble density of TiO_2-water nanofluid with heat flux at a pressure of 1.0 bar, sub cooling of 20°C and mass flux of 400 kg/m^{2}s.

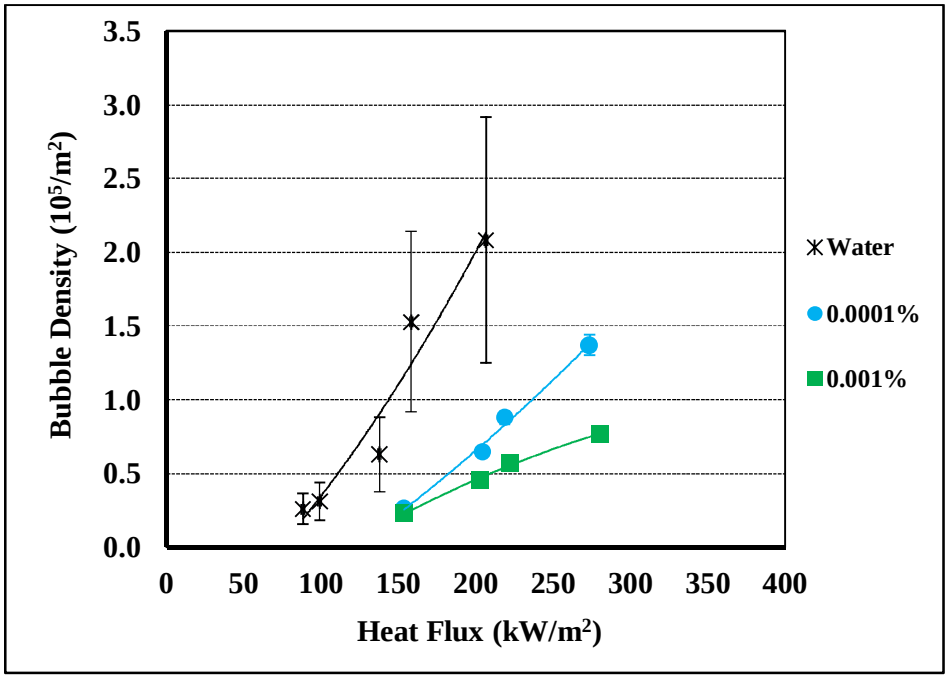

Figure 5.79. Bubble density of TiO_2-water nanofluid with heat flux at a pressure of 2.5 bar, sub cooling of 20°C and mass flux of 400 kg/m^{2}s.

5.4.2.4 Bubble Density of ZnO-Water Nanofluid

The variation in bubble density of ZnO-water nanofluid with pressure, heat flux and ZnO nanoparticle concentration is observed here. The experimental results in Fig. 5.80 and Fig. 5.81 show bubble density of 0.0001% ZnO-water nanofluid and 0.001% ZnO-water nanofluid with pressure and heat flux in an annular test section. The experimental results of bubble density of ZnO-water nanofluid and its dependence on pressure show that similar to case of Al_2O_3-water nanofluids and TiO_2-water nanofluids, pressure acts as a suppressing agent, i.e. with increase in pressure, bubble density of ZnO-water nanofluid decreases.

Figure 5.82 and Fig. 5.83 show the bubble density of for ZnO-water nanofluids with concentration and heat flux for 1.0 bar and 2.5 bar respectively.

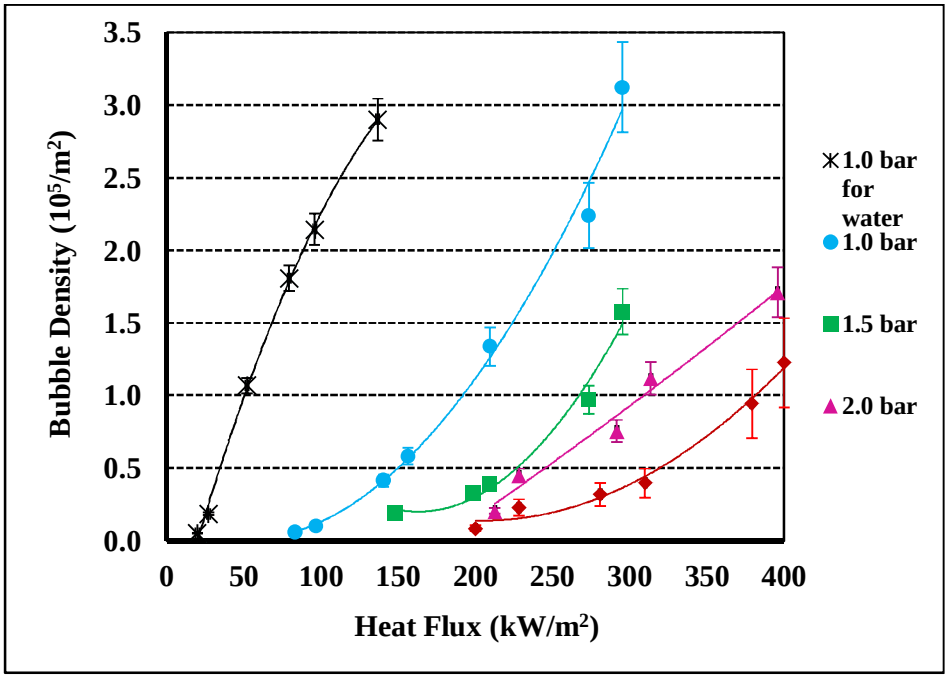

Figure 5.80. Bubble density of 0.0001% ZnO-water nanofluid with heat flux at a sub cooling of 20°C and mass flux of 400 kg/m²s.

Figure 5.82 shows that the bubble density increases with increase in heat flux but decreases with increase in concentration for ZnO-water nanofluid. It is also observed that at 1.0 bar bubble nucleation starts at higher heat flux for higher concentration of ZnO-water nanofluid. As shown in Fig. 5.83 for 2.5 bar the

bubble density is less even at higher heat flux for higher concentration of ZnO-water nanofluids over distilled water.

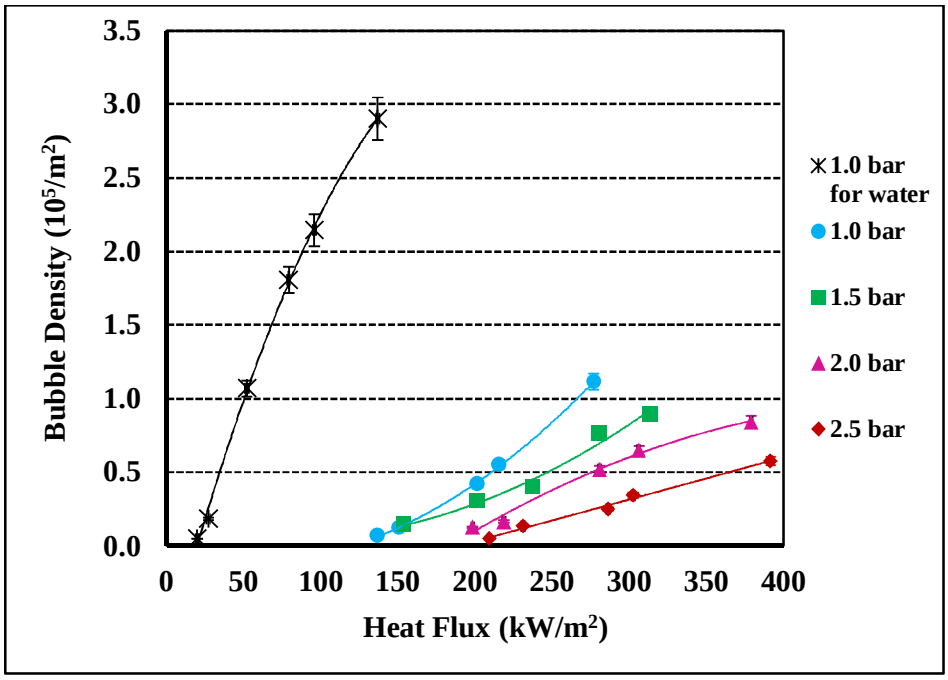

Figure 5.81. Bubble density of 0.001% ZnO-water nanofluid with heat flux at a sub cooling of 20°C and mass flux of 400 kg/m^{2}s.

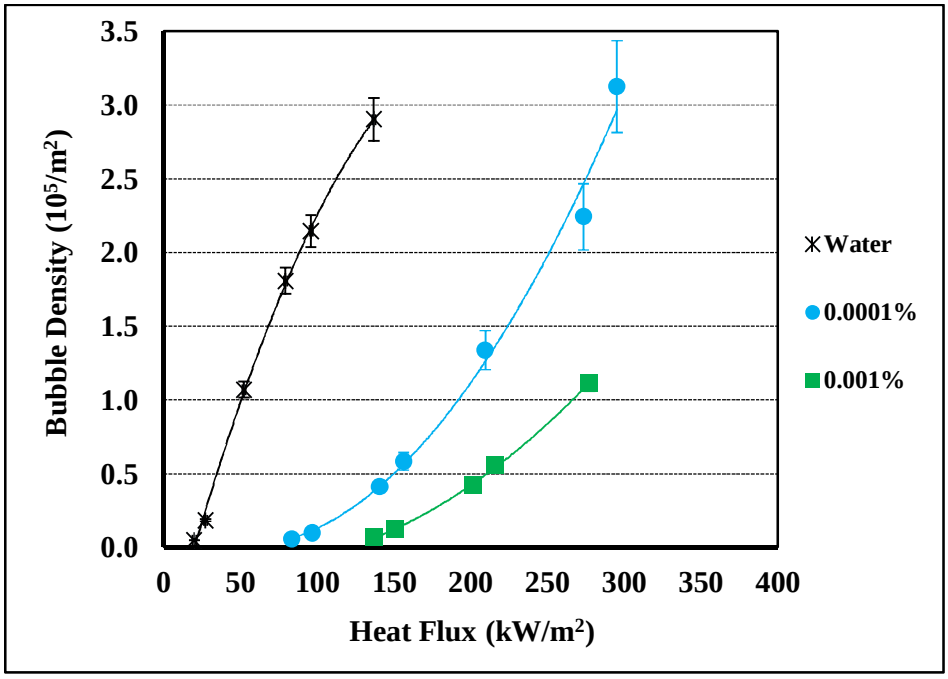

Figure 5.82. Bubble density of ZnO-water nanofluid with heat flux at a pressure of 1.0 bar, sub cooling of 20°C and mass flux of 400 kg/m^{2}s.

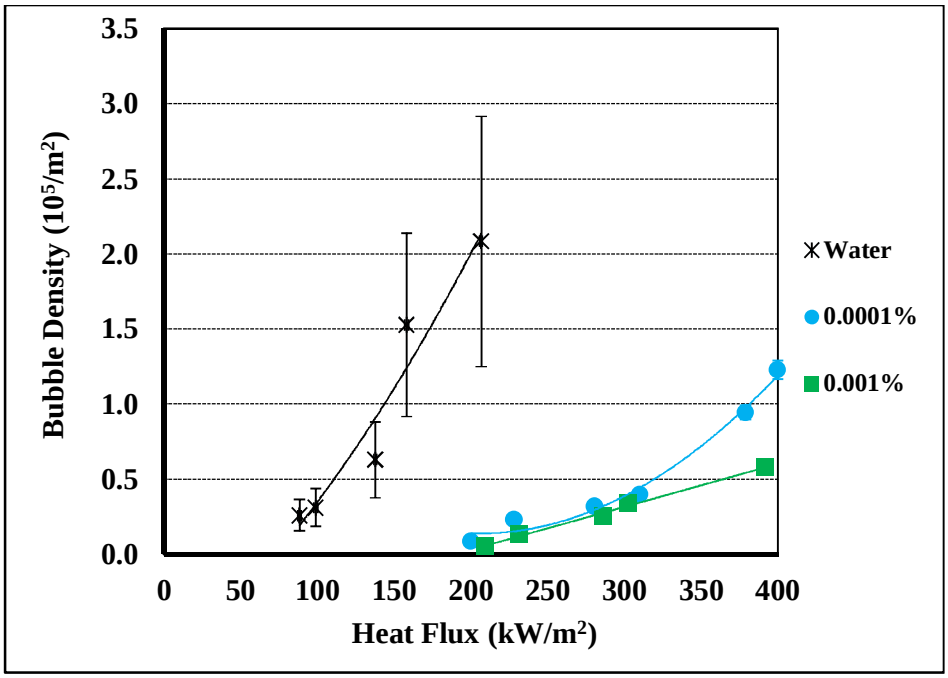

Figure 5.83. Bubble density of ZnO-water nanofluid with heat flux at a pressure of 2.5 bar, sub cooling of 20°C and mass flux of 400 kg/m^{2}s.

5.4.2.5 Bubble Density of MWCNT-Water Nanofluid

The variation in bubble density of MWCNT-water nanofluid with pressure, heat flux and MWCNT nanoparticle concentration is observed here.

The experimental results in Fig. 5.84 and Fig. 5.85 show bubble density of 0.0001% MWCNT-water nanofluid and 0.001% MWCNT-water nanofluid with pressure and heat flux in an annular test section.

The experimental results of bubble density of MWCNT-water nanofluid and its dependence on pressure show that similar to case of other selected nanofluids, pressure acts as a suppressing agent, i.e. with increase in pressure, bubble density of MWCNT-water nanofluid decreases.

Figure 5.86 and Fig. 5.87 show the bubble density of for MWCNT-water nanofluids with increase in heat flux for different concentration. It increases with heat flux but decreases with increase in concentration for MWCNT-water nanofluid, at a pressure for 1.0 bar and 2.5 bar respectively.

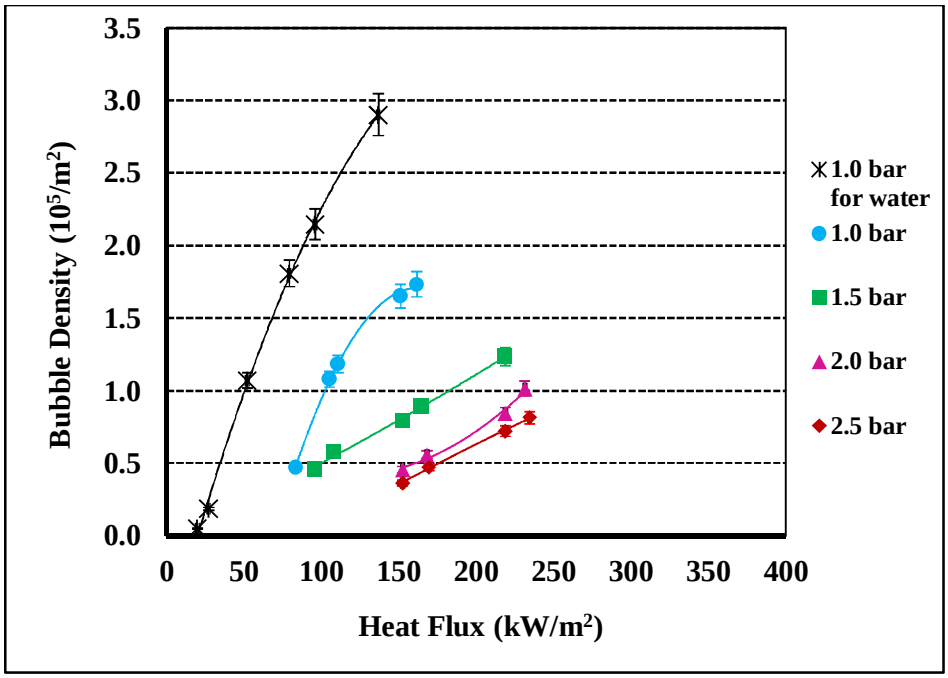

Figure 5.84. Bubble density of 0.0001% MWCNT-water nanofluid with heat flux at a sub cooling of 20°C and mass flux of 400 kg/m^{2}s.

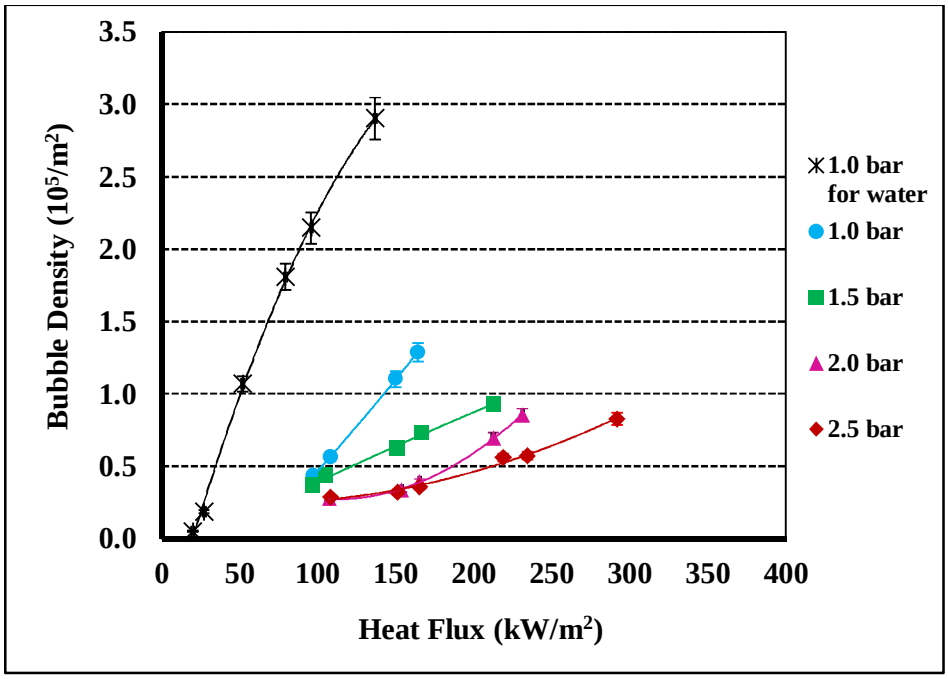

Figure 5.85. Bubble density of 0.001% MWCNT-water nanofluid with heat flux at a sub cooling of 20°C and mass flux of 400 kg/m^{2}s.

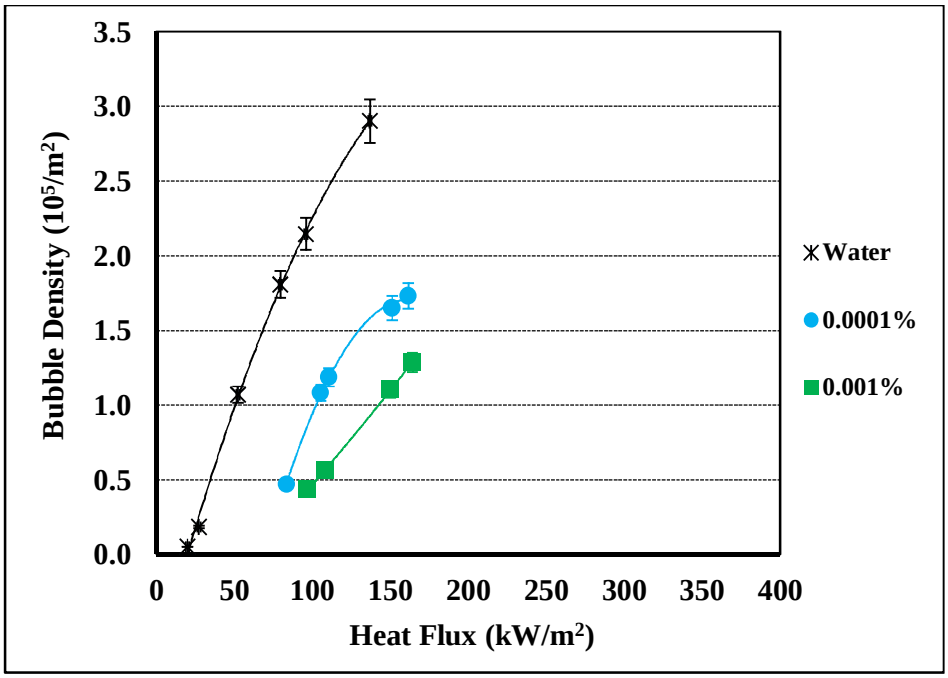

Figure 5.86. Bubble density of MWCNT-water nanofluid with heat flux at a pressure of 1.0 bar, sub cooling of 20°C and mass flux of 400 kg/m^{2}s.

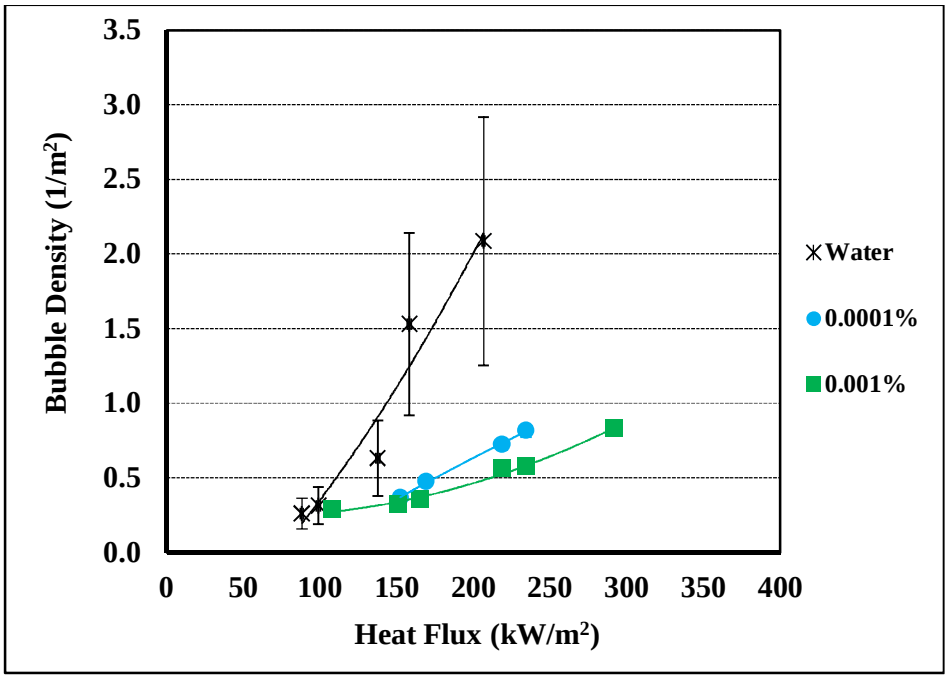

Figure 5.87. Bubble density of MWCNT-water nanofluid with heat flux at a pressure of 2.5 bar, sub cooling of 20°C and mass flux of 400 kg/m^{2}s.

5.4.3 Void Fraction

Void fraction is determined after image processing of images taken by high speed camera in the view perpendicular to the heater under proper illumination. Void fraction is the ratio of bubbles area in the unit image area of the heater surface. The void fraction, measured as empty portion in a cross sectional view depends on density of the bubbles and square of the bubble diameters.

5.4.3.1 Void Fraction of Water

The variation of void fraction of distilled water and nanofluids with pressure and heat flux has been studied. Experimental data in Fig. 5.88 show void fraction of water with applied pressure and heat flux in an annular test section.

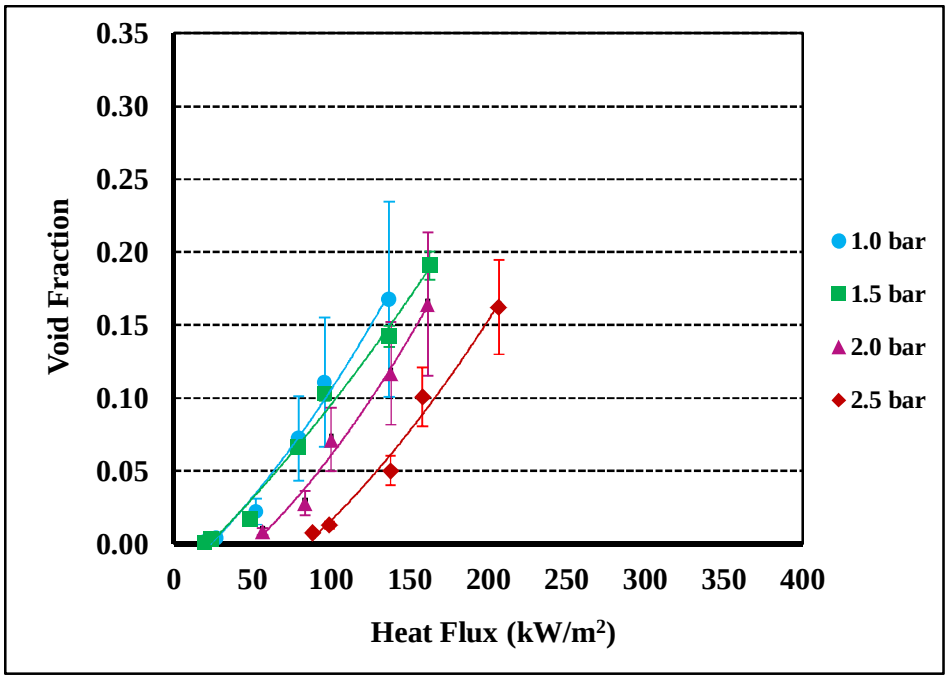

Figure 5.88. Void fraction of water with heat flux at a sub cooling of 20°C and mass flux of 400 kg/m^{2}s.

The experimental results of void fraction and its dependence on pressure show that pressure acts as a suppressor, i.e. with increase in pressure, void fraction decreases and boiling is delayed in water as higher pressure suppresses the

bubbles and due to reduced bubble diameter and bubble density overall void fraction reduces. It indicates that at high pressure, nucleation point in flow boiling of water rises, which is useful for nuclear reactors and other engineering applications. The results also show that void fraction increases with increase in heat flux.

5.4.3.2 Void Fraction of Al_2O_3-Water Nanofluid

Variation in void fraction for Al_2O_3-water nanofluid with pressure, heat flux and concentration of Al_2O_3 nanoparticles in water has been studied.

To assess the repeatability of the tests, the void fraction for 0.0001% Al_2O_3-water nanofluid tested four times. Figure 5.89 shows the repeatability plots for void fraction considering 0.0001% Al_2O_3-water nanofluid. The void fraction is plotted on the y-axis whereas heat flux is plotted on the x-axis. The four plots presented herein show that the values of void fraction show good repeatability in the experiments conducted.

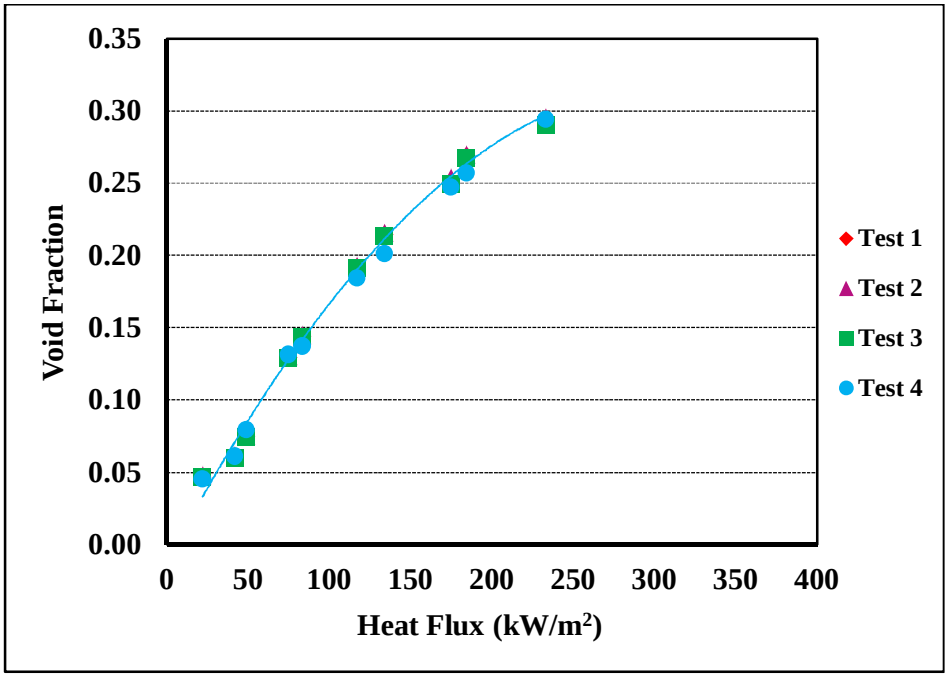

Figure 5.89. Results of repeatability test for void fraction of 0.0001% Al_2O_3-water nanofluid at a pressure of 1 bar, sub cooling of 20°C and mass flux of 400 kg/m^{2}s.

The variation of void fraction of Al_2O_3-water nanofluid with pressure, heat flux and Al_2O_3 nanoparticle concentration is studied experimentally. Fig. 5.90 and Fig. 5.91 show void fraction of 0.0001% Al_2O_3-water nanofluid and 0.001% Al_2O_3-water nanofluid with applied pressure and heat flux in an annular test section.

The experimental results of void fraction and its dependence on pressure show similar effect as water. Pressure acts as a suppressor, i.e. with increase in pressure, void fraction of Al_2O_3-water nanofluids decreases and boiling is delayed in Al_2O_3-water nanofluid as higher pressure suppresses the bubble nucleation. It is also observed that the void fraction increases with increase in heat flux applied to the test section. Figure 5.92 and Fig. 5.93 show the void fraction of for Al_2O_3-water nanofluids with concentrations and heat flux for 1.0 bar and 2.5 bar respectively. Figure 5.92 shows that the void fraction increases with increase in heat flux and concentration for Al_2O_3-water nanofluid due to larger area covered by increase in bubble diameter in an image.

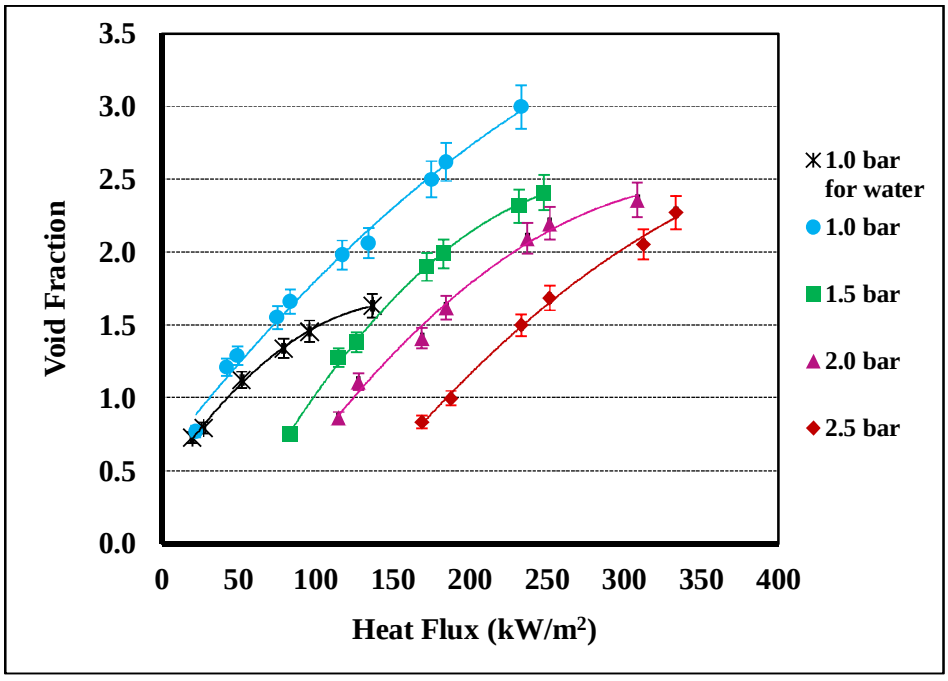

Figure 5.90. Void fraction of 0.0001% Al_2O_3-water nanofluid with heat flux at a sub cooling of 20°C and mass flux of 400 kg/m^{2}s.

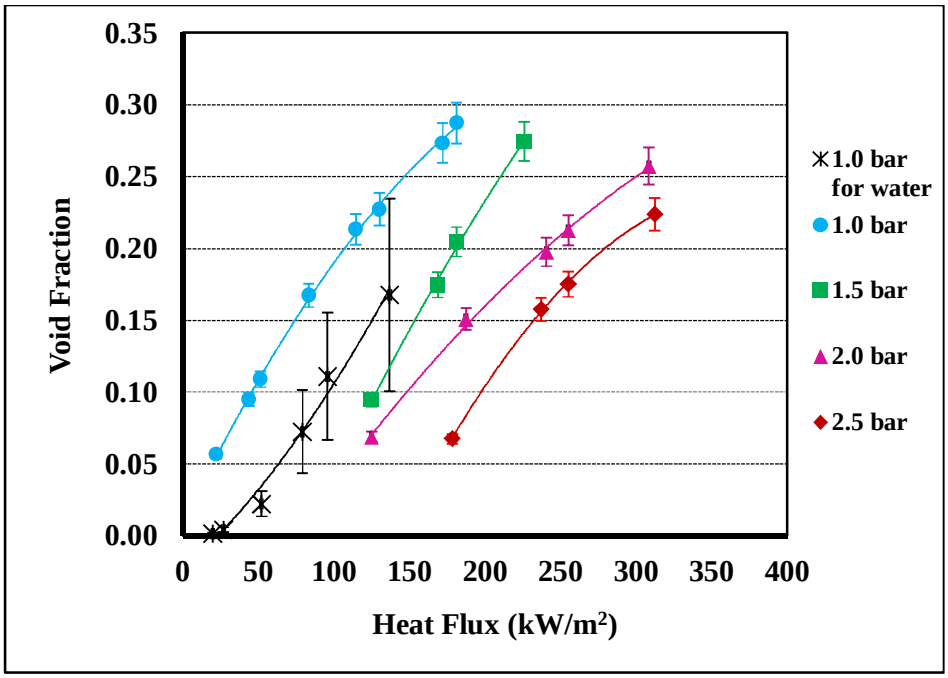

Figure 5.91. Void fraction of 0.001% Al_2O_3-water nanofluid with heat flux at a sub cooling of 20°C and mass flux of 400 kg/m^{2}s.

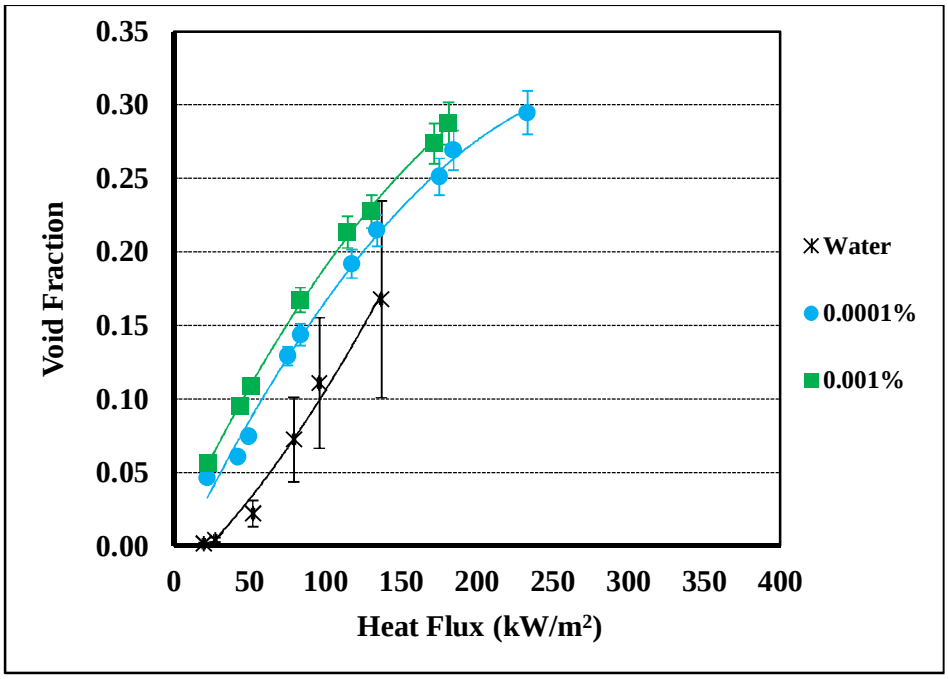

Figure 5.92. Void fraction of Al_2O_3-water nanofluid with heat flux at a pressure of 1.0 bar, sub cooling of 20°C and mass flux of 400 kg/m^{2}s.

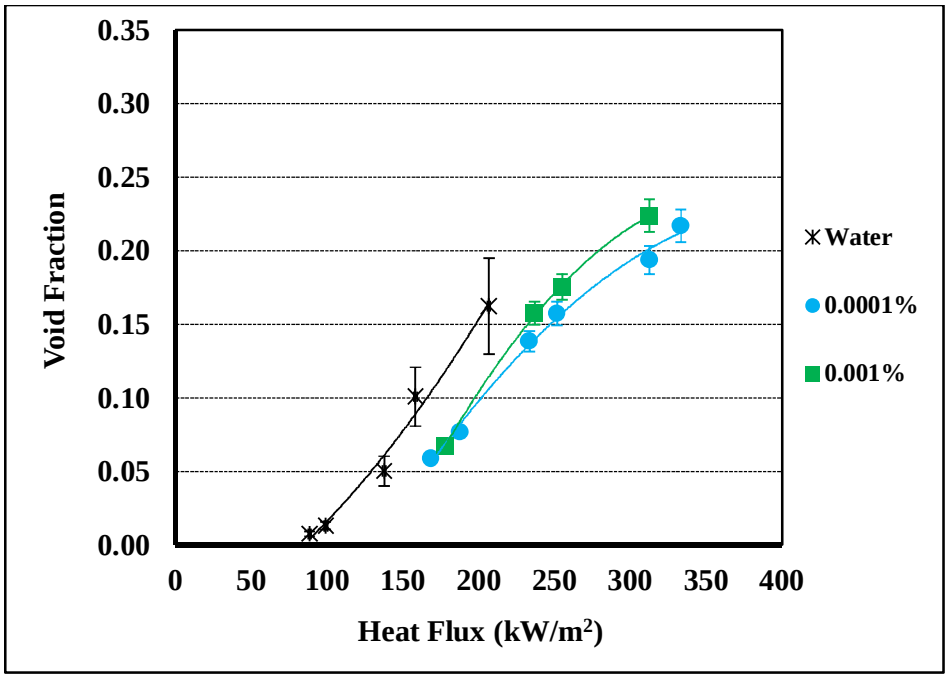

Figure 5.93. Void fraction of Al_2O_3-water nanofluid with heat flux at a pressure of 2.5 bar, sub cooling of 20°C and mass flux of 400 kg/m^{2}s.

It is also observed that at 1.0 bar bubble nucleation starts at same heat flux for both water and Al_2O_3-water nanofluids. But as shown in Fig. 5.93 for 2.5 bar the void fraction is shifted at higher heat flux for higher concentrations of Al_2O_3-water nanofluids over water.

5.4.3.3 Void Fraction of TiO_2-Water Nanofluid

The variation of void fraction of TiO_2-water nanofluid with pressure, heat flux and concentration of TiO_2 nanoparticle in water has been studied. Experimental data in Fig. 5.94 and Fig. 5.95 show void fraction of 0.0001% TiO_2-water nanofluid and 0.001% TiO_2-water nanofluid with increase in heat flux and pressure in an annular test section. The experimental results of void fraction and its dependence on pressure show similar effect as water and Al_2O_3-water nanofluids. It is observed that pressure acts as a suppressor, i.e. with increase in pressure, void fraction decreases and boiling is delayed in TiO_2-water nanofluids as higher pressure suppresses the bubbles.

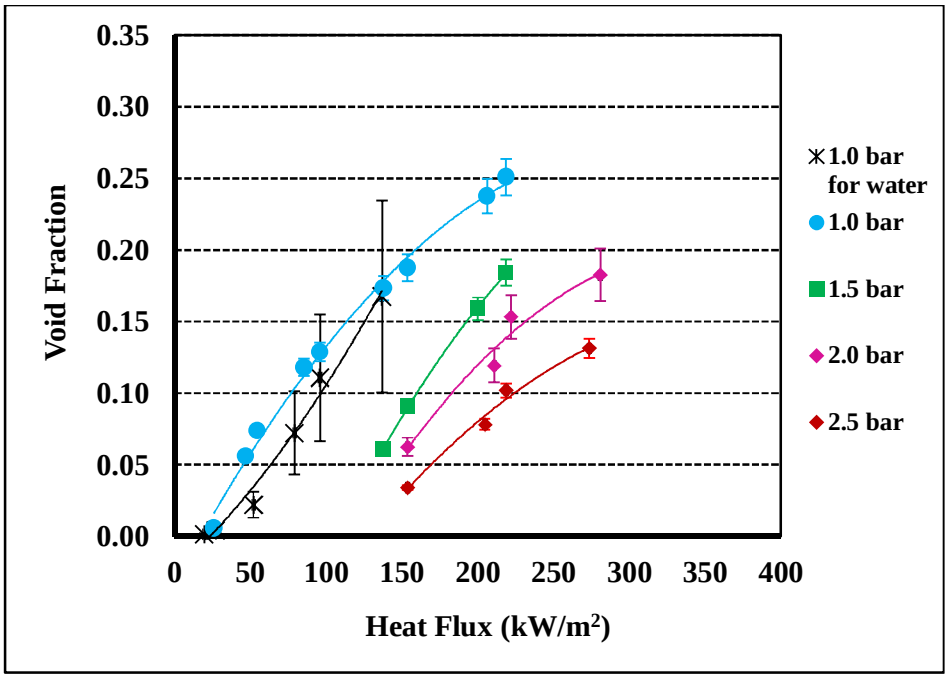

Figure 5.94. Void fraction of 0.0001% TiO_2-water nanofluid with heat flux at a sub cooling of 20°C and mass flux of 400 kg/m^{2}s.

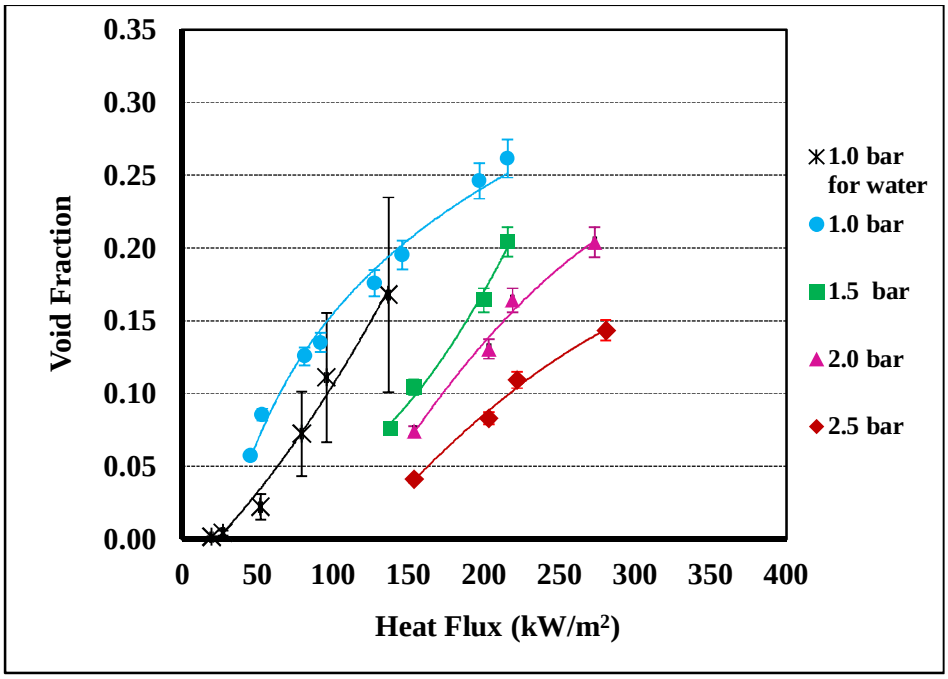

Figure 5.95. Void fraction of 0.001% TiO_2-water nanofluid with heat flux at a sub cooling of 20°C and mass flux of 400 kg/m^{2}s.

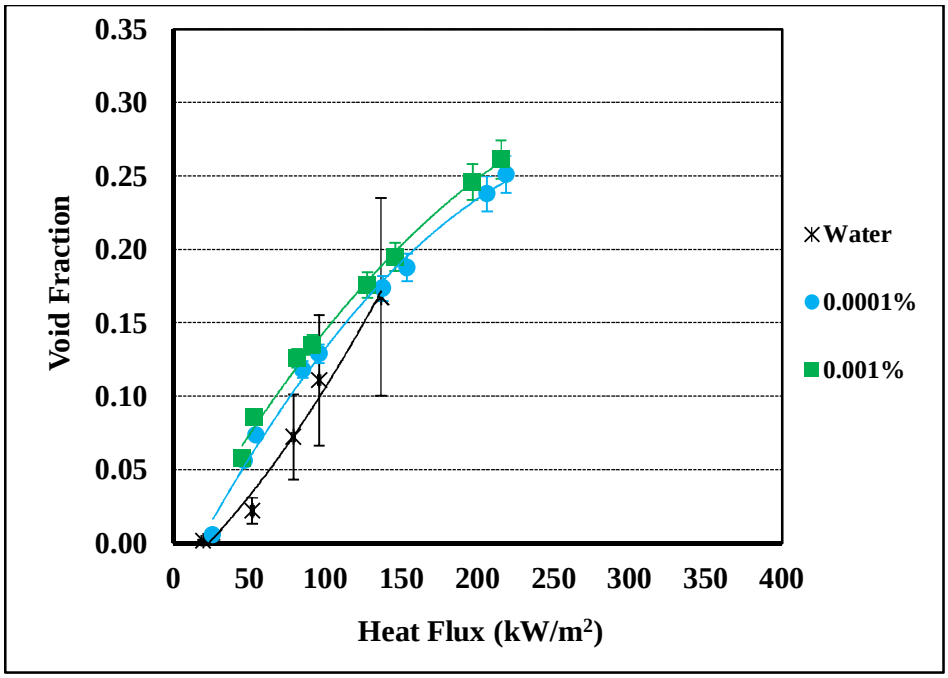

Figure 5.96. Void fraction of TiO_2-water nanofluid with heat flux at a pressure of 1.0 bar, sub cooling of 20°C and mass flux of 400 kg/m^{2}s.

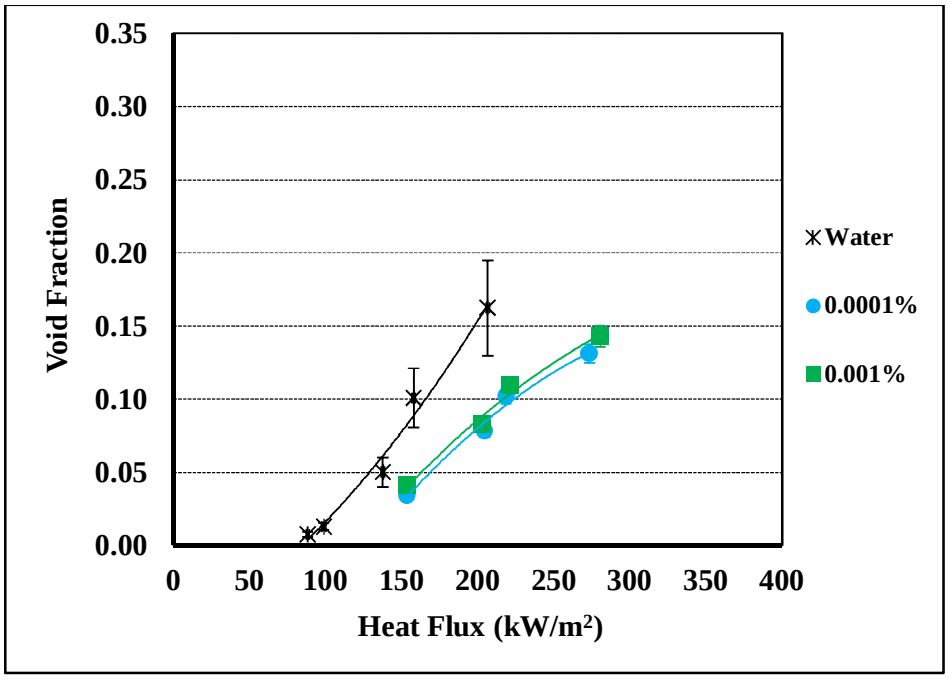

Figure 5.97. Void fraction of TiO_2-water nanofluid with heat flux at a pressure of 2.5 bar, sub cooling of 20°C and mass flux of 400 kg/m^{2}s.

Figure 5.96 and Fig. 5.97 show the void fraction of for TiO_2-water nanofluids with concentrations and heat flux for 1.0 bar and 2.5 bar respectively.

Figure 5.96 shows that the void fraction increases with increase in heat flux and concentration for TiO_2-water nanofluid. It is also observed that at 1.0 bar bubble nucleation starts at same heat flux for both water and TiO_2-water nanofluids. But as shown in Fig. 5.97 for 2.5 bar the void fraction is higher at shifted higher heat flux for higher concentrations of TiO_2-water nanofluids over distilled water.

5.4.3.4 Void Fraction of ZnO-Water Nanofluid

The variation of void fraction of ZnO-water nanofluid with pressure, heat flux and concentration of ZnO nanoparticle in water has been studied. Experimental data in Fig. 5.98 and Fig. 5.99 show void fraction of 0.0001% ZnO-water nanofluid and 0.001% ZnO-water nanofluid with applied pressure and heat flux in an annular test section.

The experimental results of void fraction and its dependence on pressure show similar effect as water, Al_2O_3-water nanofluids and TiO_2-water nanofluids. It is observed that pressure acts as a suppressor, i.e. with increase in pressure, void fraction decreases and boiling is delayed in ZnO-water nanofluids as higher pressure suppresses the bubbles.

Figure 5.100 and Fig. 5.101 show the void fraction of for ZnO-water nanofluids with concentrations of nanoparticles in water and heat flux for 1.0 bar and 2.5 bar respectively.

Figure 5.100 shows that the void fraction increases with increase in heat flux and concentration for ZnO-water nanofluid. It is also observed that at 1.0 bar bubble nucleation starts at same heat flux for both water and ZnO-water nanofluids. But as shown in Fig. 5.101 for 2.5 bar the void fraction is higher at shifted higher heat flux for higher concentrations of ZnO-water nanofluids over distilled water.

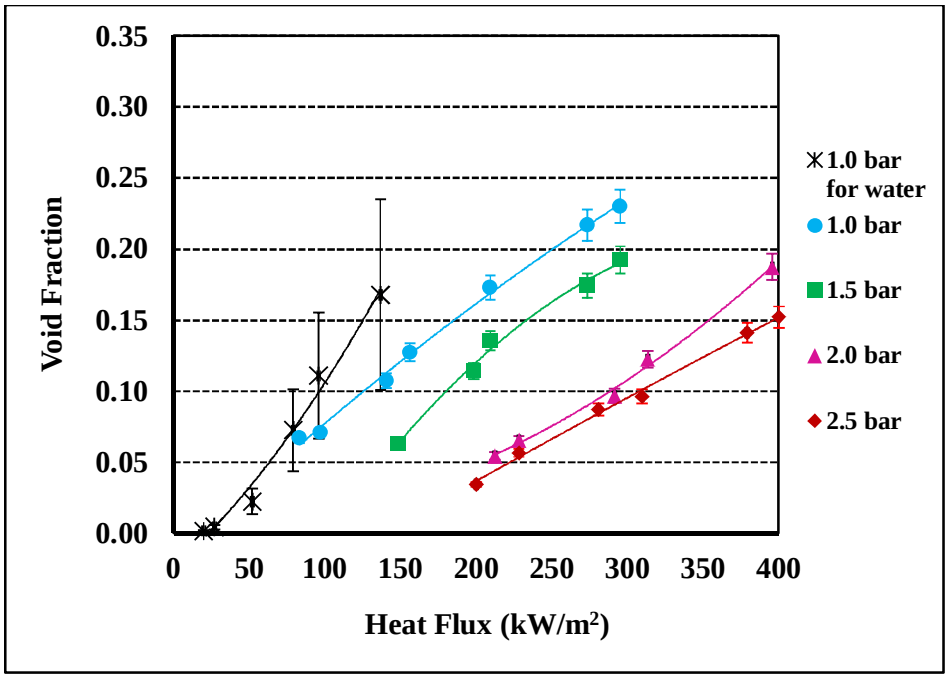

Figure 5.98. Void fraction of 0.0001% ZnO-water nanofluid with heat flux at a sub cooling of 20°C and mass flux of 400 kg/m^{2}s.

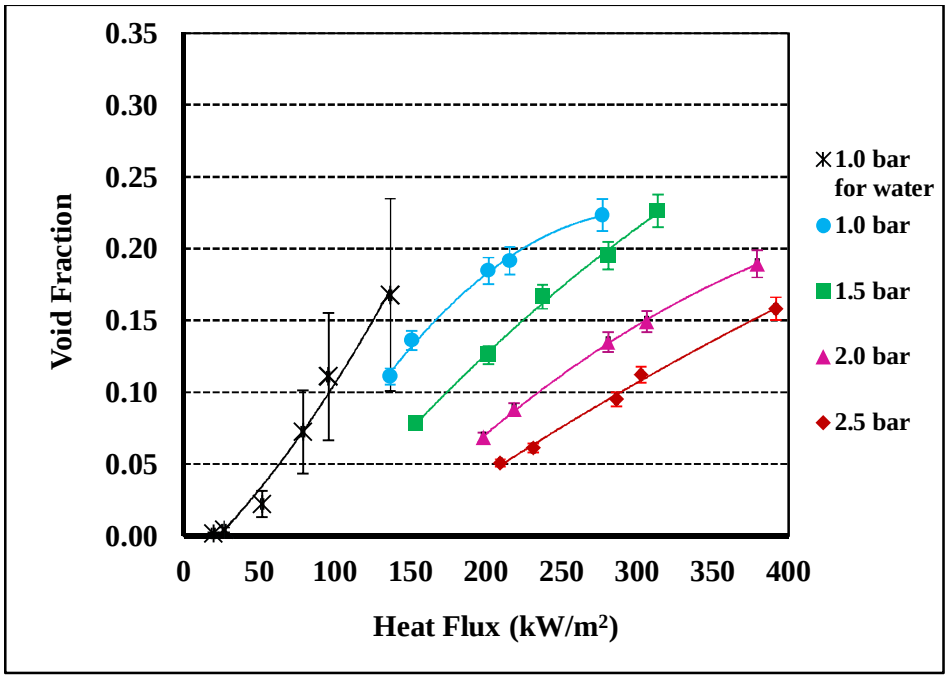

Figure 5.99. Void fraction of 0.001% ZnO-water nanofluid with heat flux at a sub cooling of 20°C and mass flux of 400 kg/m^{2}s.

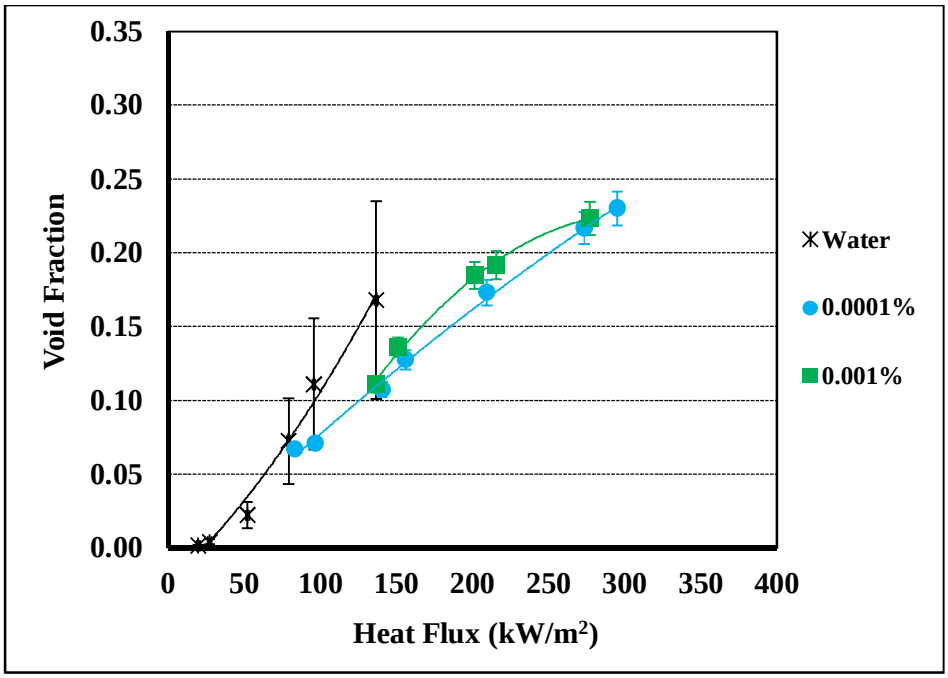

Figure 5.100. Void fraction of ZnO-water nanofluid with heat flux at a pressure of 1.0 bar, sub cooling of 20°C and mass flux of 400 kg/m^{2}s.

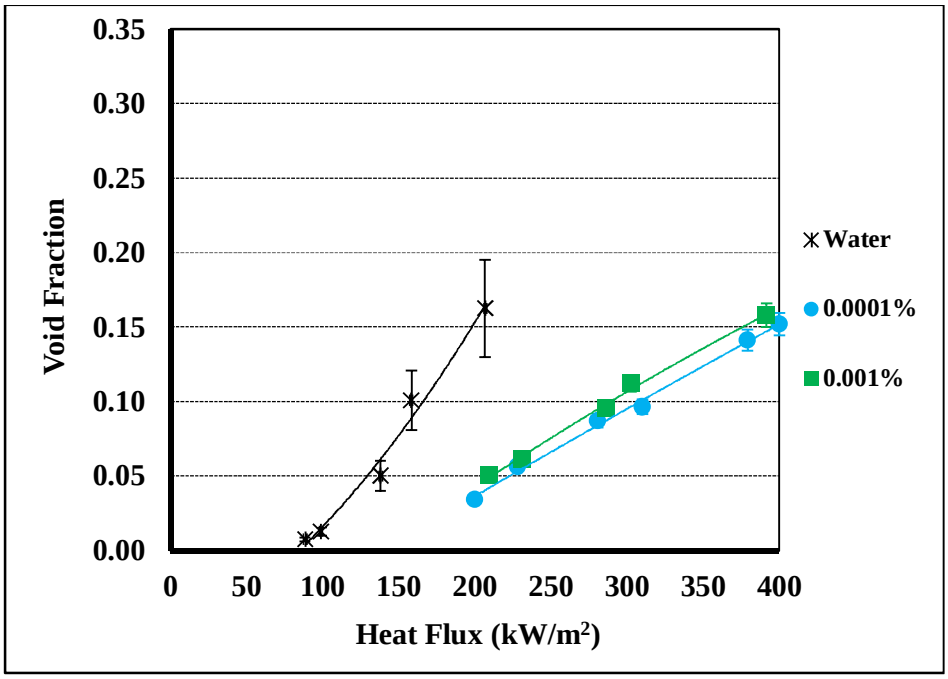

Figure 5.101. Void fraction of ZnO-water nanofluid with heat flux at a pressure of 2.5 bar, sub cooling of 20°C and mass flux of 400 kg/m^{2}s.

5.4.3.5 Void Fraction of MWCNT-Water Nanofluids

The variation of void fraction of MWCNT-water nanofluid with pressure, heat flux and concentration of MWCNT nanoparticles in water has been studied. Experimental data in Fig. 5.102 and Fig. 5.103 show void fraction of 0.0001% MWCNT-water nanofluid and 0.001% MWCNT-water nanofluid with applied pressure and heat flux in an annular test section.

The experimental results of void fraction and its dependence on pressure show similar effect as water and other selected nanofluids. It is observed that pressure acts as a suppressor, with increase in pressure, void fraction decreases and boiling is delayed in MWCNT-water nanofluids as higher pressure suppresses the bubbles and due to reduced bubble diameter and bubble density, overall void fraction reduces. It indicates that at high pressure, nucleation point in flow boiling of MWCNT-water nanofluids rises, which is useful for nuclear reactors and other engineering applications.

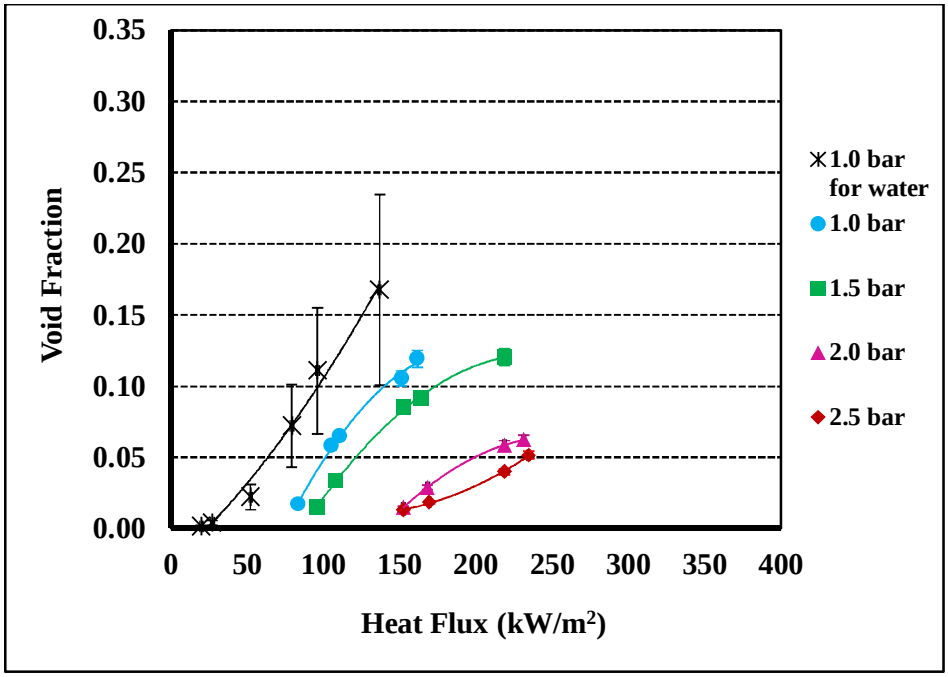

Figure 5.102. Void fraction of 0.0001% MWCNT-water nanofluid with heat flux at a sub cooling of 20°C and mass flux of 400 kg/m^{2}s.

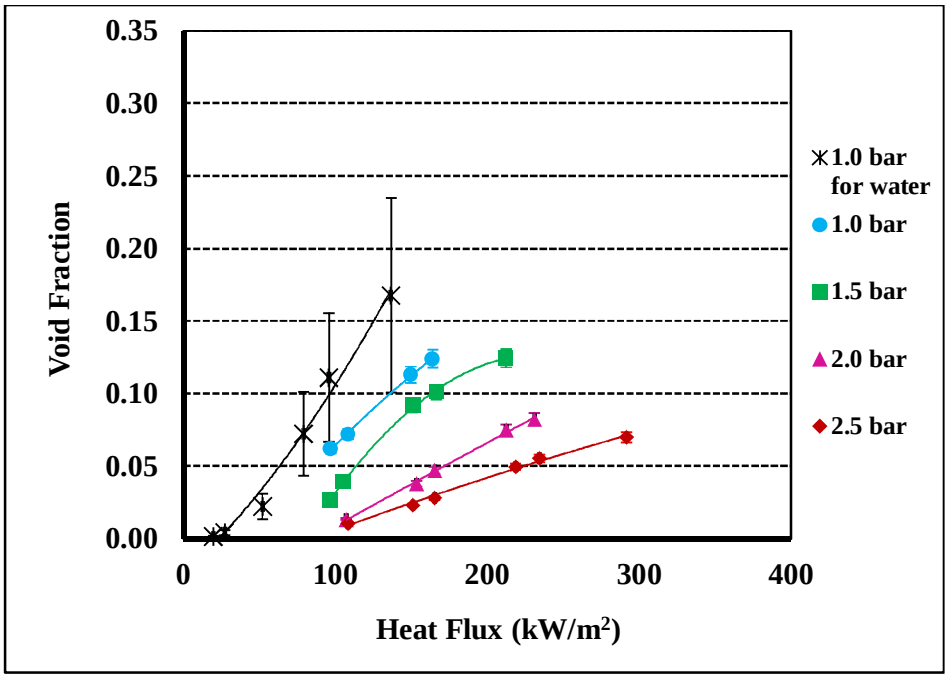

Figure 5.103. Void fraction of 0.001% MWCNT-water nanofluid with heat flux at a sub cooling of 20°C and mass flux of 400 kg/m^{2}s.

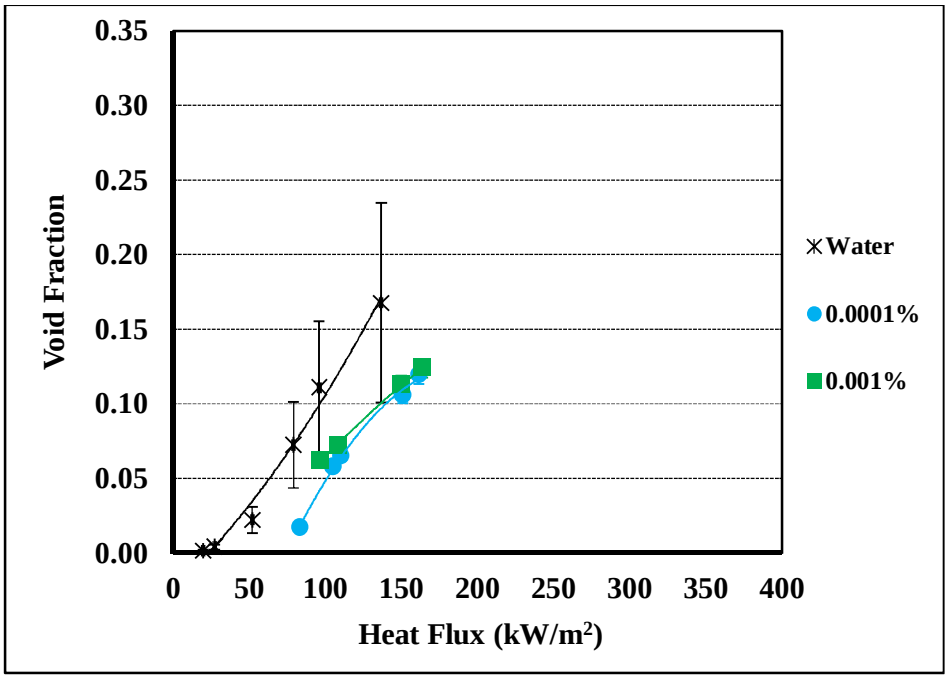

Figure 5.104. Void fraction of MWCNT-water nanofluid with heat at a pressure of 1.0 bar, sub cooling of 20°C and mass flux of 400 kg/m^{2}s.

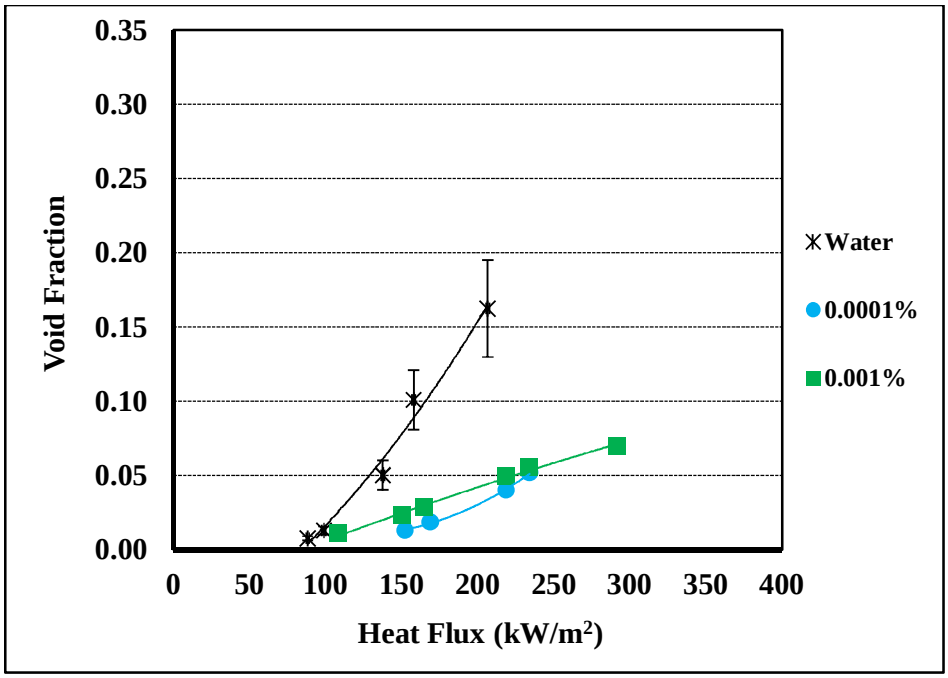

Figure 5.105. Void fraction of MWCNT-water nanofluid with heat flux at a pressure of 2.5 bar, sub cooling of 20°C and mass flux of 400 kg/m^{2}s.

Figure 5.104 and Fig. 5.105 show the void fraction of for MWCNT-water nanofluids with concentrations and heat flux for 1.0 bar and 2.5 bar respectively.

Figure 5.104 shows that the void fraction increases with increase in heat flux and concentration for MWCNT-water nanofluid. It is also observed that at 1.0 bar bubble nucleation starts at same heat flux for both water and MWCNT-water nanofluids. But as shown in Fig. 5.105 for 2.5 bar the void fraction is higher at shifted higher heat flux for higher concentrations of MWCNT-water nanofluids over distilled water.

5.5 Effect of Concentration of nanoparticles on Surface Roughness of Heater Rod

Variation in surface roughness of heater rod with concentration of nanoparticles in water has been studied.

To assess the repeatability of the tests, the surface roughness of heater rod for Al_2O_3-water nanofluid tested four times. Figure 5.106 shows the repeatability

plots for surface roughness of heater rod with Al_2O_3-water nanofluid. The surface roughness of heater rod was plotted on the y-axis whereas concentration of nanoparticles in water is plotted on the x-axis. The four plots presented here, show that the surface roughness shows good repeatability.

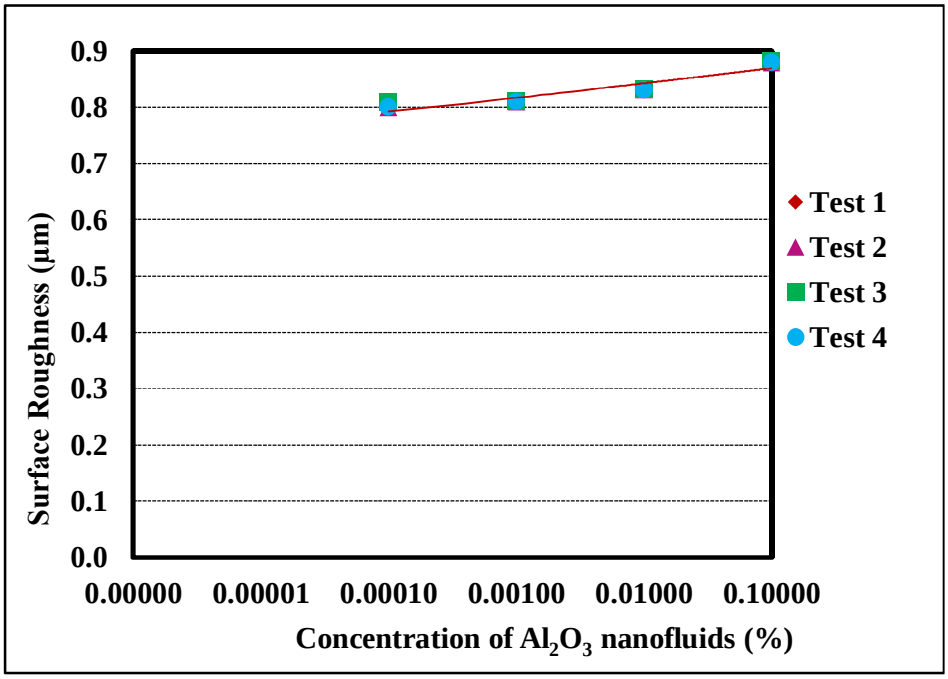

Figure 5.106. Results of repeatability test for Surface roughness of Al_2O_3-water nanofluid coated heater surface.

Figure 5.107 shows that the surface roughness, Ra (µm), of heater rod for Al_2O_3-water nanofluid, TiO_2-water nanofluid, ZnO-water nanofluid and MWCNT-water nanofluid increases gradually with increase in concentration of nanoparticles in the nanofluid.

The surface roughness for Al_2O_3-water nanofluid is maximum while that for ZnO-water nanofluid is minimum among the selected nanofluids. Surface roughness of the tube for distilled water is = 0.065 (µm), which is shown by a single point on the y-axis.

The maximum surface roughness of heater rod, after the boiling of nanofluids was 0.88, 0.64, 0.61 and 0.72 µm for boiling of distilled water, 0.1% Al_2O_3-water nanofluid, 0.1% TiO_2-water nanofluid, 0.1% ZnO-water nanofluid and 0.1% MWCNT-water nanofluid respectively.

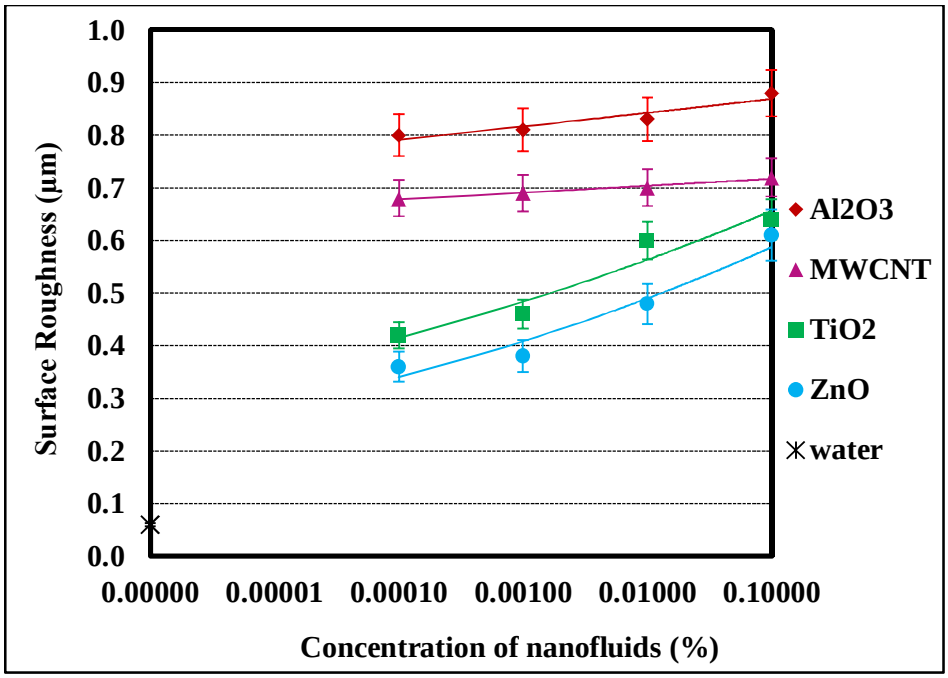

Figure 5.107. Surface roughness of stainless steel heating surface worked with nanofluids.

5.6 Summary of Experimental Results

The results and the reasons for the same have been summarized below.

5.6.1 Thermal Conductivity

The changes in the results of thermal conductivity are discussed here for the effect of sonication time and concentration of nanoparticles in the water.

5.6.1.1 Effect of Sonication Time on Thermal Conductivity

The thermal conductivity of all the nanofluids selected increased with the duration of sonication. The increment in thermal conductivity of nanofluids with sonication time varies approximately from a minimum of 65% to a maximum of 170% for the cases considered. It increases by about 170% for 0.1% Al_2O_3-water nanofluid for sonication time of six hours and by approx. 65% for 0.0001% ZnO-water nanofluid for sonication time of four hours as shown in Fig. 5.2 and Fig. 5.4.

The thermal conductivity increases as the vibrations generated by the sonication makes the mixture of nanoparticles with the base fluid more homogeneous and the agglomerate size in the nanofluids decreases. Smaller agglomerates imply a more uniform dispersion of the nanoparticles in the fluid that leads to the increase in thermal conductivity. The increase in thermal conductivity with sonication time has been reported by Murshed et al. (2005), Hays et al. (2006), Kole and Dey (2012) and Ismay et al. (2013).

However increase in thermal conductivity does not continue with increase in sonication time. Thermal conductivity reaches a maximum and then it starts decreasing with increase in sonication time. As shown in Fig. 5.2 to 5.5, sonication time for maximum thermal conductivity varies with the type of nanofluid. The sonication time at which thermal conductivity reaches maximum was 5.5-6 hrs, 2.5-3 hrs, 3.5-4 hrs and 3.5-6 hrs respectively for Al_2O_3-water nanofluid, TiO_2-water nanofluid, ZnO-water nanofluid and MWCNT-water nanofluid at different concentrations.

It was also observed that the thermal conductivity of all the nanofluids selected, decreases with sonication time after it reaches a maximum. The decrease in thermal conductivity with sonication time after it reaches a maximum was also observed by Kwak and Kim (2005), Assael et al. (2005) and Pal et al. (2015). As shown in Fig. 5.2 - 5.5, thermal conductivity of Al_2O_3-water nanofluid, TiO_2-water nanofluid and MWCNT-water nanofluid decreases slowly with sonication time while thermal conductivity of ZnO-water nanofluid decreases rapidly with sonication time after thermal conductivity attains a maximum.

5.6.1.2 Effect of Concentration on Thermal Conductivity

The thermal conductivity of all the nanofluids selected measured for 0.0001%, 0.001%, 0.01% and 0.1% nanofluid. It is observed that thermal conductivity increases with increase in concentration of nanoparticles for all the cases, refer figures 5.2 to 5.5. For all the nanofluids thermal conductivity is maximum for the highest concentration of the nanoparticles. The maximum increase in thermal conductivity was 170%, 150%, 120% and 163% for Al_2O_3-

water nanofluid, TiO_2-water nanofluid, ZnO-water nanofluid and MWCNT-water nanofluid respectively at 0.1%. Similar results were obtained by M. J. Assael et al. (2005) for Cu-water nanofluid and C-MWNT-water nanofluid, Amit Gupta et al. for Co-Ethylene Glycol and SiO_2-water nanofluids (2007), Yu et al. for CNT-water nanofluid (2007), Buongiorno et al. (2008) for Al_2O_3-water nanofluid, Soujit Sen Gupta et al. (2011) for graphene-water nanofluids and S. M. Sohel Murshed et al. (2011) for Al_2O_3-water nanofluid and TiO_2-water nanofluid, Haddad et al. for CuO-water nanofluids (2012), Jung et al. (2013) for binary nanofluids (H_2O/LiBr binary mixture with Al_2O_3 nanoparticles).

5.6.2 Heat Transfer Coefficient

The changes in the results of heat transfer coefficient are discussed here for the effect of pressure, concentration of nanoparticles in the water and heat flux.

5.6.2.1 Effect of Pressure on Heat Transfer Coefficient

Heat transfer coefficient of all the nanofluids selected measured at 1.0 bar, 1.5 bar, 2.0 bar and 2.5 bar. It was observed that for all the cases, heat transfer coefficient increases with increase in pressure. The maximum increase in HTC was 80% due to increase in pressure from 1.0 bar to 2.5 bar for 0.01% MWCNT-water nanofluid at heat flux of about 220 kW/m^2 and mass flux of 400 kg/m^2s while in case of pure water, increase in HTC was about 24% at 165 kW/m^2 heat flux and mass flux of 400 kg/m^2s.

No work has been reported on flow boiling of nanofluids at higher pressures. K.H. Bang et al. (2011) have studied the effect of increase in pressure on HTC of pure water at 2.0 bar and 16 bar and observed that pressure does not alter heat transfer coefficient significantly.

Most likely, heat transfer coefficient increases with increase in pressure due to increase in interfacial conductance, as explained by John H. Lienhard (2005). Similarly, it is expected that heat transfer coefficient of nanofluids increases with increase in pressure due to increase in interfacial conductance.

5.6.2.2 Effect of Concentration of nanoparticles on Heat Transfer Coefficient

Heat transfer coefficient of all the nanofluids selected measured for 0.0001%, 0.001%, 0.01% and 0.1% concentrations of nanofluid. It was observed that for all the cases heat transfer coefficient increases with increase in concentration. The increase in HTC was 84%, 84%, 49% and 32% over that of the base fluid for 0.1% of Al_2O_3-water nanofluid, 0.1% of TiO_2-water nanofluid, 0.1% of ZnO-water nanofluid and 0.1% of MWCNT-water nanofluid respectively at a pressure of 1.0 bar, heat flux of about 160 kW/m^2 and mass flux of 400 kg/m^{2}s.

The maximum increase in HTC was 104%, 101% and 60% over that of the base fluid for 0.1% of Al_2O_3-water nanofluid, 0.1% of TiO_2-water nanofluid, 0.1% of ZnO-water nanofluid respectively at a pressure of 2.5 bar, heat flux of about 210 kW/m^2 and mass flux of 400 kg/m^{2}s while in case of MWCNT-water nanofluid increase in HTC was about 134% over that of the base fluid at a pressure of 1.5 bar and heat flux of about 160 kW/m^2 and mass flux of 400 kg/m^{2}s.

The increase in heat transfer coefficient with increase in concentration is in similar trend as with the previous researchers Lee and Choi (1996) Xuan and Li (2003), Chien et al. (2003), Tsai et al. (2004), Wen and Ding (2004b), Ding et al. (2005), Yang et al. (2005), Heris et al. (2006), Ma et al. (2006), Heris et al. (2007), Tiwari and Das (2007), He et al. (2007), Duangthongsuk and Wongwises (2009). However Putra et al. (2003) and Wen and Ding (2005) reported drop in heat transfer coefficient. This happens due to reduced Wettability of the heating surface due to deposition of a thicker layer of nanoparticles on the heating surface at higher concentrations of nanofluids.

The main reasons for increase in heat transfer coefficient are:

- Increase in thermal conductivity of the nanofluid with increase in concentration of the nanoparticles.
- Increase in heat transfer due to increase in thermal energy of the nanoparticles.

- Increase in heat transfer due to increase in the number of nanoparticles participating in natural convection due to increase in concentration of nanoparticles.
- Increase in bubble density due to increase in concentration of nanoparticles and consequent increase in condensation of bubbles.
- Increase in conduction between nanoparticles and the surface of the heater.
- Increase in surface roughness of the heating surface due to deposition of nanoparticles on the heating surface.

5.6.2.3 Effect of Heat Flux on Heat Transfer Coefficient

Heat transfer coefficient of all the nanofluids selected was measured for heat flux varying from 0 to 400 kW/m^2. The maximum heat flux achieved for distilled water was 160 kW/m^2 and 210 kW/m^2 at a pressure for 1.0 bar and 2.5 bar respectively. At heat flux above these values for the respective pressures either the glass tube cracked or fluid leaked through the connecting ends of the tube. The maximum heat flux achieved for nanofluids at concentration of 0.1% and pressure of 2.5 bar was 295 kW/m^2, 305 kW/m^2, 390 kW/m^2 and 385 kW/m^2 for Al_2O_3-water nanofluid, TiO_2-water nanofluid, ZnO-water nanofluid and MWCNT-water nanofluid respectively at a mass flux of 400 kg/m^2s.

It was observed that for all the cases heat transfer coefficient increases with increase in heat flux. Similar results have been reported by previous researchers Mudawar and Anderson (1990), Chun et al. (2001), Liu et al. (2007), K.H. Bang et al. (2011) and Lee et al. (2014).

Heat transfer coefficient increases with increase in heat flux due to increase in energy of the nanoparticles as predicted by Mohamed Moawed (2014), and due to increase the number of active sites at the heating wall as predicted by Mudawwar (1987). Initially heat transfer coefficient increases rapidly in the convective range but at higher heat flux, heat transfer coefficient increases slowly, possibly due to coating of nanoparticles.

5.6.3 Pressure Drop

The changes in the results of pressure drop are discussed here for the effect of pressure, concentration of nanoparticles in the water and heat flux.

5.6.3.1 Effect of Pressure on Pressure Drop

The effect of pressure on pressure drop for flow boiling is not reported in the literature. Pressure drop in an annulus test section for all the nanofluids selected was measured with pressure at 1.0 bar, 1.5 bar, 2.0 bar and 2.5 bar. It was observed that for all the cases pressure drop decreases with increase in pressure.

5.6.3.2 Effect of Concentration of nanoparticles on Pressure Drop

Pressure drop along the test section for all the nanofluids selected was measured for 0.0001%, 0.001%, 0.01% and 0.1% concentration of nanoparticles. Compared to water, pressure drop for all the nanofluids selected increases significantly at all pressures tested. Thus use of nanofluids would cause extra penalty in pumping power. As shown if Fig. 5.43 - 5.46, increase in pressure drop over the distilled water at 1.0 bar was about 18%, 8%, 4% and 5% for 0.0001% Al_2O_3-water nanofluid, 0.0001% TiO_2-water nanofluid, 0.0001% ZnO-water nanofluid and 0.0001% MWCNT-water nanofluid respectively. The maximum increase in pressure drop was about 28%, 13%, 11% and 9% for 0.1% Al_2O_3-water nanofluid, 0.1% TiO_2-water nanofluid, 0.1% ZnO-water nanofluid and 0.1% MWCNT-water nanofluid respectively. The increase in pressure drop with increase in concentration is in similar trend as with the previous researchers Razi et al. (2011), Hashemi et al. (2012), Arani and Amani (2012).

The main reasons of increased pressure drop with increase in concentration of nanoparticles are increased in viscosity of the fluid, increase in surface roughness of heater surface and increased turbulence due to presence of nanoparticles.

5.6.3.3 Effect of Heat Flux on Pressure Drop

Pressure drop along the test section for all the nanofluids selected was measured with heat flux, applied at the surface heater, up to 400 kW/m^2. It was observed that for all the cases, variation in pressure drop was not observed in convective heat transfer however it was up to 28% in flow boiling heat transfer. The measured pressure drop of the selected nanofluids are similar to previous data for flow boiling of water and agree well with the previous researchers Razi et al. (2011), Hashemi et al. (2012), Arani and Amani (2012). It was also similar to previous data at 2.0 bar pressure for convective and flow boiling of water, ethylene glycol and their mixture and agree well with the previous researcher Yu et al. (2007).

5.6.4 Bubble Parameters

The visualization and image processing couldn't be done for 0.01% and higher concentrations of nanofluid due to opacity of nanofluids.

5.6.4.1 Bubble Diameter

The changes in the results of bubble diameter are discussed here for the effect of pressure, concentration of nanoparticles in the water and heat flux.

5.6.4.1.1 Effect of Pressure on the Bubble Diameter

Bubble diameter of all the nanofluids selected was measured at pressures ranging from 1 to 2.5 bar and was compared with that for distilled water. For all the cases, bubble diameter for the selected nanofluids decreases with increase in pressure. The bubble diameter decreases as increase in external pressure reduces bubbles size.

The decrease in bubble diameter with increase in pressure is similar to the results obtained by previous researchers like Tolubinsky and Kostanchuk (1970),

Bibeau and Salcudean (1991), Prodanovic et al. (2002), Klausner (2000) and Celata et al. (2007), Razi et al. (2011), Hashemi et al. (2012), Arani and Amani (2012).

The maximum bubble diameter is 1.63 mm at 140 kW/m^2, 2.47 mm at 180 kW/m^2, 2.34 mm at 220 kW/m^2, 2.17 mm at 280 kW/m^2 and 1.30 mm at 160 kW/m^2 for distilled water, 0.001% Al_2O_3-water nanofluid, 0.001% TiO_2-water nanofluid, 0.001% ZnO-water nanofluid and 0.001% MWCNT-water nanofluid respectively, as shown in Fig. 5.48, Fig. 5.51, Fig. 5.55, Fig. 5.59 and Fig. 5.63 respectively.

5.6.4.1.2 Effect of concentration of nanoparticles on the Bubble Diameter

The bubble diameter of all the nanofluids selected was measured for 0.0001% and 0.001% concentration of nanoparticles and was compared with that for water. It was observed that the bubble diameter of Al_2O_3-water nanofluid and TiO_2-water nanofluid was greater than the bubble diameters of water while the bubble diameter of ZnO-water nanofluid and MWCNT-water nanofluid was smaller than that for water at same heat flux. The results obtained agree with the results obtained by You et al. (2003) for Al_2O_3-water nanofluids and Kim et al. (2006) for boiling of nanofluids containing alumina, zirconia, or silica nanoparticles.

The heater wall which is surrounded by either Al_2O_3 nanoparticles or TiO_2 nanoparticles requires less wall superheat to initiate boiling process because these particles require less energy to change the phase while the presence of either ZnO nanoparticles or MWCNT nanoparticles deactivate the nucleation cavities and require higher wall superheat to initiate boiling process because these particles require higher energy to change the phase.

5.6.4.1.3 Effect of Heat Flux on the Bubble Diameter

The bubble diameter of all the nanofluids selected was measured for heat flux varying up to 400 kW/m^2 and was compared with that for water. It was

observed that bubble diameter for distilled water and for in all the nanofluids increases with increase in heat flux. The bubble diameter increases with increase in heat flux due to both increased wall super heat and energy gain by the nanofluids.

The bubble diameter increases with increase in heat flux due to increased wall super heat, similar predictions were taken by Abdelmessiah et al. (1972), Delvalle and Kenning (1985), Bibeau and Salcudean (1991), Chang et al. (2002), Celata et al. (2007), and Dhir (2007) and Rashidabad (2014); and possibly higher energy gain by the nanofluids compare to base fluid only.

5.6.4.2 Bubble Density

The changes in the results of bubble density are discussed here for the effect of pressure, concentration of nanoparticles in the water and heat flux.

5.6.4.2.1 Effect of Pressure on the Bubble Density

The bubble density of all the nanofluids selected was measured at pressures ranging from 1 to 2.5 bar and compared with that for water. It was observed that with increase in pressure bubble density decreases and less bubble generate at the same heat flux.

The bubble density of the selected nanofluids decreases with pressure because increased external pressure on nucleation sites prevents bubble generation. Experimental results from the study agree with the results of, Tolubinsky and Kostanchuk (1970), Bibeau and Salcudean (1991), Prodanovic et al. (2002) and Zhou (2005).

5.6.4.2.2 Effect of concentration of nanoparticles on Bubble Density

The bubble density of all the nanofluids selected was measured for 0.0001% and 0.001% concentration of nanoparticles and was compared with that

for water. It was observed that bubble density of all the nanofluids selected remains less than the bubble density of water. Experimental results of bubble density from the study agree with the results of Maurus et al. (2002) for water and Kim et al. (2006) for boiling of nanofluids containing alumina, zirconia, or silica nanoparticles.

In case of Al_2O_3-water nanofluid and TiO_2-water nanofluid, bubble diameter of all the nanofluids was greater than that for water, so less bubble density (less number of bubble) was available in same image area. As we know that, ZnO nanoparticles are very useful in corrosion resistive coating, so it may be one of the reasons for less number of bubble formations via plugging of nanoparticles at the heating rod in ZnO-water nanofluid while in case of MWCNT-water nanofluid, the surface characteristics of heating rod may also change similar to ZnO-water nanofluid. The main reason of same is not known, so further investigation is required.

5.6.4.2.3 Effect of Heat Flux on the Bubble Density

The bubble density of all the nanofluids selected was measured with heat flux varying up to 400 kW/m^2 and was compared with that for water. It was observed that the bubble density for distilled water and for all the nanofluids selected increases with increase in heat flux. Experimental results of bubble density from the study agree with the results of previous researchers Bibeau and Salcudean (1991) and Celata et al. (2007).

The bubble density of the selected nanofluid increases with increase in heat flux due to increase in driving force on bubble growth process by both wall superheat and energy gain by nanofluids.

5.6.4.3 Void Fraction

The changes in the results of void fraction are discussed here for the effect of pressure, concentration of nanoparticles in the water and heat flux.

5.6.4.3.1 Effect of Pressure on the Void Fraction

The void fraction for all the nanofluids selected was measured at pressures ranging from 1 to 2.5 bar and compared with that for water. It was observed that with increase in pressure void fraction decreases for water and for all the selected nanofluids. The void fraction decreases with increase in pressure due to reduced bubble diameter and bubble density as pressure suppresses the bubble nucleation and bubble growth.

Experimental results from the study agree with the results of Tolubinsky and Kostanchuk (1970), Bibeau and Salcudean (1991) and Prodanovic et al. (2002) for water and Kim et al. (2006) for boiling of nanofluids containing alumina, zirconia, or silica nanoparticles.

5.6.4.3.2 Effect of Concentration of nanoparticles on the Void Fraction

The void fraction for all the nanofluids selected was measured for 0.0001% and 0.001% concentration of nanoparticles and was compared with that for water. It was observed that void fraction for Al_2O_3-water nanofluid and TiO_2-water nanofluid was more than that for water while the void fraction for ZnO-water nanofluid and MWCNT-water nanofluid was less than that for water at constant heat flux and pressure.

Experimental results of void fraction from the study agree with the results of Maurus et al. (2002) for water and Kim et al. (2006) for boiling of nanofluids containing alumina, zirconia, or silica nanoparticles. The void fraction depends on bubble diameter and bubble density (i.e. fraction of bubbles in the mixture of bubbles and fluid). The void fraction for Al_2O_3-water nanofluid and TiO_2-water nanofluid increases with increase in concentration of the nanofluids due to larger area covered by increased bubble diameter in an image area. While the void fraction for ZnO-water nanofluid and MWCNT-water nanofluid was observe less than that for water due to small area covered by smaller bubble diameter in an image area of ZnO-water nanofluid and MWCNT-water nanofluid. It was

observed less due to both deactivation of the nucleation cavities and requirement of more energy to generate bubbles.

5.6.4.3.3 Effect of heat flux on the Void Fraction

The void fraction for all the nanofluids selected was measured with heat flux varying up to 400 kW/m^2 and was compared with that for water. The void fraction for distilled water and for the selected nanofluids increases with increase in heat flux. The void fraction increases with increase in heat flux due to increased vapour region in the mixture of bubbles and fluid.

Experimental results on void fraction from the study agree with the results of previous researchers Bibeau and Salcudean (1991), Zeitoun and Shoukri (1996) Maurus et al. (2002), Maurus and Sattelmayer (2006) and Celata et al. (2007).

5.6.5 The Surface Roughness

The surface roughness, Ra (μm) of heater rod for selected nanofluids increases gradually with concentration of nanoparticles. It increases due to deposition of nanoparticles on heater rod as shown in Fig. 5.104.

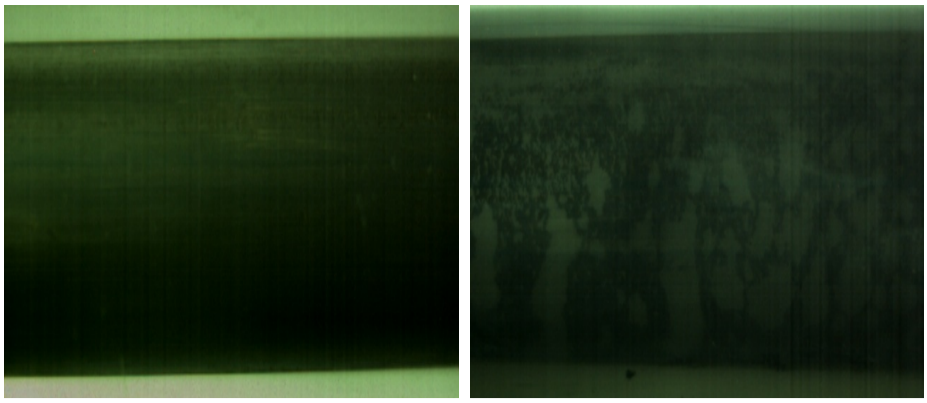

Figure 5.104. Images with 0.001% ZnO and 0.001% MWCNT deposited on heater rod.

The surface roughness for selected nanofluids was maximum for Al_2O_3-water nanofluid and minimum for ZnO-water nanofluid. Experimental results of

surface roughness from the study agree with the results of Kim et al. (2006) for boiling of nanofluids containing alumina, zirconia, or silica nanoparticles.

It was also observed that after flow boiling, a layer of nanoparticles was deposited on the surface of heater indicating bubble nucleation and growth sites. As stated by Das (2007), friction factor increases significantly in the turbulent regime with increasing tube roughness, which is one of the reasons for increase in heat transfer coefficient.

6.

EMPIRICAL RELATIONS FOR HEAT TRANSFER COEFFICIENT

In this chapter Response Surface Regression Analysis method has been used to develop empirical relations for heat transfer coefficient (HTC) of the nanofluids.

Response surface Methodology (RSM) is a collection of mathematical and statistical techniques for the modeling problems in which response is a function of several variables (Montgomery 2005). The correlations have been developed for the selected nanofluids for the operating range under consideration using free version of Minitab software,

6.1 Response Surface Regression Analysis

Heat transfer coefficient (h), the response variable, depends on concentration of nanoparticles in water (C), pressure (p) and heat flux (q) and its variation with these parameters has been studied. Thus heat transfer coefficient is expressed as

$$h = f(C, p, q) + e.$$

here, error *e* represents measurement error as well as variations not captured by this function.

If error *e* is distributed normally with its mean equal to zero, we conclude that function is a true representation of the data.

There are three models in Response Surface Regression Analysis:

1. The first-order model (linear)
2. The second-order model (square) and
3. Three-level fractional factorial model (2-way interaction)

In general all RSM problems use either one of the models or any of their combination. In these models, each variable is independent of the other variables.

Once the data are collected, the Method of Least Square for n variables (ANOVA) is used to estimate the polynomial.

Nine degrees of freedom (DF: 3 for linear model, 3 for square model and 3 for 2-way interaction model) have been considered. Adjusted sum of squared (Adj SS) values, adjusted mean of squared (Adj MS) values, values from F-test (F-Value) and value from P-test (P-Value) have been calculated for all the nine degrees through Analysis of Variance (ANOVA) method. Detailed methodology to calculate the parameters of Analysis of Variance (ANOVA) method has been presented in Appendix-I. The calculation through ANOVA and the model summery for all the nanofluids have been included in Appendix-J.

Graphical representations for following results are also generated through Minitab software for the better understanding of results. In total, four graphs have been plotted for each nanofluid.

Residual plots are used to examine the goodness of the model. Minitab provides following plots of the residuals:

1. **Normal Probability Plot of Residuals**: The points in this plot should form a straight line which means that the residuals are normally distributed. It indicates that model closely predicts the data.

2. **Residuals versus Fitted Plot**: A residual plot is a graph that shows the residuals on the vertical axis and the independent variable (here HTC) on the horizontal axis. This plot shows distribution of residuals. If a point lies far from the majority of points, it may be an outlier. There should not be any recognizable patterns in the residual plot.

3. **Histogram of the Residuals**: Histogram shows general characteristics of the residuals including typical values, spread and shape. A long tail on one side may indicate a skewed distribution. If one or two bars are far from the others, those points may be outliers.

4. **Residuals versus Observation Order of Data**. This is a plot of all residuals in the order data was collected and can be used to find non-random error,

especially due to time-related effects. This plot helps to check the assumption that the residuals are uncorrelated with each other.

The empirical relations for Al_2O_3-water nanofluids, TiO_2-water nanofluids, ZnO-water nanofluids and MWCNT-water nanofluids are presented in the following sections.

The results predicted by empirical relations and its comparison with experimental results have also been represented. Further, the effect of concentration of nanoparticles (C), pressure (p) and heat flux (q) on HTC has also been discussed.

6.2. Empirical Relation and their Validation for Al_2O_3-Water Nanofluids

The correlation for Al_2O_3-water nanofluid is given as under:

$$h_{Al2O3} = 6.63 + 28242\,C - 2.22\,p + 0.13747\,q - 24343298\,C*C + 0.904\,p*p - 0.000417\,q*q + 386\,C*p + 42.76\,C*q + 0.03123\,p*q \quad (6.1)$$

Range of the experimental data for Al_2O_3-water nanofluids, the Eq. (6.1) is, 1 bar $\leq p \leq$ 2.5 bar, $0.0001\% \leq C \leq 0.1\%$ and 0 kW/m^2 $\leq q \leq$ 400 kW/m^2.

Normal probability plot for Al_2O_3-water nanofluid is given in Fig. 6.1. Almost all the points in the graph fall on the straight line, which means that empirical relation obtained, accurately represents the experiment and there is no error in the representation except the normally distributed experimental error.

Figure 6.2 shows residuals versus fitted values of HTC for Al_2O_3-water nanofluid. There is no recognizable pattern and the predicted data differ from the experimental data by ± 5% only. As the points in the residual plot are randomly dispersed around the horizontal axis, a linear regression model is appropriate for the data of Al_2O_3-water nanofluid.

Figure 6.3 represents the residual histogram of HTC for Al_2O_3-water nanofluid. It indicates that frequency of residual. The figure shows that the residual follows the normal distribution and supports the correlation obtained.

Figure 6.4 shows the residuals versus observation order. It indicates that the residual is within the acceptable limit of ± 5% and residual doesn't depend on the order in which data was taken.

The predicted results for Al_2O_3-water nanofluids through response surface regression analysis are plotted in Fig. 6.5 for a pressure of 1.0 bar, Fig 6.6 for a pressure of 1.5 bar, Fig. 6.7 for a pressure of 2.0 bar and Fig. 6.8 for a pressure of 2.5 bar. Corresponding results obtained experimentally have also been plotted on the graphs. It is found that correlation predicts the experimental results reasonably. It is also noted that concentration of nanofluids has maximum influence on HTC of Al_2O_3–water nanofluid as it has maximum F-value = 550.55 (Appendix-J) at same P-value.

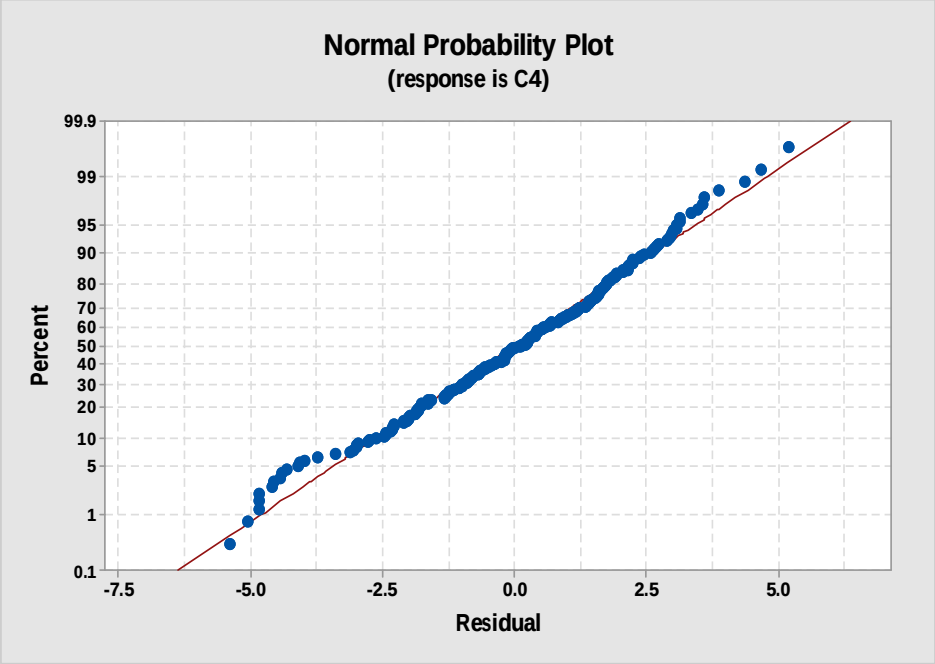

Figure 6.1. Normality probability plot of residuals of heat transfer coefficient for Al_2O_3-water nanofluid.

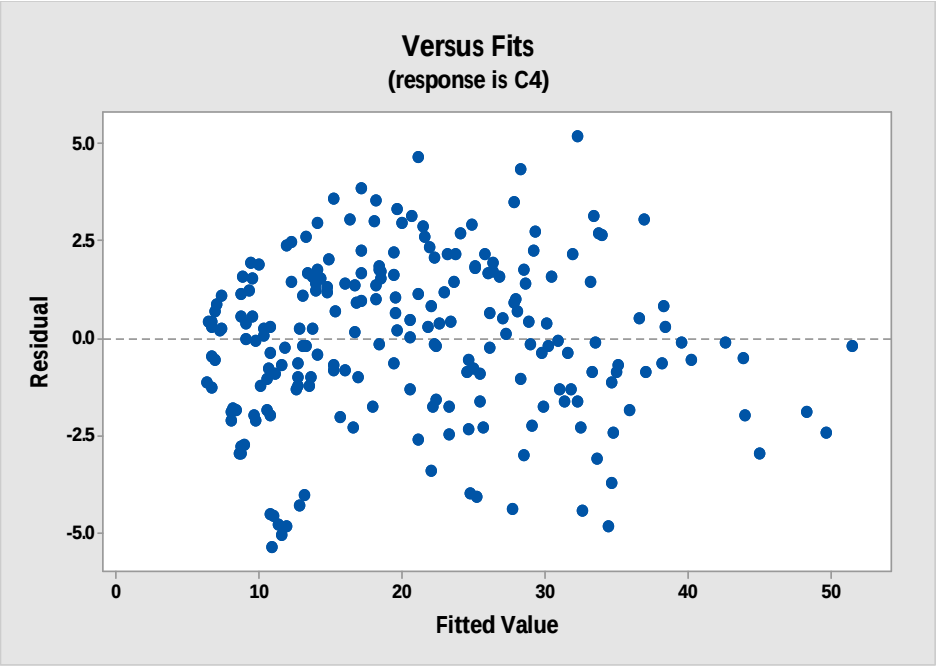

Figure 6.2. Residuals versus fits plot for heat transfer coefficient for Al_2O_3-water nanofluid.

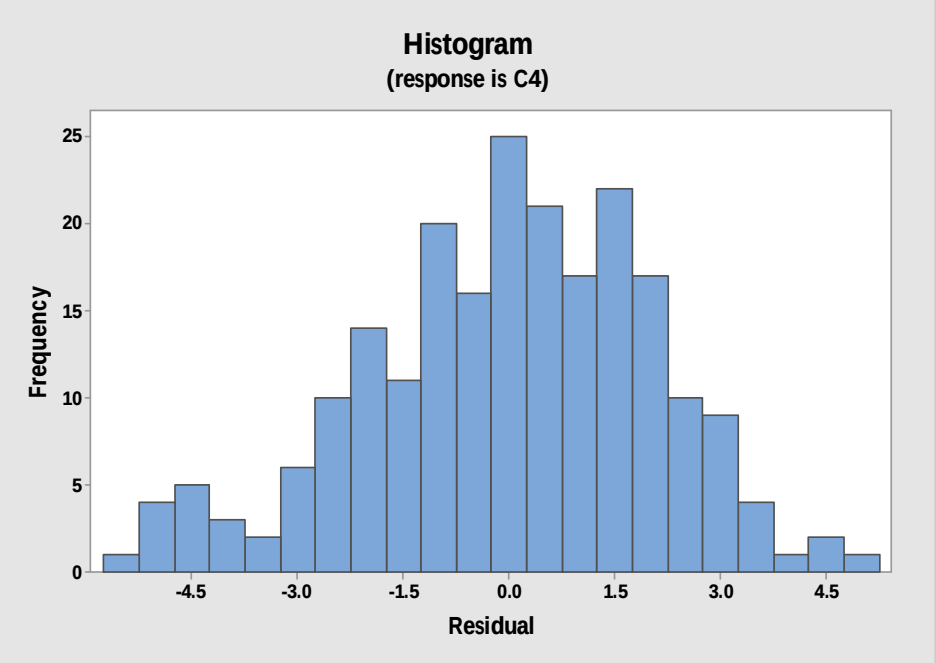

Figure 6.3. Residual histogram for heat transfer coefficient for Al_2O_3-water nanofluid.

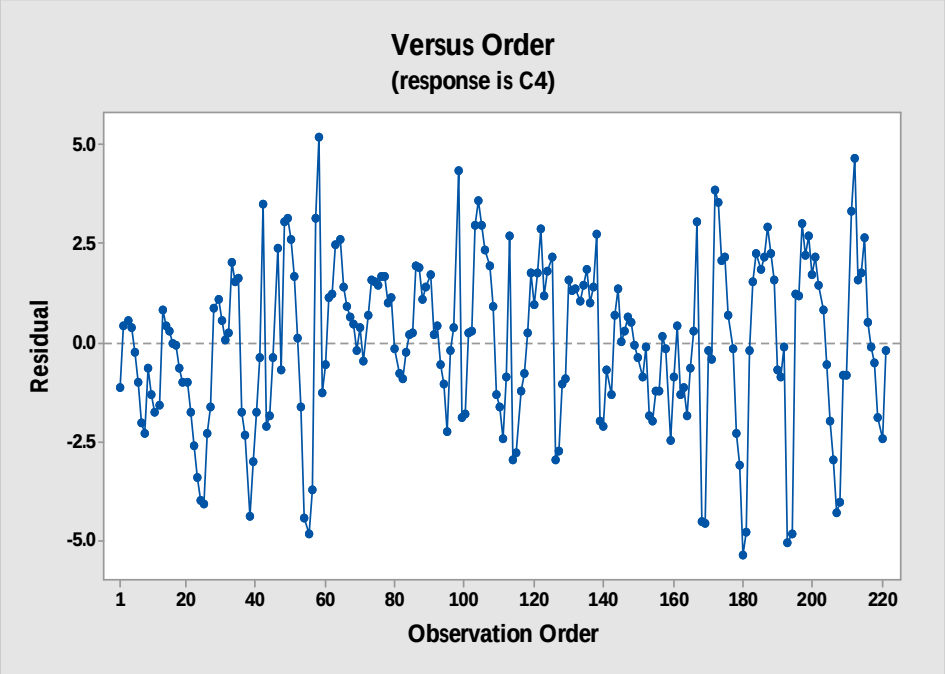

Figure 6.4. Residuals versus order for heat transfer coefficient for Al_2O_3-water nanofluid.

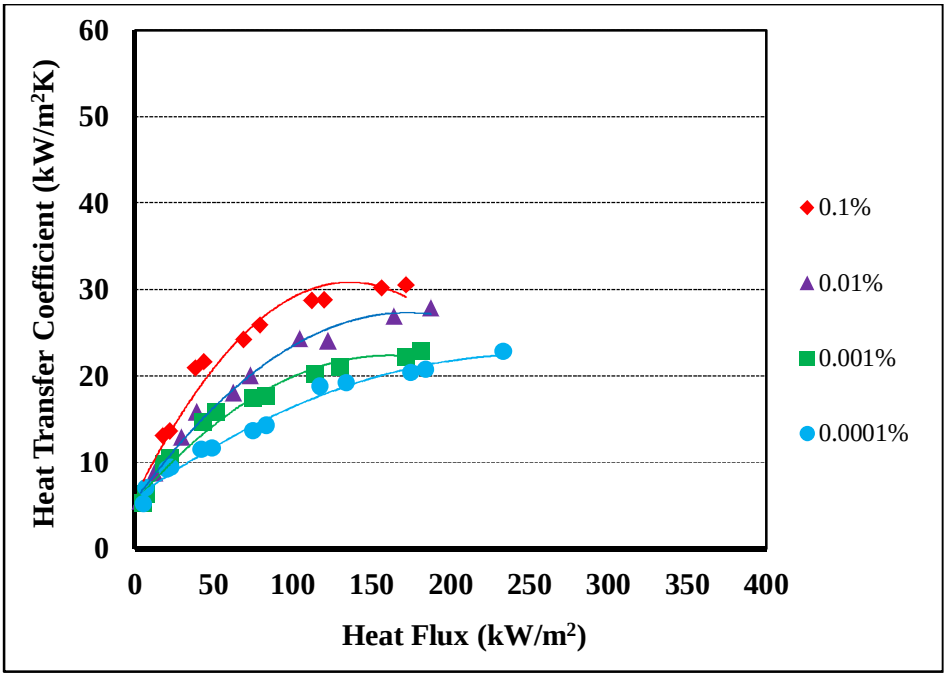

Figure 6.5. Effect of concentration of Al_2O_3 nanoparticles in water on heat transfer coefficient at 1.0 bar pressure.

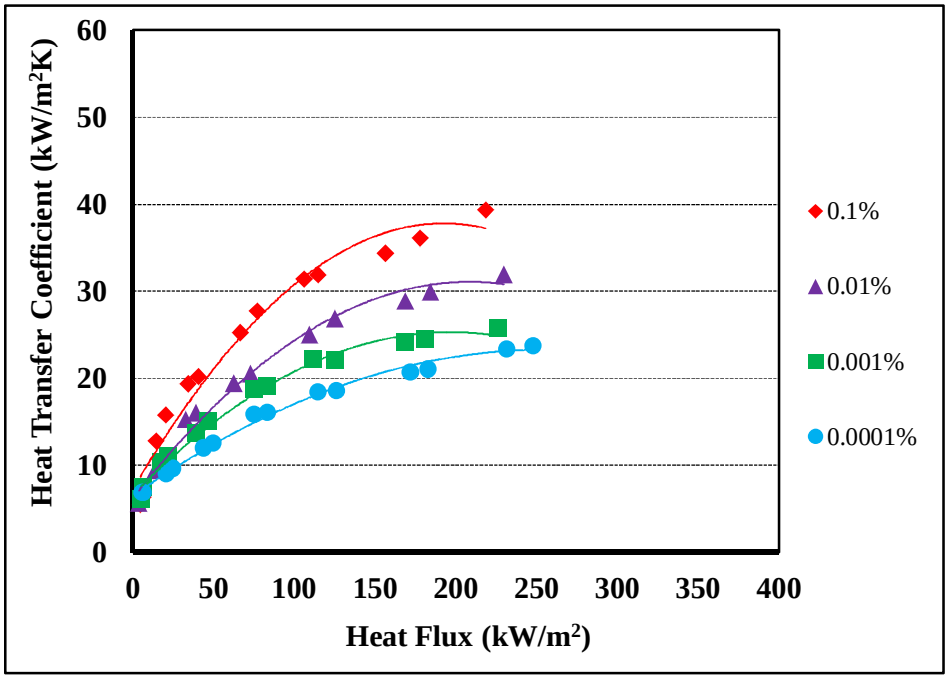

Figure 6.6. Effect of concentration of Al_2O_3 nanoparticles in water on heat transfer coefficient at 1.5 bar pressure.

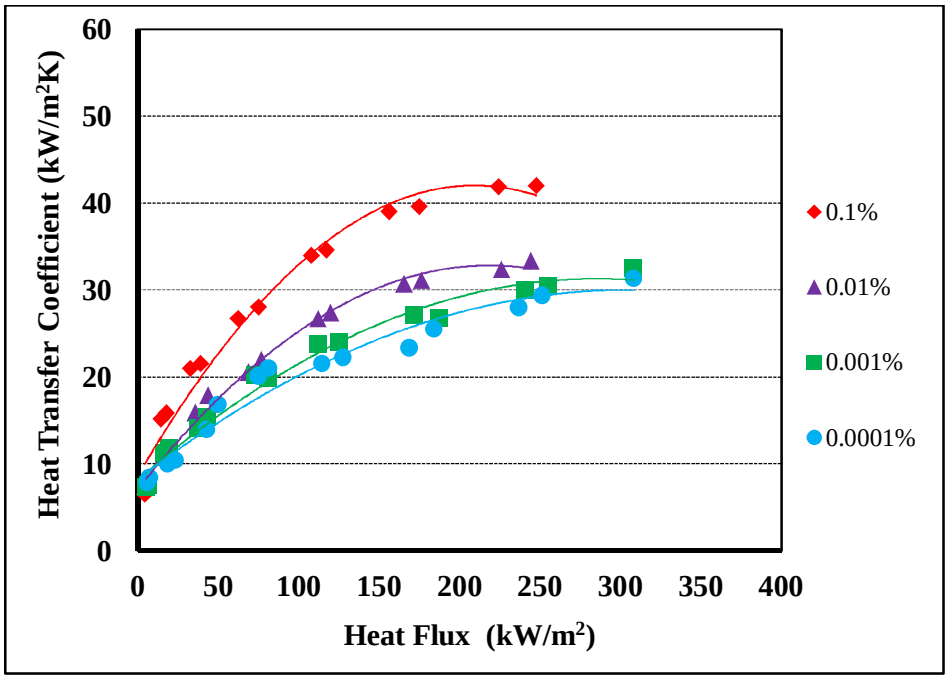

Figure 6.7. Effect of concentration of Al_2O_3 nanoparticles in water on heat transfer coefficient at 2.0 bar pressure.

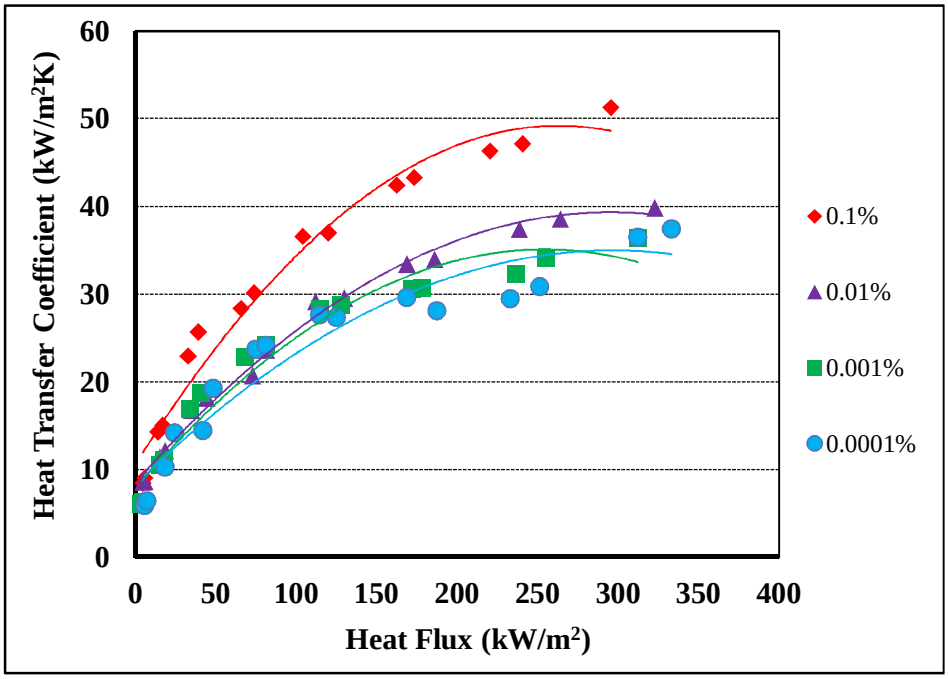

Figure 6.8. Effect of concentration of Al_2O_3 nanoparticles in water on heat transfer coefficient at 2.5 bar pressure.

The predicted results for Al_2O_3-water nanofluids through response surface regression analysis are plotted in Fig. 6.9 for 0.0001% Al_2O_3-water nanofluid, Fig. 6.10 for 0.001% Al_2O_3-water nanofluid, Fig. 6.11 for 0.01% Al_2O_3-water nanofluid and Fig. 6.12 for 0.1% Al_2O_3-water nanofluid.

Corresponding results obtained experimentally have also been plotted on the graphs.

From the comparisons of predicted results and experimental results, it is found that correlation predicts the experimental results reasonably for Al_2O_3-water nanofluids.

It is also found that pressure has less influence than concentration of nanofluids and heat flux on HTC, as model has least F-value = 215.04 (Appendix-J) at same P-value.

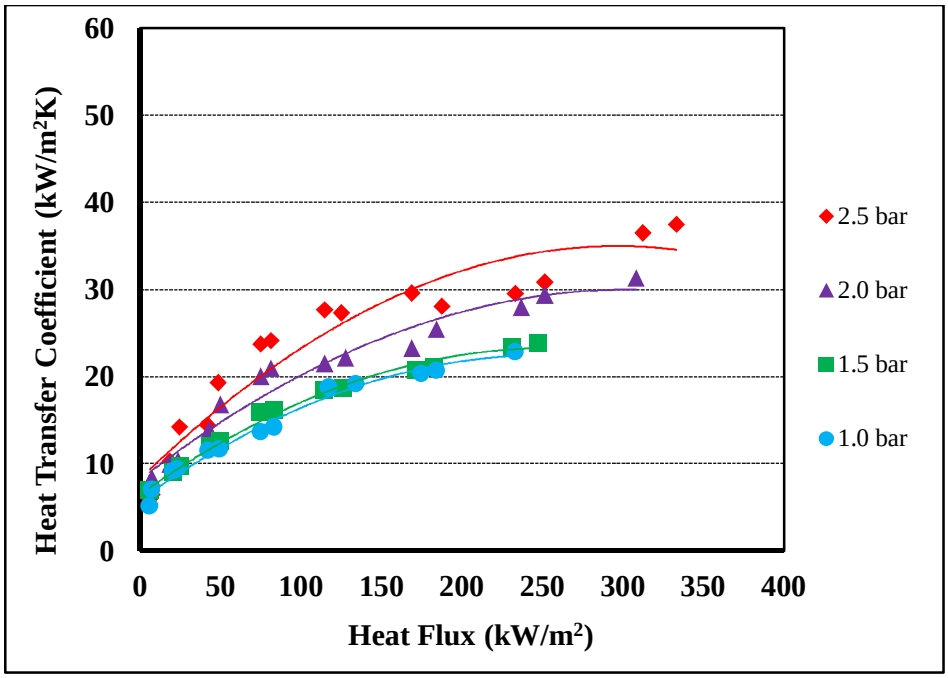

Figure 6.9. Effect of pressure on heat transfer coefficient at 0.0001% concentration of Al_2O_3 nanoparticles in water.

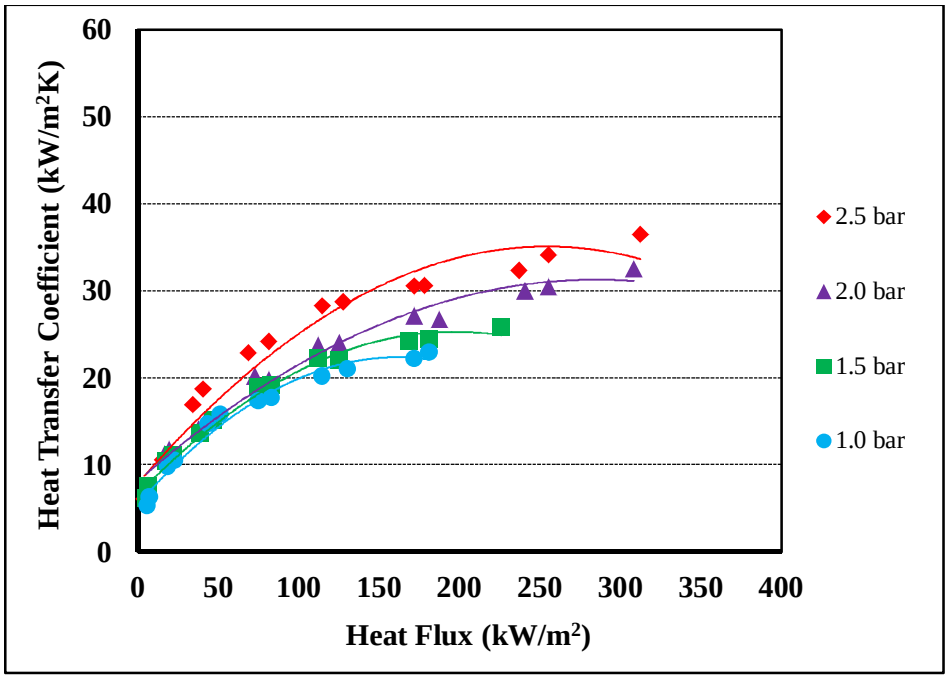

Figure 6.10. Effect of pressure on heat transfer coefficient at 0.001% concentration of Al_2O_3 nanoparticles in water.

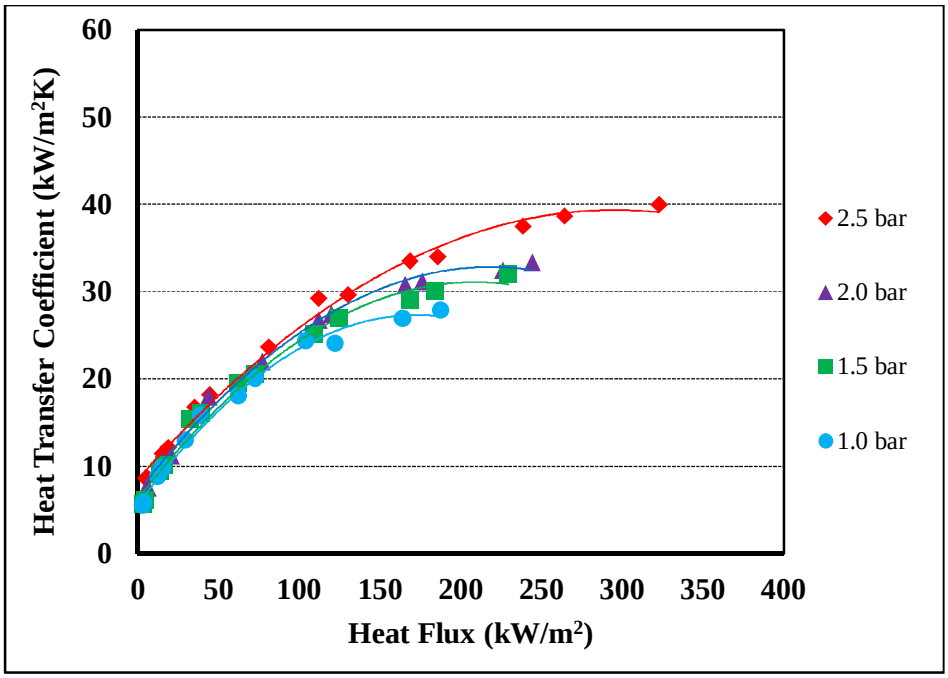

Figure 6.11. Effect of pressure on heat transfer coefficient at 0.01% concentration of Al_2O_3 nanoparticles in water.

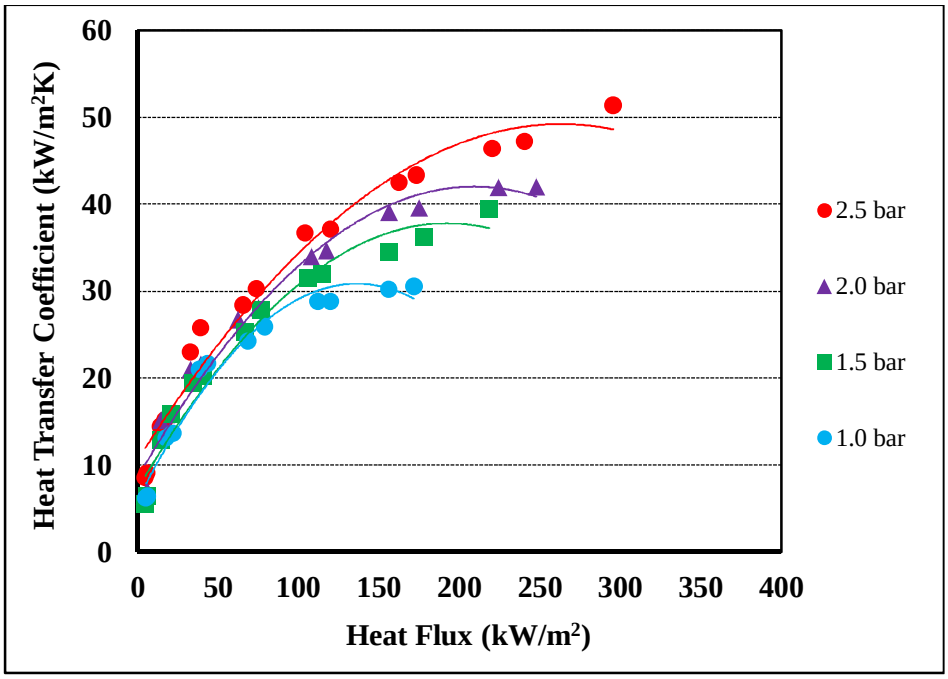

Figure 6.12. Effect of pressure on heat transfer coefficient at 0.1% concentration of Al_2O_3 nanoparticles in water.

6.3 Empirical Relation and their Validation for TiO_2-Water Nanofluids

The correlation for TiO_2-water nanofluid is given as under:

$$h_{TiO2} = 5.41 + 33357\,C - 0.80\,p + 0.14498\,q - 29139834\,C*C + 0.822\,p*p - 0.000465\,q*q - 1093\,C*p + 30.71\,C*q + 0.04007\,p*q \quad (6.2)$$

Range of the experimental data for TiO_2-water nanofluids, the Eq. (6.2) is, $1\ \text{bar} \le p \le 2.5\ \text{bar}$, $0.0001\% \le C \le 0.1\%$ and $0\ \text{kW/m}^2 \le q \le 400\ \text{kW/m}^2$.

Normal probability plot for TiO_2-water nanofluid is given in Fig. 6.13. Similar to Al_2O_3-water nanofluids, almost all the points in the graph fall on the straight line, which means that empirical relation obtained, accurately represents the experiment and there is no error in the representation except the normally distributed experimental error.

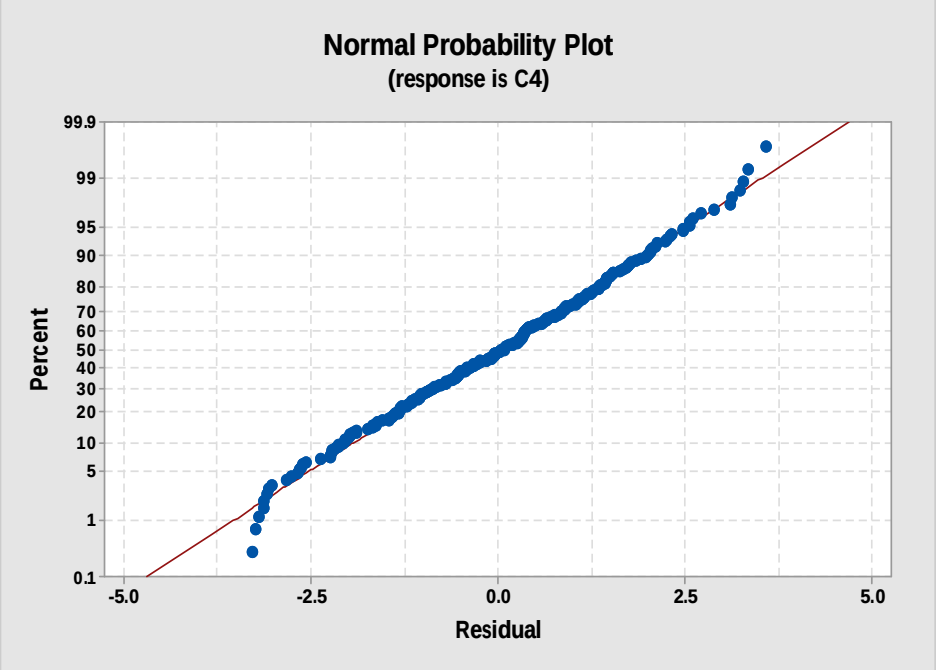

Figure 6.13. Normality plot of residuals of heat transfer coefficient for TiO_2-water nanofluid.

Figure 6.14 shows residuals versus fitted values of HTC for TiO_2-water nanofluid. There is no recognizable pattern and the predicted data differ from the experimental data by ± 5% only.

As the points in the residual plot are randomly dispersed around the horizontal axis, a linear regression model is appropriate for the data of TiO_2-water nanofluid.

Figure 6.15 represents the residual histogram of HTC for TiO_2-water nanofluid. It indicates that frequency of residual. The figure shows that the residual follows the normal distribution and supports the correlation obtained for TiO_2-water nanofluid.

Figure 6.16 shows the residuals versus observation order for TiO_2-water nanofluid. It indicates that the residual is within the acceptable limit of ± 5% and residual doesn't depend on the order in which data was taken.

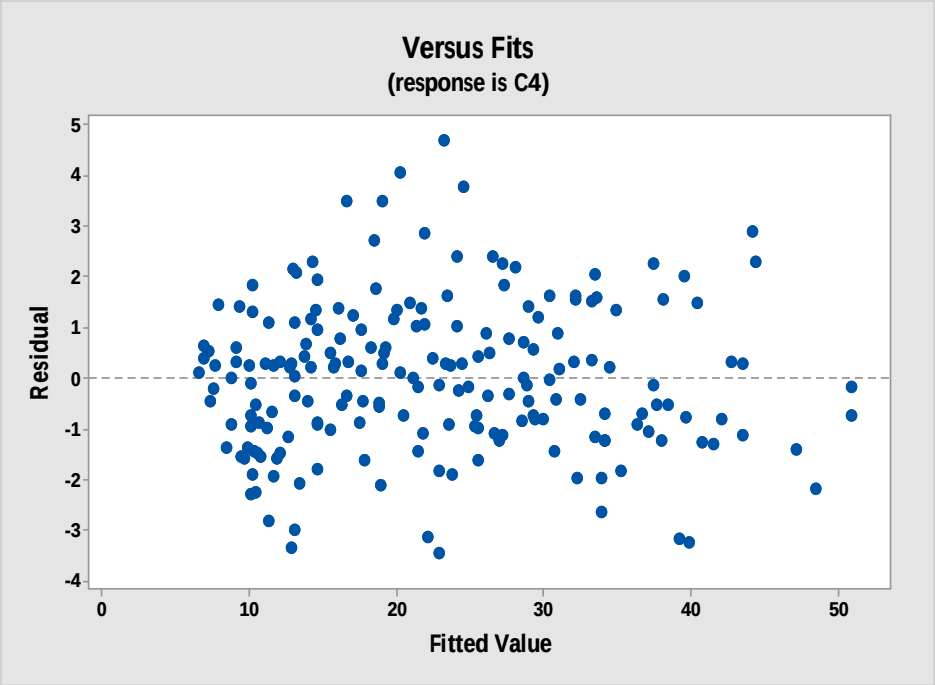

Figure 6.14. Residuals versus fits plot for heat transfer coefficient for TiO_2-water nanofluid.

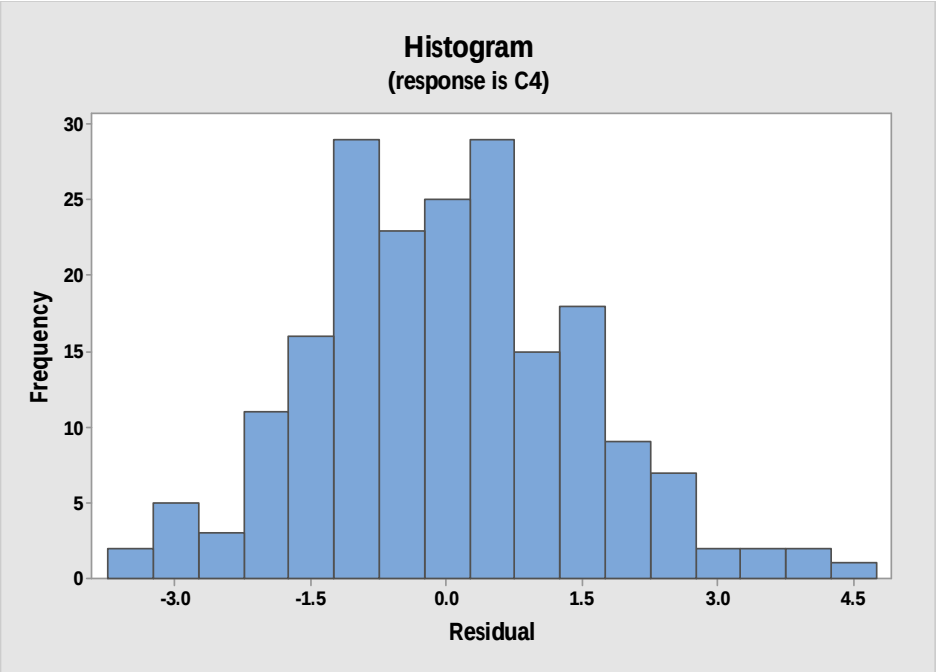

Figure 6.15. Residual histogram for heat transfer coefficient for TiO_2-water nanofluid.

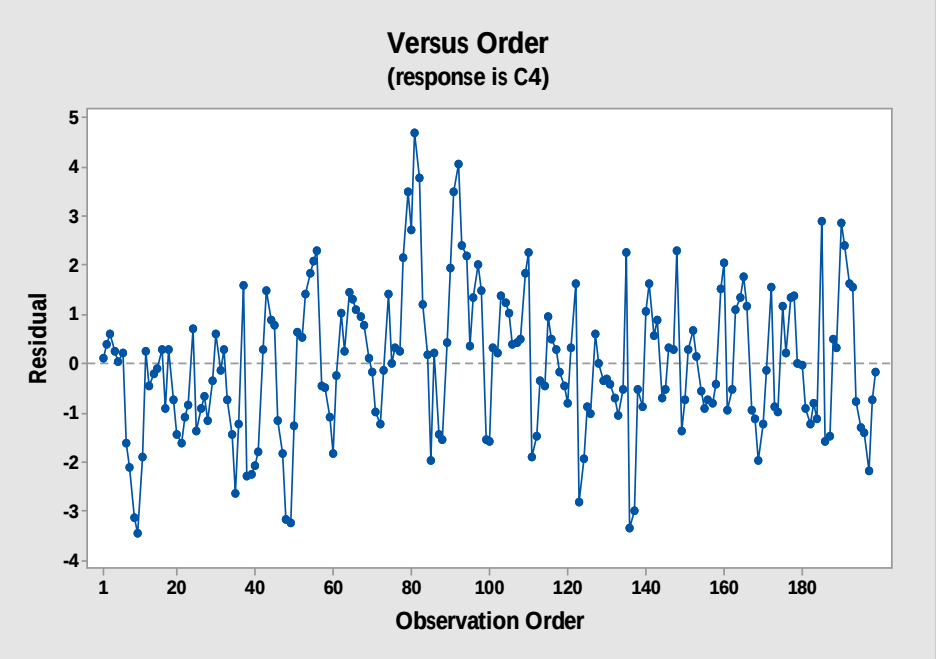

Figure 6.16. Residuals versus order for heat transfer coefficient for TiO_2-water nanofluid.

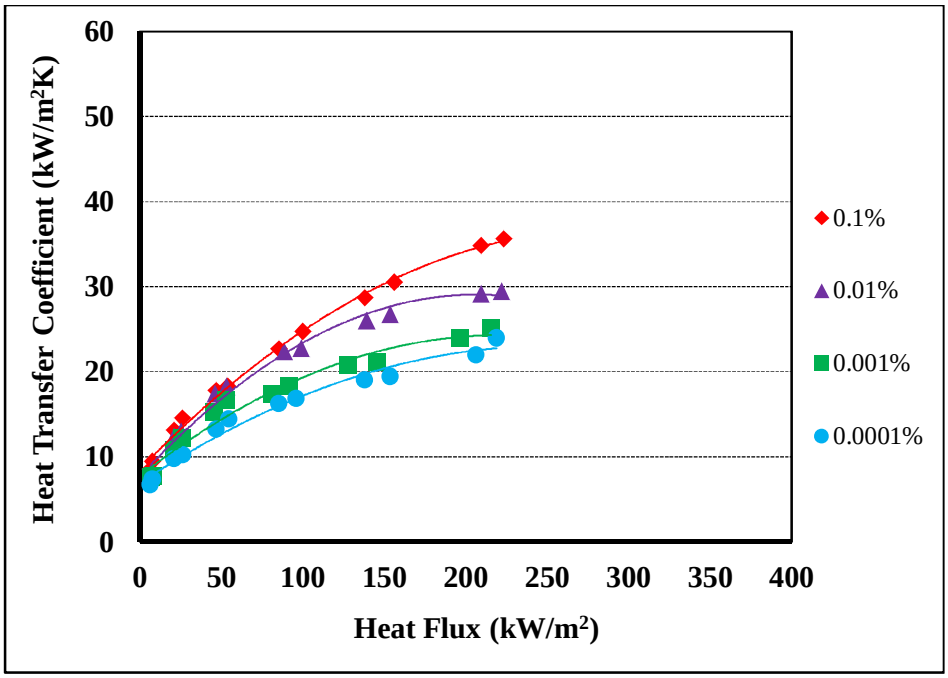

Figure 6.17. Effect of concentration of TiO_2 nanoparticles in water on heat transfer coefficient at 1.0 bar pressure.

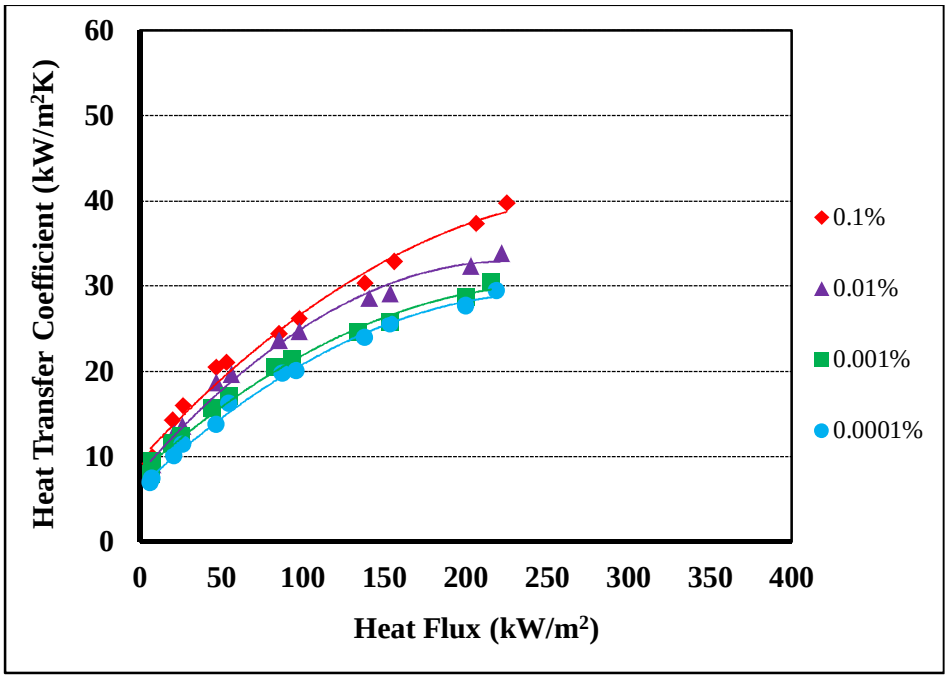

Figure 6.18. Effect of concentration of TiO_2 nanoparticles in water on heat transfer coefficient at 1.5 bar pressure.

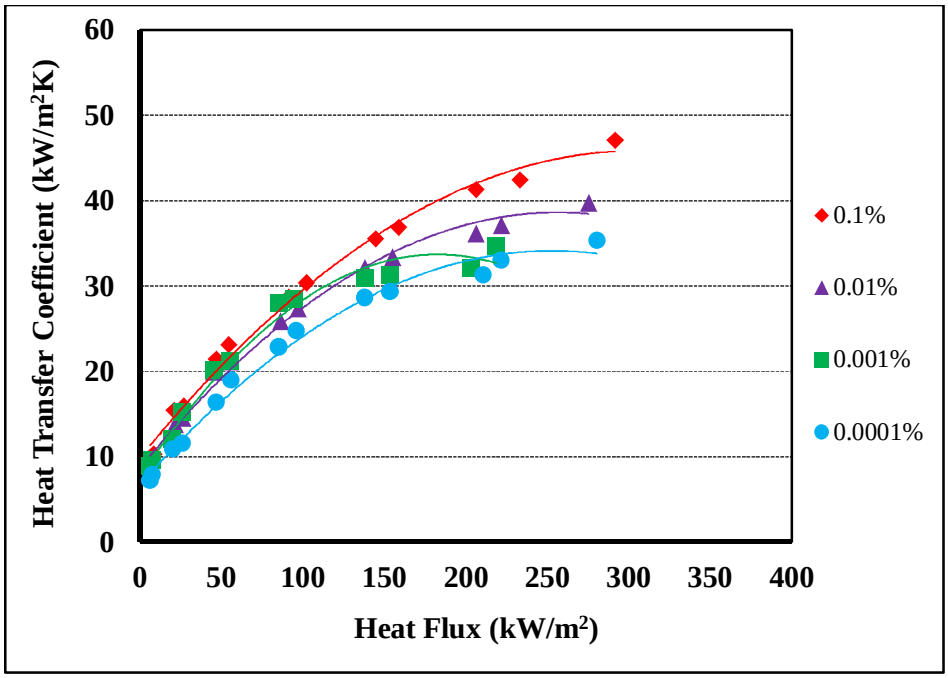

Figure 6.19. Effect of concentration of TiO_2 nanoparticles in water on heat transfer coefficient at 2.0 bar pressure.

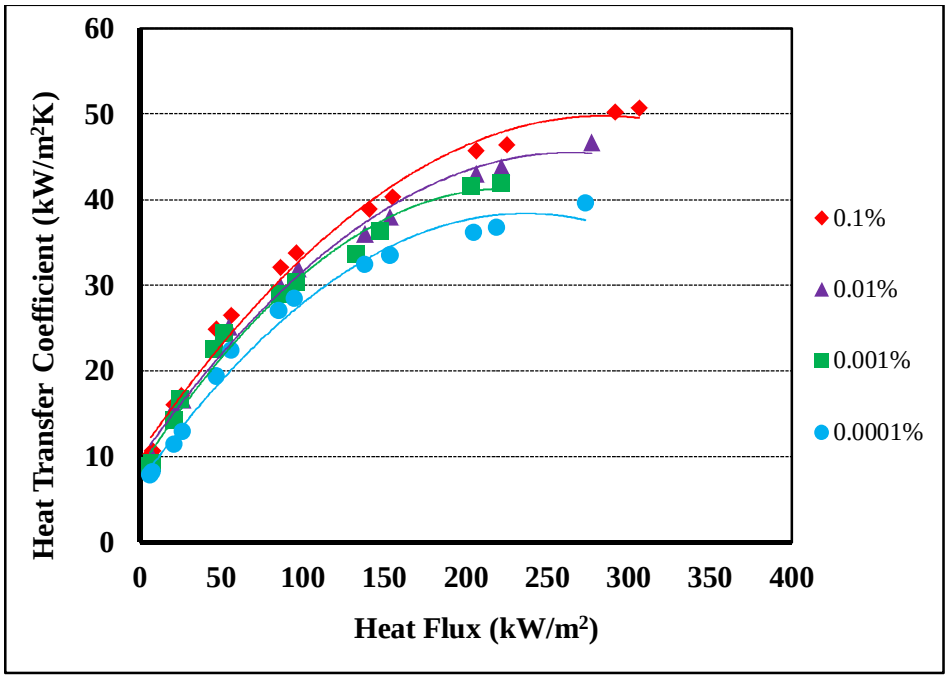

Figure 6.20. Effect of concentration of TiO_2 nanoparticles in water on heat transfer coefficient at 2.5 bar pressure.

The predicted results for TiO_2-water nanofluids through response surface regression analysis are plotted in Fig. 6.17 for a pressure of 1.0 bar, Fig 6.18 for a pressure of 1.5 bar, Fig. 6.19 for a pressure of 2.0 bar and Fig. 6.20 for a pressure of 2.5 bar. Corresponding results obtained experimentally have also been plotted on the graphs. It is found that correlation predicts the experimental results reasonably. It is also noted that heat flux has maximum influence on HTC of TiO_2–water nanofluid as it has maximum F-value = 1845.59 (Appendix-J) at same P-value.

The predicted results for TiO_2-water nanofluids through response surface regression analysis are plotted in Fig. 6.21 for 0.0001% TiO_2-water nanofluid, Fig. 6.22 for 0.001% TiO_2-water nanofluid, Fig. 6.23 for 0.01% TiO_2-water nanofluid and Fig. 6.24 for 0.1% TiO_2-water nanofluid. Corresponding results obtained experimentally for TiO_2-water nanofluids have also been plotted on the graphs. From the comparison of predicted results and experimental results, it is found that correlation predicts the experimental results reasonably.

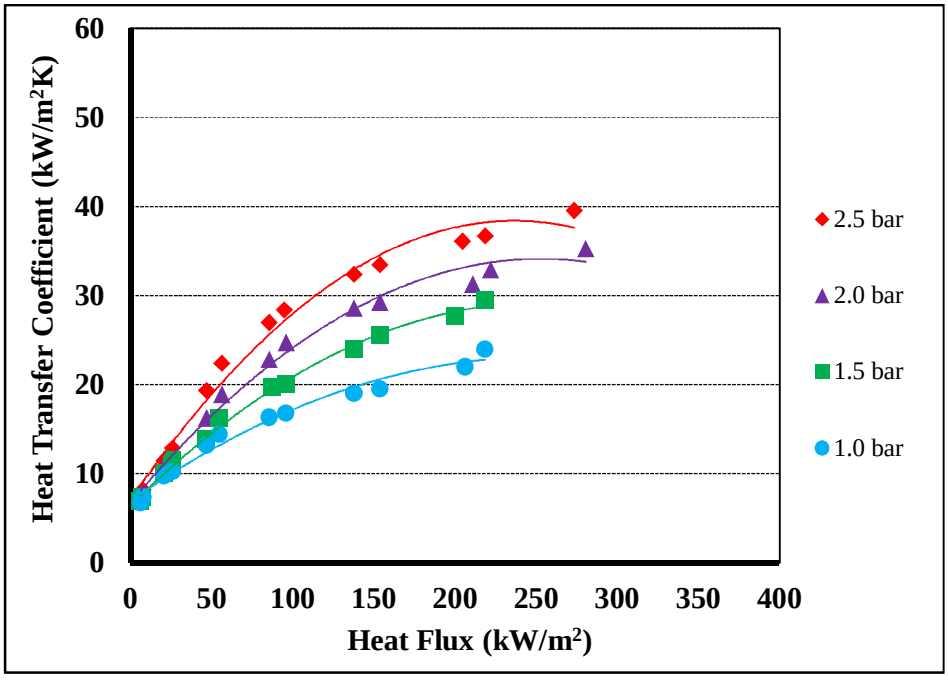

Figure 6.21. Effect of pressure on heat transfer coefficient at 0.0001% concentration of TiO_2 nanoparticles in water.

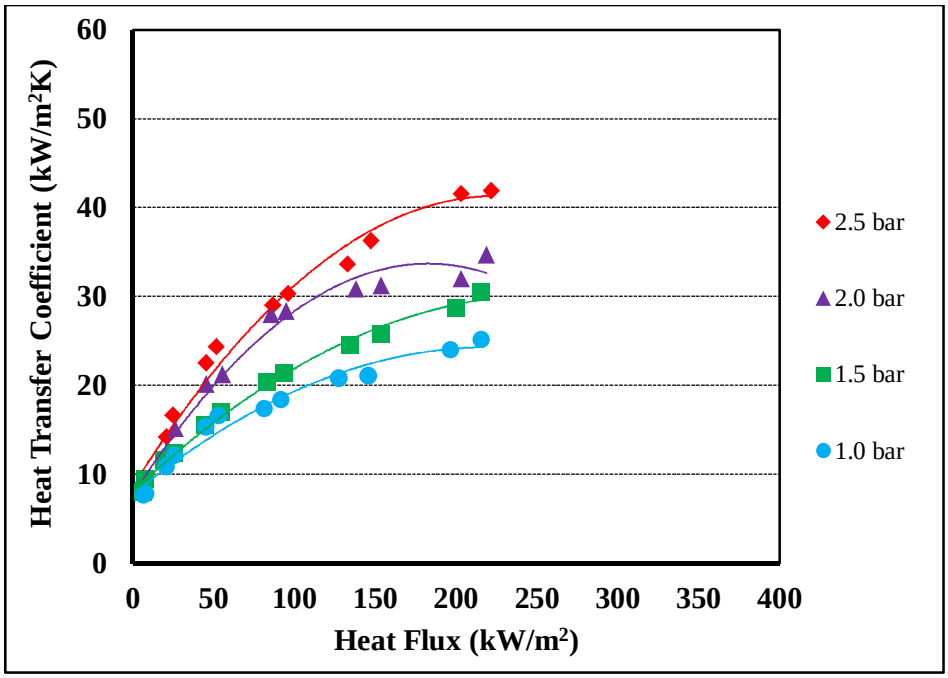

Figure 6.22. Effect of pressure on heat transfer coefficient at 0.001% concentration of TiO_2 nanoparticles in water.

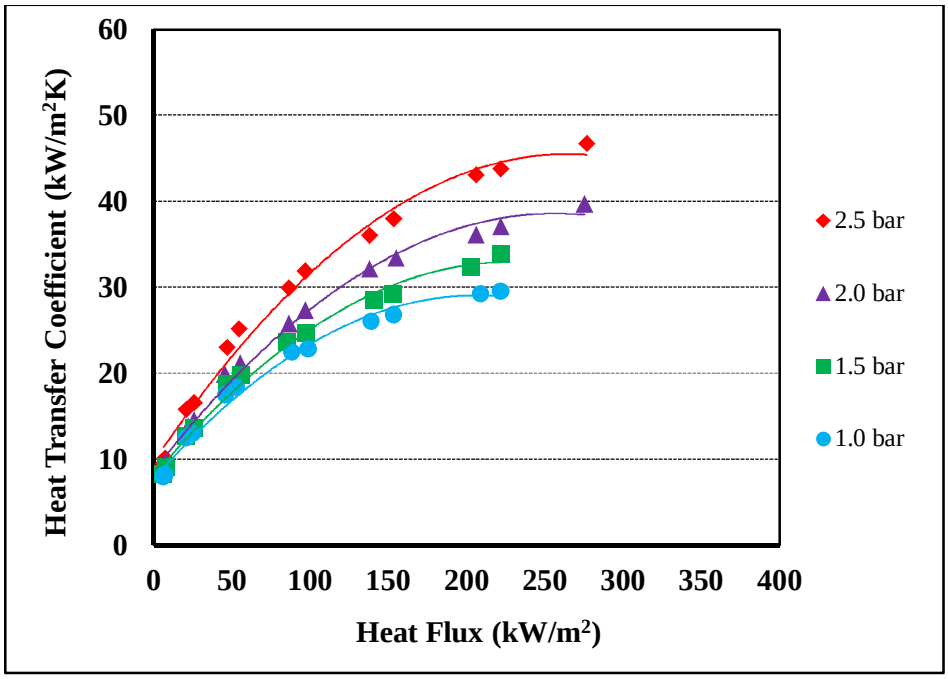

Figure 6.23. Effect of pressure on heat transfer coefficient at 0.01% concentration of TiO_2 nanoparticles in water.

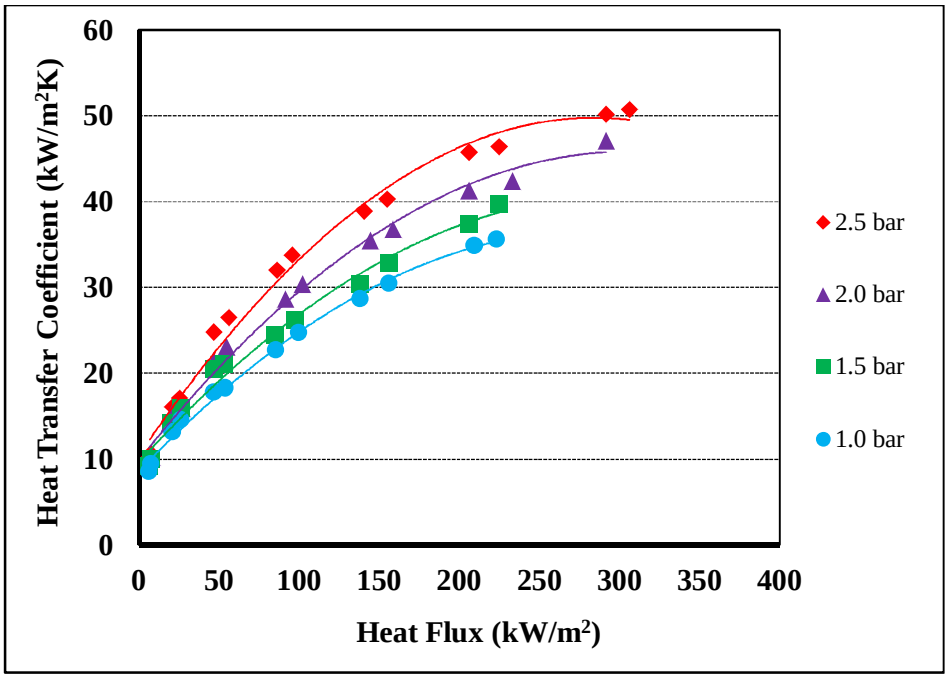

Figure 6.24. Effect of pressure on heat transfer coefficient at 0.1% concentration of TiO_2 nanoparticles in water.

It is found that the pressure has more influence than concentration of nanofluids on HTC, as model has higher F-value = 827.08 (Appendix-J) at same P-value.

6.4 Empirical Relation and their Validation for ZnO-Water Nanofluids

The correlation for ZnO-water nanofluid is given as under:

$$h_{ZnO} = 0.89 + 29395\,C + 4.68\,p + 0.08596\,q - 25725254$$
$$C*C - 0.632\,p*p - 0.000186\,q*q - 866\,C*p + 28.22$$
$$C*q + 0.02216\,p*q \qquad (6.3)$$

Range of the experimental data for ZnO-water nanofluids, The Eq. (6.3) is, 1 bar ≤ p ≤ 2.5 bar, 0.0001% ≤ C ≤ 0.1% and 0 kW/m^2 ≤ q ≤ 400 kW/m^2.

Normal probability plot for ZnO-water nanofluid is given in Fig. 6.25. Similar to Al_2O_3-water nanofluids, Almost all the points in the graph fall on the straight line, which means that empirical relation obtained, accurately represents

the experiment and there is no error in the representation except the normally distributed experimental error.

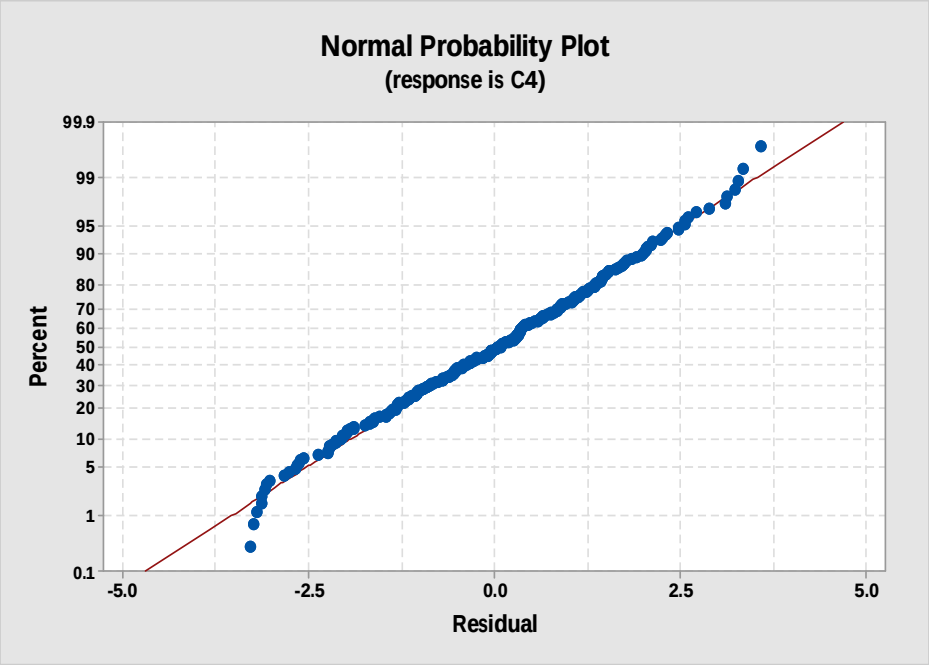

Figure 6.25. Normality plot of residuals of heat transfer coefficient for ZnO-water nanofluid.

Figure 6.26 shows the residuals versus fitted values of HTC for ZnO-water nanofluid. There is no recognizable pattern and the predicted data differ from the experimental data by ± 4% only. As the points in the residual plot are randomly dispersed around the horizontal axis, a linear regression model is appropriate for the data of ZnO-water nanofluid.

Figure 6.27 represents the residual histogram of HTC for ZnO-water nanofluid. It indicates that frequency of residual. The figure shows that the residual follows the normal distribution and supports the correlation obtained for ZnO-water nanofluid.

Figure 6.28 shows the residuals versus observation order for predicted data of HTC for ZnO-water nanofluid. It indicates that the residual is within the acceptable limit of ± 4% and residual doesn't depend on the order in which data was taken.

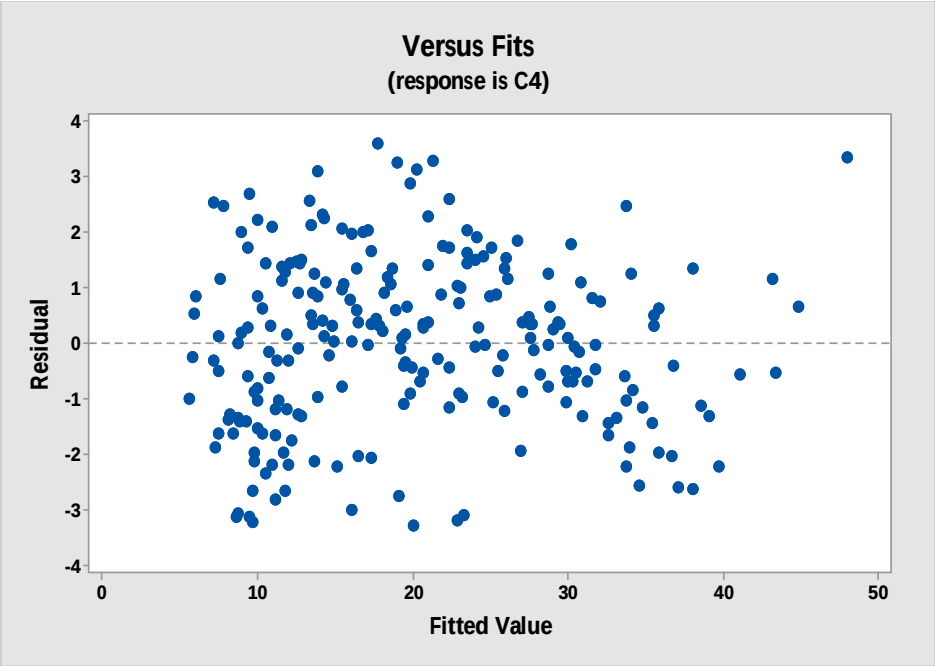

Figure 6.26. Residuals versus fits plot for heat transfer coefficient for ZnO-water nanofluid.

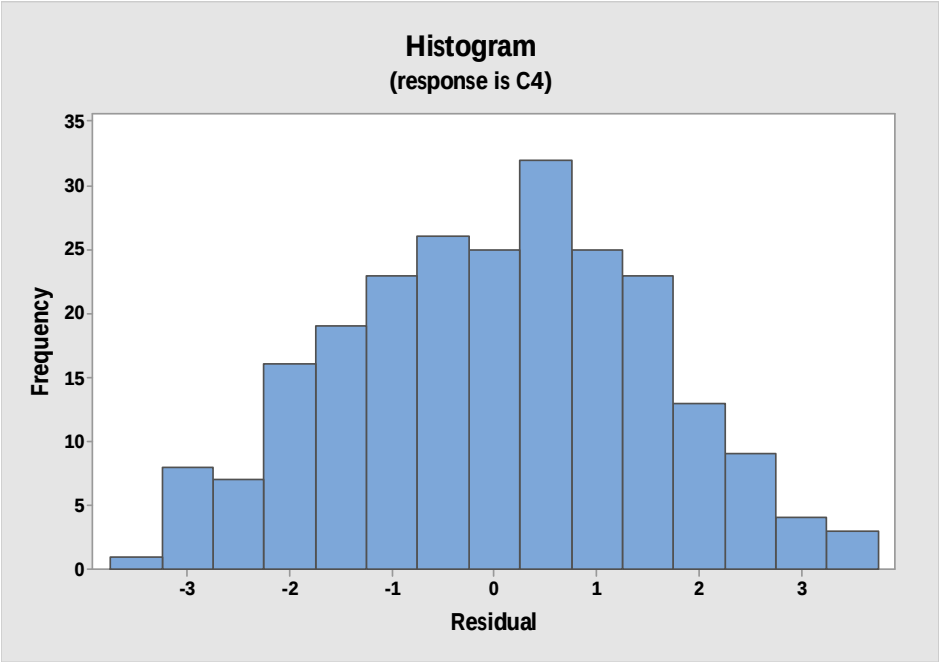

Figure 6.27. Residual histogram for heat transfer coefficient for ZnO-water nanofluid.

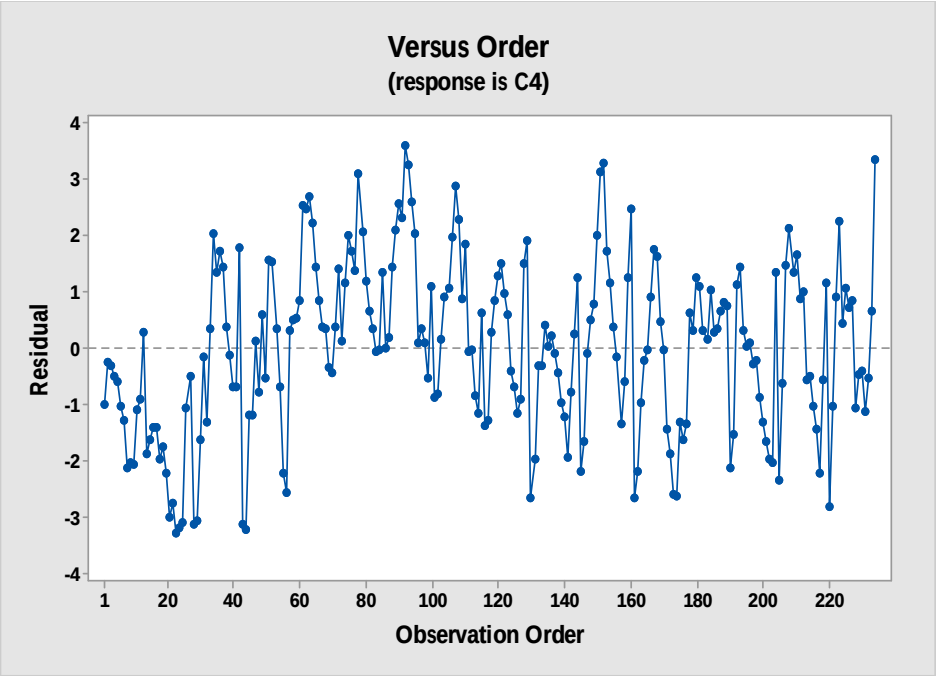

Figure 6.28. Residuals versus order for heat transfer coefficient for ZnO-water nanofluid.

The predicted results for ZnO-water nanofluids through response surface regression analysis are plotted in Fig. 6.29 for a pressure of 1.0 bar, Fig. 6.30 for a pressure of 1.5 bar, Fig. 6.31 for a pressure of 2.0 bar and Fig. 6.32 for a pressure of 2.5 bar. Corresponding results obtained experimentally have also been plotted on the graphs. It is found that correlation predicts the experimental results reasonably. It is also noted that heat flux has maximum influence on HTC of ZnO-water nanofluid as it has maximum F-value = 2826.23 (Appendix-J) at same P-value.

The predicted results for ZnO-water nanofluids through response surface regression analysis are plotted in Fig. 6.33 for 0.0001% ZnO-water nanofluid, Fig 6.34 for 0.001% ZnO-water nanofluid, Fig. 6.35 for 0.01% ZnO-water nanofluid and Fig. 6.36 for 0.1% ZnO-water nanofluid. Corresponding results obtained experimentally have also been plotted on the graphs. It is found that correlation predicts the experimental results reasonably.

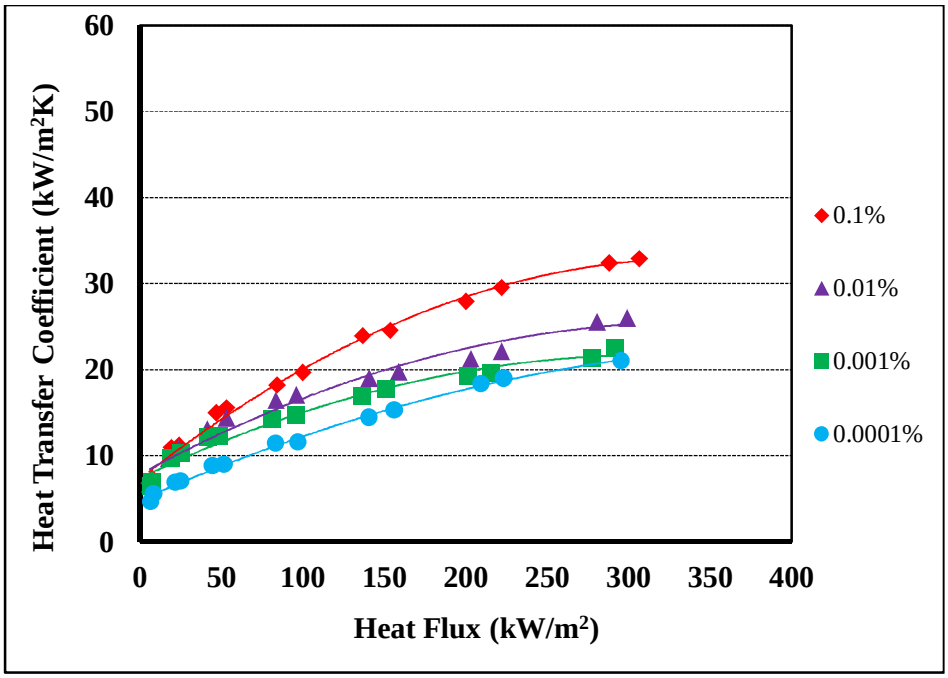

Figure 6.29. Effect of concentration of ZnO nanoparticles in water on heat transfer coefficient at 1.0 bar pressure.

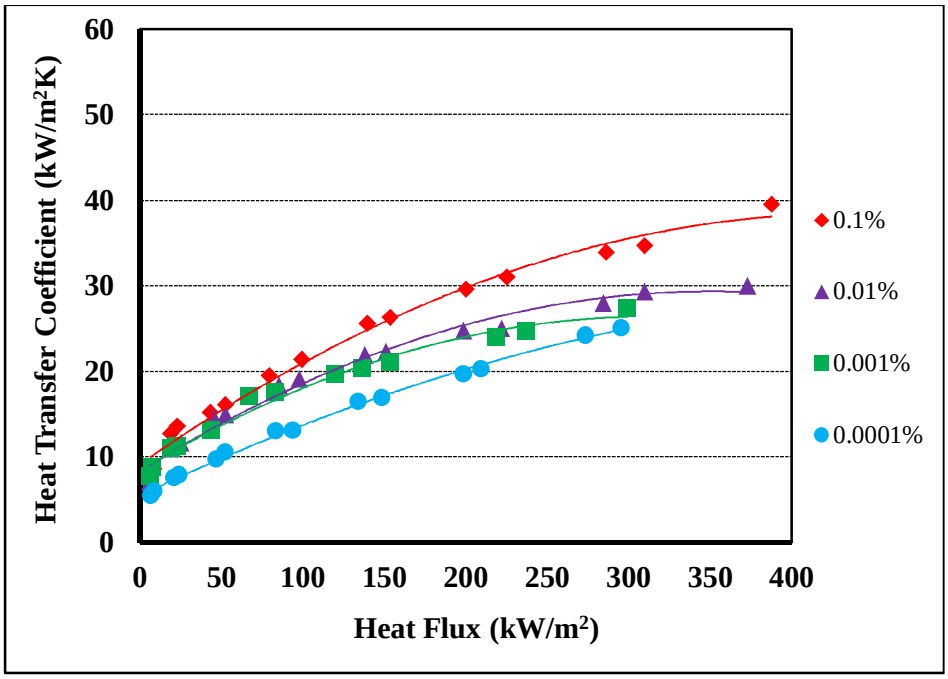

Figure 6.30. Effect of concentration of ZnO nanoparticles in water on heat transfer coefficient at 1.5 bar pressure.

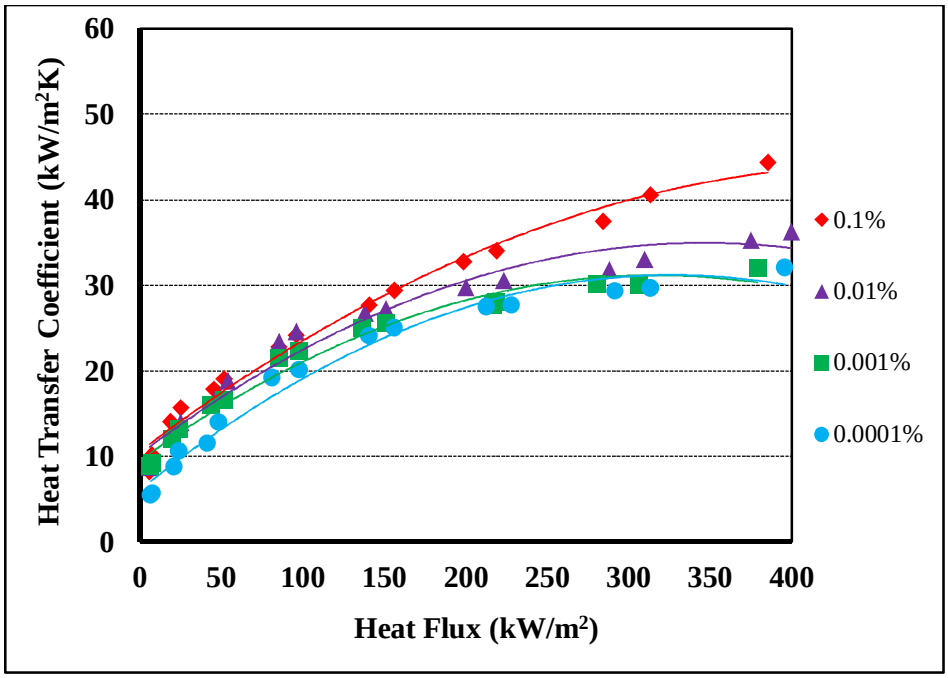

Figure 6.31. Effect of concentration of ZnO nanoparticles in water on heat transfer coefficient at 2.0 bar pressure.

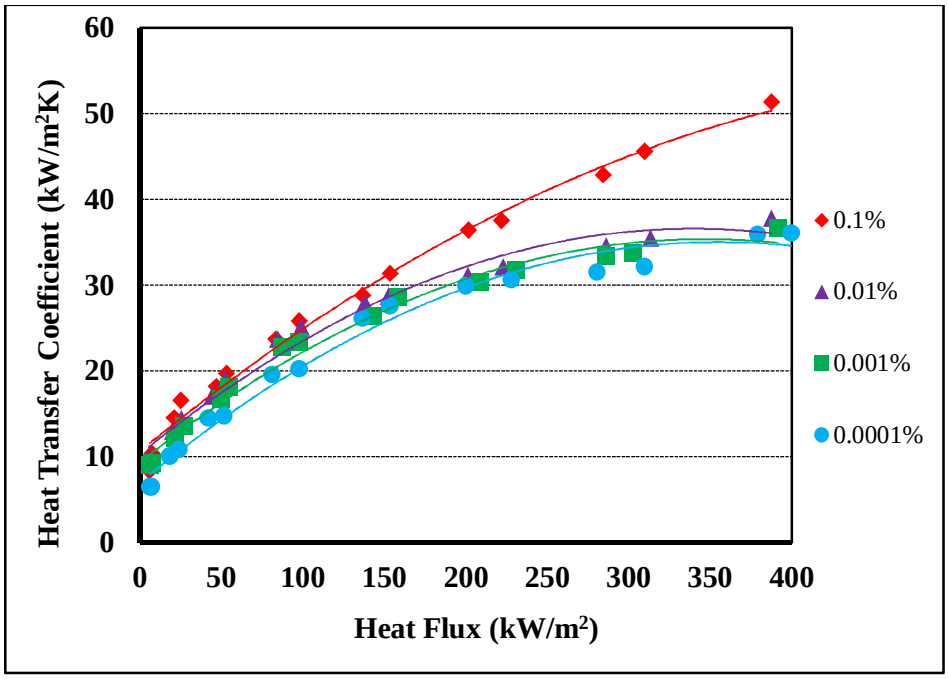

Figure 6.32. Effect of concentration of ZnO nanoparticles in water on heat transfer coefficient at 2.5 bar pressure.

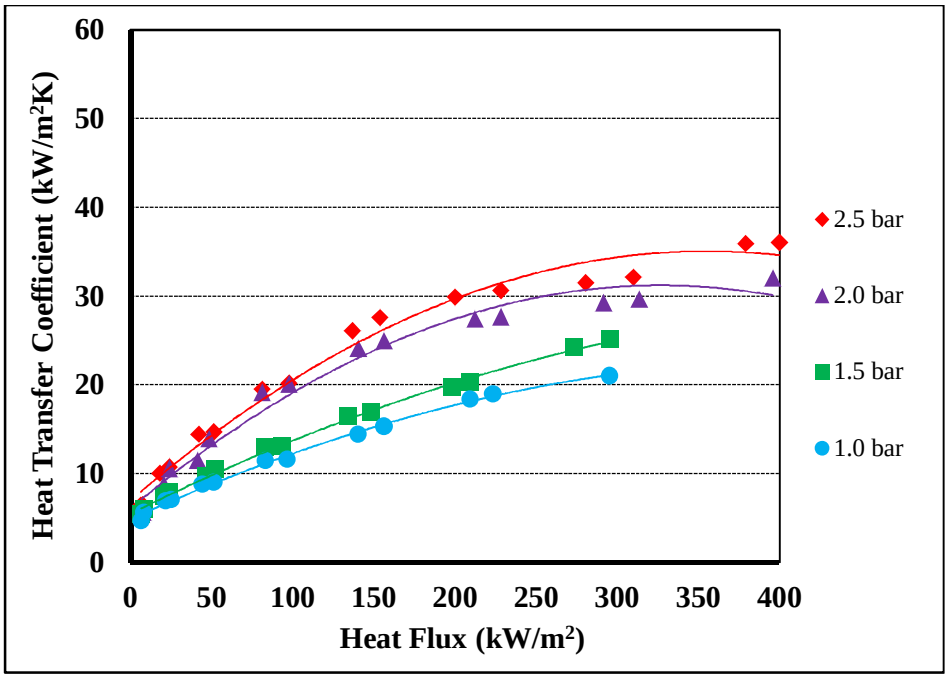

Figure 6.33. Effect of pressure on heat transfer coefficient at 0.0001% concentration of ZnO nanoparticles in water.

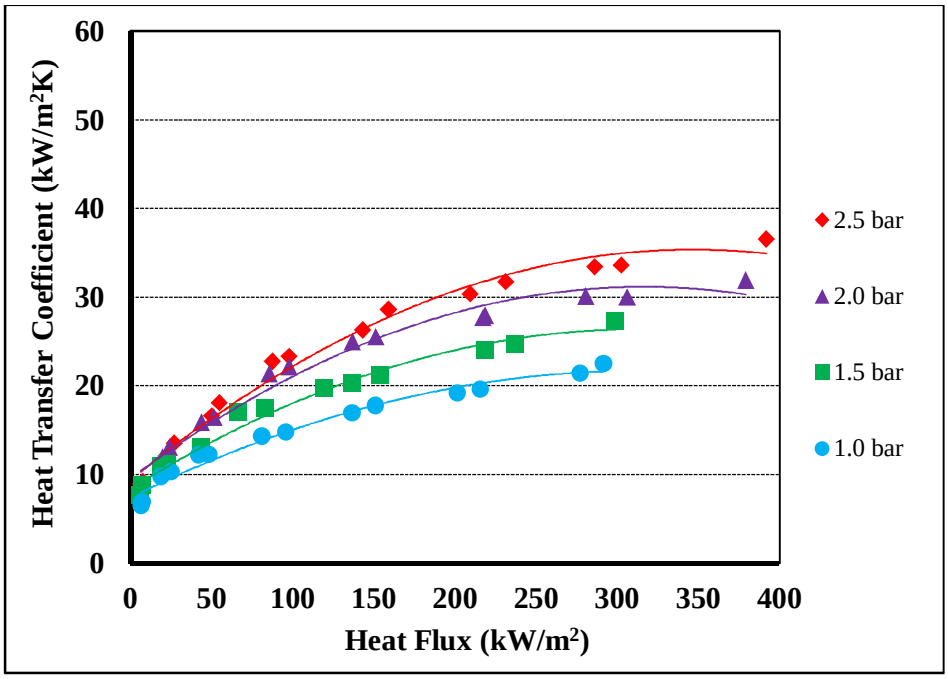

Figure 6.34. Effect of pressure on heat transfer coefficient at 0.001% concentration of ZnO nanoparticles in water.

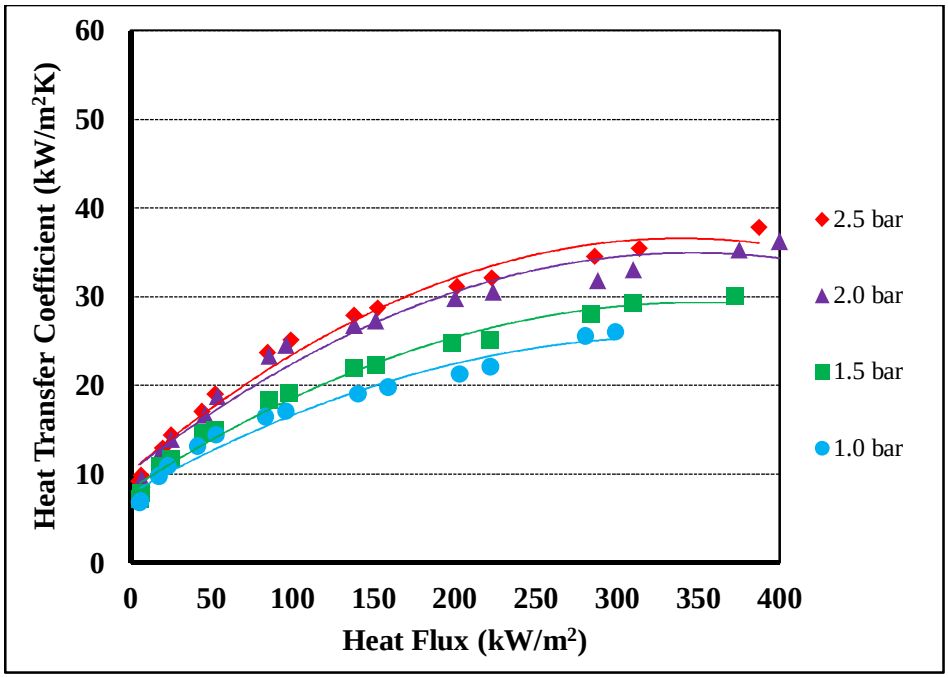

Figure 6.35. Effect of pressure on heat transfer coefficient at 0.01% concentration of ZnO nanoparticles in water.

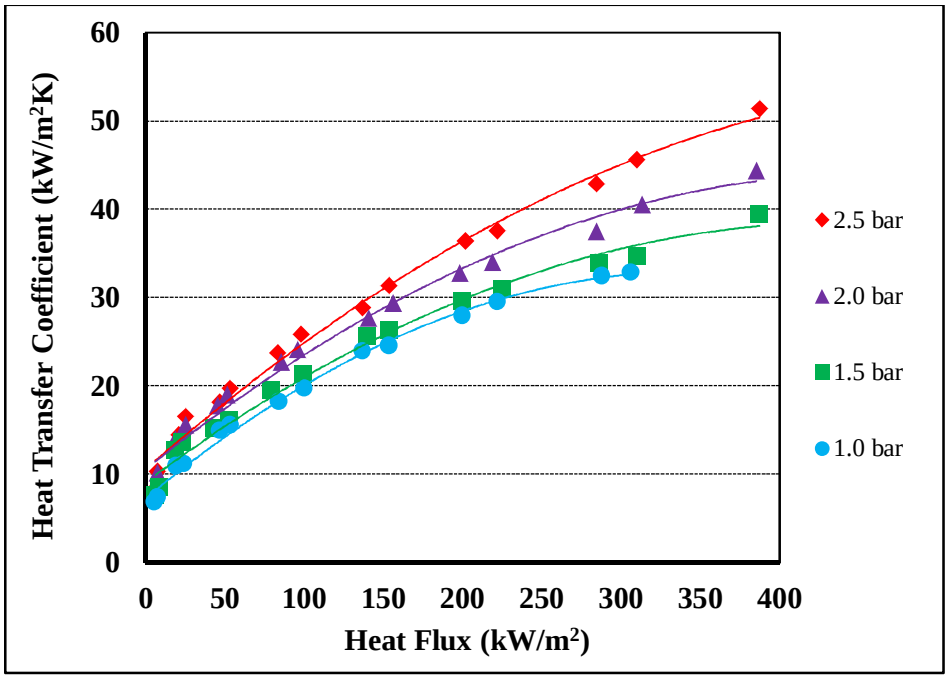

Figure 6.36. Effect of pressure on heat transfer coefficient at 0.1% concentration of ZnO nanoparticles in water.

It is also found that pressure and concentration of nanoparticles in water have approx similar influence on HTC as model has approx similar F-value = 691.59 for concentration (Appendix-J) of ZnO nanoparticle and F-value = 682.63 for pressure (Appendix-J) at same P-value.

6.5 Empirical Relation and their Validation for MWCNT-Water Nanofluids

The correlation for MWCNT-water nanofluid is given as under:

$$h_{\mathrm{MWCNT}} = -0.95 + 121278\,C + 4.99\,p + 0.1750\,q - 107150745\,C*C - 0.72\,p*p - 0.000610\,q*q - 4392\,C*p + 5.0\,C*q + 0.0248\,p*q \quad (6.4)$$

Range of the experimental data for TiO_2-water nanofluids, the Eq. (6.4) is, 1 bar $\leq$ p $\leq$ 2.5 bar, 0.0001% $\leq$ C $\leq$ 0.1% and 0 kW/m^2 $\leq$ q $\leq$ 400 kW/m^2.

Normal probability plot for MWCNT-water nanofluid is given in Fig. 6.37. Almost all the points in the graph fall on the straight line, which means that empirical relation obtained, accurately represents the experiment and there is no error in the representation except the normally distributed experimental error.

Figure 6.38 shows residuals versus fitted values of HTC for MWCNT-water nanofluid. There is no recognizable pattern and the predicted data mainly differ from the experimental data by ± 15%. This spread is rather high for overall values of HTC of about 10-60. Consequently R^2 value for the correlation is low (56%).

Figure 6.39 represents the residual histogram of HTC for MWCNT-water nanofluid. It indicates that frequency of residual. The figure shows that the residual follows the normal distribution and supports the correlation obtained for MWCNT-water nanofluid. Figure 6.40 shows the residuals versus observation order for predicted data of HTC for MWCNT-water nanofluid. It indicates that the residual is within the acceptable limit of ± 15% and residual doesn't depend on the order in which data was taken.

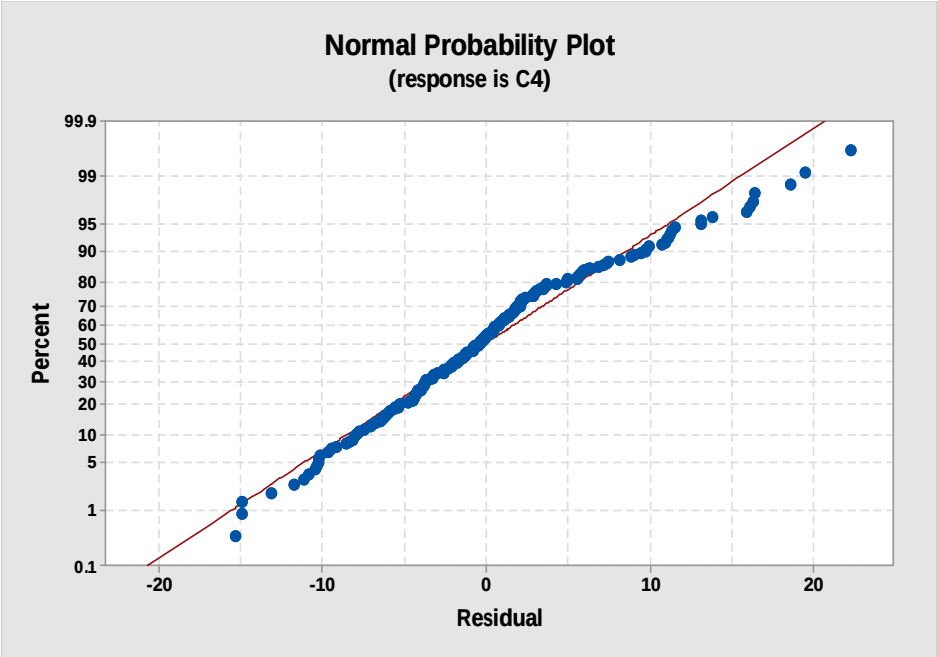

Figure 6.37. Normality probability plot of residuals of heat transfer coefficient for MWCNT-water nanofluid.

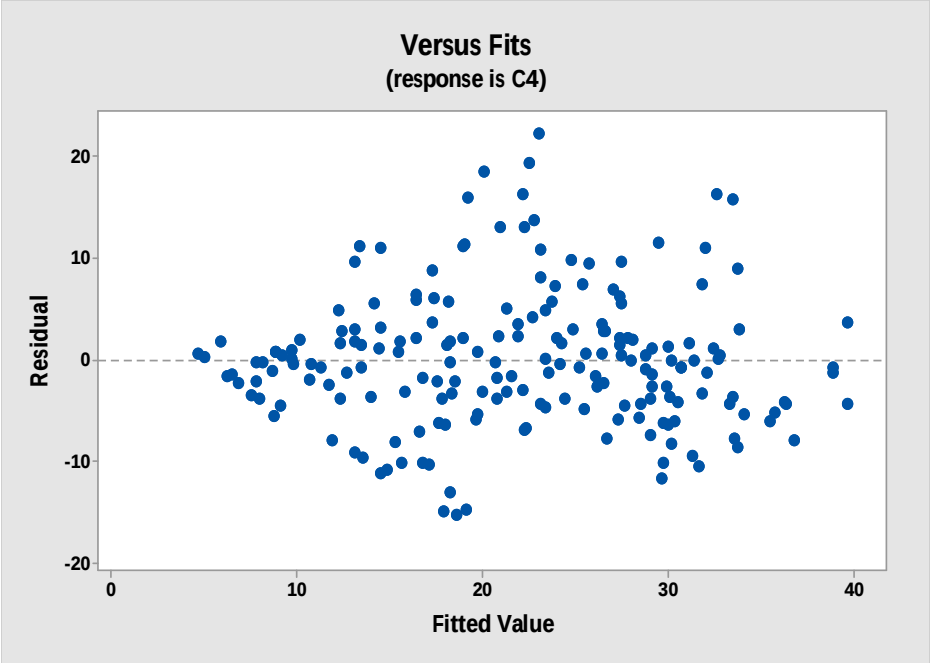

Figure 6.38. Residuals versus fits plot for heat transfer coefficient for MWCNT-water nanofluid.

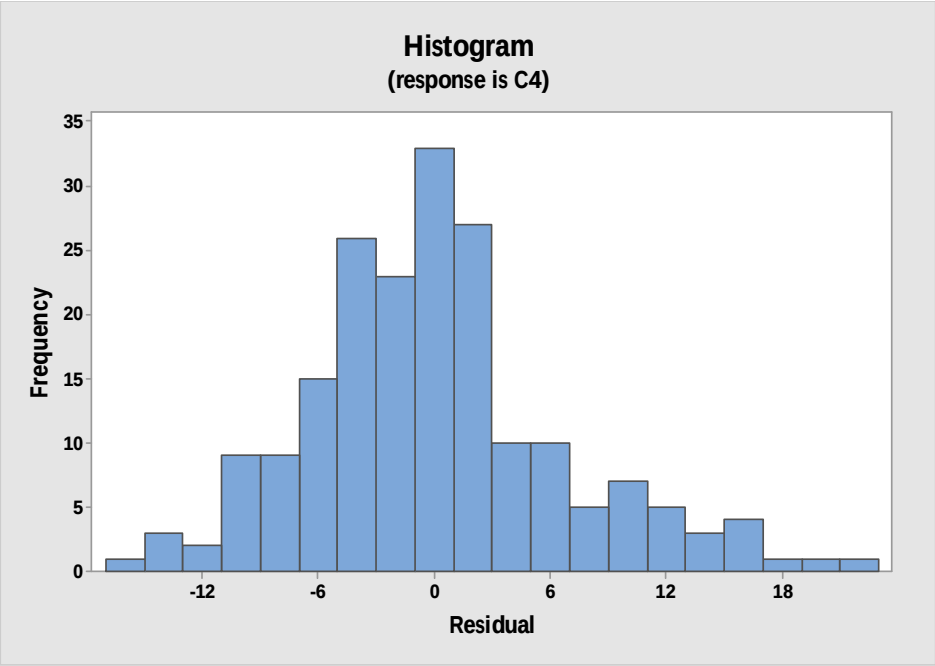

Figure 6.39. Residual histogram for heat transfer coefficient for MWCNT-water nanofluid.

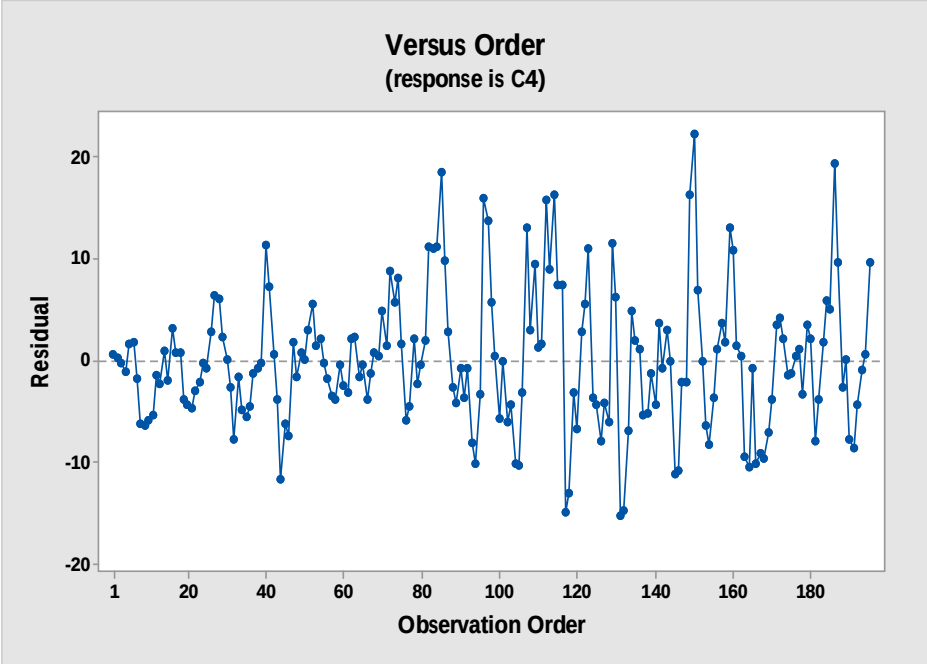

Figure 6.40. Effect of concentration of MWCNT nanoparticles in water on heat transfer coefficient at 1.0 bar pressure.

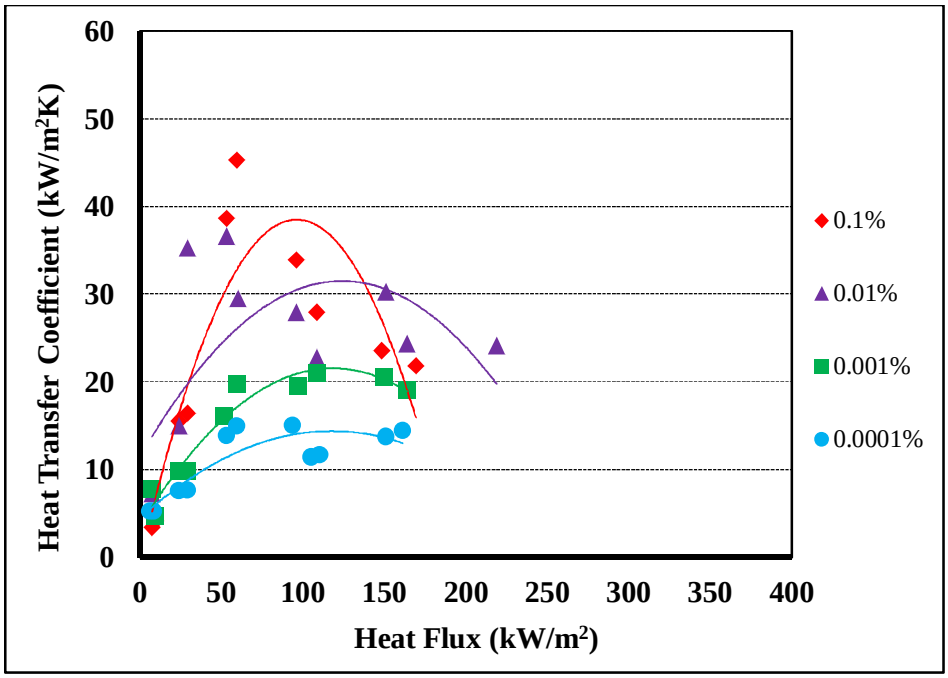

Figure 6.41. Effect of concentration of MWCNT nanoparticles in water on heat transfer coefficient at 1.0 bar pressure.

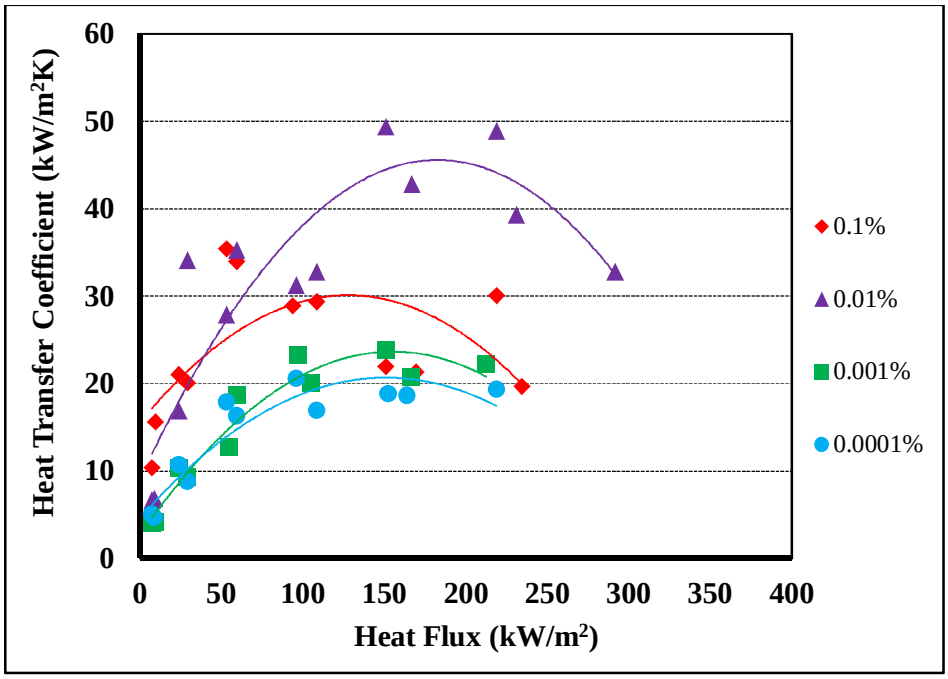

Figure 6.42. Effect of concentration of MWCNT nanoparticles in water on heat transfer coefficient at 1.5 bar pressure.

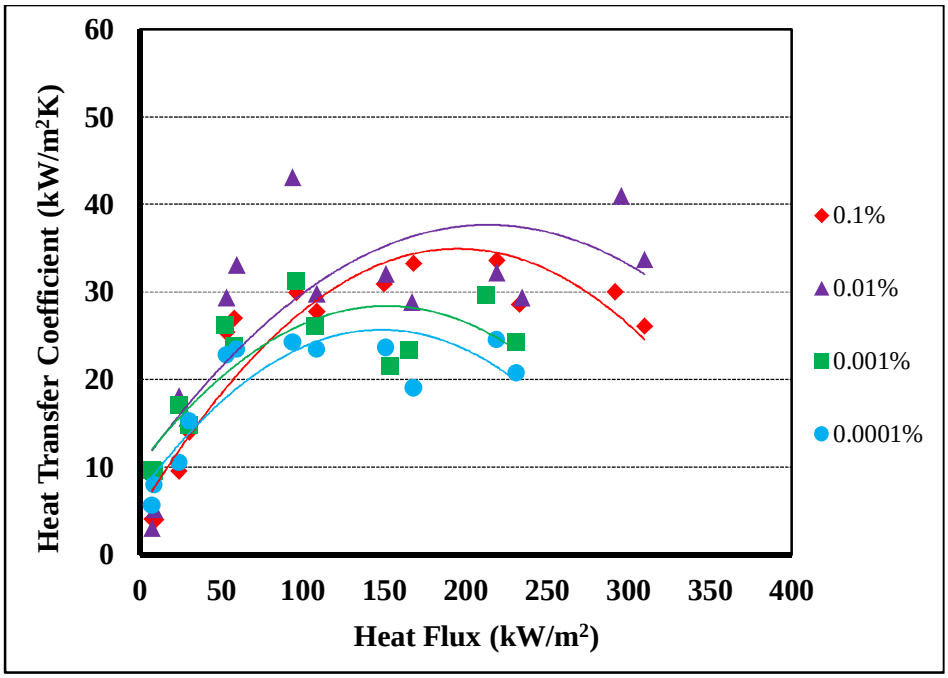

Figure 6.43. Effect of concentration of MWCNT nanoparticles in water on heat transfer coefficient at 2.0 bar pressure.

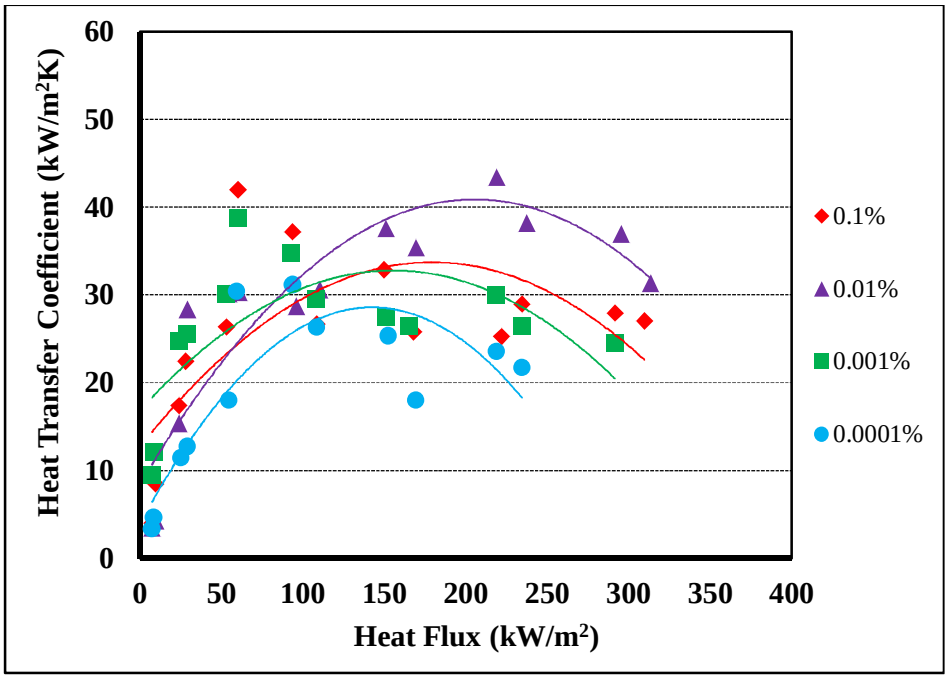

Figure 6.44. Effect of concentration of MWCNT nanoparticles in water on heat transfer coefficient at 2.5 bar pressure.

The predicted results for MWCNT-water nanofluids through response surface regression analysis are plotted in Fig. 6.41 for a pressure of 1.0 bar, Fig. 6.42 for a pressure of 1.5 bar, Fig. 6.43 for a pressure of 2.0 bar and Fig. 6.44 for a pressure of 2.5 bar.

Corresponding results obtained experimentally have also been plotted on the graphs. It is found that correlation predicts the experimental results reasonably. It is also noted that concentration has maximum influence on HTC of MWCNT-water nanofluid as it has maximum F-value = 16.38 (Appendix-J) at same P-value.

The predicted results for MWCNT-water nanofluids through response surface regression analysis are plotted in Fig. 6.45 for 0.0001% MWCNT-water nanofluid, Fig 6.46 for 0.001% MWCNT-water nanofluid, Fig. 6.47 for 0.01% MWCNT-water nanofluid and Fig. 6.48 for 0.1% MWCNT-water nanofluid.

Corresponding results obtained experimentally have also been plotted on the graphs. It is found that correlation predicts the experimental results reasonably.

It is also found that pressure has more influence than heat flux on HTC, as model has higher F-value = 8.53 (Appendix-J) for pressure at same P-value.

It is also found that the predicted R^2 values for all the nanofluids were more than 95% for Al_2O_3-water nanofluids, TiO_2-water nanofluids and ZnO-water nanofluids (Appendix-I).

So it can be concluded that the correlation correctly predicts the experimental data for Al_2O_3-water nanofluids, TiO_2-water nanofluids and ZnO-water nanofluids.

However the predicted R^2 values for MWCNT-water nanofluids was only 56% because there no exact trend was observed for experimental heat transfer coefficient. Therefore correlation for MWCNT-water nanofluid is unable to predict experimental results accurately.

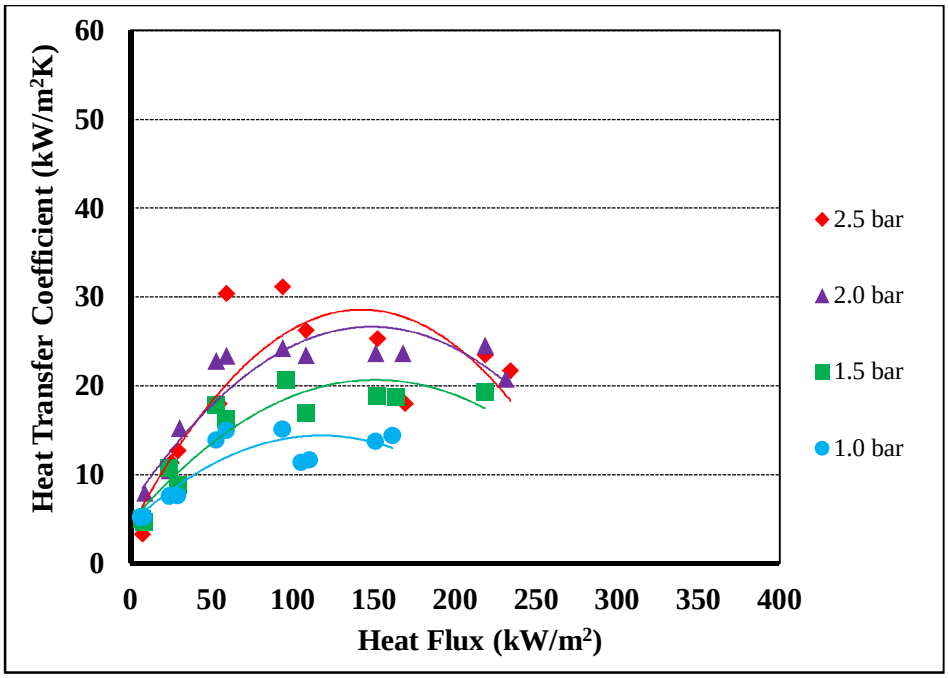

Figure 6.45. Effect of pressure on heat transfer coefficient at 0.0001% concentration of MWCNT nanoparticles in water.

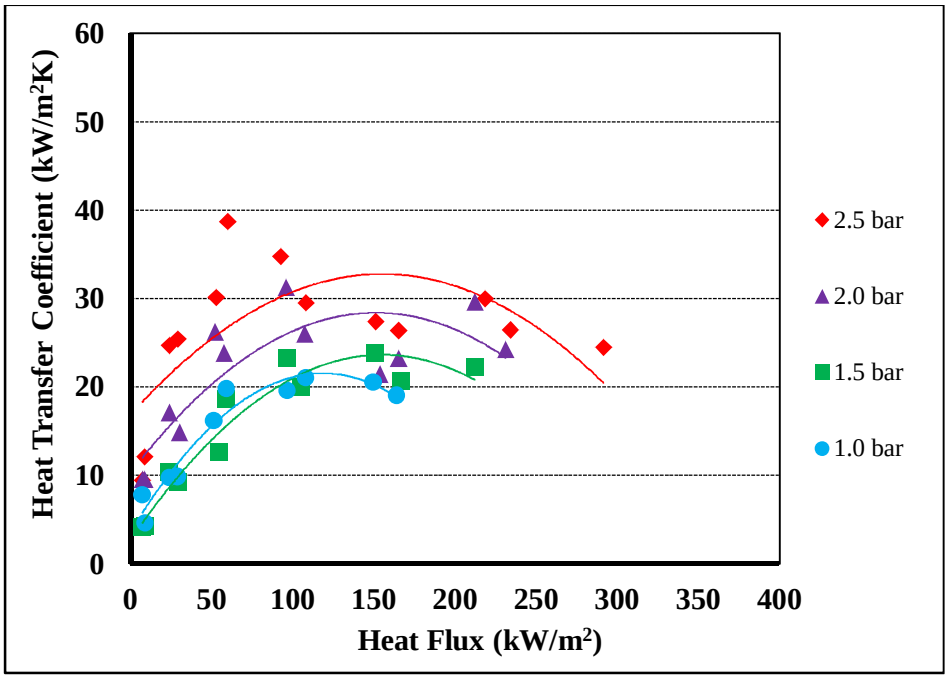

Figure 6.46. Effect of pressure on heat transfer coefficient at 0.001% concentration of MWCNT nanoparticles in water.

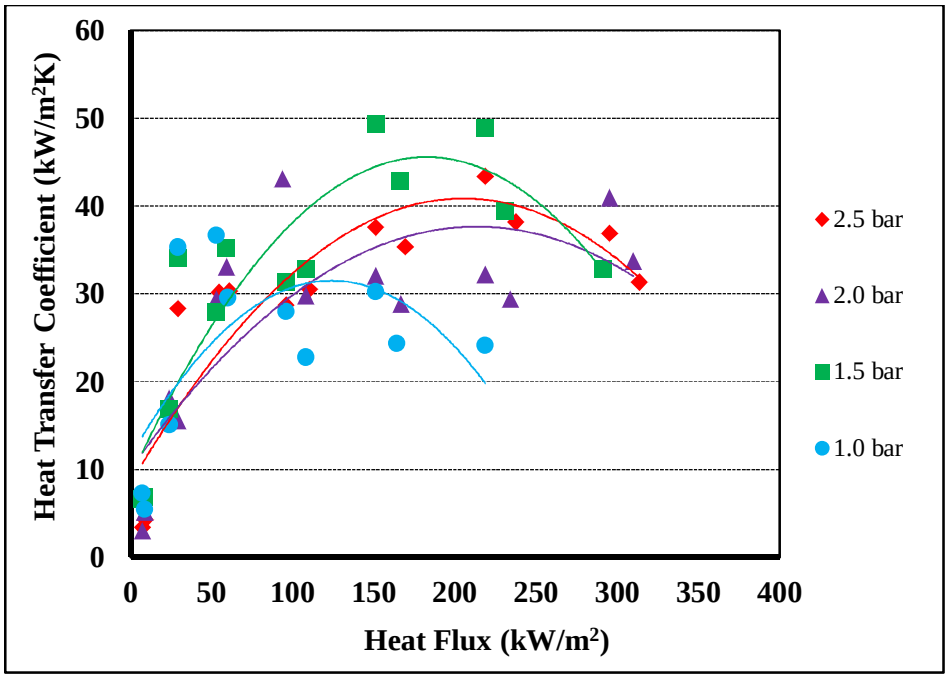

Figure 6.47. Effect of pressure on heat transfer coefficient at 0.01% concentration of MWCNT nanoparticles in water.

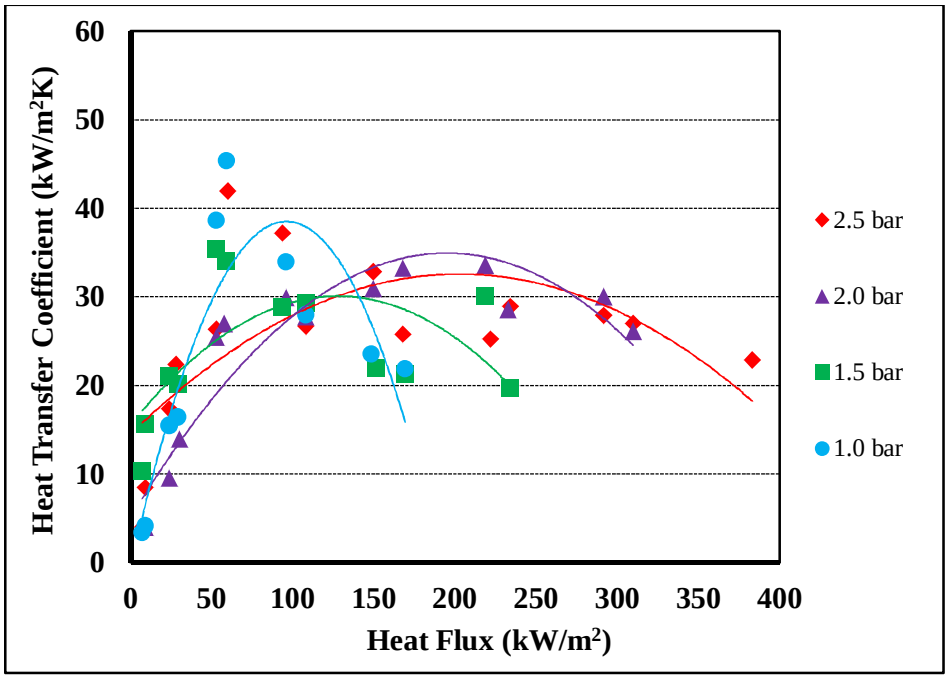

Figure 6.48. Effect of pressure on heat transfer coefficient at 0.1% concentration of MWCNT nanoparticles in water.

7.

CONCLUSIONS

An existing experimental facility was modified to study heat transfer characteristics of nanofluids in convective and boiling heat transfer. The convective and flow boiling heat transfer experiments were carried out to study effect of pressure, concentration of nanoparticles and heat flux on heat transfer coefficient, pressure drop and bubble parameters. Surface roughness of the heater rod was also measured for different concentration of nanoparticles. Following conclusions have been drawn from the study.

7.1 Thermal Conductivity

It is observed that there is no significant variation in thermal conductivity of water with sonication time. However, the thermal conductivity of Al_2O_3-water nanofluid, TiO_2-water nanofluid, ZnO-water nanofluid and MWCNT-water nanofluids increases with increase in sonication time in the beginning, reaches a maximum value and then decreases. The maximum increase in thermal conductivity was 170%, 150%, 120% and 163% for Al_2O_3-water nanofluid, TiO_2-water nanofluid, ZnO-water nanofluid and MWCNT-water nanofluid respectively at 0.1%.

7.2 Heat Transfer Coefficient

Heat transfer coefficient for flow boiling of nanofluids is not found in the literature and it is measured first time. Heat transfer coefficient of nanofluids increases with increase in concentration of nanoparticles, heat flux and pressure. The maximum increase in HTC was 80% due to increase in pressure from 1.0 bar to 2.5 bar for 0.01% MWCNT-water nanofluid at heat flux of about 220 kW/m^2 and mass flux of 400 kg/m^2s.

The maximum increase in HTC was 104%, 101% and 60% over that of the base fluid for 0.1% of Al_2O_3-water nanofluid, 0.1% of TiO_2-water nanofluid, 0.1% of ZnO-water nanofluid respectively at a pressure of 2.5 bar, heat flux of about 210 kW/m^2 and mass flux of 400 kg/m^2s while in case for 0.1% of MWCNT-water nanofluid increase in HTC was about 134% over that of the base fluid at a

pressure of 1.5 bar and heat flux of about 160 kW/m^2 and mass flux of 400 kg/m^2s.

Empirical relations were also developed for heat transfer coefficient of the nanofluids as a function of concentration of nanofluids, pressure and heat flux using free version of 'Minitab' software. The predicted results plotted in graphical form for a pressure, concentration of nanofluids and heat flux to compare with experimental results. Based on compared results and values of predicted R^2, it can be concluded that empirical relations predict the experimental results reasonably.

7.3 Pressure Drop

Pressure drop for flow boiling of nanofluids is not found in the literature and it is measured first time. For all the nanofluids used in the experiment, pressure drop increases with increase in concentration of the nanofluids. Compared with water, there was increase in pressure drop for all the nanofluids. Pressure drop decreases with increase in pressure. However there was no significant effect of heat flux on pressure drop in convection but it increases in the flow boiling.

The maximum increase in pressure drop over the distilled water was about 12%, 11%, 28% and 9% for 0.1% Al_2O_3-water nanofluid, 0.1% TiO_2-water nanofluid, 0.1% ZnO-water nanofluid and 0.1% MWCNT-water nanofluid respectively.

7.4 The Bubble Parameters

Bubble parameters, i.e. bubble diameter, bubble density and void fraction and HTC are correlated. Heat transfer coefficient increases with increase in bubble diameter for pure water, Kumar et al. (1992).

Again heat transfer coefficient increases with increase in bubble density for synthetic fuel, Kagumba (2013). However, visualization study for flow boiling of nanofluids is not found in the literature. Therefore visualization study for flow

boiling of nanofluids has been carried out and the results have been correlated with corresponding HTC.

7.4.1 Bubble Diameter

The bubble diameter for nanofluids increases with increase in concentration of the nanofluids. The bubble diameter for Al_2O_3-water nanofluid and TiO_2-water nanofluid is found to be larger than the bubble diameter for water while the bubble diameter for ZnO-water nanofluid and MWCNT-water nanofluid is found to be smaller than the bubble diameter of water.

The bubble diameter decreases with increase in external pressure for both, distilled water and selected nanofluids. Further boiling is also delayed with increase in external pressure for both, distilled water and selected nanofluids. While bubble diameter of distilled water and selected nanofluids increase with heat flux.

The maximum bubble diameter was 1.63 mm at 140 kW/m^2 for distilled water, 2.47 mm at 180 kW/m^2 for 0.001% Al_2O_3-water nanofluid, 2.34 mm at 220 kW/m^2 0.001% TiO_2-water nanofluid, 2.17 mm at 280 kW/m^2 for 0.001% ZnO-water nanofluid and 1.30 mm at 160 kW/m^2 for 0.001% MWCNT-water nanofluid respectively.

7.4.2 Bubble Density

The bubble density for nanofluids is less than the bubble density for water at constant heat flux and pressure.

The bubble density for distilled water and selected nanofluids decreases with external pressure. The bubble density for nanofluids increases with increase in concentration of nanoparticles in water. Results also show that bubble density for distilled water and selected nanofluids increases with increase in heat flux. The bubble density decreases for distilled water and the selected nanofluids with increase in external pressure.

The maximum bubble density was 2,90,198 $1/m^2$ at 140 kW/m^2 for distilled water, 1,96,605 $1/m^2$ at 235 kW/m^2 for 0.0001% Al_2O_3-water nanofluid, 3,04,493 $1/m^2$ at 220 kW/m^2 for 0.0001% TiO_2-water nanofluid, 3,12,384 $1/m^2$ at 295 kW/m^2 for 0.0001% ZnO-water nanofluid and 1,28,492 $1/m^2$ at 165 kW/m^2 for 0.0001% MWCNT-water nanofluid respectively.

7.4.3 Void Fraction

The void fraction for distilled water and selected nanofluids decreases with external pressure. Further, void fraction for distilled water and selected nanofluid increases with increase in heat flux.

The void fraction also increases with increase in concentration of the nanofluids due to larger area covered by increased bubble diameter in the image area of Al_2O_3-water nanofluid and TiO_2-water nanofluid. While the void fraction for ZnO-water nanofluid and MWCNT-water nanofluid was observed, less than that of water.

The maximum void fraction was 0.1677 at 140 kW/m^2 for distilled water, 0.2873 at 180 kW/m^2 for 0.0001% Al_2O_3-water nanofluid, 0.2611 at 220 kW/m^2 for 0.0001% TiO_2-water nanofluid, 0.2233 at 290 kW/m^2 for 0.0001% ZnO-water nanofluid and 0.1237 at 165 kW/m^2 and 0.0001% MWCNT-water nanofluid respectively.

7.5 Surface Roughness

The surface roughness, Ra (μm), of heater rod for the nanofluids used in the experiment increases monotonically with increase in concentration of nanoparticles in the nanofluid.

The maximum surface roughness of heater rod, after the boiling of working fluids was 0.06 μm for distilled water, 0.88 μm for 0.1% Al_2O_3-water nanofluid, 0.64 μm for 0.1% TiO_2-water nanofluid, 0.61 μm for 0.1% ZnO-water nanofluid and 0.72 for μm for 0.1% MWCNT-water nanofluid respectively.

7.6 Overall Conclusion

Heat transfer coefficient, pressure drop and the visualization study for flow boiling of nanofluids have not been studied before. The same have been investigated in this study.

It was found that heat transfer coefficient of nanofluids studied, increases with increase in concentration of nanoparticles, pressure and heat flux by about 135% as compared to water.

It was also found that pressure drop increases with increase in concentration of nanoparticles and with increase in heat flux in the flow boiling by about 28% as compared to water. However it decreases with increase in pressure.

The bubble diameter and void fraction increase with increase in concentration of nanoparticles and heat flux. The bubble density decreases with increase in concentration of nanoparticles however, it increases with increase in heat flux. Bubble parameters decrease with increase in pressure.

Thus, while there is a significant increase in HTC of the nanofluids selected, there is also some increase in pressure drop and coating on the surfaces. The pressure drop and coating with increase in concentration of nanoparticles and depend on type of nanoparticle. Apart from this, stability of a nanofluid is also an important issue which has not been studied here. A judicious choice for a fluid with high heat transfer coefficient shall be made based on above considerations.

7.7 Future Work

It has been observed during this study that and the effect of all the parameters on heat transfer coefficient, pressure drop bubble parameters is significant. Based on the experience gained during this study, following suggestions are given for future work.

The major fields of future research are as following:-

1. The stability of nanofluids and their heat transfer applications for higher concentrations of nanofluids needs to be investigated in more detail.
2. The chemical properties of selected nanofluids and their relation with boiling need to be studied in detail.
3. Effect of type, size and shape of nanoparticles on heat transfer characteristics of nanofluids need to be studied in more detail.
4. Effect of degree of sub cooling, flow regimes on boiling process needs to be investigated in more detail.
5. Effect of nanofluids on CHF can be investigated for flow boiling condition.

REFERENCES

A. Alsaedi, M. Awais, T. Hayat. "Effects of heat generation/absorption on stagnation point flow of nanofluid over a surface with convective boundary conditions." *Commun Nonlinear Sci Numer Simulat* 17 (2012): 4210–4223.

A. Arefmanesh, M. Aminia, M. Mahmoodi, M. Najafi. "Buoyancy-driven heat transfer analysis in two-square duct annuli filled with a nanofluid." *European Journal of Mechanics B/Fluids* 33 (2012): 95–104.

A. Mokmeli, M. Saffar-Avval. "Prediction of nanofluid convective heat transfer using the dispersion model." *International Journal of Thermal Sciences* 49 (2010): 471–478.

A. Nasiri, M. Shariaty-Niasar, A.M. Rashidi, R. Khodafarin. "Effect of CNT structures on thermal conductivity and stability of nanofluid." *International Journal of Heat and Mass Transfer* 55 (2012): 1529–1535.

A.A. Abbasian Arani, J. Amani. "Experimental study on the effect of TiO2–water nanofluid on heat transfer and pressure drop." *Experimental Thermal and Fluid Science* 42 (2012): 107–115.

A.A. Rabienataj Darzi, Mousa Farhadi, Kurosh Sedighi, Rouzbeh Shafaghat, Kaveh Zabihi. "Experimental investigation of turbulent heat transfer and flow characteristics of SiO2/water nanofluid within helically corrugated tubes." *International Communications in Heat and Mass Transfer* xxx (2012): xxx-xxx.

A.K. Nayak, P.P. Kulkarni, P.K. Vijayan. "Study on the transient and stability behaviour of a boiling two-phase natural circulation loop with Al2O3 nanofluids." *Applied Thermal Engineering* 31 (2011): 1673-1681.

A.P. Roday, M.K. Jensen. "Study of the critical heat flux condition with water and R-123 during flow boiling in microtubes. Part II – Comparison of data with correlations and establishment of a new subcooled CHF correlation." *International Journal of Heat and Mass Transfer* 52 (2009): 3250–3256.

Abdurrahim Bolukbasi, Dogan Ciloglu. "Pool boiling heat transfer characteristics of vertical cylinder quenched by SiO2ewater nanofluids." *International Journal of Thermal Sciences* 50 (2011): 1013-1021.

Abu-Nada, Eiyad. "Effects of variable viscosity and thermal conductivity of Al2O3–water nanofluid on heat transfer enhancement in natural convection." *International Journal of Heat and Fluid Flow* 30 (2009): 679–690.

Adirek Suriyawong, Somchai Wongwises. "Nucleate pool boiling heat transfer characteristics of TiO2–water nanofluids at very low concentrations." *Experimental Thermal and Fluid Science* xxx (2010): xxx–xxx.

Aida Nasiri, Mojtaba Shariaty-Niasar, Alimorad Rashidi, Azadeh Amrollahi, Ramin Khodafarin. "Effect of dispersion method on thermal conductivity and stability of nanofluid." *Experimental Thermal and Fluid Science* 35 (2011): 717–723.

Aixiang Ma, Jinjia Wei, Minzhe Yuan, Jiabin Fang. "Enhanced flow boiling heat transfer of FC-72 on micro-pin-finned surfaces." *International Journal of Heat and Mass Transfer* 52 (2009): 2925–2931.

Al-Amayreh, Mazen. "Experimental Study of Thermal Conductivity of Ethylene Glycol Water Mixtures." *European Journal of Scientific Research* 44, no. 2 (2010): 300-313.

Amir Houshang Mahmoudi, Mina Shahi, Farhad Talebi. "Effect of inlet and outlet location on the mixed convective cooling inside the ventilated cavity subjected to an external nanofluid." *International Communications in Heat and Mass Transfer* 37 (2010): 1158–1173.

Amit Gupta, Xuan Wu, Ranganathan Kumar. "Possible Mechanisms for Thermal Conductivity Enhancement in Nanofluids." *Fourth International Conference on Nanochannels, Microchannels and Minichannels.* Limerick, Ireland: ASME, 2006.

Anastasios I. Stamou, Ioannis Katsiris, Alois Schaelin. "Evaluation of thermal comfort in Galatsi Arena of the Olympics ‘‘Athens 2004’’ using a CFD model." *Applied Thermal Engineering* 28 (2008): 1206–1215.

Andrea Cioncolini, Lorenzo Santini, Marco E. Ricotti. "Effects of dissolved air on subcooled and saturated flow boiling of water in a small diameter tube at low pressure." *Experimental Thermal and Fluid Science* 32 (2007): 38–51.

Antonis Sergis, Yannis Hardalupas. "Anomalous Heat Transfer Modes of Nanofluids: a Stastical Analysis Approach Review." *9th HSTAM International Congress on Mechanics.* Limassol, Cyprus, 2010.

Apurba Kumar Santra, Niladri Chakraborty, Swarnendu Sen. "Prediction of heat transfer due to presence of copper–water nanofluid using resilient-propagation neural network." *International Journal of Thermal Sciences* 48 (2009): 1311–1318.

Apurba Kumar Santra, Swarnendu Sen, Niladri Chakraborty. "Study of heat transfer augmentation in a differentially heated square cavity using copper–water nanofluid." *International Journal of Thermal Sciences* 47 (2008): 1113–1122.

Asim Umer, Shahid Naveed, Naveed Ramzan. "Selection of a Suitable Method for the Synthesis of Copper Nanoparticles." *NANO: Brief Reports and Reviews* 7, 5 (2012): 1230005 (18 pages).

Awbi, Hazim B. "Calculation of convective heat transfer coefficients of room surfaces for natural convection." *Energy and Building* 28 (1998): 219-227.

B. Raja, D. Mohan Lal, R. Saravanan. "Flow boiling heat transfer coefficient of R-134a/R-290/R-600a mixture in smooth horizontal tubes using varied heat flux method." *Applied Thermal Engineering* 29 (2009): 1778–1785.

B.S.Haynes, D.F.Flectcher. "Subcooled flow boiling heat transfer in narrow passages." *International Journal of Heat and Mass Transfer* 46 (2003): 3673-3682.

Balasubramanian, Satish G. Kandlikar and Prabhu. "An Extension of the Flow Boiling Correlation to Transition, Laminar, and Deep Laminar Flows in

Minichannels and Microchannels." *Heat Transfer Engineering* 25, no. 3 (2010): 86-93.

Bang In Cheol, Chang Soon Heung. "Boiling heat transfer performance and phenomena of Al2O3–water nano-fluids from a plain surface in a pool." *International Journal of Heat and Mass Transfer* 48 (2005): 2407–2419.

Binglu Ruan, Anthony M Jacobi. "Ultrasonication effects on thermal and rheological properties of carbon nanotube suspensions." *Nanoscale Research Letters* 127, no. 7 (2012): 1-14.

C S Jwo, T P Teng, C J Hung, Y T Guo. "Research and development of measurement device for thermal conductivity of nanofluids." *Journal of Physics: Conference Series* 13 (2005): 55–58.

C. Codreanu, R. Gavrila, Ion Morjan. "Experimental Study Concerning the Influence of the Base Fluid Properties on the Thermal Conductivity of Nanofluids." IEEE, 2007. 81-84.

C.A. Nieto de Castro, S.M.S. Murshed, M.J.V. Lourenço, F.J.V. Santos, M.L.M. Lopes, J.M.P. França. "Enhanced thermal conductivity and specific heat capacity of carbon nanotubes ionanofluids." *International Journal of Thermal Sciences* xxx (2012): 1-6.

C.B. Chiou, D.C. Lu, C.Y. Liao, Y.Y. Su. "Experimental study of forced convective boiling for non-azeotropic refrigerant mixtures R-22/R-124 in horizontal smooth tube." *Applied Thermal Engineering* 29 (2009): 1864–1871.

C.J. Ho, L.C. Wei, Z.W. Li. "An experimental investigation of forced convective cooling performance of a microchannel heat sink with Al2O3/water nanofluid." *Applied Thermal Engineering* 30 (2010): 96–103.

C.Y. Tsai, H.T. Chien, P.P. Ding, B. Chan, T.Y. Luh, P.H. Chen. "Effect of structural character of gold nanoparticles in nanofluid on heat pipe thermal performance." *Materials Letters* 58 (2004): 1461– 1465.

Cao, Guangyu. "Indoor air flow prediction by means of CFD." Seminar report, 2006.

Celata G.P., Cumo D.Gallo, A. Mariani, G.Zummo. "A Photographic study of subcooled flow boiling burnout at high heat flux and velocity." *International Journal of Heat and Mass Transfer* 50 (2007): 283-291.

Cherng-Yuan Lin, Jung-Chang Wang, Teng-Chieh Chen. "Analysis of suspension and heat transfer characteristics of Al2O3 nanofluids prepared through ultrasonic vibration." *Applied Energy* 88 (2011): 4527–4533.

Chii-Dong Ho, Jr-Wei Tu, Shih-Cheng Yeh, Jia-Jan Guo. "Heat-transfer efficiency improvement of double-pass concentric circular heat exchangers under uniform wall fluxes." *International Communications in Heat and Mass Transfer* 35 (2008): 828–832.

Ching-Song Jwo, Tun-Ping Teng. "Experimental study on thermal properties of brines containing nanoparticles." *Rev.Adv.Mater.sci.* 10 (2005): 79-83.

Chu Nie, W.H. Marlow, Y.A. Hassan. "Discussion of proposed mechanisms of thermal conductivity enhancement in nanofluids." *International Journal of Heat and Mass Transfer* 51 (2008): 1342–1348.

Chuanhua Duan, Rohit Karnikb, Ming-Chang Lua, Arun Majumdar. "Evaporation-induced cavitation in nanofluidic channels." *PNAS*, n.d.: 1-6.

Clement Kleinstreuer, Yu Feng. "Experimental and theoretical studies of nanofluid thermal conductivity enhancement: a review." *Nanoscale Research Letters* 229, no. 6 (2011): 1-13.

Cong Tam Nguyen, Nicolas Galanis, Guillaume Polidori, Stéphane Fohanno, Catalin V. Popa, Arnaud Le Bechec. "An experimental study of a confined and submerged impinging jet heat transfer using Al2O3-water nanofluid." *International Journal of Thermal Sciences* 48 (2009): 401–411.

D. Ashtiani, M.A. Akhavan-Behabadi, M. Fakoor Pakdaman. "An experimental investigation on heat transfer characteristics of multi-walled CNT-heat transfer oil nanofluid flow inside flattened tubes under uniform wall temperature condition." *International Communications in Heat and Mass Transfer* xxx (2012): xxx–xxx.

D. Tsoukalas, P. Dimitrakis, S. Kolliopoulou, P. Normand. "Recent advances in nanoparticle memories." *Materials Science and Engineering B* 124-125 (2005): 93–101.

D.B.R., Delvalle V.H. and Kenning. "Subcooled flow boiling at high heat flux." *International Journal of Heat Transfer* 28 (1988): 1907-1920.

D.M. Hargreaves, N.G. Wright. "On the use of the k–e model in commercial CFD software to model the neutral atmospheric boundary layer." *Journal of Wind Engineering and Industrial Aerodynamics* 95 (2007): 355–369.

D.V. Kuznetsov, S.P. Bardakhanov, A.V. Nomoev, S.A. Novopashin, V.Z. Lygdenov. "Heat Conductivity of Nanofluids Based on Al2O3, SiO2, and TiO2." *Journal of Engineering Thermophysics* 19 (2010): 138–143.

Devdatta P. Kulkarni, Debendra K. Das, Ravikanth S. Vajjha. "Application of nanofluids in heating buildings and reducing pollution." *Applied Energy* 86 (2009): 2566–2573.

Devdatta P. Kulkarni, Ravikanth S. Vajjha, Debendra K. Das, Daniel Oliva. "Application of aluminum oxide nanofluids in diesel electric generator as jacket water coolant." *Applied Thermal Engineering* 28 (2008): 1774–1781.

Dongsheng Wen, Michael Corr, Xiao Hua, Guiping Lin. "Boiling heat transfer of nanofluids: The effect of heating surface modification." *International Journal of Thermal Sciences* 50 (2011): 480-485.

Dongsheng Wen, Yulong Ding. "Experimental investigation into convective heat transfer of nanofluids at the entrance region under laminar flow conditions." *International Journal of Heat and Mass Transfer* 47 (2004): 5181–5188.

Dongsheng Wen, Yulong Ding. "Natural Convective Heat Transfer of Suspensions of Titanium Dioxide Nanoparticles (Nanofluids)." *IEEE Transactions on Nanotechnology* 5 (2006): 220-227.

Duangthongsuk W, Wongwises S. "Heat transfer enhancement and pressure drop characterstics of TiO2-water nanofluid in adouble-tube counter flow heat exchanger." *International Journal of Heat and Mass Transfer*, 2009: 2059-2067.

Dumbre, A. V. "Augmentation of Heat Transfer by Using Nano-Fluids Using Nano-Fluids." *International Journal of Researchers, Scientists and Developers* 1 (2013): 7-11.

E. Espi, Ph. Berne, P. Duverneuil. "Using CFD to understand the air circulation in a ventilated room." *Computers chsm. Engng* 22 (1998): S751-S754,.

E. Natarajan, R. Sathish. "Role of nanofluids in solar water heater." *Int J Adv Manuf Technol*, 2009.

Eden, Mamut. "Characterization of Heat and Mass Thransfer Properties of Nanofluids." *Romanian Journal of Physics* 51 (2006): 5–12.

Erfeng Chen, Yanzhong Li, Xianghua Cheng. "CFD simulation of upward subcooled boiling flow of refrigerant-113 using the two-fluid model." *Applied Thermal Engineering* (ELSEVIER) 29 (2009): 2508–2517.

Eric Forrest, Erik Williamson, Jacopo Buongiorno, Lin-Wen Hu, Michael Rubner, Robert Cohen. "Augmentation of nucleate boiling heat transfer and critical heat flux using nanoparticle thin-film coatings." *International Journal of Heat and Mass Transfer* 53 (2010): 58–67.

F.M. Hady, F.S. Ibrahim, S.M. Abdel-Gaied, M.R. Eid. "Effect of heat generation/absorption on natural convective boundary-layer flow from a vertical cone embedded in a porous medium filled with a non-Newtonian nanofluid." *International Communications in Heat and Mass Transfer* 38 (2011): 1414–1420.

Frank M, Anderson D, Weeks E.R. "Particle migration in pressure-driven flow of a Brownian suspension." *Journal of Fluid Mechanics* 493 (2003): 363-378.

G. Harish, V. Emlin, V. Sajith. "Effect of surface particle interactions during pool boiling of nanofluids." *International Journal of Thermal Sciences* 50 (2011): 2318-2327.

G. Vinayak Rao, A.R. Balakrishnan. "Heat transfer in nucleate pool boiling of multicomponent mixtures." *Experimental Thermal and Fluid Science* 29 (2004): 87–103.

Georgia A. Pilkington, Wuge H. Briscoe. "Nanofluids mediating surface forces." *Advances in Colloid and Interface Science* 179-182 (2012): 68–84.

Gherhardt Ribatski, Leszek Wojtan, John R. Thome. "An analysis of experimental data and prediction methods for two-phase frictional pressure drop and flow boiling heat transfer in micro-scale channels." *Experimental Thermal and Fluid Science* 31 (2006): 1–19.

Gilles Roy, Iulian Gherasim, François Nadeau, Gérard Poitras, Cong Tam Nguyen. "Heat transfer performance and hydrodynamic behavior of turbulent nanofluid radial flows." *International Journal of Thermal Sciences* 58 (2012): 120-129.

Guangyao Lu, Jing Wang. "Experimental investigation on heat transfer characteristics of water flow in a narrow annulus." *Applied Thermal Engineering* 28 (2008): 8-13.

Gwang Hyeok Seo, Gyoodong Jeun, Sung Joong Kim. "A Review of Wettability Effect on Boiling Heat Transfer Enhancement." Jeju, Korea: Transactions of the Korean Nuclear Society Spring Meeting, 2012.

Gwon Hyun Ko, Kyoungyoon Heo, Kyoungjun Lee, Dae Seong Kim, Chongyoup Kim, Yangsoo Sohn, Mansoo Choi. "An experimental study on the pressure drop of nanofluids containing carbon nanotubes in a horizontal tube." *International Journal of Heat and Mass Transfer* 50 (2007): 4749–4753.

H. Almohammadi, Sh. Nasiri Vatan, E. Esmaeilzadeh, A. Motezaker, A. Nokhosteen. "Experimental Investigation of Convective Heat Transfer and Pressure Drop of Al2O3/Water Nanofluid in Laminar Flow Regime inside a Circular Tube." *International Science Index* 6, no. 8 (2012): 1887-1892.

H.E. Patel, K.B. Anoop, T. Sundararajan, Sarit K.Das. "Model for Thermal Conductivity of CNT-Nanofluids." *Bulletin of Material Science* 31 (2008): 387–390.

Haas, Christoph. Critical Heat Flux for Flow Boiling of Water at Low Pressure on Smooth and Micro-Structured Zircaloy Tube Surfaces. Karlsruhe: KIT Scientific Publishing, 2012.

Hai Trieu Phan, Nadia Caney, Philippe Marty, Stéphane Colasson, Jérôme Gavillet. "Flow boiling of water in a minichannel: The effects of surface wettability on two-phase pressure drop." *Applied Thermal Engineering* 31 (2011): 1894-1905.

Hamid Reza Seyf, Morteza Feizbakhshi. "Computational analysis of nanofluid effects on convective heat transfer enhancement of micro-pin-fin heat sinks." *International Journal of Thermal Sciences* 58 (2012): 168-179.

Hao Peng, Guoliang Ding, Haitao Hua. "Effect of surfactant additives on nucleate pool boiling heat transfer of refrigerant-based nanofluid." *Experimental Thermal and Fluid Science* 35 (2011): 960–970.

Hao Peng, Guoliang Ding, Weiting Jiang, Haitao Hu, Yifeng Gao. "Heat transfer characteristics of refrigerant-based nanofluid flow boiling inside a horizontal smooth tube." *International Journal of refrigeration* 32 (2009): 1259–1270.

Hartmut Presting, Ulf Konig. "Future nanotechnology developments for automotive applications." *Materials Science and Engineering C* 23 (2003): 737–741.

Heris, Saeed Zeinali. "Experimental investigation of pool boiling characteristics of low-concentrated CuO/ethylene glycol–water nanofluids." *International Communications in Heat and Mass Transfer* 38 (2011): 1470–1473.

Hone, J. "Carbon Nanotubes: Thermal Properties." *Dekker Encyclopedia of Nanoscience and Nanotechnology* (Dekker Encyclopedia of Nanoscience and Nanotechnology), 2004: 603-610.

Hoo-Kyu Oh, Chang-Hyo Son. "Flow boiling heat transfer and pressure drop characteristics of CO2 in horizontal tube of 4.57-mm inner diameter." *Applied Thermal Engineering* 31 (2011): 163-172.

Huaqiang Chu, Boming Yu. "A new comprehensive model for nucleate pool boiling heat transfer of pure liquid at low to high heat fluxes including CHF." *International Journal of Heat and Mass Transfer* 52 (2009): 4203–4210.

Huaqing Xie, Wei Yu, Yang Li, Lifei Chen. "Discussion on the thermal conductivity enhancement of nanofluids." *Nanoscale Research Letters* 124 (2011): 6.

Hyungdae Kim, Jeongbae Kim, Moohwan Kim. "Experimental Study of CHF Characteristics on CHF Characteristics of Water-TiO2 Nanofluids." *Nuclear Engineering and Technology* 38, no. 1 (2006): 61-68.

I. Mohammed Sadiq, Basudev Chowdhury, Natarajan Chandrasekaran, Amitava Mukherjee. "Antimicrobial sensitivity of Escherichia coli to alumina nanoparticles." *Nanomedicine: Nanotechnology, Biology, and Medicine* xx (2009): xxx–xxx.

Ibrahim Palabiyik, Zenfira Musina, Sanjeeva Witharana, Yulong Ding. "Dispersion Stability and Thermal Conductivity of Propylene Glycol Based Nanofluids." n.d.

In Cheol Bang, Soon Heung Chang. "Boiling heat transfer performance and phenomena of Al2O3–water nano-fluids from a plain surface in a pool." *International Journal of Heat and Mass Transfer* 48 (2005): 2407–2419.

Incropera, F.P., DeWitt, D.P. *Fundamentals of Heat and Mass Transfer*. 3rd. New York: Wiley, 1990.

J. Darabi, M.M. Ohadi, M.A. Fanni, S.V. Dessiatoun, M. A. Kedzierski. "Effect of Heating Boundary Conditions on Pool Boiling Experiments." *HVAC&R RESEARCH*, 1999: 1-14.

J.M. Horan, D.P. Finn. "CFD reliability issues in analysis of naturally ventilated buildings." *International Conference "Passive and Low Energy Cooling for the Built Environment", .* Greece, 2005. 53-58.

J.R.Thome, L. Wojtan, T. Ursenbacher. "Investigation of flow boiling in horizontal tubes: part II – development of a new heat transfer model for stratified-

wavy, dryout and mist flow regimes." *Int. J. Heat Mass Transfer* 48 (2005): 2970–2985.

J.Y.Tu. "The influence of bubble size on void fraction distribution in subcooled flow boiling at low pressure." *Int. Comm. Heat Mass Transfer* 26 (1999): 607-616.

Jacqueline B. Copetti, Mario H. Macagnan, Flávia Zinani, Nicole L.F. Kunsler. "Flow boiling heat transfer and pressure drop of R-134a in a mini tube: an experimental investigation." *Experimental Thermal and Fluid Science* 35 (2011): 636–644.

Jaeseon Lee, Issam Mudawar. "Critical heat flux for subcooled flow boiling in micro-channel heat sinks." *International Journal of Heat and Mass Transfer* 52 (2009): 3341–3352.

Janusz T Cieslinski, Tomasz Z Kaczmarczyk. "Pool boiling of water-Al2O3 and water-Cu nanofluids on horizontal smooth tubes." *Nanoscale Research Letters* 6:220 (2011): 1-9.

Ji-Hwan Lee, Kyo Sik Hwang, Seok Pil Jang, Byeong Ho Lee, Jun Ho Kim, Stephen U.S. Choi, Chul Jin Choi. "Effective viscosities and thermal conductivities of aqueous nanofluids containing low volume concentrations of Al2O3 nanoparticles." *International Journal of Heat and Mass Transfer* 51 (2008): 2651–2656.

Jin Xie, Sheng Peng, Nathan Brower, Nader Pourmand, Shan X.Wang and Shouheng Sun. "One-pot synthesis of monodisperse iron oxide nanoparticles for potential biomedical applications." *Pure Appl. Chem.* 78 (2006): 1003–1014.

Jing Fan, Liqiu Wang. "Constructal design of nanofluids." *International Journal of Heat and Mass Transfer* 53 (2010): 4238–4247.

Jing Fan, Liqiu Wang. "Heat conduction in nanofluids: Structure–property correlation." *International Journal of Heat and Mass Transfer* 54 (2011): 4349–4359.

John H. Lienhard IV, John H. Lienhard V. *A Heat Transfer Textbook.* Cambridge, Massachusetts, U.S.A.: Phlogiston Press, 2005.

John R. Thome, Gherhardt Ribatski. "State-of-the-art of two-phase flow and flow boiling heat transfer and pressure drop of CO2 in macro- and micro-channels." *International Journal of Refrigeration* 28 (2005): 1149–1168.

Johnathan S. Coursey, Jungho Kim. "Nanofluid boiling: The effect of surface wettability." *International Journal of Heat and Fluid Flow* 29 (2008): 1577–1585.

Jonathan A. Olivier, Jackson B. Marcinichen, Arnaud Bruch, John Thome. "Green Cooling of High Performance Microprocessors: Parametric Study Between Flow Boiling and Water Cooling." *Journal of Thermal Science and Engineering Applications* 3 (2011): 041003-1-12.

Jong Hyuk Lee, Taeseung Lee, Yong Hoon Jeong. "Experimental study on the pool boiling CHF enhancement using magnetite-water nanofluids." *International Journal of Heat and Mass Transfer* 55 (2012): 2656–2663.

Jongwoo Lim, Kedar Hippalgaonkar, Sean C. Andrews, Arun Majumdar, and Peidong Yang. "Quantifying Surface Roughness Effects on Phonon Transport in Silicon Nanowires." *Nano Letters* 12 (2012): 2475−2482.

Juan Abanto, Daniel Barrero, Marcelo Reggio, Benoit Ozell. "Air flow modelling in a computer room." *Building and Environment* 39 (2004): 1393 – 1402.

Jungho Kim, John F. Benton, Derek Wisniewski. "Pool boiling heat transfer on small heaters: effect of gravity and subcooling." *International Journal of Heat and Mass Transfer* 45 (2002): 3919–3932.

K. Balasubramanian, P.S. Lee, C.J. Teo, S.K. Chou. "Flow boiling heat transfer and pressure drop in stepped fin microchannels." *International Journal of Heat and Mass Transfer* 67 (2013): 234–252.

K. Balasubramanian, P.S. Lee, L.W. Jin, S.K. Chou, C.J. Teo, S. Gao. "Experimental investigations of flow boiling heat transfer and pressure drop in straight and expanding microchannels e A comparative study." *International Journal of Thermal Sciences* 50 (2011): 2413-2421.

K. Visagavel, P.S.S. Srinivasan. "Analysis of single side ventilated and cross ventilated rooms by varying the width of the window opening using CFD." *Solar Energy* 83 (2009): 2–5.

K.B. Anoop, T. Sundararajan, Sarit K. Das. "Effect of particle size on the convective heat transfer in nanofluid in the developing region." *International Journal of Heat and Mass Transfer* 52 (2009): 2189–2195.

K.V. Sharma, L. Syam Sundar, P.K. Sarma. "Estimation of heat transfer coefficient and friction factor in the transition flow with low volume concentration of Al2O3 nanofluid flowing in a circular tube and with twisted tape insert." *International Communications in Heat and Mass Transfer* 36 (2009): 503–507.

Kandlikar, S. G. "Critical Heat Flux in Subcooled Flow Boiling an Assesment of current understanding and Future irections for Research." *Multiphase Science and Technology* 13, no. 3 (2001): 207-232.

Kandlikar, S.G. "A General Correlation for Saturated Two-Phase Flow Boiling Heat Transfer Inside Horizontal and Vertical Tubes." *Journal of Heat Transfer* 112 (1990): 219-228.

Kandlikar, Satish G. "Heat Transfer Mechanisms During Flow Boiling in Microchannels." *Transactions of the ASME* 126 (2004): 8-16.

Kedzierski, Mark A. "Effect of CuO Nanoparticle Concentration on R134A/Lubricant Pool Boiling Heat Transfer." *Micro/Nanoscale Heat Transfer International Conference.* Tainan, Taiwan: Proceedings of MNHT2008, 2008. 1-8.

Khwanchit Wongcharee, Smith Eiamsa-ard. "Enhancement of heat transfer using CuO/water nanofluid and twisted tape with alternate axis." *International Communications in Heat and Mass Transfer* 38 (2011): 742–748.

Khwanchit Wongcharee, Smith Eiamsa-ard. "Heat transfer enhancement by using CuO/water nanofluid in corrugated tube equipped with twisted tape." *International Communications in Heat and Mass Transfer* 39 (2012): 251–257.

Ki-Jung Park, Dongsoo Jung. "Boiling heat transfer enhancement with carbon nanotubes for refrigerants used in building air-conditioning." *Energy and Buildings* 39 (2007): 1061–1064.

Ki-Jung Park, Dongsoo Jung. "Enhancement of nucleate boiling heat transfer using carbon nanotubes." *International Journal of Heat and Mass Transfer* 50 (2007): 4499–4502.

Ki-Jung Park, Dongsoo Jung, Sang Eun Shim. "Nucleate boiling heat transfer in aqueous solutions with carbon nanotubes up to critical heat fluxes." *International Journal of Multiphase Flow* 35 (2009): 525–532.

Kim SJ, Bang IC, Buongiorno J, Hu LW. "Effects of nanoparticle deposition on surface wettability influencing boiling heat transfer in nanofluids." *Applied Physics Letters* 89, no. 15 (2006): 153107-1-3.

Kim, Hyungdae. "Enhancement of critical heat flux in nucleate boiling of nanofluids: a state-of-art review." *Nanoscale Research Letters* 6:145 (2011): 1-18.

Kiyuel Kwak, Chongyoup Kim. "Viscosity and thermal conductivity of copper oxide nanofluid dispersed in ethylene glycol." *Korea-Australia Rheology Journal* 17, no. 2 (2005): 35-40.

Klausner J.F. "Bubble forces and detachment models." Boiling 2000: Phenomena and Emerging Applications. Keynote Lecture. 2000.

Konstantinos Ritos, Yiannis Lihnaropoulos , Stergios Naris & Dimitris Valougeorgis. "Pressure and Temperature-Driven Flow Through Triangular and Trapezoidal Microchannels." *Heat Transfer Engineering* 32 (2011): 1101-1107,.

Kristen Henderson, Young-Gil Park, Liping Liu, Anthony M. Jacobi. "Flow-boiling heat transfer of R-134a-based nanofluids in a horizontal tube." *International Journal of Heat and Mass Transfer* 53 (2010): 944–951.

Kyo Sik Hwang, Ji-Hwan Lee, Seok Pil Jang. "Buoyancy-driven heat transfer of water-based Al2O3 nanofluids in a rectangular cavity." *International Journal of Heat and Mass Transfer* 50 (2007): 4003–4010.

L. Syam Sundar, K.V. Sharma. "Heat transfer enhancements of low volume concentration Al2O3 nanofluid and with longitudinal strip inserts in a circular tube." *International Journal of Heat and Mass Transfer* 53 (2010): 4280–4286.

L. Syam Sundar, M.T. Naik, K.V. Sharma, M.K. Singh, T.Ch. Siva Reddy. "Experimental investigation of forced convection heat transfer and friction factor in a tube with Fe3O4 magnetic nanofluid." *Experimental Thermal and Fluid Science* 37 (2012): 65–71.

L. Syam Sundar, N.T. Ravi Kumar, M.T. Naik, K.V. Sharma. "Effect of full length twisted tape inserts on heat transfer and friction factor enhancement with Fe3O4 magnetic nanofluid inside a plain tube: An experimental study." *International Journal of Heat and Mass Transfer* 55 (2012): 2761–2768.

L. Vasiliev, E. Hleb, A. Shnip, D. Lapotko. "Bubble generation in micro-volumes of ‘‘nanofluids”." *International Journal of Heat and Mass Transfer* 52 (2009): 1534–1539.

Liang Zhang, Liwu Fan, Zitao Yu, Kefa Cen. "An experimental investigation of transient pool boiling of aqueous nanofluids with graphene oxide nanosheets as characterized by the quenching method." *International Journal of Heat and Mass Transfer* 73 (2014): 410–414.

Lixin Cheng, Lei Liu. "Boiling and two-phase flow phenomena of refrigerant-based nanofluids: Fundamentals, applications and challenges." *international journal of refrigeration* 36 (2013): 421-446.

M, Zeitoun O and Shoukri. "Bubble behaviour and mean diameter in subcooled flow boiling." *Transaction of ASME Journal of Heat Transfer* 26 (1996): 110-116.

M. Chandrasekar, S. Suresh, A. Chandra Bose. "Experimental investigations and theoretical determination of thermal conductivity and viscosity of Al2O3/water nanofluid." *Experimental Thermal and Fluid Science* 34 (2010): 210–216.

M. Chandrasekar, S. Suresh, A. Chandra Bose. "Experimental studies on heat transfer and friction factor characteristics of Al2O3/water nanofluid in a circular

pipe under laminar flow with wire coil inserts." *Experimental Thermal and Fluid Science* 34 (2010): 122–130.

M. Fakoor Pakdaman, M.A. Akhavan-Behabadi, P. Razi. "An experimental investigation on thermo-physical properties and overall performance of MWCNT/heat transfer oil nanofluid flow inside vertical helically coiled tubes." *Experimental Thermal and Fluid Science* 40 (2012): 103–111.

M. Kostic, Kalyan C.Simham. "Computerized, Transient Hot-Wire Thermal Conductivity (HWTC) Apparatus for Nanofluids." *6th WSEAS International Conference on HEAT and MASS TRANSFER*. 2009. 71-78.

M. Misale, G. Guglielmini, A. Priarone. "HFE-7100 pool boiling heat transfer and critical heat flux in inclined narrow spaces." *International Journal of Refrigeration* 32 (2009): 235-245.

M. Nasiri, S.Gh. Etemad, R. Bagheri. "Experimental heat transfer of nanofluid through an annular duct." *International Communications in Heat and Mass Transfer* 38 (2011): 958–963.

M. Raja, R. Vijayan, S. Suresh, R Vivekananthan. "Effect of heat transfer enhencement and NOx emission using Al2O3/Water nanofluid as coolent in CI engine." *Indian Journal of Engineering & Materials Science* 20 (2013): 443-449.

M. Saeedinia, M.A. Akhavan-Behabadi, M. Nasr. "Experimental study on heat transfer and pressure drop of nanofluid flow in a horizontal coiled wire inserted tube under constant heat flux." *Experimental Thermal and Fluid Science* 36 (2012): 158–168.

M., Bibeau E.L and Salcudean. "Experimental investigation of subcooled void growth for upward and downward flow at low velocities and low pressure." *Experimental Heat Transfer, Fluid Mechanics and Thermodynamics*, 1991.

M.A. Akhavan-Behabadi, M. Fakoor Pakdaman, M. Ghazvini. "Experimental investigation on the convective heat transfer of nanofluid flow inside vertical helically coiled tubes under uniform wall temperature condition." *International Communications in Heat and Mass Transfer* 39 (2012): 556–564.

M.A.Kedzierski. "Effect of CuO nanoparticle concentration on R134A/lubricant pool boiling heat transfer." *Micro/Nanoscale Heat Transfer International Conference.* Tainan, 2008.

M.H. Kayhani, H. Soltanzadeh, M.M. Heyhat, M. Nazari, F. Kowsary. "Experimental study of convective heat transfer and pressure drop of TiO2/water nanofluid." *International Communications in Heat and Mass Transfer* 39 (2012): 456–462.

M.M. Sarafraz, F. Hormozi. "Convective boiling and particulate fouling of stabilized CuO-ethylene Convective boiling and particulate fouling of stabilized CuO-ethylene." *International Communications in Heat and Mass Transfer* 53 (2014): 116–123.

M.R. Khosravi Nikou, M.R. Ehsani. "Turbulence models application on CFD simulation of hydrodynamics, heat and mass transfer in a structured packing." *International Communications in Heat and Mass Transfer* 35 (2008): 1211–1219.

M.S. Dresselhaus, G. Dresselhaus, J C. Charlier. "Electronic, thermal and mechanical properties of carbon nanotubes." *Phil. Trans. R. Soc. Lond. A* 362 (2004): 2065–2098.

Majid Emami Meibodi, Mohsen Vafaie-Sefti, Ali Morad Rashidi, Azadeh Amrollahi, Mohsen Tabasi, Hossein Sid Kalal. "Simple model for thermal conductivity of nanofluids using resistance model approach." *International Communications in Heat and Mass Transfer* 37 (2010): 555–559.

Majid Moosavi, Elaheh K. Goharshadi, Abbas Youssefi. "Fabrication, characterization, and measurement of some physicochemical properties of ZnO nanofluids." *International Journal of Heat and Fluid Flow* 31 (2010): 599–605.

Mamalis, A.G. "Recent advances in nanotechnology." *Journal of Materials Processing Technology* 181 (2007): 52–58.

Manoj Chopkar, Prasanta K. Dasb, Indranil Mannaa. "Synthesis and characterization of nanofluid for advanced heat transfer applications." *Scripta Materialia* 55 (2006): 549–552.

Maurus R., Ilchenko V., Sattelmayer T. "Study of the bubble characteristics and the local void fraction in subcooled flow boiling using digital imaging and analyzing techniques." *Experimental Thermal and Fluid Science* 26 (2002): 147-155.

Milnes P. David, Josef Miler, Julie E. Steinbrenner, Yizhang Yang, Maxat Touzelbaev, Kenneth E. Goodson. "Hydraulic and thermal characteristics of a vapor venting two-phase microchannel heat exchanger." *International Journal of Heat and Mass Transfer* 54 (2011): 5504–5516.

Mina Shahi, Amir Houshang Mahmoudi, Abbas Honarbakhsh Raouf. "Entropy generation due to natural convection cooling of a nanofluid." *International Communications in Heat and Mass Transfer* 38 (2011): 972–983.

Ming-Chang Lu Renkun Chen, Vinod Srinivasan, Van P. Carey, Arun Majumdar. "Critical heat flux of pool boiling on Si nanowire array-coated surfaces." *International Journal of Heat and Mass Transfer* 54 (2011): 5359–5367.

Min-Sheng Liu, Mark Ching-Cheng Lin, I-Te Huang, Chi-Chuan Wang. "Enhancement of thermal conductivity with carbon nanotube for nanofluids." *International Communications in Heat and Mass Transfer* 32 (2005): 1202–1210.

Mohammad Kalteh, Abbas Abbassi, Majid Saffar-Avval, Jens Harting. "Eulerian–Eulerian two-phase numerical simulation of nanofluid laminar forced convection in a microchannel." *International Journal of Heat and Fluid Flow* 32 (2011): 107–116.

Mousa, M.G. "Effect of nanofluid concentration on the performance of circular heat pipe." *Ain Shams Engineering Journal* xxx (2011): xxx-xxx.

N., Zuber. *Hydrodynamic Aspects of Boiling Heat Transfer*. AEC Report No. AECU-4459, Physics and Methamatics, 1959.

N.B. Kaye, Y. Ji, M.J. Cook. "Numerical simulation of transient flow development in a naturally ventilated room." *Building and Environment* 44 (2009): 889–897.

Nor Azizah Yacob, Anuar Ishak, Roslinda Nazar, Ioan Pop. "Falkner–Skan problem for a static and moving wedge with prescribed surface heat flux in a nanofluid." *International Communications in Heat and Mass Transfer* 38 (2011): 149–153.

Norfifah Bachok, Anuar Ishak, Ioan Pop. "Flow andheattransferoverarotatingporousdiskinananofluid." *Physica B406* 406 (2011): 1767–1772.

O. Ahmed, M.S. Hamed. "Experimental investigation of the effect of particle deposition on pool boiling of nanofluids." *International Journal of Heat and Mass Transfer* 55 (2012): 3423–3436.

O.S. Prajapati, A.K. Rajvanshi. "Effect of Pressure on Subcooled Flow Boiling of TiO2-Water Nanofluids." Lausanne, Switzerland: Ecole Polytechnique Fédérale de Lausanne, 2012.

Olivier Zürcher, John R. Thome, Daniel Favrat. "An onset of nucleate boiling criterion for horizontal flow boiling." *Int. J. Therm. Sci.* 39 (2000): 909–918.

Om Shankar Prajapati, Dr. A.K. Rajvanshi. "Al2O3-Water Nanofluids in Convective Heat Transfer." *Applied Mechanics and Materials* 110-116 (2012): 3667-3672.

Ooi Yongsona, Irfan Anjum Badruddina, Z.A. Zainala, P.A. Aswatha Narayana. "Airflow analysis in an air conditioning room." *Building and Environment* 42 (2007): 1531–1537.

P. Rana, R. Bhargava. "Flow and heat transfer of a nanofluid over a nonlinearly stretching sheet: A numerical study." *Commun Nonlinear Sci Numer Simulat* 17 (2012): 212–226.

P. Rohdin, B. Moshfegh. "Numerical predictions of indoor climate in large industrial premises. A comparison between different k–e models supported by field measurements." *Building and Environment* 42 (2007): 3872–3882.

P. Selvakumar, S. Suresh. "Convective performance of CuO/water nanofluid in an electronic heat sink." *Experimental Thermal and Fluid Science* 40 (2012): 57–63.

Paritosh Garg, Jorge L. Alvarado, Charles Marsh, Thomas A. Carlson, David A. Kessler, Kalyan Annamalai. "An experimental study on the effect of ultrasonication on viscosity and heat transfer performance of multi-wall carbon nanotube-based aqueous nanofluids." *International Journal of Heat and Mass Transfer* 52 (2009): 5090–5101.

Patricia E. Gharagozloo, John K. Eaton, Kenneth E. Goodson. "Diffusion, aggregation, and the thermal conductivity of nanofluids." *APPLIED PHYSICS LETTERS* 93 (2008): 103-110.

Peter Vassallo, Ranganathan Kuma, Stephen D'Amico. "Pool boiling heat transfer experiments in silica–water nano-fluids." *International Journal of Heat and Mass Transfer* 47 (2004): 407–411.

Ping-Yang Wang, Xiu-Juan Chen, Zhen-Hua Liu, Yi-Peng Liu. "Application of nanofluid in an inclined mesh wicked heat pipes." *Thermochimica Acta* 539 (2012): 100-108.

Pooyan Razi, M.A. Akhavan-Behabadi, M. Saeedinia. "Pressure drop and thermal characteristics of CuO–base oil nanofluid laminar flow in flattened tubes under constant heat flux." *International Communications in Heat and Mass Transfer* 38 (2011): 964–971.

Prajapati O.S., A.K. Rajvanshi. "Effect of Al2O3-Water Nanofluids in Convective Heat Transfer." *International Journal of Nanoscience* 11 (No. 3 (2012)): 1240005 (4 pages).

Prodanovic V., Fraser. D and Salcudean.M. "Bubble behaviour in subcooled flow boiling of water at low pressures and low flow rates." *International Journal of Multiphase Flow* 28 (2002): 1-19.

R. Ben Mansour, N. Galanis, C.T. Nguyen. "Experimental study of mixed convection with watereAl2O3 nanofluid in inclined tube with uniform wall heat flux." *International Journal of Thermal Sciences* 50 (2011): 403-410.

R. Mastrullo, A.W. Mauro, J.R. Thome, D. Toto, G.P. Vanoli. "Flow pattern maps for convective boiling of CO2 and R410A in a horizontal smooth tube:

Experiments and new correlations analyzing the effect of the reduced pressure." *International Journal of Heat and Mass Transfer* 55 (2012): 1519–1528.

R. Maurus, V. Ilchenko, T. Sattelmayer. "Study of the bubble characteristics and the local void fraction in subcooled flow boiling using digital imaging and analysing techniques." *Experimental Thermal and Fluid Science* 26 (2002): 147–155.

Rafael C. Gonzalez, Richard E. Woods. *Digital Image Processing*. second. Tom Robbins, 2002.

Ramin Hajian, Mohammad Layeghi, Kamal Abbaspour Sani. "Experimental study of nanofluid effects on the thermal performance with response time of heat pipe." *Energy Conversion and Management* 56 (2012): 63–68.

Ravikanth S. Vajjha, Debendra K. Das. "Experimental determination of thermal conductivity of three nanofluids and development of new correlations." *International Journal of Heat and Mass Transfer* 52 (2009): 4675–4682.

Reiyu Chein, Jason Chuang. "Experimental microchannel heat sink performance studies using nanofluids." *International Journal of Thermal Sciences* 46 (2007): 57–66.

Robert A. Taylor, Patrick E. Phelan. "Pool boiling of nanofluids: Comprehensive review of existing data and limited new data." *International Journal of Heat and Mass Transfer* 52 (2009): 5339–5347.

Roghayeh Lotfi, Ali Morad Rashidi, Azadeh Amrollahi. "Experimental study on the heat transfer enhancement of MWNT-water nanofluid in a shell and tube heat exchanger." *International Communications in Heat and Mass Transfer* 39 (2012): 108–111.

Russel, W. B. "Brownian Motion of Small Particles Suspended in Liquids." *Anrt Rev. Fluid Mectt* 13 (1981): 425-55.

S. Marre, Y. Roig, C. Aymonier. "Supercritical microfluidics: Opportunities in flow-through chemistry and materials science." *Journal of Supercritical Fluids* 66 (2012): 251– 264.

S. Mirmasoumi, A. Behzadmehr. "Effect of nanoparticles mean diameter on mixed convection heat transfer of a nanofluid in a horizontal tube." *International Journal of Heat and Fluid Flow* 29 (2008): 557–566.

S. Soltani, S. Gh. Etemad, J. Thibault. "Pool boiling heat transfer of non-Newtonian nanofluids." *International Communications in Heat and Mass Transfer* 37 (2010): 29–33.

S. Suresh, K.P. Venkitaraj, P. Selvakumar, M. Chandrasekar. "Effect of Al2O3–Cu/water hybrid nanofluid in heat transfer." *Experimental Thermal and Fluid Science* 38 (2012): 54–60.

S. Suresh, M. Chandrasekar, S. Chandra Sekhar. "Experimental studies on heat transfer and friction factor characteristics of CuO/water nanofluid under turbulent flow in a helically dimpled tube." *Experimental Thermal and Fluid Science* 35 (2011): 542–549.

S. Suresh, P. Selvakumar, M. Chandrasekab, V. Srinivasa Raman. "Experimental studies on heat transfer and friction factor characteristics of Al2O3/water nanofluid under turbulent flow with spiraled rod inserts." *Chemical Engineering and Processing* 53 (2012): 24– 30.

S. Zeinali Heris, M. Nasr Esfahany, S.Gh. Etemad. "Experimental investigation of convective heat transfer of Al2O3/water nanofluid in circular tube." *International Journal of Heat and Fluid Flow* 28 (2007): 203–210.

S. Zeinali Heris, S.Gh. Etemad, M. Nasr Esfahany. "Experimental investigation of oxide nanofluids laminar flow convective heat transfer." *International Communications in Heat and Mass Transfer* 33 (2006): 529–535.

S.G.Kandlikar. "Critical Heat Flux in subcooled flow boiling – An assessment of current understanding and future direction for research." *Multiphase Science and Technology* 13 (2001): 207-232.

S.G.Kandlikar. "Heat tranfer characteristics in partial boiling, fully devloped boiling, and significant void flow regions of subcooled flow boiling." *Journal of heat transfer* 120 (1998): 395-401.

S.H. Noie, S. Zeinali Heris, M. Kahani, S.M. Nowee. "Heat transfer enhancement using Al2O3/water nanofluid in a two-phase closed thermosyphon." *International Journal of Heat and Fluid Flow* 30 (2009): 700–705.

S.M. Aminossadati, B. Ghasemi. "Enhanced natural convection in an isosceles triangular enclosure filled with a nanofluid." *Computers and Mathematics with Applications* 61 (2011): 1739–1753.

S.M. Fotukian, M. Nasr Esfahany. "Experimental investigation of turbulent convective heat transfer of dilute c-Al2O3/water nanofluid inside a circular tube." *International Journal of Heat and Fluid Flow* 31 (2010): 606–612.

S.M. Fotukian, M. Nasr Esfahany. "Experimental study of turbulent convective heat transfer and pressure drop of dilute CuO/water nanofluid inside a circular tube." *International Communications in Heat and Mass Transfer* 37 (2010): 214–219.

S.M. Hashemi, M.A. Akhavan-Behabadi. "An empirical study on heat transfer and pressure drop characteristics of CuO–base oil nanofluid flow in a horizontal helically coiled tube under constant heat flux." *International Communications in Heat and Mass Transfer* 39 (2012): 144–151.

S.M. Sohel Murshed, C.A. Nieto de Castro. "Contribution of Brownian Motion in Thermal Conductivity of Nanofluids." *Proceedings of the World Congress on Engineering 2011 Vol III.* London, U.K., 2011.

S.M. Sohel Murshed, Keon Vereen, Darton Strayer, Ranganathan Kumar. "An experimental investigation of bubble nucleation of a refrigerant in pressurized boiling flows." *Energy* 35 (2010): 5143-5150.

S.U.S.Choi. "Nanofluid technology: Current status and future research." sponsored work report by an agency of the United States Government, Argonne, 1999.

S.U.S.Choi. "Nanofluids: From Vision to Reality Through Research." *Journal of Heat Transfer* 131 (2009): 1-9.

Sadik Kakaç, Anchasa Pramuanjaroenkij. "Review of convective heat transfer enhancement with nanofluids." *International Journal of Heat and Mass Transfer* 52 (2009): 3187–3196.

Saeid Vafaei, Dongsheng Wen. "Flow boiling heat transfer of alumina nanofluids in single microchannels and the roles of nanoparticles." *J Nanopart Res* 13 (2011): 1063–1073.

Saide Soltani, Seyed Gholamreza Etemad, Jules Thibault. "Pool boiling heat transfer performance of Newtonian nanofluids." *Heat Mass Transfer* 45 (2009): 1555–1560.

Salma Parvin, M.A. Alim, N.F. Hossain. "Prandtl number effect on cooling performance of a heated cylinder in an enclosure filled with nanofluid." *International Communications in Heat and Mass Transfer*, 2012.

Sang M. Kwark, Ratan Kumar, Gilberto Moreno, Jaisuk Yoo, Seung M. You. "Pool boiling characteristics of low concentration nanofluids." *International Journal of Heat and Mass Transfer* 53 (2010): 972–981.

Sanjeeva Witharana, Haisheng Chen, Yulong Ding. "Stability of nanofluids in quiescent and shear flow fields." *Nanoscale Research Letters* 231, no. 6 (2011): 1-6.

Sarit K. Das, G. Prakash Narayan, Anoop K. Baby. "Survey on nucleate pool boiling of nanofluids: the effect of particle size relative to roughness." *J Nanopart Res* 10 (2008): 1099–1108.

Sarit K. Das, Nandy Putra, Wilfried Roetze. "Pool boiling characteristics of nano-fluids." *International Journal of Heat and Mass Transfer* 46 (2003): 851–862.

Sarit K. Das, Nandy Putra, Wilfried Roetzel. "Pool boiling of nano-fluids on horizontal narrow tubes." *International Journal of Multiphase Flow* 29 (2003): 1237–1247.

Sarit K. Das, Stephen U. S. Choi, Wenhua Yu, T. Pradeep. *Nanofluids: Science and Technology*. United States of America: A JOHN WILEY & SONS, INC., PUBLICATION, 2010.

Sarit Kumar Das, Stephen U.S. Choi, Hrishikesh E. Patel. "Heat Transfer in Nanofluids-A Review." *Heat Transfer Engineering* 27, no. 10 (2006): 3–19.

Satish G Kandlikar, Mark E Steinke. "Predicting heat transfer during flow boiling in minichannels and microchannel." *ProQuest Science Journals* 109 (2003): 667-676.

Sattelmayer, Maurus Reinhold and Thomas. "Bubble and boundary layer behaviour in subcooled flow boiling." *International Journal of Thermal Sciences* 45 (2006): 257-268.

Seok Pil Jang, Kyo Sik Hwang, Ji-Hwan Lee, Jun Ho Kim, Byeong Ho Lee, Stephen U.S. Choi. "Effective Thermal Conductivities and Viscosities of Water-based Nanofluids Containing Al2O3 with Low Concentration." *International Conference on Nanotechnology*. Hong Kong: Proceedings of the 7th IEEE, 2007.

Seok Pil Jang, Stephen U. S. Choi. "Effects of Various Parameters on Nanofluid Thermal Conductivity." *Journal of Heat Transfer* 129 (2007): 617-623.

Seyyed Abdolreza Fazeli, Seyyed Mohammad Hosseini Hashemi, Hootan Zirakzadeh, Mehdi Ashjaee. "Experimental and numerical investigation of heat transfer in a miniature heat sink utilizing silica nanofluid." *Superlattices and Microstructures* 51 (2012): 247–264.

Seyyed Mohammad Hosseini Hashemi, Seyyed Abdolreza Fazeli, Hootan Zirakzadeh, Mehdi Ashjaee. "Study of heat transfer enhancement in a nanofluid-cooled miniature heat sink." *International Communications in Heat and Mass Transfer* 39 (2012): 877–884.

Sh. Allahyari, A. Behzadmehr, S.M. Hosseini Sarvari. "Conjugate heat transfer of laminar mixed convection of a nanofluid through a horizontal tube with circumferentially non-uniform heating." *International Journal of Thermal Sciences* 50 (2011): 1963-1972.

Shailesh Kumar, Santosh Kumar Prasad, Jyotirmay Banerjee. "Analysis of flow and thermal field in nanofluid using a single phase thermal dispersion model." *Applied Mathematical Modelling* 34 (2010): 573–592.

Sheng-shan Bi, Lin Shi, Li-li Zhang. "Application of nanoparticles in domestic refrigerators." *Applied Thermal Engineering* 28 (2008): 1834–1843.

Shive Dayal Pandey, V.K. Nema. "Experimental analysis of heat transfer and friction factor of nanofluid as a coolant in a corrugated plate heat exchanger." *Experimental Thermal and Fluid Science* 38 (2012): 248–256.

Sidi El Becaye Maiga, Samy Joseph Palm, Cong Tam Nguyen, Gilles Roy, Nicolas Galanis. "Heat transfer enhancement by using nanofluids in forced convection flows." *International Journal of Heat and Fluid Flow* 26 (2005): 530–546.

Sodja, Jurij. "Turbulence models in CFD." Ljubljana, 2007.

Sourav Mitra, Sandip K. Saha, Subhrakanti Chakraborty, Sumitesh Das. "Study on boiling heat transfer of water-TiO2 and water-MWCNT nanofluids based laminar jet impingement on heated steel surface." *Applied Thermal Engineering* 37 (2012): 353-359.

Stefan S. Bertsch, Eckhard A. Groll, Suresh V. Garimella. "Effects of heat flux, mass flux, vapor quality, and saturation temperature on flow boiling heat transfer in microchannels." *International Journal of Multiphase Flow* 35 (2009): 142–154.

Sung Joong Kim, Tom McKrell, Jacopo Buongiorno, Lin-Wen Hu. "Experimental Study of Flow Critical Heat Flux in Alumina-Water, Zinc-Oxide-Water, and Diamond-Water Nanofluids." *Journal of Heat Transfer* 131 (2009): 1-7.

Sung Joong Kim, Tom McKrell, Jacopo Buongiorno, Lin-wen Hu. "Subcooled flow boiling heat transfer of dilute alumina, zinc oxide, and diamond nanofluids at atmospheric pressure." *Nuclear Engineering and Design* 240 (2010): 1186–1194.

Suvankar Ganguly, Sudipta Sikdar, Somnath Basu. "Experimental investigation of the effective electrical conductivity of aluminum oxide nanofluids." *Powder Technology* 196 (2009): 326–330.

Tae Il Kim, Yong Hoon Jeong, Soon Heung Chang. "An experimental study on CHF enhancement in flow boiling using Al2O3 nano-fluid." *International Journal of Heat and Mass Transfer* 53 (2010): 1015–1022.

Tae-Keun Hong, Ho-Soon Yang. "Nanoparticle-Dispersion-Dependent Thermal Conductivity in Nanofluids." *Journal of the Korean Physical Society* 47 (2005): S321-S324.

Tae-Keun Hong, Ho-Soon Yang. "Study of the enhanced thermal conductivity of Fe nanofluids." *JOURNAL OF APPLIED PHYSICS* 97 (2005): 064311,1-4.

Takahiro Harada, Hiroshi Nagakura, Tomio Okawa. "Dependence of bubble behavior in subcooled boiling on surface wettability." *Nuclear Engineering and Design* xxx (2010): xxx–xxx.

Tawatchai Charinpanitkul, Kajornsak Faungnawakij, Wiwut Tanthapanichakoon. "Review of Recent Research on Nanoparticle Production in Thailand." *Advanced Powder Technology* 19 (2008): 443–457.

Teng, Ching-Song Jwo and Tun-Ping. "Experimental Study on Thermal Properties of Brines Containing Nanoparticles." *Rev.Adv.Mater.Sci.* 10 (2005): 79-83.

Thome, John R. "Boiling in microchannels: a review of experiment and theory." *International Journal of Heat and Fluid Flow* 25 (2004): 28–139.

TieJun Zhang, Yoav Peles, John T. Wen, Tao Tong, Je-Young Chang, Ravi Prasher, Michael K. Jensen. "Analysis and active control of pressure-drop flow instabilities in boiling microchannel systems." *International Journal of Heat and Mass Transfer* 53 (2010): 2347–2360.

Ting-Yu Lin, Satish G. Kandlikar. "An Experimental Investigation of Structured Roughness Effect on Heat Transfer During Single-Phase Liquid Flow at Microscale." *JOURNAL OF HEAT TRANSFER* 134 (2012,): 101701-9.

Tolubinsky V.I., Kostanchuk D.M. "Vapour bubbles growth rate and heat transfer intensity at subcooled water boiling." *4th Int. Heat Transfer Conference.* 1970.

Tomio Okawa, Kenta Nagano, Takahiro Hirano. "Boiling heat transfer during single nanofluid drop impacts onto a hot wall." *Experimental Thermal and Fluid Science* 36 (2012): 78–85.

Tomio Okawa, Masahiro Takamura, Takahito Kamiya. "Boiling time effect on CHF enhancement in pool boiling of nanofluids." *International Journal of Heat and Mass Transfer* 55 (2012): 2719–2725.

Tong-Bou Chang, Siou-Ci Syu, Yen-Kai Yang. "Effects of particle volume fraction on spray heat transfer performance of Al2O3–water nanofluid." *International Journal of Heat and Mass Transfer* 55 (2012): 1014–1021.

Tu, J. Y. "The Influence of Bubble Size on Void fraction Distribution in Subcooled Flow Boiling at Low Pressure." *Int. Comm. Heat Mass Transfer* 26 (1999): 607-616.

Ugandhar Puli, A.K. Rajvanshi. "An image analysis technique for determination of void fraction in subcooled flow boiling of water in horizontal annulus at high pressures." *International Journal of Heat and Fluid Flow* xxx (2010): xxx–xxx.

V Vasu, K Rama Krishna and A C S Kumar. "Analytical prediction of forced convective heat transfer of fluids embedded with nanostructured materials (nanofluids)." *PRAMANA journal of physics* 69, no. 3 (2007): 411-421.

V. Dupont, J. R. Thome. "Evaporation in microchannels: influence of the channel diameter on heat transfer." *Microfluid Nanofluid* 1 (2005): 119–127.

V. Prodanovic, D. Fraser, M. Salcudean. "Bubble behaviour in subcooled flow boiling of water at low pressure and low flow rates." *international journal of Multiphase flow* 28 (2002): 1-19.

V. Vasu, K. Rama Krishna, A.C.S. Kumar. "Analytical prediction of forced convective heat transfer of fluids embedded with nanostructured materials (nanofluids)." *Pramana journal of physics* 69 (2007): 411–421.

Vikash Khanikar, Issam Mudawar, Timothy Fisher. "Flow Boiling in a Micro-Channel Coated with Carbon Nanotubes." IEEE, 2008. 960-969.

Vinod Srinivasan, Ming-Chang Lu, Je-Young Chang, Arun Majumdar. "Enhanced Heat Transfer in Biporous Wicks in the Thin Liquid Film Evaporation and Boiling Regimes." *Journal of Heat Transfer* 134 (2012): 101501-1.

Visinee Trisaksri, Somchai Wongwises. "Critical review of heat transfer characteristics of nanofluids." *Renewable and Sustainable Energy Reviews* 11 (2007): 512-523.

Visinee Trisaksri, Somchai Wongwises. "Nucleate pool boiling heat transfer of TiO2–R141b nanofluids." *International Journal of Heat and Mass Transfer* 52 (2009): 1582–1588.

W. Yu, D.M. France, S.U.S. Choi, J.L. Routbort. "Review and Assessment of Nanofluid Technology for Transportation and Other Applications." Sponsored work report by an agency of the United States Government, Oak Ridge, 2007.

Wang, Junye. "Experimental investigation of the transient thermal performance of a bent heat pipe with grooved surface." *Applied Energy* 86 (2009): 2030–2037.

Weerapun Duangthongsuk, Somchai Wongwises. "Effect of thermophysical properties models on the predicting of the convective heat Effect of thermophysical properties models on the predicting of the convective heat." *International Communications in Heat and Mass Transfer* 35 (2008): 1320–1326.

Weerapun Duangthongsuk, Somchai Wongwises. "Heat transfer enhancement and pressure drop characteristics of TiO2–water nanofluid in a double-tube counter flow heat exchanger." *International Journal of Heat and Mass Transfer* 52 (2009): 2059–2067.

Wei Tong, Arthur E. Bergles, Michael K. Jensen. "Pressure Drop with Highly Subcooled Flow Boiling in Small-Diameter Tubes." *Experimental Thermal and Fluid Science* 15 (1997): 202-212.

Weilin Qu, Issam Mudawar. "Flow boiling heat transfer in two-phase micro-channel heat sinks—I. Experimental investigation and assessment of correlation methods." *International Journal of Heat and Mass Transfer* 46 (2003): 2755–2771.

Wen, Dongsheng. "Mechanisms of thermal nanofluids on enhanced critical heat flux (CHF)." *International Journal of Heat and Mass Transfer* 51 (2008): 4958–4965.

Wenhua Yu, David M. France, David S. Smith, Dileep Singh, Elena V. Timofeeva, Jules L. Routbort. "Heat transfer to a silicon carbide/water nanofluid." *International Journal of Heat and Mass Transfer* 52 (2009): 3606–3612.

X. Fu, S.L. Qi, P. Zhang, R.Z. Wang. "Visualization of flow boiling of liquid nitrogen in a vertical mini-tube." *International Journal of Multiphase Flow* 34 (2008): 333–351.

X. Zhang, H. Gu, M. Fujii. "Experimental Study on the Effective Thermal Conductivity and Thermal Diffusivity of Nanofluids." *International Journal of Thermophysics* 27, no. 2 (2006): 569-580.

Xiangdong Li, Wei Wei, Rongshun Wang, Yumei Shi. "Numerical and experimental investigation of heat transfer on heating surface during subcooled boiling flow of liquid nitrogen." *International Journal of Heat and Mass Transfer* 52 (2009): 1510–1516.

Xiang-Qi Wang, Arun S. Mujumdar. "A Review on Nanofluids - Part II: Experimental and Applications." *Brazilian Journal of Chemical Engineering* 25, no. 4 (2008): 631 - 648.

Xiang-Qi Wang, Arun S. Mujumdar. "Heat transfer characteristics of nanofluids: a review." *International Journal of Thermal Sciences* 46 (2007): 1–19.

Xiao Tang, Yao-Hua Zhao, Yan-hua Diao. "Experimental investigation of the nucleate pool boiling heat transfer characteristics of d-Al2O3-R141b nanofluids on a horizontal plate." *Experimental Thermal and Fluid Science* 52 (2014): 88–96.

Xiaohao Wei, Haitao Zhu, Tiantian Kong, Liqiu Wanga. "Synthesis and thermal conductivity of Cu2O nanofluids." *International Journal of Heat and Mass Transfer* 52 (2009): 4371–4374.

Yang Y, Grulke EA, Zhang ZG, Wu G. "Thermal and rheological properties of carbon nanotube-in-oil dispersions." *Journal of Applied Physics* 99 (2006): 114307–114308.

Yi-Hsuan Hung, Tun-Ping Teng, Tun-Chien Teng, Jyun-Hong Chen. "Assessment of heat dissipation performance for nanofluid." *Applied Thermal Engineering* 32 (2012): 132-140.

Yimin Xuan, Qiang Li. "Heat transfer enhancement of nanofluids." *International Journal of Heat and Fluid Flow* 21 (2000): 58-64.

Yimin Xuan, Wilfried Roetzel. "Conceptions for heat transfer correlation of nanofluids." *International Journal of Heat and Mass Transfer* 43 (2000): 3701-3707.

You SM, Kim JH, Kim KH. "Effect of nanoparticles on critical heat flux of water in pool boiling heat transfer." *Applied Physics Letters* 83 (2003): 3374-3376.

Yuan-Yang, Zhen-Hua Liu and. "A new frontier of nanofluid research – Application of nanofluids in heat pipes." *International Journal of Heat and Mass Transfer* xxx (2012): xxx–xxx.

Yujin Hwang, Jae-Keun Lee, Jong-Ku Lee, Young-Man Jeong, Seong-ir Cheong, Young-Chull Ahn, Soo H. Kim. "Production and dispersion stability of nanoparticles in nanofluids." *Powder Technology* 186 (2008): 145–153.

Yulong Ding, Haisheng Chen, Liang Wang, Chane-Yuan Yang, Yurong He, Wei Yang, Wai Peng Lee, Lingling Zhang, Ran Huo. "Heat Transfer Intensification Using Nanofluids." *KONA Powder and Particle Journal* 25 (2007): 23-38.

Yurong He, Yi Jin, Haisheng Chen, Yulong Ding, Daqiang Cang, Huilin Lu. "Heat transfer and flow behaviour of aqueous suspensions of TiO2 nanoparticles (nanofluids) flowing upward through a vertical pipe." *International Journal of Heat and Mass Transfer* 50 (2007): 2272–2281.

Yurong He, Yubin Men, Yunhua Zhao, Huilin Lu, Yulong Ding. "Numerical investigation into the convective heat transfer of TiO2 nanofluids flowing through a straight tube under a laminar flow conditions." *Applied Thermal Engineering* 35 (2009): 1965-1972.

Z, Haddad. "Natural convection in nanofluids: Are the thermophoresis and Brownian motioneffects significant in nanofluid heat transfer enhancement." *International Journal of Thermal Science*, 2012: 152-162.

Zhang Lin, T.T. Chow, C.F. Tsang. "Effect of door opening on the performance of displacement ventilation in a typical office building." *Building and Environment*, 2007: 1335–1347.

Zhen-hua Liu, Jian-guo Xiong, Ran Bao. "Boiling heat transfer characteristics of nanofluids in a flat heat pipe evaporator with micro-grooved heating surface." *International Journal of Multiphase Flow* 33 (2007): 1284–1295.

Zhen-Hua Liu, Xue-Fei Yang, Jian-Guo Xiong. "Boiling Characteristics of carbon nanotubes suspensions under sub-atmospheric pressuer." *International Journal of Thermal Science* 49 (2010): 1156-1164.

Zhen-Hua Liu, Yuan-Yang Li. "A new frontier of nanofluid research – Application of nanofluids in heat pipes." *International Journal of Heat and Mass Transfer* xxx (2012): xxx–xxx.

Zhen-Hua Liu, Yu-Hao Qiu. "Boiling heat transfer characteristics of nanofluids jet impingement on a plate surface." *Heat Mass Transfer* 43 (2007): 699–706.

Zhou, D.W. "Heat transfer enhancement of copper nanofluid with acoustic cavitation." *International Journal of Heat and Mass Transfer* 47 (2004): 3109–3117.

APPENDICES

APPENDIX A: Specification of the Test Section

Table A-A: The specifications of the test section.

S. No.	Characteristics	Size
1	Glass tube inner diameter (mm)	21.8
2	Heater rod outer diameter (mm)	12.7
3	Cross-sectional Area (mm^2)	246.56
4	Glass tube length (mm)	780
5	Heater length (mm)	500
6	Entrance length (mm)	230
7	Exit length (mm)	50
8	Hydraulic Diameter (mm)	9.1
9	Heated Perimeter (mm)	39.89
10	Wetted perimeter (mm)	108.39

APPENDIX B: Specifications of UVM "Deep Drawn Tanks Model SW 24".

Table A-B: The specifications of UVM.

Overall dimensions (mm)	L 590	W 390	H 410
Tank size (mm)	L 500	W 300	H 150
Liquid Level (mm)	130		
Tank Volume (liter)	24		
Ultrasonic Capacity (Watt)	300		
Drain valve available with fabricated tanks only	0.5 inch		
Main Supply	220V AC, 50 Hz		
Ultrasonic Frequency	27±3 KHz		

APPENDIX C: Uncertainty Analysis

The experimental uncertainty of the present work was determined by following ASME guidelines on reporting uncertainties in experimental measurements in multiphase flow. [2]

1. Uncertainties in the dimensions of the test section:

Inner diameter of the annulus, $d_i = 12.7 \times 10^{-3}$ m

Absolute error, $|\Delta d_i| = 0.1 \times 10^{-3} m$

Uncertainty, $\left|\frac{\Delta d_i}{d_i}\right| = 0.78\%$

Outer diameter of the annulus, $d_o = 21.8 \times 10^{-3}$ m

$|\Delta d_o| = 0.1 \times 10^{-3} m$

$\left|\frac{\Delta d_o}{d_o}\right| = 0.45\%$

Length of the heater, $L = 500 \times 10^{-3}$ m

$|\Delta L| = 1 \times 10^{-3} m$

$\left|\frac{\Delta L}{L}\right| = 0.2\%$

Flow area of the annulus,

$$A_f = \frac{\pi}{4}\left(d_o^{\,2} - d_i^{\,2}\right)$$

$$= \frac{\pi}{4}\left(21.8^2 - 12.7^2\right) \times 10^{-6} m^2$$

$$= 246.58 \times 10^{-6} m^2$$

$$|\Delta A_f| = \frac{\pi}{4}\left(\sqrt{\left(2d_o|\Delta d_o|\right)^2 + \left(2d_i|\Delta d_i|\right)^2}\right)$$

$$= \frac{\pi}{4}\left(\sqrt{\left(2 \times 21.8 \times 10^{-3}\left|0.1 \times 10^{-3}\right|\right)^2 + \left(2 \times 12.7 \times 10^{-3}\left|0.1 \times 10^{-3}\right|\right)^2}\right)$$

$$= 1.64 \times 10^{-6} m^2 \Rightarrow \left|\frac{\Delta A_f}{A_f}\right| = 0.66\%$$

Heated surface area,

$A_h = \pi\, d_i\, L = \pi \times 12.7 \times 10^{-3} \times 500 \times 10^{-3}$

$= 19949.11 \times 10^{-6}\ m^2$

$$\left|\frac{\Delta A_h}{A_h}\right| = \sqrt{\left|\frac{\Delta d_i}{d_i}\right|^2 + \left|\frac{\Delta L}{L}\right|^2}$$

$$= \sqrt{0.78^2 + 0.2^2}$$

$$= 0.81\%$$

Hydraulic Diameter,

$$\boldsymbol{d_h = d_o - d_i = 21.8 \times 10^{-3} - 12.7 \times 10^{-3} = 9.1 \times 10^{-3}\ m}$$

$$\left|\Delta d_h\right| = \sqrt{\left|\Delta d_o\right|^2 + \left|\Delta d_i\right|^2} = 0.14 \times 10^{-3} \Rightarrow \left|\frac{\Delta d_h}{d_h}\right| = 1.53\%$$

2. Uncertainty in the measurement of flow rate:

The total uncertainty in measuring volumetric flow rate is obtained as the quadratic sum of the following three components:

(i). The maximum uncertainty claimed by manufacturer is 1 %. Maximum flow, V_p is 18 lpm

Therefore, $\left|\frac{\Delta V_p}{V_p}\right|_1 = 1\% \Rightarrow \left|\Delta V_p\right|_1 = 0.18\ lpm$

(ii). Maximum uncertainty in the calibration of turbine flow meter along with DAQ = 3 x standard deviation of calibration curve fit

$\left|\Delta V_p\right|_2 = 3 \times 0.0626 = 0.1878\ lpm$

(iii) Maximum uncertainty in estimation of average of 10 readings

$\left|\Delta V_p\right|_3$ = 3 x standard deviation of the mean = 3 x 0.021 = 0.063 lpm

Total uncertainty in measuring the volumetric flow rate

$$\left|\Delta V_p\right| = \sqrt{\left|\Delta V_{p_1}\right|^2 + \left|\Delta V_{p_2}\right|^2 + \left|\Delta V_{p_3}\right|^2}$$

$$= \sqrt{(0.18)^2 + (0.1878)^2 + (0.063)^2}$$

$$= 0.28 \text{ lpm}$$

Therefore, $\left|\frac{\Delta V_p}{V_p}\right| = 1.6\%$

3. Uncertainty in measurement of Pressure

(i) Maximum uncertainty claimed by manufacturer = 1%

Therefore, $\left|\frac{\Delta p_1}{p}\right| = 1\% \Rightarrow |\Delta p_1| = 0.01 \text{ bar}$

(ii) Maximum uncertainty in the calibration of pressure sensor along with DAQ = 3 x standard deviation of calibration curve fit

Therefore, $|\Delta p_2|$ = 3 x 0.04844 = 0.14532 bar

(iii) Maximum uncertainty in estimation of average of 10 readings

$|\Delta p_3|$ = 3 x standard deviation of the mean = 3 x 0.02 = 0.06 bar

Total uncertainty in measuring pressure

$$|\Delta p| = \sqrt{|\Delta p_1|^2 + |\Delta p_2|^2 + |\Delta p_3|^2}$$
$$= \sqrt{(0.01)^2 + (0.14532)^2 + (0.06)^2}$$
$$= 0.158 \text{ bar}$$

Therefore, $\left|\frac{\Delta p}{p}\right| = 1.58\%$

4. Uncertainty in measurement of Temperature

(i) Maximum uncertainty claimed by manufacturer = 0.1%

Therefore, $\left|\frac{\Delta T_1}{T}\right| = 0.1\% \Rightarrow |\Delta T_1| = 0.473$ K

(ii) Maximum uncertainty in the calibration of Thermocouple

= 3 x standard deviation of calibration curve fit

Therefore, $|\Delta T_2|$ = 3 x 0.6434 = 1.93 K

(iii) Maximum uncertainty in estimation of average of 10 readings

$|\Delta T_3|$ = 3 x Standard deviation of mean= 3 x 0.01= 0.03 K

Total uncertainty in measuring temperature

$$|\Delta T| = \sqrt{|\Delta T_1|^2 + |\Delta T_2|^2 + |\Delta T_3|^2}$$
$$= \sqrt{0.473^2 + 1.93^2 + 0.03^2}$$
$$= 1.98 \text{ K}$$

Therefore, $\left|\frac{\Delta T}{T}\right| = 0.4\%$

5. Uncertainty in the measurement of Power:

Maximum Power,

P = V x I

P = 32 x 2000/1000 = 64 kW

As per the suppliers claim,

$|\Delta V| = 0.2$ Volts and $|\Delta I| = 10$ amp

$$|\Delta P| = \sqrt{\left(|\Delta V|^2\right) + \left(|\Delta I|^2\right)}$$

$$\left|\frac{\Delta P}{P}\right| = \sqrt{\left(\left|\frac{\Delta V}{V}\right|^2 + \left|\frac{\Delta I}{I}\right|^2\right)} = \sqrt{\left(\left|\frac{0.2}{32}\right|^2 + \left|\frac{10}{2000}\right|^2\right)} = 0.8\%$$

Uncertainty in the measurement of heat flux (q):

$$\left|\frac{\Delta q}{q}\right| = \sqrt{\left(\left|\frac{\Delta P}{P}\right|^2 + \left|\frac{\Delta A_h}{A_h}\right|^2\right)}$$

$$= \sqrt{0.8^2 + 0.81^2}$$

$$= 1.14\ \%$$

APPENDIX D: Specifications of (KD2 Pro)

Table A-D: The specifications of the thermal property analyzer (KD2 Pro).

S. No.	Parameters	KD2 Pro
1.	Measurement Time	1 minute
2.	Accuracy	5% specific heat 5% Thermal conductivity/Resistivity 10% Thermal Diffusivity
3.	Range of Measurement	K: 0.02 to 2 Wm^{-1} C^{-1} D: 0.1 to 1.0 mm^2s^{-1} R: 0.5 to 50 mC W^{-1} C: 0.5 to 4 MJ m^{-3} C^{-1}
4.	Operating Environment	- 50℃ to 150°C
5.	Weight	0.95 kg
6.	Power	4 x 'AA' batteries

APPENDIX E: Specifications of the KS-1 Sensor of KD2 Pro.

Table A-E: The specifications of the KS-1 Sensor of KD2 Pro.

S. No.	Parameters	KS-1
1.	Diameter	1.3 mm
2.	Length	60 mm
3.	Thermal conductivity range	0.02 to 2.00 (W/mK)
4.	Thermal Resistivity range	0.50 to 50 (mK/W)
5.	Accuracy (Conductivity)	±5%
6.	Cable length	0.8 m

APPENDIX F: Properties of Nanoparticles

Aluminum Oxide (Alumina, alpha-Al_2O_3)
White nanopowder
Purity: 99.0+%
Average Particle Size (APS): 40 nm
Specific Surface Area (SSA): ~ 60 m^2/g
Applications: Ceramic, catalyst, polishing, phosphor….

Titanium Oxide (TiO_2, rutile)
Purity: 99.5%
Appearance: white nanopowder
D50: 10-30 nm
SSA: ~ 50 m^2/g

Zinc Oxide (ZnO)
Purity: 99.8%
Appearance: white ~ light yellow nanopowder
D50: 10-30 nm
SSA: 30-50 m^2/g

Multi Walled Carbon Nanotubes (MWCNT)
Purity: > 95 wt%
Outside diameter: 10-20 nm
Inside diameter: 3-5 nm
Length: 5-30um
SSA: > 350 m^2/g
Ash: < 1.0 wt%
Amorphous carbon: < 3.0%
Electrical conductivity: > 100 s/cm
Bulk density: 0.27g/cm^3
True density: ~2.1 g/cm^3
Manufacturing method: Catalytic CVD

APPENDIX G: Thermal Properties of Water.

- Maximum density at 4^{o}C - 1,000 kg/m^3, 1.940 slugs/ft^3
- Specific Weight at 4^{o}C - 9.807 kN/m^3, 62.43 Lbs./Cu.Ft, 8.33 Lbs./Gal., 0.1337 Cu.Ft./Gal.
- Freezing temperature - 0^{o}C (Ice at 0^{o}C)
- Boiling temperature - 100^{o}C
- Latent heat of melting - 334 kJ/kg
- Latent heat of evaporation - 2,270 kJ/kg
- Critical temperature - 380^{o}C - 386^{o}C
- Critical pressure - 221.2 bar, 22.1 MPa (MN/m^2)
- Specific heat capacity water - 4.187 kJ/kgK
- Specific heat capacity ice - 2.108 kJ/kgK
- Specific heat capacity water vapor - 1.996 kJ/kgK
- Thermal expansion from 4^{o}C to 100^{o}C - 4.2x10^{-2}
- Bulk modulus elasticity - 2.15 x 10^9 (Pa, N/m^2)

Table A-G: Thermal properties of water

Temperature - *t* -	**Absolute pressure - *p* -**	**Density - ρ -**	**Specific volume - *v* -**	**Specific Heat - c_p -**	**Specific entropy - *e* -**
(^{o}C)	(kN/m^2)	(kg/m^3)	10^{-3} (m^3/kg)	(kJ/kgK)	(kJ/kgK)
0 (Ice)		916.8			
4 (maximum density)	0.9	1000.0			
25	3.2	997.1	1.00	4.181	0.367
80	47.5	972	1.03	4.198	1.076
100	101.33	958	1.04	4.219	1.307

Temperature - *t* -	**Absolute pressure - *p* -**	**Dynamic viscosity - μ -**	**Kinematic viscosity - *v* -**	**Expansion coefficient**	**Specific enthalpy**	**Prandtl's no.**
(^{o}C)	(kN/m^2)	(Centipoise)	10^{-6} (m^2/s)	10^{-3} (l/K)	(kJ/kg)	
4	0.9	1.52		0.160	21.0	
25	3.2	0.890		0.257	104.8	
80	47.5	0.355	0.365	0.643	335.3	2.23
100	101.33	0.281	0.295	0.752	419.1	1.75

APPENDIX H: Thermal Conductivity of Nanoparticles.

Thermal conductivity of some common materials and products are indicated in the table below.

1 W/(mK) = 1 W/(m^{o}C) = 0.85984 kcal/(hr m^{o}C) = 0.5779 Btu/(ft hr ^{o}F)

Table A-H: Thermal conductivity of some common materials

Thermal Conductivity - k - (W/mK)			
Material/Substance	Temperature (^{o}C)		
	25	125	225
Aluminum Oxide	≈ 30		
Titanium Oxide	≈ 10		
Zinc Oxide	≈ 60		
MWCNT	>500		
Steel, Carbon 1%	≈ 43		
Stainless Steel	≈ 16	≈ 17	≈ 19
Water	0.58		

APPENDIX I: ANOVA Method

The results of an ANOVA are presented in tabular form. The components of results of an ANOVA are presented as following:

1. **Source**: It indicates the source of variation, either from the factor, the interaction, or the error. The total is a sum of all the sources.

2. **DF**: It is degrees of freedom from each source. It indicates the number of independent elements in the sum of squares. The degrees of freedom for each component of the model are:

   DF (Factor) $= r - 1$

   DF (Error) $= n_T - r$

   Total $= n_T - 1$

   where n_T = the total number of observations and r = *the number of factor levels.*

3. **SS**: It is sum of squares between groups (factor) and the sum of squares within groups (error). SS Total is the total variation in the data. SS (Factor) is the deviation of the estimated factor level mean around the overall mean. It is also known as the sum of squares between treatments. SS Error is the deviation of an observation from its corresponding factor level mean. It is also known as error within treatments. Its calculations can be done by:

   SS (Factor) $= \sum(\hat{Y} - \bar{Y})^2$

   SS Error $= \sum(Y - \hat{Y})^2$

   SS Total $= \sum(\hat{Y} - \bar{Y})^2 + \sum(Y - \hat{Y})^2 = \sum(Y - \bar{Y})^2$

   where Y = value of the observation, $\bar{Y}$ = mean of the observations, $\hat{Y}$ = fitted response for n (no. of observations).

   Minitab breaks down the SS Regression or Treatments component of variance into the **adjusted sum of squares (Adj SS)** for the main effects, interactions, blocks, and each covariate. The adjusted sum of squares does not depend on the order the factors are entered into the model. It is the unique portion of SS Regression explained by a factor, given all other factors in the model, regardless of the order they were entered into the model.

For example, in our case the model has three factors: C, P, and q. The adjusted sum of squares for P shows how much of the remaining variation P explains, given that C and q are also in the model. The calculations for the adjusted sum of squares for three factors are:

SSR (q | C, P) = SSE (C, P) – SSE (C, P, q) or

SSR (q | C, P) = SSR (C, P, q) – SSR (C, P)

where SSR (q | C, P) is the adjusted sum of squares for q, given that C and P are also in the model.

SSR (P, q | C) = SSE (C) – SSE (C, P, q) or

SSR (P, q | C) = SSR (C, P, q) – SSR (C)

where SSR(P, q | C) is the adjusted sum of squares for P and q, given that C is also in the model.

4. **MS**: These are mean of squares values, found by dividing the sum of squares by the degrees of freedom. The calculations for the mean square for the factor and error can be done by:

$$MS\ (Factor) = \frac{SS\ (Factor)}{DF\ (Factor)}$$

$$MS\ (Error) = \frac{SS\ (Error)}{DF\ (Error)}$$

The **adjusted mean of squared** (**Adj MS**) values is calculated as:

$$Adj\ MS = \frac{Adj\ (SS)}{DF}$$

5. **F-value**: It is calculated by dividing the factor MS by the error MS. An F-test evaluates whether the observed statistic exceeds a critical value from the distribution. If the observed F-statistic exceeds the critical value, reject the null hypothesis. For example, in one-way analysis of variance, the F-statistic is a ratio of the mean square of the factor and the mean square error. An F-statistic that is larger than the critical value from the F-distribution, using the appropriate confidence level and degrees of freedom, supports rejecting the null hypothesis that the means are equal.

F- test is a test to determine whether the factor means are equal or not. The formula of F value is:

$$F = \frac{\text{MS (Factor)}}{\text{MS (Error)}}$$

The degrees of freedom for the numerator are (r – 1) and for the denominator are $(n_T - r)$. Larger values of F support rejecting the null hypothesis that the means are equal.

6. **P-value**: It is used to determine whether a factor is significant or not; typically compare against an alpha value of 0.05. If the p-value is lower than 0.05, then the factor is significant.

7. **S: -** It is the standard error of the regression in Analysis of Variance method for Al_2O_3-water nanofluid. It represents the average distance that the observed values fall from the regression line. It is calculated as:

$$S = \sqrt{MS(Error)}$$

The S provides important information that R-squared does not. S is 2.10459 for Al_2O_3-water nanofluids, which defines that the average distance of the data points from the fitted line is about 2.1% HTC.

8. **R-square (R^2)**: These values are higher than 0.95. It indicates that model representation is significant. When R^2 is closer to the 1, the better the estimation of regression equation fits the sample data. In general, the R^2 measures percentage of the variation of Y around Y that is explained by the regression equation. Its formula is:

$$R^2 = \frac{SS\ (Factor)}{SS\ (Total)} = 1 - \frac{SS\ (Error)}{SS\ (Total)} = 1 - \frac{\sum(Y - \hat{Y})^2}{\sum(Y - \bar{Y})^2}$$

9. **Adjusted R^2**: accounts for the number of predictors in ANOVA model and is useful for comparing models with different numbers of predictors. While the calculations for adjusted R^2 can produce negative values, Minitab displays zero for these cases. The formula for adjusted R^2 is:

$$R^2\ (Adj) = 1 - \frac{MS\ (Error)}{SS\ (Total) \Big/ DF\ (Total)}$$

10. **Predicted R^2**: Indicates how well the model predicts responses for new observations, whereas R^2 indicates how well the model fits the data. The formula for predicted R^2 is:

$$R^2(\text{Pred.}) = 1 - \frac{PRESS}{SS\,(Total)} = 1 - \sum_{1}^{n} \frac{(\frac{e_i}{1-h_i})^2}{\sum(Yi - \tilde{Y})^2}$$

e_i = i^{th} residual
h_i = i^{th} diagonal element of $\mathbf{X\,(X'\,X)^{-1}\,X'}$
X = predictor matrix

where PRESS = prediction sum of squares and SS (Total) = total sum of squares.

Predicted R^2 can prevent over-fitting the model, means it fits the model too closely to the data in the current data set, so it is not useful for predicting new data. Predicted R^2 can be more useful than adjusted R^2 for comparing models because it is calculated with observations that are not included in model calculation. Predicted R^2 values lie between 0 and 1; larger values of predicted R^2 suggest models of greater predictive ability. While the calculations for predicted R^2 can produce negative values, Minitab displays zero for these cases.

The results of analysis of variance and model summary are presented in **Appendix-J** for all the nanofluids.

APPENDIX J: Results of ANOVA and Summery Reports

1. Analysis of Variance for Al_2O_3-water nanofluid:

Source	**DF**	**Adj SS**	**Adj MS**	**F-Value**	**P-Value**
Model	9	21777.3	2419.70	546.29	0.000
Linear	3	7246.9	2415.63	545.37	0.000
C	1	2438.5	2438.54	550.55	0.000
P	1	952.5	952.48	215.04	0.000
q	1	2322.3	2322.32	524.31	0.000
Square	3	1768.8	589.61	133.12	0.000
C*C	1	166.1	166.12	37.51	0.000
P*P	1	11.0	11.02	2.49	0.116
q*q	1	1558.9	1558.89	351.95	0.000
2-Way Interaction	3	818.3	272.75	61.58	0.000
C*P	1	1.7	1.71	0.39	0.535
C*q	1	411.4	411.43	92.89	0.000
P*q	1	325.3	325.29	73.44	0.000
Error	211	934.6	4.43		
Total	220	22711.9			

The summery for Al_2O_3-water nanofluids the model:

S	R^2	R^2 (adj)	R^2 (pred)
2.10459	95.89%	95.71%	95.37%

2. Analysis of Variance for TiO_2-water nanofluid

Source	DF	Adj SS	Adj MS	F-Value	P-Value
Model	9	22378.6	2486.51	1084.97	0.000
Linear	3	10030.7	3343.58	1458.95	0.000
C	1	1081.2	1081.16	471.76	0.000
P	1	1895.5	1895.48	827.08	0.000
q	1	4229.7	4229.67	1845.59	0.000
Square	3	1541.5	513.85	224.21	0.000
C *C	1	217.3	217.28	94.81	0.000
P*P	1	8.4	8.38	3.66	0.057
q*q	1	1336.9	1336.86	583.33	0.000
2-Way Interaction	3	817.3	272.44	118.88	0.000
C *P	1	13.1	13.10	5.71	0.018
C *q	1	222.1	222.11	96.92	0.000
P*q	1	568.6	568.61	248.11	0.000
Error	189	433.1	2.29		
Total	198	22811.7			

Model Summary for TiO_2-water nanofluid

S	R-sq	R-sq(adj)	R-sq(pred)
1.51386	98.10%	98.01%	97.88%

3. Analysis of Variance for ZnO-water nanofluid

Source	**DF**	**Adj SS**	**Adj MS**	**F-Value**	**P-Value**
Model	9	20831.4	2314.60	964.13	0.000
Linear	3	11084.2	3694.73	1539.02	0.000
C	1	1660.3	1660.30	691.59	0.000
P	1	1638.8	1638.79	682.63	0.000
q	1	6785.0	6784.96	2826.23	0.000
Square	3	1219.1	406.38	169.27	0.000
C *C	1	201.0	200.99	83.72	0.000
P*P	1	5.8	5.79	2.41	0.122
q*q	1	1049.5	1049.53	437.17	0.000
2-Way Interaction	3	746.6	248.87	103.67	0.000
C *P	1	9.5	9.48	3.95	0.048
C *q	1	414.4	414.37	172.60	0.000
P*q	1	383.4	383.42	159.71	0.000
Error	224	537.8	2.40		
Total	233	21369.2			

Model Summary for ZnO-water nanofluid

S	**R-sq**	**R-sq(adj)**	**R-sq(pred)**
1.54942	97.48%	97.38%	97.26%

4. Analysis of Variance for MWCNT-water nanofluid

Source	**DF**	**Adj SS**	**Adj MS**	**F-Value**	**P-Value**
Model	9	13455.5	1495.06	31.92	0.000
Linear	3	1274.4	424.79	9.07	0.000
C	1	767.2	767.22	16.38	0.000
P	1	399.6	399.55	8.53	0.004
q	1	103.7	103.66	2.21	0.139
Square	3	5568.7	1856.22	39.63	0.000
C *C	1	2846.4	2846.35	60.77	0.000
P*P	1	6.1	6.06	0.13	0.719
q*q	1	3463.1	3463.14	73.94	0.000
2-Way Interaction	3	363.5	121.18	2.59	0.054
C *P	1	191.2	191.22	4.08	0.045
C *q	1	6.4	6.39	0.14	0.712
P*q	1	173.9	173.88	3.71	0.056
Error	185	8664.5	46.84		
Total	194	22120.1			

Model Summary for MWCNT-water nanofluid

S	R-sq	R-sq(adj)	R-sq(pred)
6.84362	60.83%	58.92%	55.70%

PUBLICATION

INTERNATIONAL JOURNALS

1. Prajapati, O.S. and Rohatgi, N., "Flow Boiling Heat Transfer Enhancement by Using ZnO-Water Nanofluids" Science and Technology of Nuclear Installations, Vol. 2014, Article ID 890316, 8 pages, (2014).
2. Prajapati, O.S., Rohatgi, N. and Rajvanshi, A.K., "Heat Transfer Behaviour of Nanofluid at High Pressure", Journal of Materials Science & Surface Engineering, Vol. 1, pp. 1-3, (2013).
3. Prajapati, O.S. and Rajvanshi, A.K., "Al_2O_3-Water Nanofluids in Convective Heat Transfer", International Journal of Applied Mechanics and Materials, Vol. 110-116, Page 3667-3672, (2012).
4. Prajapati, O.S. and Rajvanshi, A.K., "Effect of Al_2O_3-Water Nanofluids in Convective Heat Transfer", International Journal of Nanoscience, Vol. 11, No. 3, 1240005 (4 pages), (2012).

INTERNATIONAL CONFERENCES

1. Prajapati, O.S. and Rajvanshi, A.K., "Effect of Ultrasonication on ZnO-water Nanofluid's Thermal Conductivity" International Conference on Emerging Trends on Mirco & Nano, ETMN-2013, BIT's Goa, India, (2013).
2. Prajapati, O.S. and Rajvanshi, A.K., "Heat Transfer Behaviour with ZnO-water Nanofluids" 2nd Virtual Nanotechnology Poster Conference, (2012).
3. Prajapati, O.S. and Rajvanshi, A.K., "Effect of Pressure on Subcooled Flow Boiling of TiO_2-water Nanofluids" ECI - 8th International Conference on Boiling and Condensation Heat Transfer, at Ecole Polytechnique Fédérale de Lausanne (EPFL) Lausanne, Switzerland, (2012).
4. Prajapati, O.S. and Rajvanshi, A.K., "Nanofluid Behaviour in Flow Boiling Heat Transfer" Workshop on Phase-change Thermal Systems, PCTS-2012, IIT Kanpur, Kanpur, India, (2012).

5. Prajapati, O.S. and Rajvanshi, A.K., "TiO_2-Water Nanofluid Behavior at High Pressure in Convective Heat Transfer" 2nd International Conference on Renewable Energy: Generation and Applications, ICREGA'12, Al Ain, United Arab Emirates, (2012).
6. Prajapati, O.S. and Rajvanshi, A.K., "Flow Boiling Heat Transfer with TiO_2-Water Nanofluid" INDO-JAPAN Conference on Frontier NanoMaterials for Energy, FNE-2012, Sharda University, Greater Noida, India, (2012).
7. Om Shankar Prajapati and A.K.Rajvanshi, "Al_2O_3-Water Nanofluids in Convective Heat Transfer" International Conference on Mechanical and Aerospace Engineering, (ICMAE 2012), held at University of Delhi, Delhi, India, (2011).
8. Prajapati, O.S. and Rajvanshi, A.K., "Effect of Nanofluid in Flow Boiling Heat Transfer" International Conference on Nanomaterials & Nanotechnology, ICNANO 2011, University of Delhi, Delhi, India, (2011).
9. Om Shankar Prajapati and A.K.Rajvanshi, "Critical Heat Flux in Boiling Heat Transfer" Sharjah International Symposium on Nuclear and Renewable Energies for the 21st Century, held at University of Sharjah, Sharjah, United Arab Emirates, (2011).
10. Prajapati, O.S. and Rajvanshi, A.K., "Convective Heat Transfer with Al_2O_3-Water Nanofluids" International Conference on Renewable Energy, University of Rajasthan, Jaipur, India, (2011).
11. Prajapati , O.S. and Rajvanshi, A.K., "Effect of Al2O3-water Nanofluids in Convective Heat Transfer" International Conference on Nanoscience, Nanotechnology and Advanced Materials held at GITAM Institute of Science, GITAM University, Vishakhapatnam, India (2010).
12. Prajapati, O.S. and Rajvanshi, A.K., "Heat Transfer Enhancement with Al_2O_3 Nanofluid in Convective Heat Transfer" International Conference on Power and Energy systems, International Association of Science and Technology for Development (IASTED), Phuket, Thailand, (2010).
13. Prajapati, O.S. and Rajvanshi, A.K., "Heat Transfer Characteristics of Al_2O_3 Nanofluids in Convective Heat Transfer" International Conference

on Advances in Renewable Energy, ICARE, Maulana Azad National Institute of Technology, Bhopal, India, (2010).

NATIONAL CONFERENCES

1. Om Shankar Prajapati and A.K. Rajvanshi, “Heat Transfer Behaviour of Nanofluids at High Pressure” presented at All India Seminar on Nanotechnology Applications (NTA-2012) held at Design Center, Malaviya National Institute of technology Jaipur, jaipur, India, (2012).
2. Om Shankar Prajapati and A. K. Rajvanshi, “Critical Heat Flux of Nanofluids” presented at All India Seminar on Nanotechnology & Its Applications (NTA-2011) held at Arya College of Engg. & I. T., Jaipur, India, (2011).
3. O.S. Prajapati and A.K. Rajvanshi, “Science and Technology of Nano Size Structures”, presented at National Conference on Recent Developments in Mechanical Engineering held at Laxmi Devi Institute of Engineering & Technology, Alwar, India, (2010) .

BOOKS

1. Om Shankar Prajapati and A.K. Rajvanshi “Heat Transfer with nanofluids”, ISBN: 978-3-8465-4922-3, Lap Lambart, Germany, 2011.
2. Akash Vajpai, A. K. Rajvanshi And O. S. Prajapati, “Thermal Conductivity of Nanofluids”, ISBN: 978-3-8484-4831-9, Lap Lambart, Germany, 2012.

BIO-DATA

O.S. Prajapati

Mr. O.S. Prajapati joined the technical teaching faculty in the Department of Mechanical Engineering at Rajasthan Technical University, Kota, India on 18.06.2013 where he is Assistant Professor of Mechanical Engineering. He has additional charges of Dy. Chairman Library, Proctor, AICTE Co-coordinator and Departmental Coordinator for NBA in the same University. He was Assistant Professor of Mechanical Engineering during the period of 28.02.2013-17.06.2013 in the Department of Mechanical Engineering at M.L.V. Government Textile and Engineering College, Bhilwara, Rajasthan, India. He was Senior Research Fellow and Junior Research fellow of the Bhabha Atomic Research Center, Department of Atomic Energy, Mumbai, India sponsored research project "Investigation of Heat Transfer Characteristics of Nano-fluids in Subcooled Flow Boiling (Sanction No.: 2009/36/95-BRNS/3234" in the Mechanical Engineering Department at Malaviya National Institute of Technology, Jaipur, India during the period of 17.09.2012-27.02.2013 and 17.09.2010-16.09.2012. He worked as Q.A. Engineer at KCWPL, Jaipur form 16.10.2007-15.07.2008. He obtained B.E. degree in Mechanical Engineering from University of Rajasthan, Jaipur, India in 2007 and M.Tech. degree in Energy Engineering from Malaviya National Institute of Technology, Jaipur, India in 2010. He has 2 year 11 month teaching experience, 2 year 5 month research experience and 9 month industrial experience. He has published 3 International Books, 3 National Books and 4 research papers in International journals. He also presented 13 research papers in International conferences and 9 papers in National conferences.

Out of all publications, 2 research papers in International journals and 7 research papers in International conferences and 3 research papers in National conferences are contribution to his Ph.D. work.